2016

The role of the prion-like protein SOD1 and macropinocytosis in the propagation of disease in ALS; an infectious idea

Rafaa Zeineddine
University of Wollongong

The role of the prion-like protein SOD1 and macropinocytosis in the propagation of disease in ALS; an infectious idea

A thesis submitted in fulfilment of the requirements for the award of the degree

Doctor of Philosophy

from

UNIVERSITY of WOLLONGONG

by

Rafaa Zeineddine

Bachelor of Medical Biotechnology (Adv) (Hons)

School of Biological Sciences

Centre for Medical and Molecular Bioscience

Illawarra Health and Medical Research Institute (IHMRI)

2016

THESIS CERTIFICATION

I, Rafaa Zeineddine, declare that this thesis, submitted in fulfilment of the requirements for the award of Doctor of Philosophy, in the Department of Biological Sciences, University of Wollongong, is wholly my own work unless otherwise referenced on acknowledged. The document has not been submitted for qualifications at any other academic institution.

Rafaa Zeineddine

2016

ACKNOWLEDGEMENTS

First and foremost, I would like to express my sincere gratitude to my supervisor Dr Justin Yerbury. The endless support, guidance, advice , patience inspiration, motivation and care you have provided me throughout the past few years has allowed to me to carry out all my tasks and responsibilities in my PhD research successfully and competently. I am also very thankful for the great opportunities you provided me with, which have allowed me to attain new skills, more knowledge and the confidence to carry out a career in medical research. Your excellent supervision has been greatly appreciated. Thank you. I would also like to thank my co-supervisor Senior Professor Mark Wilson for your advice and the opportunities you have provided me with.

I would like to acknowledge and thank the University of Wollongong's Global Challenges Program for supporting and funding me with the opportunity to travel overseas for a conference in Germany.

I would like to thank Dr Elise Stewart for her assistance in the lab, especially with specialised imaging techniques at the University of Wollongong's innovation campus. Your continuous support and readiness to assist has made those aspects of my work much more convenient and time saving.

A big thank you to all past and current members of the Yerbury and Wilson labs, and of office 228, for all your problem-solving support and assistance in experimenting and other lab work, especially Natalie, Kate, Luke, Daniel, Bella, Bec and Amy. To my other friends, Rachael, Diane, Aleta and Natalie your never-ending support, your kind offers and suggestions and willingness to always assist during my most stressful times has made my PhD experience much more joyful and rewarding. Thank you for always being there for me when I need it the most, you guys are an important part of my life.

To my unconditionally loving immediate family, I give you my most heartfelt appreciation for your support, love, patience, care and your belief in me. With a special mention to my mother, you have always been there for me, and always taught me my education is important and reminded me daily that I will get through my challenges, your love, faith and strength is what helps me achieve and succeed, I am eternally grateful for everything you are and everything you do. To my brother Mohamed, sister in-law Chantelle and father, thank you for all your support and love, with special mention to the new addition to the family who has brought nothing but happiness and joy to our lives, my nephew Idris. A huge thank you to my both my aunties and their families, thank you for your moral and emotional support and lift when needed. I would also like to thank my fiancé Ahmed for his unconditional support, love and motivation to always achieve my best. I would also like to acknowledge and thank my other family and family friends, especially Javed Rana for his support throughout the years.

Lastly, thank you to everyone in my life who has helped me grow, learn and develop into a better person.

TABLE OF CONTENTS

LIST OF FIGURES

LIST OF TABLES

ABBREVIATIONS

A265	Absorbance at 265 nm
A280	Absorbance at 280 nm
Ab	Antibody
ABR	Australian Bioresources
Abs	Antibodies
AEC	Anion exclusion chromatography
ALEXA488	ALEXA fluor® 488
ALEXA633	ALEXA fluor® 633
ALS	Amyotrophic lateral sclerosis
ALS	Amyotrophic lateral sclerosis
Amp	Ampicillin
AST1	Astrocyte-like cells
Az	Sodium azide
bp	Base pair
BSA	Bovine serum albumin
BSA	Bovine albumin serum
CB	Carbenicillin
CE	Cytoplasmic extract
CNS	Central nervous system
CSF	Cerebrospinal fluid
dH_2O	Distilled water
DIC	Differential interference contrast
DMEM:F12	Dulbecco's modified Eagles medium: Hams F-12
DMSO	Dimethyl sulfoxide
DTT	Dithiothreitol
E.coli	*Escherichia coli*
ECL	Enhanced chemiluminescence
EDTA	Ethylenediaminetetraacetic acid
EGFP	Enhanced green fluorescent protein
ELISA	Enzyme-linked immunosorbent assay
Em	Emission
ER	Endoplasmic reticulum
Ex	Excitation
FBS	Fetal bovine serum
FESEM	Field emission scanning electron microscopy
FITC	Fluorescein isothiocyanate
FloIT	Flow cytometric characterisation of inclusions and trafficking
FSC	Forward scatter
FUS/TLS	Fused in sarcoma/translocated in liposarcoma protein
g	Relative centrifugal force (9.8 m.s-2)

G93A	G93A mutant
GFP	Green fluorescent protein
GST	Glutathione-S-transferase
H	Hour
h	Hour(s)
HDC	Heat-denatured casein
HDC/PBS	1% heat denatured casein and 0.01% thimerosal in PBS
HEK	Human embryonic kidney
HMW	High molecular weight
HR	High resolution
HRP	Horseradish peroxidase
hSOD1	Human SOD1
Ig	Immunoglobulin
iPSC	Induced pluripotent stem cell
IPTG	Isopropyl-β-D- thiogalactopyranoside
kDa	Kilo daltons
KO	Knock-out
LB	Lysogeny broth
mAb	Monoclonal antibody
ME	Memrane extract
MFI	Mean fluorescence intensity
mg132	Carbobenzoxy-Leu-Leu-leucinal
min	Minutes
MTT	3-(4,5-Dimethylthiazol-2-yl)-2,5-diphenyltetrazolium bromide
MW	Molecular weight
MWCO	Molecular weight cut off
n	Number
NCIs	Neuronal cytoplasmic inclusions
NE	Nuclear extract
ng	Nanograms
NSC-34	Motor neuron-like cells
NT	Non-transfected
pAb	Polyclonal antibody
PBS	Phosphate-buffered saline
PCR	Polymerase chain reaction
PDL	Poly-D-lysine
PE	Pellet extract
PFA	Paraformaldehyde
PMA	Phorbol 12-myristate 13-acetate
rpm	Revolutions per minute
RT	Room temperature
s	Seconds
SA	Streptavidin

SDS	Sodium dodecyl sulphate
SDS-PAGE	Sodium dodecyl sulphate-polyacrylamide gel electrophoresis
SEC	Size exclusion chromatography
SOD1	$Cu^{2+,}$ Zn^{2+} superoxide dismutase 1
SOD1 G93A	Glycine substituted to alanine at position 93 SOD1 mutation
SSC	Side scatter
TAE	Tris-acetate-EDTA
TDP-43	Transactivation response DNA-binding protein
TEM	Transmission electron microscopy
ThT	Thioflavin T
TMED	N,N,N',N'- tetramethylethylenediamine
TR	Tomato red
UV	Ultraviolet
V	Volts
WT	Wild type
ΔCt	Difference in crossing points

PUBLICATIONS FROM THESIS

Work presented as part of this thesis contributed to the following publications as referenced in the relevant chapters.

- **Zeineddine R**, Pundavela JF, Corcoran L, Stewart EM, Do-Ha D, Bax M, Guillemin G, Vine KL, Hatters DM, Ecroyd H, Dobson CM, Turner BJ, Ooi L, Wilson MR, Cashman NR and Yerbury JJ (2015) SOD1 protein aggregates stimulate macropinocytosis in neurons to facilitate their propagation. Molecular neurodegeneration 10:57 (Chapter 1 and 4)

- **Zeineddine R** and Yerbury JJ (2015) The role of macropinocytosis in the propagation of protein aggregation associated with neurodegenerative diseases. Frontiers in physiology 6:277. (Chapter 1 and 4)

- Grad LI, Yerbury JJ, Turner BJ, Guest WC, Pokrishevsky E, O'Neill MA, Yanai A, Silverman JM, **Zeineddine R**, Corcoran L, Kumita JR, Luheshi LM, Yousefi M, Coleman BM, Hill AF, Plotkin SS, Mackenzie IR and Cashman NR (2014) Intercellular propagated misfolding of wild-type Cu/Zn superoxide dismutase occurs *via* exosome-dependent and -independent mechanisms. Proc Natl Acad Sci U S A. (Chapter 1)

- Roberts K, **Zeineddine R**, Corcoran L, Li W, Campbell IL and Yerbury JJ (2013) Extracellular aggregated Cu/Zn superoxide dismutase activates microglia to give a cytotoxic phenotype. Glia 61:409-419. (Chapter 1)

- Sundaramoorthy V, Walker AK, Yerbury J, Soo KY, Farg MA, Hoang V, **Zeineddine R**, Spencer D and Atkin JD (2013) Extracellular wildtype and mutant SOD1 induces ER-Golgi pathology characteristic of amyotrophic lateral sclerosis in neuronal cells. Cellular and molecular life sciences: CMLS 70:4181-4195. (Chapter 1)

Work presented in this thesis contributes to the following publications currently in preparation:

- **Zeineddine R,** Whiten D, McAlary L and Yerbury JJ (2016) Exogenously added recombinant SOD1 protein aggregates are associated with TDP-43 protein mislocalisation and aggregation. *Currently in preparation* (Chapter 3)

- **Zeineddine R,** McAlary L and Yerbury JJ (2016) The transfer and seeding of SOD1 between neurons. *Currently in preparation* (Chapter 2)

LIST OF CONFERENCE PRESENTATIONS

Zeineddine R, Yerbury JJ "SOD1 protein aggregates stimulate macropinocytosis in neurons to facilitate their propagation". Poster presentation. *Mechanisms of Neurodegeneration*, EMBL Heidelberg, Germany **2015**.

Zeineddine R and Yerbury JJ SOD1 "Protein aggregates stimulate macropinocytosis in neurons to facilitate their propagation ". Poster presentation. *1st Australian Neurodegeneration and Dementia Conference*, Melbourne, Australia, **2015**.

Zeineddine R Yerbury JJ "SOD1 protein aggregates activate macropinocytosis in neurons to facilitate their entry". Poster presentation. *MND Australia Research Meeting*, Sydney, Australia, **2015**.

Zeineddine R Yerbury JJ "Macropinocytosis: A key player in the propagation of disease in ALS". Oral presentation. *Proteostasis & Disease Research Centre Seminar Series*¸ Wollongong, Australia, **2015**.

Zeineddine R and Yerbury JJ "Macropinocytosis as a Mechanism for the Cellular Entry of Mutant SOD1 Aggregates into Neurons". Poster presentation. *39th Lorne Conference on Protein Structure and Function*, Lorne, Australia, **2014**.

Zeineddine R Yerbury JJ "Gobbling and Gulping: Neuronal macropinocytosis, a way in for SOD1 aggregates to mediate propagation of ALS or MND". Oral presentation. *Proteostasis and Disease Symposium*¸ Wollongong, Australia, **2014**.

Zeineddine R Yerbury JJ "Neuronal macropinocytosis: a pathway to SOD1-mediated disease in ALS". Oral presentation. *Proteostasis & Disease Research Centre Seminar Series*¸ Wollongong, Australia, **2014**.

Zeineddine R Yerbury JJ "Neuronal macropinocytosis; a way in for SOD1 aggregates to mediate propagation of disease in ALS". Oral presentation. *School of Biological Sciences Postgraduate Conference*, Kioloa, Australia, **2014**.

Zeineddine R Yerbury JJ "Investigating the mechanisms of entry of SOD1-ALS aggregates into neuronal cells". Oral presentation. *Proteostasis & Disease Research Centre Seminar Series*¸ Wollongong, Australia, **2013**.

Zeineddine R Yerbury JJ "The Prion-Like Action of SOD1 and TDP-43 in Amyotrophic Lateral Sclerosis". Oral presentation. *School of Biological Sciences Postgraduate Conference*, Kioloa, Australia, **2013**.

Zeineddine R Yerbury JJ "The prion-like action of SOD1: an infectious idea". Poster presentation. *MND Australia Research Meeting*, Sydney, Australia, **2013**.

Zeineddine R Yerbury JJ "The Prion-Like Action of SOD1: an Infectious Idea". Poster presentation. *Proteostasis and Disease Symposium*¸ Wollongong, Australia, **2012**.

Zeineddine R Yerbury JJ "The Prion-Like Action of SOD1: an Infectious Idea". Oral presentation. *School of Biological Sciences Postgraduate Conference*, Kioloa, Australia, **2012**.

Zeineddine R Yerbury JJ "Elucidating the role of protein inclusions in the transfer of pathology in ALS". Oral presentation. *Proteostasis & Disease Research Centre Seminar Series*¸ Wollongong, Australia, **2012**.

ABSTRACT

With the onset of the rapidly increasing population, the impact of age related neurodegenerative diseases including Amyotrophic lateral sclerosis, Alzheimer's disease, Creutzfeldt-Jakob disease, Parkinson's disease, Huntington's disease and frontotemporal dementia is becoming a predominant health and economic concern. Amyotrophic lateral sclerosis (ALS) is a devastating neuromuscular degenerative disease that currently has no effective treatment or therapeutics. ALS is characterised by a focal onset of motor neuron loss, followed by contiguous outward spreading of pathology throughout the nervous system, resulting in paralysis and death generally within a few years after diagnosis. The mechanisms underlying neurodegeneration of motor neurons and disease progression are currently unknown; however, current evidence implicates a range of cellular mechanisms. These mechanisms include, deficient protein quality control, aberrant RNA metabolism, oxidative stress, endoplasmic reticulum stress, glutamate excitotoxicity, mitochondrial dysfunction, fragmentation of the Golgi apparatus, activated glia, axonal transport defects and neuroinflammation. These dysfunctional cellular pathways may be associated with the protein aggregates that are hallmarks of ALS pathology. However, the dysfunction in several cellular processes does not explain the spreading of pathology, here the aberrant release and uptake of toxic proteins including SOD1 and TDP-43 and their subsequent accumulation and deposition in motor neurons may contribute. Given this hypothesis, the work presented in this thesis aimed to further examine the role of SOD1 and TDP-43 in the propagation of neurodegeneration in ALS, and investigate whether the proteins exhibit prion-like properties. The term "Prion-like" as used here refers to the misfolding and aggregation of a disease specific protein that subsequently escapes the cellular environment and seeds aggregation in a naïve cell.

The main aims of this thesis were to: investigate the mechanisms underpinning the uptake of SOD1 aggregates into murine NSC-34 cells (Chapter 2); Examine the subsequent release of SOD1 into the cytosol, detect released extracellular SOD1, and observe for secreted SOD1 internalisation into NSC-34 motor neurons, then identify and quantify seeding activity in recipient cells expressing SOD1 and characterise this interaction using a novel flow cytometry method to quantify protein aggregation; Flow cytometric characterisation of inclusions and trafficking (FloIT) (Chapter 3); determine whether exogenous recombinant SOD1 protein aggregates can induce and/or contribute to TDP-43 pathology (Chapter 4); determine if SOD1 aggregates can enter humanised models of motor neurons *via* the same mechanism of action using both iPSC derived motor neurons and primary neurons (Chapter 5).

In Chapter 2, the aggregation and internalisation of SOD1 proteins, inhibition of SOD1 aggregates; macropinocytosis-associated membrane protrusions, fluid-phase uptake and activation of RAC1 in NSC-34 motor neurons were investigated using transmission electron microscopy, pharmacological inhibitors, flow cytometric measurements, confocal microscopy, field emission scanning electron microscopy and enzyme-linked immunosorbent assays (ELISAs). Flow cytometric measurements indicated that SOD1 aggregates could enter into naïve NSC-34 cells *in vivo*. Furthermore, internalisation of SOD1 aggregates into NSC-34 cells was shown to be mediated *via* a macropinocytosis pathway. SOD1-induced the activation of macropinocytosis in NSC-34 cells, which was dependent on the activation of RAC1 as assessed by ELISA. This in turn triggered the formation of ruffles and blebs in the plasma membrane as assessed by field emission scanning electron microscopy and fluorescent measurements of the FM1-43FX membrane binding dye. This resulted in the uptake of SOD1 aggregates and fluid from the extracellular environment as assessed by fluorescent measurements of 10 kDa dextran conjugated to Alexa Fluor. Significant cell

death in NSC-34 motor neurons was not observed during this process. Collectively, this data suggests that SOD1 aggregates are capable of mediating the activation of macropinocytosis-like pathways to facilitate their entry into in NSC-34 cells.

In chapter 3, spontaneous aggregation of $SOD1^{WT}$ and mutant $SOD1^{G93A}$-EGFP proteins in NSC-34 motor neurons was measured using the flow cytometric characterisation of inclusions and trafficking (FloIT) technique. The transient expression of $SOD1^{WT}$ and mutant $SOD1^{G93A}$-EGFP in NSC-34 motor neurons was shown to correlate with cell death over time, indicative of toxicity. SOD1 aggregate release from transiently transfected NSC-34 cells was examined by immunoblotting pelletable fractions of conditioned media from these cells at end point (72 h). Although the mechanisms of release were not confirmed, an increase in cell death was observed concomitant with inclusion formation; consistent with a possible role for passive release from SOD1 transfected NSC-34 cells. The now extracellular (released) SOD1 aggregates were internalised into naïve NSC-34 cells as demonstrated by confocal microscopy and immunoblotting of cell lysates. Next, the transfer of $SOD1^{WT}$ tdTomato and mutant $SOD1^{G93A}$-EGFP from transfected NSC-34 cells was assessed by flow cytometry and the FloIT technique. The transfer of $SOD1^{WT}$ tdTomato and mutant $SOD1^{G93A}$-EGFP proteins was confirmed by the detection of dual fluorescent NSC-34 cells, indicating the presence of both proteins. Furthermore, immunoblotting and microscopic observations following the uptake of SOD1 aggregates suggested that recombinant WT and mutant SOD1 aggregates were found to escape membrane bound vesicles and enter into the cytosol; a similar process has previously been observed during virus entry. The ability of SOD1 to rupture membrane bound compartments was confirmed by haemoglobin red blood cell assay, the use of liposomes, and fluorescent measurements of the Galectin-3 protein. The seeding activity of mutant SOD1 was assessed by co-culturing NSC-34 cells expressing either $SOD1^{WT}$ tdTomato or mutant $SOD1^{G93A}$-EGFP. Flow cytometric analysis and FloIT measurements

indicated that mutant SOD1^{G93A}-EGFP induced the aggregation of SOD1^{WT} tdTomato proteins at 72 h, in a prion like fashion. The FloIT analysis of two colour aggregates also demonstrates that SOD1^{G93A}-EGFP and SOD1^{WT} tdTomato are co-aggregating. The seeding activity of mutant SOD1 was further confirmed, when recombinant mutant SOD1 G93A aggregates were found to enhance the number of inclusion bodies containing SOD1^{WT} tdTomato red aggregates as assessed by flow cytometric analysis and FloIT measurements. Together, this data supports a role for SOD1 in the infectious prion-like spread of protein aggregation in neuronal cells.

In Chapter 4, spontaneous aggregation of TDP-43^{WT} tdTomato and mutant TDP-43^{G124A}-EGFP fusion proteins in NSC-34 motor neurons was demonstrated using flow cytometry and measured using the flow cytometric characterisation of inclusions and trafficking (FloIT) technique. However, a significant reduction in the number of inclusions was observed at 72 h, indicating loss of cells containing inclusions, likely through cell death. The transfer of TDP-43^{WT} tdTomato and mutant TDP-43^{G124A}-EGFP from transfected donor to recipient NSC-34 cells was assessed by flow cytometry and the FloIT technique. The transfer of TDP-43^{WT} tdTomato and mutant TDP-43^{G124A}-EGFP proteins was confirmed by the detection of dual fluorescent NSC-34 cells, indicating the presence of both proteins. Furthermore, the seeding activity of mutant TDP-43 was assessed by co-culturing NSC-34 cells expressing either TDP-43^{WT} tdTomato or mutant TDP-43^{G124A}-EGFP. Flow cytometric analysis and FloIT measurements indicated that mutant TDP-43^{G124A} induced the aggregation of TDP-43^{WT} from 48 to 72 h. These data also demonstrate that TDP-43^{G124A} and TDP-43^{WT} tdTomato are co-aggregating. Incubation of TDP-43^{WT} tdTomato transfected NSC-34 cells with recombinant SOD1 aggregates was found to induce the mislocalisation and aggregation of TDP-43^{WT} into the cytosol at 2 h and 72 h. To confirm these results, flow cytometric analysis and FloIT measurements were used to quantify inclusion formation. Recombinant mutant SOD1 G93A

aggregates were found to significantly enhance the number of inclusion bodies containing TDP-43^{WT} tdTomato red aggregates. Furthermore, confocal microscopy demonstrated that recombinant SOD1 aggregates could induce the same TDP-43 pathology in TDP-43^{WT} tdTomato transfected human embryonic kidney (HEK-293) cells. Collectively, this data suggests that TDP-43 can spontaneously form aggregates, transfer between cultured motor neuron cells and induce the aggregation of TDP-43^{WT} mediated by mutant TDP-43^{G124A}. This is similar to those observed for SOD1. Furthermore, this study suggests a role for the interplay between SOD1 and TDP-43 where SOD1 aggregates may contribute to TDP-43 pathology.

In Chapter 5, a role for macropinocytosis in humanised models was studied. Human iPSC derived motor neurons and human primary neurons were both used to confirm the ability of protein aggregates to stimulate macropinocytosis using confocal microscopy and flow cytometry. Incubation of human iPSC derived motor neurons and neurons with WT and mutant G93A SOD1 recombinant aggregates were found to internalise into these cells, and this could be significantly inhibited by pre-incubation with inhibitors of macropinocytosis including EIPA and RAC1W56. Furthermore, confocal microscopy observations demonstrated that SOD1 aggregate internalisation into these cells induced the formation of membrane ruffling and blebbing, as assessed by field emission scanning electron microscopy and fluorescent measurements of the FM1-43FX membrane binding dye. In addition, the internalisation of SOD1 aggregates was shown to coincide with the uptake of extracellular fluid as assessed by fluorescent measurements of 10 kDa dextran conjugated to Alexa Fluor. This data supports a role for SOD1 aggregate mediated activation of macropinocytosis in human neurons, demonstrating that similar mechanisms are possible *in vivo*. Moreover, the role of macropinocytosis in other protein aggregates including recombinant TDP-43, Huntingtin (Htt_{ex1}46Q) and α-synuclein associated with ALS/FTLD, Huntington's and

Parkinson's disease was assessed in NSC-34 motor neurons. Incubation of NSC-34 motor neurons with TDP-43, Huntingtin ($Htt_{ex1}46Q$) and α-synuclein recombinant aggregates was found to result in aggregate internalisation, which could be significantly inhibited by pre-incubation with inhibitors of macropinocytosis including EIPA (exception in the case of α-synuclein). Furthermore, internalisation of these aggregates into these NSC-34 motor neurons induced the formation of membrane perturbations as assessed by field emission scanning electron microscopy; this coincided with the activation of RAC1 as assessed by ELISA and the uptake of extracellular fluid as assessed by fluorescent measurements of 10 kDa dextran conjugated to Alexa Fluor. Furthermore, the model proteins α-lactalbumin reduced and carboxymethylated (RCM) and amorphous proteins were also able to internalize into NSC-34 motor neurons, induce membrane perturbations and fluid uptake from the extracellular environment, in a similar manner to that of SOD1, however, this occurred in the absence of the activation of RAC1 suggesting that a broad range of aggregated proteins, both amorphous and amyloid-like, may be able to induce varied macropinocytosis-like pathways to facilitate their cellular uptake. Overall, this data suggests that activation of macropinocytosis-like pathways induced by a range of protein aggregates including SOD1, TDP-43, Huntingtin ($Htt_{ex1}46Q$) and α-synuclein aggregates may facilitate their entry into motor neurons *in vivo*, similar to those observed during the propagation of aggregation during ALS progression.

Collectively, this thesis demonstrated that SOD1 and TDP-43 protein aggregates, as well as other protein aggregates including Huntingtin ($Htt_{ex1}46Q$) and α-synuclein aggregates are capable of being internalising by neuronal cells, through stimulating the activation of macropinocytosis, an endocytic pathway also commonly employed by viruses during infection. Once internalised, SOD1 and TDP-43 aggregates were shown to behave in a prion-like manner, propagating aggregation between motor neuron cells in culture, a mechanism that potentially contributes to the progression of disease in ALS. However, given that an

array of other genes have been recently implicated in disease pathogenesis and the multi-systemic and multifactorial nature of ALS, findings from this thesis may only represent one pathway which may act in concert with other pathways and mechanisms to induce motor neuron degeneration. Given this, further research into the pathological mechanisms underlying the progressive cycle of disease progression of ALS is necessary for *viable* therapeutic treatments of ALS.

Chapter 1

LITERATURE REVIEW

1.1 Amyotrophic Lateral sclerosis: A common motor neuron disorder

Amyotrophic lateral sclerosis (ALS) was first described by Jean-Martin Charcot in 1869, as a paralytic disorder associated with lesions observed in the central nervous system (CNS) (Goetz, 2000). ALS is the most common form of motor neuron disease with adult onset. It is a progressive and fatal neurodegenerative disease characterised by the selective degeneration of both the upper and lower motor neurons which extend through the brainstem and spinal cord to innervate skeletal muscle (Boillée et al., 2006) **(**Figure 1.1). Premature degeneration and death of these motor neurons leads to progressive spasticity, exaggerated reflexes of facial muscles (bulbar onset) or limbs (spinal onset), muscle weakness and atrophy that affects the muscles of mobility, speech, swallowing and respiration, eventually resulting in paralysis and death of the patient generally within 3-5 years from clinical onset (Cleveland and Rothstein, 2001; Tandan and Bradley, 1985). Although in general cell loss in ALS is specific for motor neurons, thus sparing cognitive ability, in approximately 5-10% of ALS cases, patients also develop frontotemporal lobar dementia (FTLD) (Lomen-Hoerth et al., 2002).

1.2 Clinical features and disease course in ALS

Diagnosis of ALS is achieved by clinical examination and electromyography (EMG) analysis (Redler and Dokholyan, 2012). ALS is a heterogeneous disorder, characterised by variations in i) the region(s) of onset, ii) contribution of upper and lower motor neuron deficits and iii) the rate of disease progression between affected individuals (Ravits and Spada, 2009). Irrespective of this, the majority of ALS cases are defined by a focal site of clinical onset of motor neuron degeneration, followed by outward spreading of pathology through adjacent contiguous anatomic paths, affecting motor neurons that are proximal to the region of onset, followed by more distal pools of motor neurons and other cells within the interconnected

regions (Ravits et al., 2007; Ravits and Spada, 2009). Recent evidence however, suggests that onset of motor neuron degeneration can start at one or more focal points (multifocal) (Braak et al., 2013), followed by local propagation of pathology from these regions (Sekiguchi et al., 2014). Although contiguous propagation of pathology through the neuroaxis is considered the most significant clinical feature of ALS (Ravits and Spada, 2009), the molecular mechanisms underlying anatomical spread are currently unknown. Given the progression and spread observed in ALS cases, it is likely disease pathology is spread cell to cell and region to region by a yet to be understood mechanism.

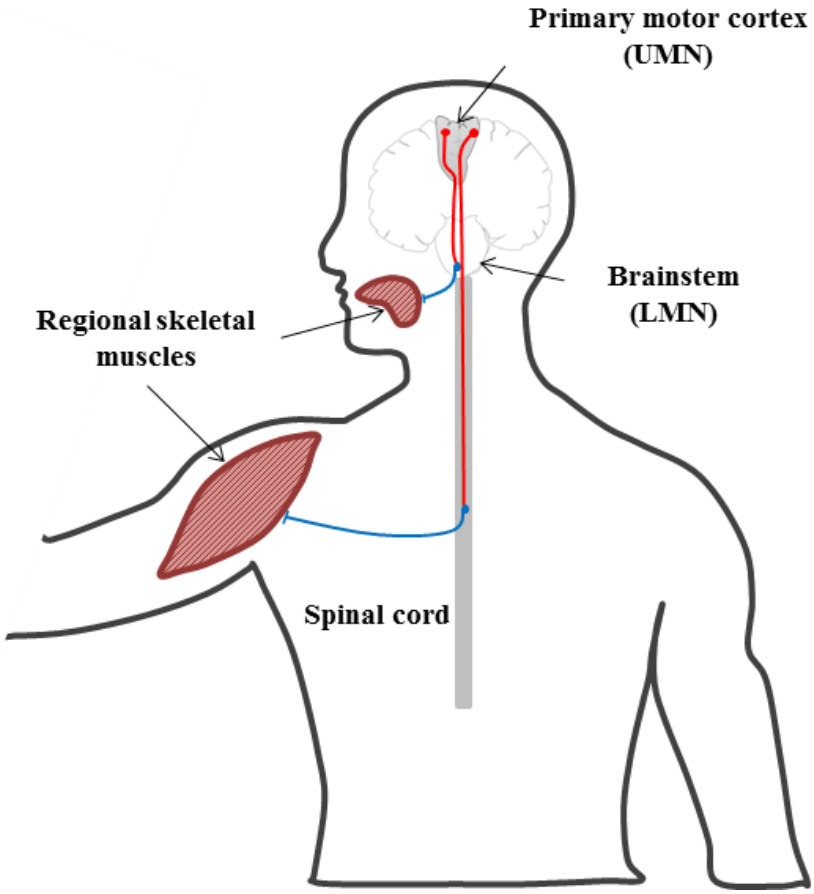

Figure 1.1 ALS disease onset and regional spread of pathology involves the anatomy of the motor system. The functional motor system consists of upper motor neurons (UMNs), lower motor neurons (LMNs), and regional skeletal muscles. Upper motor neurons (solid red line) are located in the primary motor cortex of the brain with their axons projecting to the brainstem or spinal cord to form synapses with LMN cell bodies (blue dots). LMN axons then extend from the brainstem or the spinal cord to communicate with target muscles of the head and neck or trunk and proximal limb muscles through synaptic connectivity respectively (blue line). At the initiation of disease in ALS, pathology is observed to have propagated and distributed within the functional motor system, followed by propagation of pathology by regional contiguous spread (Ravits, 2014; Ravits and Spada, 2009), affecting muscle tissues responsible for controlling voluntary movements (Rowland and Shneider, 2001), and therefore resulting in the progressive paralysis.

1.3 Incidence, Risk factors and therapeutics

ALS has an incidence of approximately 2-3 people per 100,000 (Logroscino et al., 2010; Strong and Rosenfeld, 2003), with a slight male predominance in Caucasian populations (Logroscino et al., 2010), although the incidence between men and women is relatively similar in familial ALS (Kiernan et al., 2011). The major risk factors for ALS are age, with onset commonly occurring at 45-65 years, and family history of the disease (Kiernan et al., 2011). There is increasing evidence to suggest that specific environmental factors may have a role in the etiology of some ALS cases. Such environmental factors thought to increase the risk of developing ALS include engaging in a lifetime of intensive physical activity (Scarmeas et al., 2002; Veldink et al., 2005) and geographically limited populations including Gulf War veterans (Haley, 2003) and Italian soccer players (Chio et al., 2005). The overall population-based lifetime risk of ALS is 1:350 and 1:400 for men and women respectively (Kiernan et al., 2011), with a rapid decrease in incidence after the age of 80 (Logroscino et al., 2010).

Currently, ALS is managed by limited pharmacological treatments which have prioritised the symptoms rather than the causes of ALS, with more potentially supportive therapies being investigated, such as Tauroursodeoxycholic acid (Elia et al., 2016; Lu et al., 2016). Despite this, there are no definitive treatment options to cure or even significantly slow ALS disease progression. Riluzole is the only clinically approved disease-modifying therapeutic treatment available (Orsini et al., 2015). However this drug only provides modest improvement in survival (3-6 months) attributed to its transient effects on modulating excitotoxicity (Geevasinga et al., 2016). Consequently, understanding the pathological mechanisms of neurodegeneration in ALS disease progression is necessary for better treatment options that aim to improve disease course and potentially lead to preventative treatments for ALS that will act as specific disease targets.

1.4 Disease Aetiology

The aetiology of ALS is currently unknown, however, it is suggested that the complexity of ALS is attributed to the multi-factorial and multi-systemic nature of the disease, some of which will be outlined below. Previous findings from studies of ALS patients, transgenic animal models and *in vivo* cell culture systems implicate several pathological processes that may potentially be responsible for, or contribute to, the pathogenesis of ALS resulting in it being classed as either a proteinopathy, a ribonucleopathy, an axonopathy, or a disease related to the neuronal microenvironment (Riancho et al., 2016).

There are currently multiple and interconnected molecular and pathological mechanisms implicated in ALS. These mechanisms include, deficient protein quality control, aberrant RNA metabolism, oxidative stress, endoplasmic reticulum stress, glutamate excitotoxicity, mitochondrial dysfunction, fragmentation of the Golgi apparatus, axonal transport defects and neuroinflammation (reviewed in Harikrishnareddy et al., 2015; Redler and Dokholyan, 2012). However, recent work presents convincing evidence to suggest that these mechanisms are occurring simultaneously, rather than individually, to mediate motor neuron degeneration and death (reviewed in Soo et al., 2011), and therefore are potential targets for therapeutic intervention.

1.5 Protein misfolding and aggregation

Neurodegenerative diseases are closely linked to the formation and deposition of protein aggregates, quite often fibrillar, that accumulate intracellularly, such as α-synuclein in Parkinson's disease, or extracellularly, such as the Aβ peptide plaques associated with Alzheimer's disease (Chiti and Dobson, 2006). Although the peptides and proteins that aggregate are seemingly unrelated in terms of primary or tertiary structure, often the resulting deposits are remarkably similar, often sharing a rope-like fibrillar morphology, a common

cross-β core structure, and the ability to bind specific dyes such as thioflavin T and Congo red (Dobson, 2003).

Protein aggregation, or more specifically fibril formation, can be described as a nucleated self-assembly reaction. In this context, misfolded monomeric proteins or peptides must first aggregate to form stable nuclei from which fibril growth can occur *via* addition of further monomer. *In vivo*, using bulk measurements such as light scattering or thioflavin T fluorescence, protein aggregation reactions display sigmoidal growth kinetics (Figure 1.2). Initially, there is a lag phase which is thought to reflect the time it takes for the nuclei to form, and throughout which time the formation of fibrils is below the threshold of detection (Pedersen et al., 2004; Serio et al., 2000). In solution, there are two predominant species; monomer and fibrils (Figure 1.2A), while oligomeric aggregates are thought to be present in small amounts (< 2% of total species). However, during the elongation phase the concentration of fibrils increases dramatically as the monomer concentration decreases. This is thought to be due to increasing numbers of actively growing fibrils *via* fragmentation of fibrils creating new 'growing ends' and/or secondary nucleation (Figure 1.2B; where available sites on existing fibrils catalyse the nucleation of new aggregates)(Arosio et al., 2014; Knowles et al., 2014). This rapid growth proceeds until such time as the process reaches a plateau where the equilibrium between available monomer and fibrillar protein is reached (Figure 1.2A) (Chiti and Dobson, 2006; Wilson et al., 2008). The lag phase can be circumvented by the addition of exogenous nuclei or 'seed' in the form of preformed fibrils (Jarrett and Lansbury, 1993). As a consequence of seeding, the lag time is eliminated (Jarrett et al., 1993) resulting in a first-order growth polymerisation (Figure 1.2C).

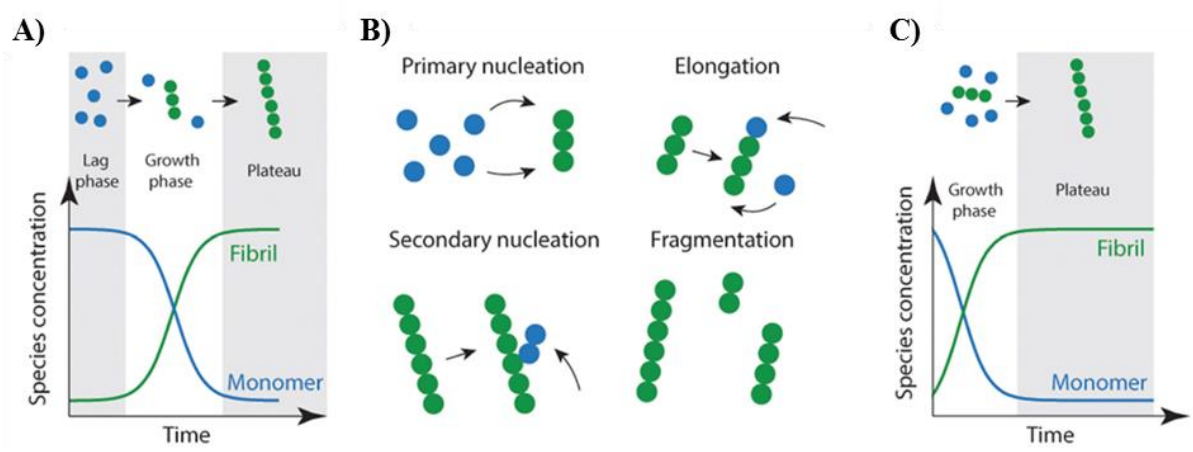

Figure 1.2 Schematic representation of amyloid fibril formation. (A-B) Fibril formation can be characterised by a lag phase where nucleation events occur, following critical nucleation a growth/elongation phase is observed which can proceed *via* primary (monomer addition) or secondary (fragmentation/secondary nucleation) events. During the latter stages, mature fibrils are formed which often display strong ThT emission signals. (C) Addition of fibrils or other functional seeds to the start of the reaction allows elongation to proceed without the requirement for primary nucleation removing the lag phase.

1.6 Genetic factors

While the majority of clinical ALS is sporadic (sALS; 90-95%) with no known obvious cause, the remainder of cases are familial or inheritable in nature (fALS; 10%) (Haverkamp et al., 1995) and are predominantly associated with Mendelian-inherited mutations in genes encoding Cu/ Zn superoxide dismutase (SOD1), 43-kDa trans-activating response region DNA-binding protein (TDP-43), fused in sarcoma/translocated in liposarcoma (FUS/TLS), and C9ORF72 (Belzil et al., 2009; Brettschneider et al., 2012; Mackenzie et al., 2007; Rosen, 1993). Familial ALS is commonly inherited in an autosomal dominant pattern (Li and Wu, 2016). Furthermore, some gene mutations have been identified in sALS cases including the ataxin-2 repeat expansions (Elden et al., 2010) and more recently loss-of-function NEK1 variants have been associated with approximately 3% of ALS cases (Kenna et al., 2016). In addition, there is accumulating evidence to suggest that that mutations in these genes associated with fALS are also identified in sALS cases (Al-Chalabi et al., 2012). Given the similarities in pathological and clinical features between sporadic and familial forms of ALS, it is suggested that similar downstream pathogenic mechanisms are involved in the final

pathway for ALS (Al-Chalabi et al., 2012; Kabashi et al., 2007), and therefore information into mechanistic insights and therapeutic advances may be translatable to all forms of ALS and increase our understanding of the aetiology of ALS.

To date, at least 19 major genes with mutations and various functions including DNA and/or RNA processing, and protein transport, trafficking and degradation have been directly linked to fALS, in which a summary of these main genes are outlined in Table 1.1 (see Li and Wu, 2016). Although other studies and genome wide analysis databases have reported approximately 125 genes as potential modifiers of ALS susceptibility (ALS Online Genetics Database; http://alsod.iop.kcl.ac.uk), mutations in most of these genes are only identified in a small fraction of ALS patients and therefore contribute minimally to the development of ALS disease (Li and Wu, 2016). Furthermore, some polymorphisms identified in ALS patients may represent genetic risk factors rather than causative mutations including mutations in the neurofilament-heavy subunit (NFH), vascular endothelial growth factor (VEGF) and ciliary neurotrophic factor (CNTF) (see Redler and Dokholyan, 2012).

The first causative gene was identified in 1993 as Cu^{2+}, Zn^{2+} superoxide dismutase 1 (SOD1) (Rosen, 1993). SOD1, a well-studied gene linked with several variants of familial ALS, and has contributed significantly to the current understanding of the molecular mechanisms of other forms of ALS. Mutations in SOD1 are very common, accounting for approximately 20% fALS and 1-2 % sALS cases (Deng et al., 1993; Rosen, 1993). The majority of these SOD1 mutations are missense mutations, with an autosomal dominant inheritance, with the exception of the D90A polymorphism, which can also result in a recessive inheritance pattern (Al-Chalabi et al., 1998). In addition to SOD1, TDP-43, which binds RNA and DNA, is an additional key player in ALS, with mutations in TDP-43 identified in approximately 5% sALS and 3% fALS (Rutherford et al., 2008; Sreedharan et al., 2008).

Table 1.1 The genetics of familial amyotrophic lateral sclerosis

Gene	Protein	Clinical presentations	Function	Mode of Inheritance
ALS 2	Alsin	UMN, LMN, Bulbar	DNA/RNA processing	AR
ANG	Angiogenin	UMN, LMN, Bulbar	DNA/RNA processing	AD
ATXN2	Ataxin 2	UMN, LMN	DNA/RNA processing	AD
C9orf72	Chromosome 9 open reading frame 72	UMN, LMN, Bulbar	Protein degradation	AD
CHMP2B	Charged multivesicular body protein 2B	UMN, LMN, Bulbar	DNA/RNA processing	AD
CHMP2B	Charged multivesicular body protein 2B	UMN, LMN, Bulbar	DNA/RNA processing	AD
CCNF	cyclin F	UMN	Protein degradation	AD
DCTN1	Dynactin	UMN, LMN, Bulbar	Axonal transport and vesicle trafficking	-
FUS	Fused in sarcoma	UMN, LMN, Bulbar	DNA/RNA processing	AD,AR,DN
NEFH	Neurofilament heavy chain	UMN, LMN, Bulbar	Cytoskeletal network	AD
OPTN	Optineurin	UMN, LMN	Protein degradation (autophagy)-	AD, AR
PRPH	Peripherin	LMN, Bulbar	Cytoskeletal network	-
PFN1	Profilin 1	LMN, Bulbar	Cytoskeletal network	AD
SETX	Senataxin	UMN, LMN, Bulbar	DNA/RNA processing	AD
SOD1	Cu2+, Zn2+ superoxide dismutase 1	UMN, LMN, Bulbar	Antioxidant	AD,AR,DN
SQSTM1	Sequestosome 1	UMN, LMN, Bulbar	Protein degradation	-
TAF15	TAF15 RNA polymerase II,	UMN, LMN	DNA/RNA processing	AD, AR
TARDBP	TAR DNA binding protein	UMN, LMN, Bulbar	DNA/RNA processing	AD, AR
UBQLN2	Ubiquilin 2	UMN, LMN, Bulbar	Protein degradation	SD
VAPB	Vesicle-associated membraneprotein-associated protein B	UMN, LMN, Bulbar	Axonal transport and vesicle trafficking	AD
VCP	Valosin-containing protein	UMN, LMN, Bulbar	Protein degradation	AD

Mode types: AD, autosomal dominant; AR, autosomal recessive; DN, de novo; (-) unknown information at current. Information obtained from ALSoD database (http://alsod.iop.kcl.ac.uk/) and from the following literature (Al-Chalabi et al., 2012; Chen et al., 2013; Li and Wu, 2016; Marangi and Traynor, 2015; Webster et al., 2016; Williams et al., 2016).

1.6.1 Superoxide dismutase 1 (SOD1) in ALS

SOD1 is a ubiquitously expressed, cytosolic 32 kDa homodimeric enzyme, which plays an important role as a cellular antioxidant to prevent oxidative stress. The primary function of SOD1 is to convert (dismutase) the highly reactive free-radical superoxide formed during biological processes, to a less damaging species (hydrogen peroxide) (Beckman and Koppenol, 1996). More than 180 disease-associated mutations have been described in ALS patients, mainly identified as point mutations present throughout all 5 exons of the SOD1 gene (http://alsod.iop.kcl.ac.uk/; Tortelli et al., 2013). Although some of these SOD1 mutations can impair enzymatic function, others are not associated with a loss of dismutase function, rather they retain enzymatic activity comparatively similar to wild-type levels (Bruijn et al., 1997; Gurney et al., 1994). However, these mutations may result in varying dimer stability, aggregation propensity, metal ion binding affinity, intracellular protein trafficking and rates of disease progression (Kaur et al., 2016).

Some of the most common SOD1-ALS mutations include G93A, G37R, G85R, A4V and D90A (Al-Chalabi et al., 1998; Bruijn et al., 1997; Polling et al., 2014; Robertson et al., 2007; Weisberg et al., 2012). To further characterise the role of SOD1 in ALS, *in vivo* models including transgenic mice and rats have been engineered to over-express fALS associated mutated forms of either the human or murine SOD1. These genetically engineered (transgenic) animal models subsequently develop progressive motor neuron degeneration, reminiscent of human ALS disease, and are therefore used as *in vivo* experimental ALS models (reviewed in Turner and Talbot, 2008). To more accurately analyse SOD1 behaviour *in vivo,* recent studies have developed mice expressing both human WT and mutant SOD1 protein, since most patients with familial ALS exhibit heterozygous mutations (Fukada et al., 2001; Jaarsma et al., 2000). Interestingly, co-expression of WT SOD1 accelerated disease phenotypes of mutant SOD1 expressing mice (Deng et al., 2006; Wang et al., 2009).

Increasing evidence implicates a toxic gain of function acquired by mutant forms of SOD1, which is directly responsible for motor neuron death (Andersen et al., 1995; Gurney et al., 1994; Yim et al., 1996). This idea was initially supported by observations that transgenic mice lacking SOD1 do not develop an ALS-like motor neuron disease or do not die prematurely at least up to 6 months of age (Reaume et al., 1996). Conversely, rodents expressing mutant SOD1 develop a progressive motor neuron disease, recapitulating many features of ALS including motor neuron loss, deficient axonal transport, mitochondrial dysfunction as well as pathological hallmarks (Gurney et al., 1994; Nagai et al., 2001; Ripps et al., 1995) similar to that observed in human ALS patients (Dal Canto and Gurney, 1997). However, the development of ALS-like symptoms in these mice varies depending on the type of SOD1 mutation; transgene expression level, gender and genetic background (Heiman-Patterson et al., 2011; Mancuso et al., 2012). Although it is widely accepted that different mutants of SOD1 exert their toxicity through a gain of function, the precise cytotoxicity of mutant SOD1 and its specificity for motor neurons remain to be elucidated.

A common feature that nearly all forms of mutant SOD1 exhibit is a higher propensity to misfold and/or aggregate compared to WT SOD1 (Andersen et al., 1995; Furukawa and O'Halloran, 2005; Gurney et al., 1994). Indeed, the relative aggregation propensities among variants of mutant SOD1 has been reported to vary significantly in culture (Prudencio et al., 2009), with certain mutations in SOD1 that exhibit aggressive clinical phenotypes having a higher propensity to aggregate (Radunovic and Leigh, 1996). Although protein aggregation is central to mutant SOD1 pathogenesis, it is unclear how mutation in SOD1 results in protein misfolding and thus disease. However, aggregation-prone segments that interact to induce aggregation in SOD1 have recently been identified, indicating that protein destabilisation of the native fold may play a role in SOD1 mutant pathogenicity (Ivanova et al., 2014). Furthermore, dimer disassociation has been reported to be a critical step for triggering SOD1

aggregation, thus making aggregation prone residues more accessible (Rakhit et al., 2004). However, additional factors such as RNA granule dysregulation and dysfunction of protein degradation pathways may also underlie aggregation more generally in ALS (see Blokhuis et al., 2013). Using *in vivo* analysis of mutant SOD1 aggregation profiles and survival time of fALS patients, it has been reported that a higher protein instability and aggregation rate correlate inversely with survival time (Bystrom et al., 2010; Wang et al., 2008). In addition, under certain denaturing conditions, WT SOD1 has also been shown to form aggregates *in vivo* (Chia et al., 2010), suggesting that aberrant oligomerisation of SOD1 could be a shared pathogenic feature of ALS, irrespective of genotype (Redler and Dokholyan, 2012).

1.6.2 TDP-43 in ALS

In addition to SOD1, pathogenic forms of TDP-43, that are mislocalised to the cytoplasm, hyperphosphorylated, and ubiquitinated within protein inclusions are a significant pathological characteristic of motor neurons in ALS where SOD1 mutations are excluded. TDP-43 is a heterogeneous RNA/DNA binding protein that is ubiquitously expressed and involved in a range of processes in RNA metabolism including mRNA splicing and localisation and gene regulation (Ayala et al., 2008; Johnson et al., 2009). Specifically, TDP-43 has been implicated in ALS as a key player due to its presence in neuronal cytoplasmic inclusions found in the spinal cord of sporadic ALS patients (Arai et al., 2006; Neumann et al., 2006). In addition, mutations in TDP-43 have been associated with both familial and sporadic ALS disease (Kabashi et al., 2008; Sreedharan et al., 2008; Van Deerlin et al., 2008). Of note, most mutations identified in the TARDBP gene are located in the exon encoding the C-terminal domain (Rutherford et al., 2008; Sreedharan et al., 2008), which has been suggested to be highly aggregation prone (Zhang et al., 2009). It remains to be determined if mutations in TDP-43 cause a gain or loss of function, with current evidence suggesting both a toxic gain of function, a loss of function or a combination thereof (Lee et

al., 2012). Similar to other misfolding disease related proteins, a gain of toxic function may result from the mislocalisation of TDP-43 from the nucleus to the cytosol, where it fragments, aggregates and forms inclusions (Johnson et al., 2009). However, it has been proposed that the sequestration of functional TDP-43 into cytoplasmic inclusions may deplete nuclear TDP-43 and result in the toxic loss of function of nuclear TDP-43 (Budini et al., 2015).

1.7 Cytoplasmic inclusion bodies in ALS

1.7.1 Overview

The central pathological hallmark of ALS is the presence of cytoplasmic proteinaceous deposits known as inclusion bodies in degenerating motor neurons and neighbouring cells (Blokhuis et al., 2013). The most common types of aggregates identified in ALS patients are ubiquitinated aggregates in the form of Lewy body-like hyaline inclusions, skein-like, or round ubiquitin positive inclusions (Kato, 1999; Murayama et al., 1989). In addition, Bunina bodies and round hyaline inclusions (without a halo) are also found is ALS (Mizusawa, 1993; Okamoto et al., 2008). Multiple proteins have been found associated with these inclusions including; SOD1, TDP-43, FUS/TLS, optineurin (OPTN), Ubiquilin-2 (UBQLN2) and C9ORF72 (reviewed in Blokhuis et al., 2013). Of note, TDP-43 is thought to be the major component of ubiquitinated inclusions in most cases of ALS and many cases of FTLD (Arai et al., 2006; Neumann et al., 2006). Therefore, not only are these misfolded protein aggregates a significant pathological hallmark of ALS, but also have an important role in mediating disease initiation and progression (see section 1.4).

1.7.2 Misfolded SOD1 in inclusion bodies

Inclusion bodies containing aggregated SOD1 have been detected in human most-mortem spinal cord tissues from both familial and to a lesser extent sporadic ALS patients (Bosco et al., 2010; Forsberg et al., 2010; Shibata et al., 1994) and in spinal cord tissues from SOD1 ALS mouse (Bruijn et al., 1997; Shibata et al., 1994; Watanabe et al., 2001). However, these cytoplasmic inclusions are not limited to the spinal cord, rather are found in other brain regions including the hippocampus, cerebellum and frontal and temporal cortices (reviewed in Al-Chalabi et al., 2012). The appearance of these inclusion bodies coincide with disease onset in mouse models and are therefore thought to be an early pathological event in ALS, which then accumulate progressively throughout the course of the disease (Turner et al., 2003; Wang et al., 2002). Furthermore, recent studies have used conformation specific antibodies to show that misfolded WT SOD1 can be detected in human post-mortem tissues from non-SOD1 sporadic ALS individuals (Bosco et al., 2010; Forsberg et al., 2010; Pokrishevsky et al., 2012).

While SOD1 misfolding and/or aggregation are features of pathogenesis in both familial and sporadic ALS, including non-SOD1 linked familial and sporadic ALS (Matias-Guiu et al., 2008), the role of SOD1 misfolding in motor neuron death has not yet been conclusively determined. A study of transgenic familial ALS mice over time reported that soluble misfolded SOD1 is concentrated in motor neurons from birth (Rakhit et al., 2007; Zetterstrom et al., 2007), and that large insoluble aggregates are detected primarily in the later stages of disease (Karch et al., 2009). Its thus appears that smaller soluble or misfolded SOD1 species may be responsible for initial toxicity, and eventually begin to cause symptoms once a disease-specific threshold has been reached. However, the relative toxicities of small soluble oligomers and large-scale aggregates of SOD1 remain to be directly proven. It has been postulated that oligomeric species present in solution prior to the appearance of fibrils are

more likely to be responsible for cellular toxicity more generally (Kayed et al., 2003). However, it is probable that all aggregate species provoke some level of cellular stress. One potential mechanism of toxicity is through exposed hydrophobic residues found on protein aggregates that have been shown to interact with cell receptors and membranes (Bolognesi et al., 2010; Stefani and Dobson, 2003), leading to membrane disruption and inappropriate signaling cascades. Moreover, the toxicity exerted by misfolded and aggregated SOD1 has been reportedly linked with a range of pathological cellular effects including organelle dysfunction (mitochondria, endoplasmic reticulum and the Golgi), cytoskeletal disruption, caspase activation and dysfunction of proteasomal and autophagic pathways (Bendotti et al., 2012).

Evidence from post mortem tissue demonstrates that protein aggregation is linked closely to motor neuron death in ALS (Brettschneider et al., 2014).However, nucleation of protein aggregation appears to be a stochastic process (Hortschansky et al., 2005), suggesting that protein aggregation alone should cause a random pattern of cell death. In contrast, cell death in ALS occurs in an ordered and progressive manner in human ALS patients, and therefore protein aggregation contained within individual cells is not likely the sole cause of this spread. Rather, one way to explain such an ordered progression is the prion-like propagation of protein misfolding and aggregation between adjacent cells.

1.8 Patterns of Neurodegenerative Pathology in Humans

Major neurodegenerative diseases, such as ALS, Alzheimer's disease, Tauopathies such as Frontotemporal Dementia, Parkinson's disease, Huntington's disease, and transmissible spongiform encephalopathies (TSEs), have common pathological changes such as loss of neurons and the presence of pathological protein aggregates into either intracellular inclusions bodies or extracellular plaques. However, generally speaking, the main

aggregating protein is disease specific; for example SOD1, β-amyloid, α-synuclein, Huntingtin and the prion protein (PrP) aggregate in ALS, Alzheimer's disease, Parkinson's disease, Huntington's disease and Creutfeldt-Jakob disease respectively (reviewed in Brundin et al., 2010). Distinctive anatomical patterns of disease spread are consistent with a spreading of pathology from one part of the brain to another in all of these neurodegenerative diseases (Brundin et al., 2010).

The progression of these disorders, which is also associated with increasing clinical severity, has enabled the development of several staging systems based on location of protein aggregates (Braak et al., 2006; Braak et al., 2003; Brettschneider et al., 2014; Brettschneider et al., 2013). The resulting patterns suggest that pathology is not only propagated between nearby cells, but that it also remotely connects regions of the brain along axonal pathways (Brettschneider et al., 2015; Brundin et al., 2010). Together these data are consistent with a propagation of protein misfolding and aggregation reminiscent of those underpinning prion diseases (reviewed in Zeineddine and Yerbury, 2015).

1.9 Prion-like propagation of aggregation in neurodegenerative diseases

1.9.1 Prion Disease

Over 30 years ago, a significant development in the field of infectious diseases and protein biochemistry research was made, it was identified that "infectious" proteins known as prions, could transmit disease between organisms without the requirement of nucleic acid (Prusiner, 1998). The mammalian prion protein is a self-propagating transmissible agent that mainly consists of the abnormal misfolded/aggregated form of the prion protein (Prion Protein Scrapie; PrP^{Sc}), known to transmit between cells and between individuals of the same species (species barriers) (Diener et al., 1982; Prusiner, 1984). Prions can exhibit multiple phenotypes (prion strains) and are responsible for a spectrum of aggressive

neurodegenerative diseases in humans including Kuru and Creutzfeldt-Jakob disease (CJD), and in animal populations in the form of scrapie in sheep and bovine spongiform encephalopathy (BSE), also known as mad cow disease in cattle, and several other species have their own version of prion-opathies (Diener et al., 1982; Prusiner, 1982). In these prion diseases, the PrP^{Sc} protein can replicate by inducing the misfolding and aggregation of the recruited natively folded cellular prion protein (PrP^{C}), resulting in the aggregation of the newly formed pathological prion protein converting it the protease resistant and insoluble state. Therefore, prions act as abnormal templates that induce template-directed protein misfolding and progressive aggregation (Prusiner, 1998).

There are two hypotheses on the molecular mechanisms of PrP^{Sc}-induced conversion of PrP^{C}, including template-directed refolding or nucleated polymerisation. Template-directed misfolding involves a cyclical propagation whereby PrP^{Sc} induces PrP^{C} (substrate) formation, and these newly formed pathogenic proteins go on to convert subsequent PrP^{C} proteins, thus amplifying infectious agents (Aguzzi and Calella, 2009). The nucleated polymerisation hypothesis suggests that the misfolding of PrP^{C} to PrP^{Sc} is a reversible process and the PrP^{Sc} can be stabilised by contact with PrP^{Sc} protein aggregates (Aguzzi and Calella, 2009).

1.9.2 Prion-like activity in neurodegenerative disease

1.9.2.1 Overview

Misfolded proteins associated with common neurodegenerative diseases are thought to be capable of propagating the misfolding and aggregation of their natively folded counterparts, potentially contributing to the transmission and spread of pathology from cell to cell within and between tissues beyond the site of original protein conversion (reviewed in Brettschneider et al., 2015). Mounting evidence has implicated a ‘prion-like’ mechanism in the propagation of a pathology associated with common neurodegenerative diseases also

known collectively as proteinopathies including; ALS, Alzheimer's, Parkinson's and Huntington's disease. Proteins known to aggregate in these disorders including SOD1, β-amyloid, tau, α-synuclein and fibrillar polyQ aggregates ($K_2Q_{44}K_2$), a model for polyQ expansion, are all thought to share a "prion-like" mechanism of cell to cell spread, to propagate misfolding (see Aguzzi and Calella, 2009; Brundin et al., 2010).

Prion-like propagation involves these protein aggregates entering into cells, crossing cellular membranes to transmit pathogenic proteins in a 'prion-like' manner through the triggering of the misfolding of their normally structured counterparts in cells, tissues, and animal models (Brettschneider et al., 2015). The precise mechanism by which pathogenic proteins gain access to the cytoplasmic compartment to propagate misfolding and aggregation remains incompletely understood (Clavaguera et al., 2009; Desplats et al., 2009; Grad et al., 2014; Ren et al., 2009).

These non-infectious proteopathies do not involve the prion protein but typically their disease specific misfolded protein (Marciniuk et al., 2013). However, it is useful to model the progression of neurodegenerative diseases associated with protein aggregation on the spread of prion diseases within a host. It may provide an explanation for the apparent clinically observed patterns of pathology in ALS, Parkinson's, Alzheimer's and Huntington's disease. There is indeed evidence amassing that suggests this might be the case (Table1.2).

Table 1.2 Evidence of Prion-like mechanisms of disease specific proteins in models of common neurodegenerative disorders.

Disease	Disease specific protein	Cellular location of misfolded protein	Cell to cell spread	*Self-propagation	Disease transmission
Transmissible prion encephalopathies	Prion	Intracellular (Yamasaki et al., 2012) Extracellular (Fevrier et al., 2004)	Yes	Yes	Yes
Parkinson's	α-Synuclein	Intracellular (Bick et al., 2008; Eisbach and Outeiro, 2013) Extracellular (Desplats et al., 2009; Gustafsson et al., 2016; Loov et al., 2016; Ren et al., 2016)	Yes (Luk et al., 2012a)	Yes (Desplats et al., 2009; Ibrahim and McLaurin, 2016; Pinotsi et al., 2016)	Yes (Li et al., 2008; Luk et al., 2012a; Luk et al., 2012b)
Alzheimer's	β-amyloid	Intracellular (Moon et al., 2012) Extracellular (Kumar et al., 2011)	Yes (Nath et al., 2012; Tasaki et al., 2010)	Yes (Kane et al., 2000; Tjernberg et al., 1999)	Yes (Kane et al., 2000; Meyer-Luehmann et al., 2006)
Alzheimer's	Tau	Extracellular (Schwab et al., 1998; Yamaguchi et al., 1991)	Yes (Kfoury et al., 2012; Mohamed et al., 2013; Saman et al., 2012)	Yes (Frost et al., 2009; Stancu et al., 2015; Stohr et al., 2012; Vasconcelos et al., 2016)	Yes (Iba et al., 2013; Lasagna-Reeves et al., 2012)
Huntington's	Huntingtin (Poly Q)	Intracellular (Petrasch-Parwez et al., 2007)	Yes (Herrera et al., 2011; Pearce et al., 2015)	Yes (Ren et al., 2009; Yang et al., 2002)	No
ALS	SOD1	Intracellular (Cereda et al., 2013) Extracellular (Grad et al., 2011; Turner et al., 2005a; Urushitani et al., 2006)	Yes (Grad et al., 2014; Münch et al., 2011)	Yes (Chia et al., 2010; Grad et al., 2011; Grad et al., 2014; Münch et al., 2011)	Yes (Ayers et al., 2014; Ayers et al., 2016)
ALS	TDP-43	Intracellular (Nonaka et al., 2009b)	Yes (Feiler et al., 2015; Nonaka et al., 2013)	Yes (Feiler et al., 2015; Furukawa et al., 2011; Nonaka et al., 2013; Shimonaka et al., 2016)	Yes (Nonaka et al., 2013)

*** Self propagation refers to the ability of the disease proteins to seed the aggregation of soluble endogenous proteins.**

1.9.2.2 Parkinson's Disease

Parkinson's disease is a movement disorder characterised by the formation of Lewy bodies and Lewy neurite inclusions, containing predominately α-synuclein, which has been implicated as a key mediator in vesicular transport (Braak et al., 2003; Uversky, 2007). Mutations within the α-synuclein gene is linked with inherited forms of Parkinson's disease and over expression of the wild-type form of α-synuclein has been reported to induce toxicity, similar to that observed in the disease (Dauer and Przedborski, 2003).

Similar to ALS, in Parkinson's disease α-synuclein aggregates have been reported to spread in a topographically predictable manner as disease pathology progresses through the CNS (Braak et al., 2006; Braak et al., 2003). Furthermore, previous studies have observed the propagation of α-synuclein aggregates from cell to cell in human cultured human neurons and in animal models, initiating the formation of Lewy body- like aggregates in naïve cells (Desplats et al., 2009; Hansen et al., 2011; Lee et al., 2010). Cell culture studies have shown that extracellular α-synuclein in various forms (fibrils, oligomers, and monomers) can be internalised by cultured neuronal cells (Lee et al., 2010). Furthermore, mouse cortical neuronal stem cells were shown to internalise extracellular aggregated α-synuclein either applied as recombinantly produced protein aggregates or from co-culture with cells overexpressing and subsequently releasing α-synuclein aggregates (Steiner et al., 2011). In addition, CNS injections of brain homogenates derived from mice exhibiting α-synuclein pathology or recombinant α-synuclein amyloid fibrils induced the formation of intracellular inclusions and the onset of Parkinson's symptoms in recipient transgenic and wild-type non-transgenic mice (Luk et al., 2012a; Luk et al., 2012b).

The most startling evidence for a prion-like mechanism of α-synuclein involves the observation that healthy tissue transplants grafted into the brains of people with Parkinson's disease acquire (as early as four years) intracellular deposits of α-synuclein, known as Lewy bodies (Li et al., 2008). This was further demonstrated in post mortem studies that showed that approximately 2-5% of normal embryonic neurons transplanted in the brains of Parkinson's disease patients acquired α-synuclein rich Lewy bodies over a period of 5 years (Brundin et al., 2008; Hansen et al., 2011). The host to graft pathological α- synuclein cell-to-cell transfer and seeding aggregation in recipient neurons (neuroblastoma cell line) and *in vivo* in mice, where α-synuclein was shown to propagate from a mouse host brain cells to grafted dopaminergic neurons (Hansen et al., 2011) and demonstrates the transmissibility of α- synuclein. A more recent study has been able to show, using more advanced imaging techniques including super resolution microscopy, that α- synuclein can be taken up in its monomeric form into neuronal cells, and nucleate the aggregation of endogenous α-synuclein (Pinotsi et al., 2016).

1.9.2.3 Alzheimer's Disease

Alzheimer's disease is characterised by the formation of amyloid plaques which are extracellular deposits composed primarily of insoluble β-amyloid aggregates and cytoplasmic inclusion bodies containing hyperphosphorylated tau protein (Alonso et al., 1996). β-amyloid is a proteolytic cleavage product of amyloid precursor protein (APP) which is a transmembrane protein which may act as a signaling nexus, transducing information about extracellular conditions (van der Kant and Goldstein, 2015). Cytoplasmic inclusion bodies containing hyperphosphorylated tau protein aggregates or tangles are known to progressively spread through the brain in an anatomically stereotypical manner (Alonso et al., 1996; Goedert et al., 2006).

In a similar paradigm to α-synuclein in Parkinson's disease models, the transmissibility of β-amyloid (Aβ) peptide plaques have been initially shown to resemble a prion-like mechanism in a study in which non-human primates were injected with human brain tissue derived from AD patient (Baker et al., 1993; 1994). Similarly, injection of autopsy-derived brain extracts from Alzheimer's disease patients in to transgenic mouse models of Alzheimer's disease engineered to produce large amounts of APP, induces β-amyloid (Aβ) peptide plaque formation around the injection site indicating that a single inoculation of brain extract can initiate β-amyloid plaque formation *in vivo* (Kane et al., 2000). In addition, one study implanted steel wires coated with brain extracts derived from human Alzheimer's disease patients and demonstrated plaque formation which were observed to spread from the point of seeding into neighbouring tissues (Eisele et al., 2009). This transmissibility was shown to be inhibited by neutralising antibodies specific for β- amyloid, therefore indicating that the agent responsible for this self-propagation mechanism is β-amyloid (Meyer-Luehmann et al., 2006). Furthermore, intraperitoneal injections of β-amyloid rich transgenic brain homogenates into transgenic mice induced widespread cerebral β-amyloidosis and associated pathologies (Eisele et al., 2010), which was confirmed in another study which traced *in vivo* Aβ propagation using bioluminescence imaging (Stohr et al., 2012).

In addition to β-amyloid, tau protein aggregates have been shown to self-propagate from cell to cell in cultured cells (Kfoury et al., 2012). Similar to β-amyloid, injected brain extracts containing misfolded tau into the brains of transgenic mice can seed the propagation of tau misfolding and transmit this misfolding from the site of injection into neighbouring regions of the brain (Clavaguera et al., 2009). More recently, pre-aggregated β-amyloid aggregates were shown to directly induce Tau aggregation by cross-seeding in a prion-like manner and therefore propagating Tau pathology *in vivo* (Vasconcelos et al., 2016).

1.9.2.4 Huntington's Disease

Huntington's disease is a genetic autosomal dominantly inherited disease associated with mutations in the gene encoding huntingtin and is characterised mainly by involuntary movements and dementia. Huntingtin protein has been implicated in DNA transcription, vesicle and axonal transport and synaptic function (Cattaneo et al., 2005). Mutations in the huntingtin protein associated with disease are in the form of variable expansions within a polyglytamine repeat (CAG) in exon 1 and induce the misfolding and aggregation of Huntingtin resulting in the formation of inclusion bodies (Duyao et al., 1993). A direct correlation between the extent of polyQ expansion with the propensity to misfold or aggregate, disease severity and initiation of onset has been suggested (Davies et al., 1997; Duyao et al., 1993; Scherzinger et al., 1997). Like α-synuclein, β-amyloid and tau, Huntingtin has also been reported to exhibit prion-like mechanisms of propagation. Aggregates of pathogenic polyQ expansion peptides have been shown to resemble scrapie prions (fibrillar or ribbon-like morphology) (Scherzinger et al., 1997) and transmit from cell to cell (Ren et al., 2009; Yang et al., 2002). Importantly, large aggregates of huntingtin peptides have been shown to self-propagate through a seeding nucleation mechanism that persists for several passages following the initial incubation of the cells with the extracellular aggregates (Ren et al., 2009).

1.10 Regional spread of disease in ALS

1.10.1 Overview

It has been known for decades that fibril formation can be seeded *in vivo* through addition of preformed fibrils, removing the rate limiting lag phase (see Figure 1.2). Just as *in vivo* fibril formation of purified proteins is a nucleation dependent process, recent work using 2-photon imaging demonstrates that Aβ plaque formation in the brain is also a nucleation dependent

process (Burgold et al., 2014). This propagation is easily understandable given that Aβ aggregates do not have to cross plasma membranes to seed further aggregation as amyloid plaques are present outside of cells. It may be less likely that aggregates formed intracellularly such as SOD1, could propagate aggregation inside another cell. However, there is a wave of research that demonstrates that this is possible. At present, two major proteins associated with pathogenesis of ALS have demonstrated intermolecular requirements of prion-like activity: including SOD1 and TDP-43 (see Grad et al., 2015). In SOD1-ALS disease models, the propagation of SOD1 protein aggregates from cell to cell in neuronal and other cell lines and the template-directed seeding of SOD1 has been suggested as a possible explanation for the toxic intercellular spread of pathology. (Furukawa et al., 2013; Grad et al., 2014; Münch et al., 2011).

Given that ALS associated inclusions are intracellular, there are two vital steps that must occur in order to propagate aggregation between cells; aggregates must first be released from the originating neuron to the extracellular space and then the aggregates must cross the cell membrane barriers to be taken up by neighbouring neuron cells to seed further aggregation in the cytosol of naïve cells.

1.10.2 SOD1

1.10.2.1 SOD1 aggregates can be released from neurons

Misfolded SOD1 aggregates that are suggested to exhibit thermodynamic and conformational stability are able to better thrive in the hostile extracellular environments (Grad et al., 2015). SOD1 aggregates are generally found to be intracellular in human ALS patient samples, however both WT and mutant SOD1 have been detected in the cerebrospinal fluid of ALS patients (Zetterstrom et al., 2011) and in spinal cord cultured derived from transgenic SOD1 mouse models (Urushitani et al., 2006), suggesting that release of SOD1 occurs *in vivo*. In

addition, SOD1 can also be secreted from motor neuron like-cells in culture (Gomes et al., 2007). Although the mechanism of release of protein aggregates is incompletely understood, SOD1 secretion can occur in both a passive manner associated with cell death or actively through exocytosis pathways (Gomes et al., 2007; Grad et al., 2014). In addition, SOD1 associates with secretory chaperone-like proteins, including chromogranins which are components of neurotransmitter enriched secretory vesicles, facilitating the release of SOD1 (Huttner et al., 1991; Urushitani et al., 2006). Of note, prior to secretion, mutant SOD1 aggregates can accumulate in the endoplasmic reticulum-Golgi compartments of the endocytic pathways (Urushitani et al., 2008). Misfolded WT and mutant SOD1 have been shown to be secreted from neuron-like cells in association with exosomes (Basso et al., 2013), which are subsequently taken up by neuron-like cells in culture (Grad et al., 2014). Furthermore, exosomes obtained from mouse astrocytes were observed to transfer mutant SOD1 to spinal neurons, resulting in the selective death of motor neurons (Basso et al., 2013). Collectively these data leaves open the possibility that both cell death and active secretion mechanisms are acting in concert to promote aggregate release *in vivo*.

1.10.2.2 SOD1 uptake

In order to facilitate the propagation of intracellular aggregation in neurodegenerative diseases, such as ALS, Parkinson's, Alzheimer's and Huntington's diseases, active aggregate nuclei or seeds must internalise into cells and gain access to the cytosol of naïve cells. Indeed, a number of recent studies have observed that exogenously applied SOD1 aggregates derived recombinantly or from conditioned media can be taken up efficiently and rapidly into living cells (Furukawa et al., 2013), such as motor neuron like cells in a time dependant manner, followed by localisation of SOD1 to the cytosol of neurons (Münch et al., 2011) and cultured glial cells (Roberts et al., 2013). However, it is currently unknown how exogenous SOD1 aggregates gain access to the cytosol and subsequently accumulate in cytosolic inclusions

(Sundaramoorthy et al., 2013). Moreover, exogenously added aggregated WT and mutant SOD1 have been shown to be taken up into mouse NSC-34 and human SH-SY5Y neuronal cells (Sundaramoorthy et al., 2013).

1.10.2.3 Prion-like action of SOD1

Increasing experimental evidence now indicate that misfolded SOD1 has the ability to induce conformational changes from one molecule, seeding aggregation to another analogous to that of prion-like propagation (Chia et al., 2010; Grad et al., 2011; Grad et al., 2014; Münch et al., 2011).

Furthermore, similar to prions, there is evidence to suggest that propagation of misfolding and aggregation of both mutant and WT SOD1 occurs *via* two mechanisms including, nucleated polymerisation and template-directed misfolding (Grad et al., 2015). Given the highly stable conformation of native SOD1 and its ability to stabilise mutant misfolded SOD1 (Prudencio et al., 2010), it has been suggested that this may enable native SOD1 to act as a thermodynamically favourable substrate for template directed seeded polymerisation (Grad et al., 2015). Furthermore, another study has also demonstrated that the intracellular conversion of WT SOD1 potentially occurs *via* template-directed misfolding, using surface plasmon resonance (Grad et al., 2011). However, it is possible that mutant SOD1 that is highly aggregation prone may utilise both seeded polymerisation and template directed misfolding. Moreover, newly formed misfolded SOD1 can act as template for propagation of misfolding, given that the misfolding of SOD1 can persist in the absence of the misfolded seed in cell culture (Grad et al., 2014).

Misfolded and aggregated forms of SOD1 derived from recombinant protein or from homogenates of spinal cords of transgenic mice expressing human mutant SOD1 have been observed to trigger the formation of SOD1 protein aggregates in naïve cells, thus acting as

seeds (Figure 1.3) (Chia et al., 2010). In addition, the co-aggregation of mutant and WT SOD1 have been detected in post-mortem tissue derived from familial ALS patients, indicative of intermolecular conversion of protein misfolding (Bruijn et al., 1998). Supporting this, familial associated mutations in SOD1 (G127X and G85R) expressed in human mesenchymal and neural cell lines were observed to trigger the conversion of endogenous wild-type native SOD1 to a misfolded form, revealed by conformation-specific antibodies specific for epitopes present in SOD1 only when it is in a misfolded state. The conversion of human WT SOD1 to a misfolded form was shown to be dependent on a tryptophan (Trp) amino acid residue at position 32 (Grad et al., 2011). Interestingly, the same study showed that SOD1 mutations containing a serine substitution at position 32 failed to trigger the misfolding of WT SOD1 in human cell lines. Similarly, expression of these human SOD1 mutants in cells lines did not induce the misfolding of endogenous murine WT SOD1 which inherently exhibits a serine at position 32, indicating species specific barriers. Similarly, prions also have species specific barriers that limit their transmission of disease between different species (Raymond et al., 2000), therefore further supporting the prion-like behaviour of SOD1 ALS.

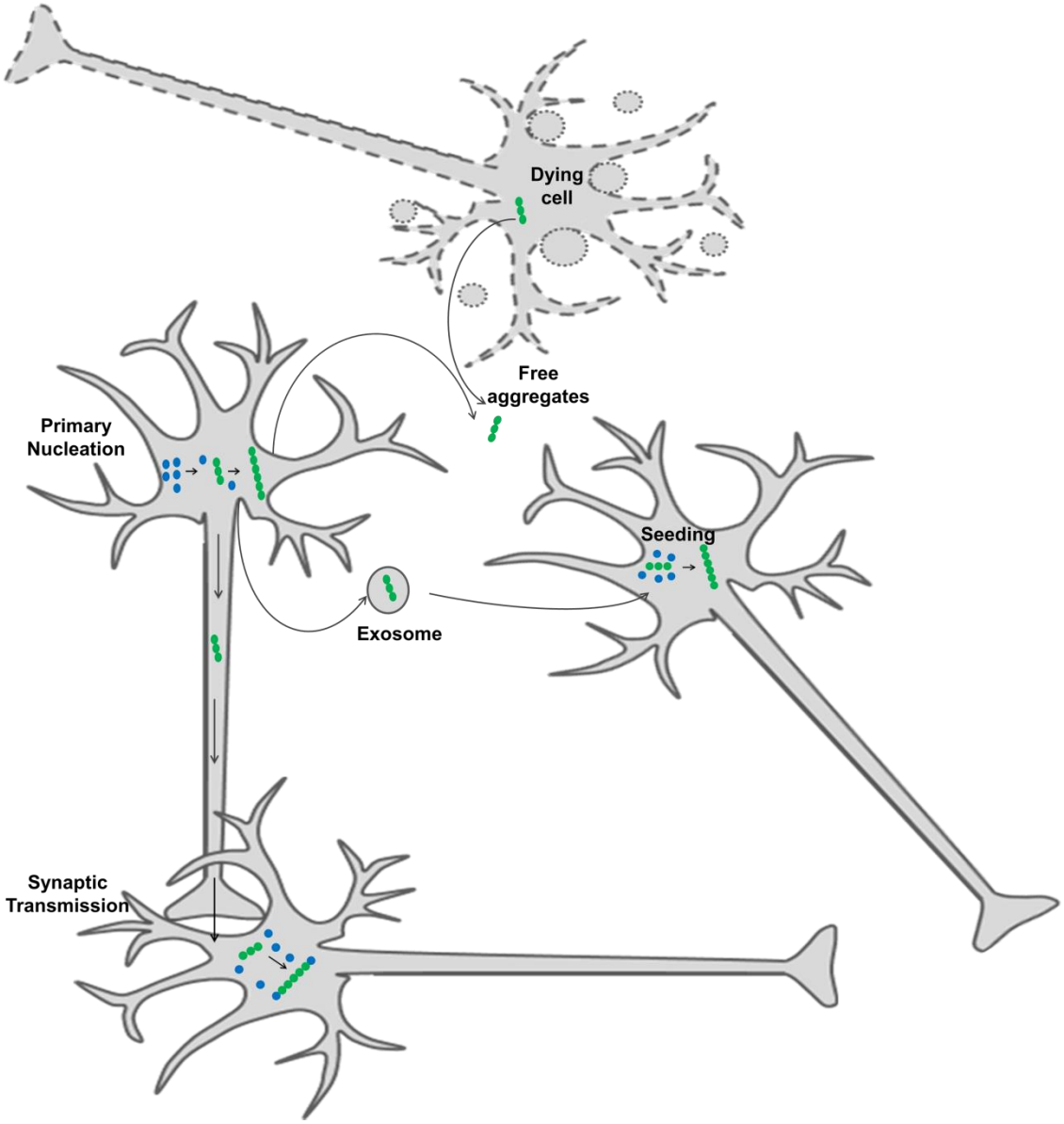

Figure 1.3 Proposed model of the role of SOD1 propagation of aggregation in amyotrophic lateral sclerosis. Protein aggregates form in neurons (primary nucleation) and have the potential to further nucleate the aggregation of other proteins. These protein aggregates can transfer directly from cell to cell through synaptic transfer, or be actively released *via* secretion mechanisms (e.g. exosomes) or in their naked forms from newly dying/dead motor neurons which is suggested to occur in the easily stages of the diseases to neighbouring interconnecting neurons. The uptake of such aggregates nucleates aggregation in naïve cells, a process that resembles the prion-like propagation of aggregation.

To further support this, murine SOD1 protein is not associated with inclusions of human mutant SOD1 in SOD1 mice (Deng et al., 2006; Prudencio et al., 2009; Wang et al., 2009). Furthermore, human WT SOD1 does not exacerbate motor neuron disease in mice expressing murine mutant SOD1 G86R (Audet et al., 2010). In addition, recombinant G127X aggregates

were able to trigger the misfolding of recombinant human WTSOD1 in a cell-free system under reducing conditions, supporting the idea of "protein-only" conversion. This therefore provides direct evidence of intermolecular conversion of natively structured WT SOD1 by misfolded SOD1 in a physiological intracellular environment (Grad et al., 2011). Furthermore, other work has observed that exogenously applied mutant SOD1 aggregates can induce the misfolding of soluble transgenically expressed mutant protein in mouse neuroblastoma cells, transmitting the pathology from cell to cell, indicative of self-propagation of aggregation, similar to the disease mechanics in prion diseases (Münch et al., 2011). Similarly, exogenously applied recombinant human mutant SOD1 fibrils can internalise into mouse neuroblastoma cells that are engineered to express the same human SOD1 mutant and subsequently induce intracellular aggregation (Furukawa et al., 2013)

These findings are supported by the results of two other studies which demonstrate for the first time, *in vivo* evidence for prion-like transmission of SOD1 toxic aggregate species in mediating pathology in ALS. Recently, it has been demonstrated that spinal cord homogenates derived from symptomatic (paralysed) $SOD1_{G93A}$ mice when injected into the spinal cords of genetically vulnerable mice (newborn) expressing low amounts of another form of mutant SOD1 ($SOD1_{G85R}$-YFP) triggered a spinal inclusion pathology and ALS-like disease phenotype (Ayers et al., 2014). Interestingly, when second passage homogenates derived from these mice were injected into new $SOD1_{G85R}$ mice, an early onset of clinical disease was observed, again featuring abundant $SOD1_{G85R}$ inclusion-like pathology (Ayers et al., 2014). Furthermore, it was observed in this study that spinal cord homogenates derived from WT SOD1 transgenic mice injected into transgenic mice triggered widespread $SOD1_{G85R}$ containing inclusion-like pathology in one third of inoculated $SOD1_{G85R}$ mice, implicating WT SOD1 in the pathogenesis of disease progression in sporadic ALS. In a more recent study that extends these findings, spinal homogenates from paralysed mutant

$SOD1_{G93A}$ mice were injected into the sciatic nerves of adult $SOD1_{G85R}$ expressing mice (rather than newborn) (Ayers et al., 2016). Similar to the previous study above, these mice developed ALS-like disease characterised by rapidly spreading $SOD1_{G85R}$ containing inclusion pathology and motor neuron loss, similar to clinical and pathological findings in human ALS.

1.10.3 TDP-43

In addition to SOD1, propagation of TDP-43 aggregation has also been suggested to resemble that of a prion-like seeding mechanism. TDP-43 pathology in ALS is clinically similar to SOD1 pathology in SOD1 familial ALS, with ubiquitinated inclusions throughout the spinal cord and motor cortex. There is also evidence of regional spreading of TDP-43 associated pathology occurring in a sequential pattern through the neuroaxis (Brettschneider et al., 2013). Recent evidence suggests that phosphorylated and ubiquitinated TDP-43 aggregates may be able to propagate from cell to cell in cultured neuroblastoma cells and induce TDP-43 aggregation in the cells expressing human TDP-43 in a self-templating fashion (Nonaka et al., 2013). Similar to SOD1, TDP-43 and its C-terminal fragments have a high propensity to misfold *in vivo* (Johnson et al., 2009) with mutations enhancing aggregation (Guo et al., 2011; Johnson et al., 2009). Furthermore, aggregated full length TDP-43 has been detected in exosome fractions derived from conditioned media of human neuroblastoma cells treated with seeds from ALS disease patient brain extracts, similar to prions and therefore this gives evidence for the prion-like properties of pathological TDP-43 aggregates from diseased brains (Nonaka et al., 2013). It has been suggested that TDP-43 contains a yeast prion-like domain in the C-terminal region which is highly aggregation prone (Mousavi and Hotta, 2005). Specifically, one study has reported that the prion-like domain of TDP-43 is critical for aggregation, cytoplasmic mislocalisation and toxicity (Johnson et al., 2008). Pathological aggregates of TDP-43 also contains aggregates of its C-terminal fragment (Arai et al., 2006)

which have been characterised as fibril-like structures (Hasegawa et al., 2008). Other studies have demonstrated that recombinant exogenously applied fibrillar aggregates of full-length TDP-43 can internalise into human embryonic kidney cells, and triggered the mislocalisation of endogenous nuclear TDP-43 to the cytoplasm, where it is found to co-localise with the seeding aggregates and form inclusions *via* prion-like nucleated polymerisation (Furukawa et al., 2011). These induced aggregates are ubiquitinated, similar to that observed in ALS disease and therefore supporting an important role for pathological TDP-43 in disease progression. More recently, it was observed that TDP-43 fibrils triggered the seed-dependant aggregation of WT TDP-43 or TDP-43 lacking a nuclear localisation signal, and different peptides sequences of TDP-43 were able to produce fibrils that induced different TDP-43 associated pathologies (Shimonaka et al., 2016).

A role for a prion-like propagation of WT SOD1 misfolding induced by toxic TDP-43 has recently been reported. Aberrant accumulation of mislocalised cytosolic TDP-43 has been shown to induce the misfolding of SOD1 (Pokrishevsky et al., 2012). Misfolding-specific antibodies revealed misfolded SOD1 in both spinal cord tissue derived from SOD1-familial ALS and in sporadic ALS with cytoplasmic TDP-43 inclusions. In addition, this was also supported by *in vivo* evidence using human neuroblastoma SH-SY5Y cells and murine spinal neural cultured cells transgenic for human WT SOD1. However, misfolded SOD1 was not co-localised with cytosolic TDP-43, suggesting an indirect induction of SOD1 misfolding, followed by the propagation of SOD1 misfolding (Pokrishevsky et al., 2012). Similar to the prion protein, tissue-derived TDP-43 aggregates are resistant to protease digestion, heat and formic acid (Nonaka et al., 2013), however, it remains to be determined whether propagated aggregation persists in the absence of the seed. In addition, induced aggregates of TDP-43 are toxic to cultured neuroblastoma cells (Nonaka et al., 2013).

1.11 Endocytosis

The mechanisms involved in the propagation of misfolded proteins from cell to cell or from region to region in CNS tissues are not completely understood. However, there may be several mechanisms involved in disease-associated protein aggregate entry into recipient neurons depending on the nature of the protein aggregate, activation of signals and the fate of the internalised material (Mercer and Helenius, 2009).

Endocytosis can occur by multiple mechanisms that are generally classified into two broad categories, including pinocytosis which involves the uptake of fluid and solutes, and phagocytosis which involves the uptake of large particles (see Conner and Schmid, 2003). Phagocytosis is used to internalise large particles like bacteria and viruses, but only a few cell types have the ability to use this mechanism. Pinocytosis is characterised by a range of unrelated and highly regulated mechanisms including clathrin-mediated endocytosis, cavelolar-mediated endocytosis, clathrin and cavelolar-independent endocytosis, lipid raft mediated endocytosis and macropinocytosis (Mercer and Helenius, 2009).

1.11.1 Clathrin-mediated endocytosis

Clathrin mediated endocytosis previously known as receptor mediated endocytosis involves concentrating transmembrane receptors and their bound soluble ligands into coated pits formed by the arrangement of cytosolic clathrin proteins embedded in the plasma membrane, which eventually invaginate and pinch off to form endocytic vesicles which are transported into the cell (Brodsky et al., 2001; Schmid, 1997).

1.11.2 Caveolae -mediated endocytosis

Similarly, caveolae-mediated endocytosis involves caveolin which is a dimeric protein found on the surface of most cells and represents a cholesterol-rich microdomain on the plasma

membrane, which facilitates the import of molecules (including pathogens) and transports them to specific locations within the cell. Caveolin binds cholesterol and inserts into the inner leaflet of the plasma membrane where it self-associates, forming the caveolin coat on the surface of the membrane invagination, in which many signalling molecules and membrane transporting molecules are concentrated (Anderson, 1998).

1.11.3 Clathrin and caveolin dependant -mediated endocytosis

Clathrin and cavelolar-independent endocytosis occurs in neurons and neuroendocrine cells which may constitute a specialised high capacity endocytic pathway for fluids and lipids, including recovering secreted membrane proteins, however, this remains poorly understood (Artalejo et al., 2002; Kirkham and Parton, 2005). Lipid-raft mediated endocytosis involves lipid rafts which are microdomains embedded in the plasma membrane characterised by a unique lipid environment enriched in cholesterol and sphingolipids, which concentrate receptors and therefore regulate the induction of signalling pathways (Marmor and Julius, 2001).

1.11.4 Macropinocytosis

Macropinocytosis, also known as a form of fluid-phase endocytosis, is a unique and transient actin dependent process that leads to the non-selective internalisation of extracellular fluid, membrane and other particles (Watts and Marsh, 1992).

Fluid-phase and receptor-mediated endocytosis have been implicated in the cellular uptake of protein aggregates associated with neurodegenerative diseases. Extracellular α-synuclein fibrils and oligomers are thought to enter into neuronal cells *via* receptor mediated endocytosis (Lee et al., 2008), with more recent evidence that α-synuclein fibrils bind heparan sulfate proteoglycans (HSPGs) to mediate their entry into in cultured cells and

primary neurons (Holmes et al., 2013). Similarly, tau aggregates bind HSPGs to trigger their cellular uptake *via* macropinocytosis, although how this relates to activation of macropinocytosis and to entry of other neurodegenerative disease aggregates is unclear (Holmes et al., 2013). However, monomeric α-synuclein and mutant huntingtin aggregates have been observed to directly translocate and penetrate the plasma membrane, respectively, without passage though endocytic compartments (Lee et al., 2008; Ren et al., 2009).

Several studies now suggest that macropinocytosis may be involved in the uptake of protein aggregates associated with various neurodegenerative diseases (Grad et al., 2014; Holmes et al., 2013; Münch et al., 2011; Sundaramoorthy et al., 2013). Interestingly, endocytic uptake of the pathogenic prion protein can be mediated by lipid-raft dependant macropinocytosis (Wadia et al., 2008). Collectively these data show that, despite their size, aggregates from a range of neurodegenerative diseases can be efficiently taken up by cells and most importantly this can occur in neurons. Given the similar structure and large size of these aggregates it is likely that similar mechanisms are used by various subsets of neurons to engulf such large aggregates.

1.12 Hijacking macropinocytosis for SOD1 aggregate entry into cells

Fluid phase endocytosis has been gaining importance in SOD1-ALS pathogenesis, where large SOD1 aggregates have been shown to enter into cells through macropinocytosis (Grad et al., 2014; Münch et al., 2011; Sundaramoorthy et al., 2013; Zeineddine and Yerbury, 2015). Supporting this, the large size of the protein aggregates argues against neuronal entry by caveolae (generally used for particle sizes from 50 - 100 nm) (Richter et al., 2008) or clathrin-coated pits (for particle sizes < 200 nm) (Traub, 2009) and the fact that neurons are incapable of phagocytosis.

Specifically, macropinocytosis is a signal-dependent process generally triggered by growth factors but can be triggered by a variety of other particles such as bacteria, apoptotic bodies, necrotic cells and viruses (Mercer and Helenius, 2012). The activation of macropinocytosis is a result of a number of cell-specific downstream signalling events including activating receptor tyrosine kinases that in turn trigger a signalling cascade that induces changes in the dynamics of actin filaments and trigger plasma membrane ruffling (or membrane extensions and blebbing). Membrane ruffles can take the form of planar lamellipodia, circular ruffles or blebs, dependant on the nature of the cell type and ligand (reviewed in Mercer and Helenius, 2009). These ruffles can then fold back onto themselves to fuse with the plasma membrane creating large, fluid filled randomly sized vacuoles (0.5-10 μM) termed macropinosomes that lack supporting coating molecules (Meier et al., 2002).

Various factors and signalling pathways are required for macropinocytosis, including the Ras superfamily GTPases which activate the RAC1, Rab5, Arf6, and the phosphatidylinositol-3-kinase (PI(3)K) signalling pathways (Bar-Sagi et al., 1987). Kinases, including p21-activated kinase 1 (Pak1) activated by RAC1, regulate cytoskeleton dynamics and motility, and are required throughout the whole process of macropinocytosis (Dharmawardhane et al., 2000). In addition, other factors including Na+/H+ exchangers that maintain pH required for GTPase activity are vital for macropinocytosis (West et al., 1989). Following these signalling events, macropinosome closure occurs, which involves fusion of membrane folds (Swanson, 2008) regulated by kinases, myosins and GTPases (Sun et al., 2003). Once macropinosomes are formed they are trafficked into the cytoplasm of the cell, however some macropinosomes are recycled to the cell surface, where their contents are released into the extracellular space (Hewlett et al., 1994), although the fate of macropinosomes is not completely understood, the trafficking process depends on the cell type and mode of induction (Mercer and Helenius, 2009).

Studies on the propagation of SOD1 aggregation by Münch et. al were the first to show that mutant SOD1 ALS protein aggregates enter into N2A cells *via* endocytic vesicles mediated by ATP and lipid raft dependent macropinocytosis (Münch et al., 2011), through the use of a large panel of inhibitors of a range of cellular functions to systematically rule out specific pathways of endocytosis including as caveolin and clatherin dependent endocytosis. Specifically, inhibitors of Na+/H+ exchangers (EIPA), kinases (rottlerin), phosphoinositide 3-kinase and a cholesterol depleting agent were able to strongly diminish the uptake of aggregates composed of mutant SOD1 protein into neuronal cells (Münch et al., 2011). Furthermore, these mutant SOD1 aggregates were capable of transiently co-localising with fluorescent dextran, a marker of fluid phase uptake and therefore together suggests that mutant SOD1 aggregates selectively use macropinocytosis to enter the cells. Interestingly, it was proposed that once internalised, these mutant SOD1 aggregates can rapidly exit the macropinocytic compartment to enter into the cytosol, where these aggregates seed the aggregation of their soluble counterparts in a prion-like fashion (Münch et al., 2011).

In addition, a recent study demonstrated that that uptake of both extracellular WT and mutant SOD1 soluble forms into NSC-34 cells can be inhibited by the small molecule EIPA which is sometimes considered a specific inhibitor of macropinocytosis (Sundaramoorthy et al., 2013). EIPA (ethylisopropylamiloride) is an analogue of amiloride that is an inhibitor of Na^+/H^+ exchangers and is thought to be specific to macropinocytosis due to the susceptibility of GTPases such as RAC1 to pH changes (Koivusalo et al., 2010). Further, the protein kinase C inhibitor, rottlerin, was also able to inhibit SOD1 uptake consistent with macropinocytosis facilitating the uptake of WT and mutant SOD1 (Sundaramoorthy et al., 2013). Following the internalisation of the aggregated WT and mutant SOD1 *via* macropinocytosis, these aggregates were observed to form SOD1 containing foci or inclusions which inhibited transport from the endoplasmic reticulum to the Golgi apparatus. This resulted in the

induction of neurodegenerative pathways reminiscent of ALS pathology, including endoplasmic reticulum stress and fragmentation of the Golgi resulting and subsequent neuronal cell death (Sundaramoorthy et al., 2013). This further supports the role of misfolded WT SOD1 in ALS and therefore the idea that similar mechanisms of neurodegeneration spread may be occurring in familial and sporadic ALS.

Viruses, including vaccinia virus (Huang et al., 2008) and the Adenovirus 3 (Meier et al., 2002), are known to hijack macropinocytosis pathways to enter cells and likely rupture the unsupported and unstructured vacuole to gain entry to the cytosol, including the Japanese encephalitis virus that infects neurons (Kalia et al., 2013). The African swine fever virus also uses macropinocytosis to internalise into host cells (Sanchez et al., 2012). Interestingly, this virus is able to directly stimulate macropinocytosis through induction of cytoplasmic membrane perturbation in the form of blebbing and ruffles, fluid (measured using dextran) uptake, actin reorganisation, activity of Na+/H+ exchangers and signalling events required for macropinocytosis including Pak1 kinases and the Rho-GTPase RAC1 activation. Similar to previous studies, EIPA significantly reduced virus entry and infection (Sanchez et al., 2012).

Although there is now growing evidence that fluid phase endocytosis and in particular macropinocytosis may play a role in SOD1- mediated ALS, the mechanisms by which SOD1 aggregates utilise macropinocytosis to gain entry into cells and potentially nucleate the aggregation of endogenous soluble proteins and if the form of pinocytosis is constitutive or stimulated is currently unknown (Figure 1.4).

1.13 Overview

It is becoming increasingly evident that the propagation of protein aggregation is a key event in the progressive nature of several neurodegenerative diseases such as ALS, Alzheimer's

disease, Parkinson's disease and Huntington's disease. This may be explained by the nucleation of aggregation in nearby or connected neurons. In the cases where protein aggregates are intracellular, in order for this propagation to occur aggregates must be able to gain access to the cytosol of naïve neurons. It is; however, clear that SOD1 protein aggregates are able to spread to naïve cells in culture gaining access to the cytosol in an unknown manner linked with fluid phase endocytosis. Evidence is accumulating that implicates neuronal macropinocytosis in the uptake of protein aggregates. Although this process is very complex and may involve other processes and factors, the literature published to date on the role of macropinocytosis in ALS allows for further detailed investigations into the role of SOD1 and macropinocytosis in the propagation of aggregation in neuronal cells in a prion-like manner. Furthermore, the involvement of fluid phase endocytosis in the prion-like propagation of disease proteins in Parkinson's, Alzheimer's and Huntingtons disease implicates a unifying mechanism of pathogenesis in these proteinopathies. Overall, it appears that misfolded disease proteins associated with neurodegenerative disorders exhibit similar patterns of disease propagation to prion protein, and interestingly may use similar mechanisms of uptake to that of viruses. It is there vital then to understand this mechanism to identify targets that will halt passage of the "infectious" particle in a strategy analogous to drugs blocking viral entry.

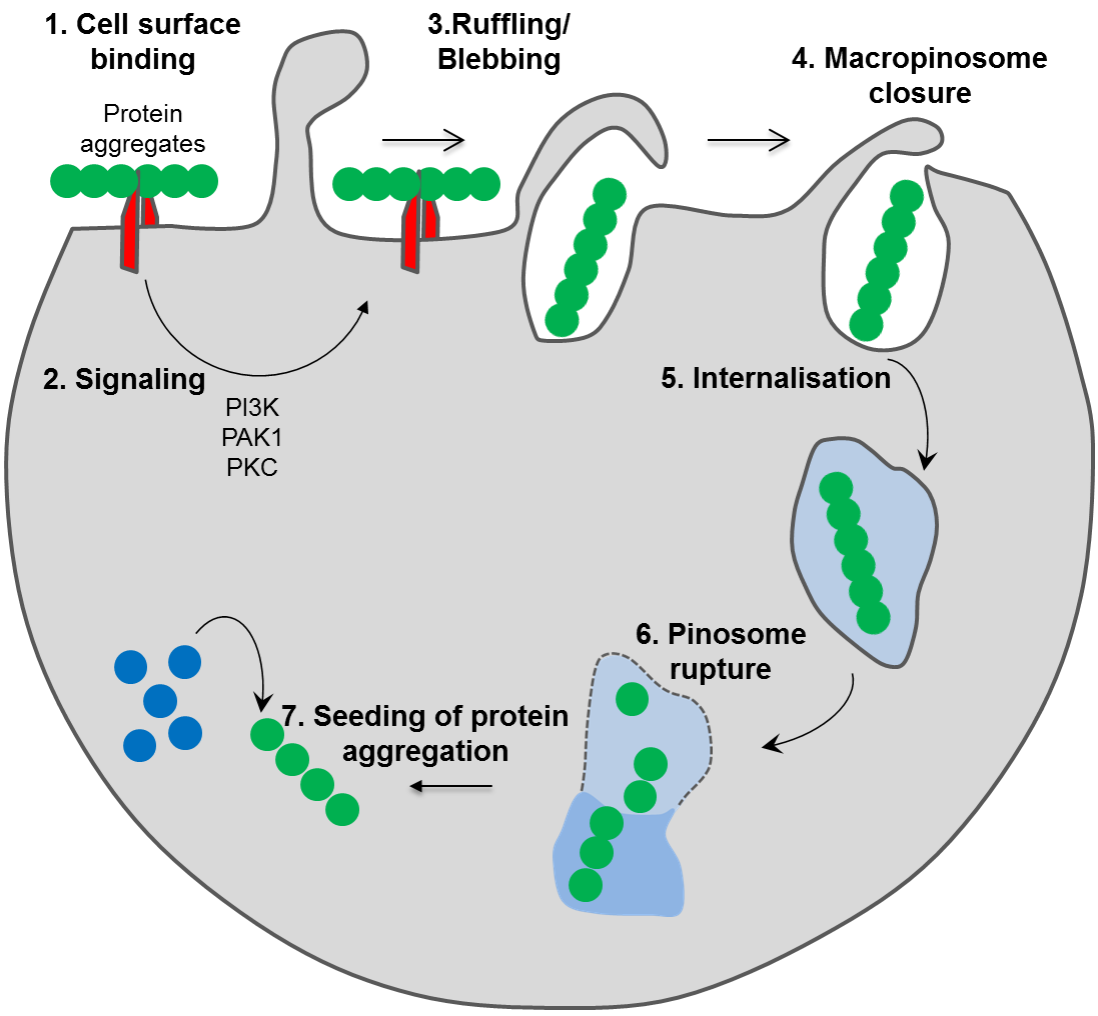

Figure 1.4 Proposed mechanism for aggregate uptake *via* macropinocytosis. Aggregates may interact with cell surface receptors (such as HSG) (1) and promote the clustering and activation of signalling receptors such as receptor tyrosine kinases. This may result in the activation of signalling pathways such as those regulated by RAC1 (2), PAK1 and PKC and subsequent mobilisation of actin and formation of ruffles/blebs (3). Upon macropinosome closure (4) the structure is internalised (5). Given the unstructured nature of the macropinosomes it is likely that rigid aggregate structures may cause rupture (6) and allow access of the aggregates to the cytosol where nucleation of aggregation can proceed (7).

1.14 Summary

ALS is a deadly adult-onset neurodegenerative disease affecting thousands of people globally. With no effective or promising therapies available at present, the need to understand and decipher the mechanisms involved in disease progression is important. This knowledge may help slow or halt the propagation of disease in ALS, and eventualy manage quality of life and survival rates.

Emerging evidence implicates the prion-like activity of SOD1 and processes such as macropinocytosis as important players in the propagation of disease in ALS. The uptake of aggregates *via* macropinocytosis may have broader implications as a common mechanism facilitating spread of protein misfolding in neurodegenerative diseases of aging. Although it has been well established previously that common proteinopathies cannot spread between humans, reports from post-mortem studies now revealed that some patients who developed iatrogenic Creutzfeldt-Jakob disease (CJD) as a result of treatment with human cadaveric pituitary-derived growth hormone contaminated with prions exhibited parenchymal and vascular amyloid-beta deposition. Given that none of these patients had pathogenic mutations or other high risk alleles associated with easrly onset of Alzheimer's disease, these findings are consistent with iatrogenic transmission of amyloid-beta pathology in addition to CJD (Jaunmuktane et al., 2015).

The major difference between PrP and SOD1 is that the pathological PrP is highly stable and protease resistant, compared to misfolded SOD1 which becomes protease sensitive (Grad et al., 2011), and thus less likely to be able to transmit from one person to another. However, the ability of misfolded SOD1 to transmit from cell to cell and region to region posssibly *via* macropinocytosis is thought to be critical for disease progression. However, further detailed research is required to understand how SOD1 aggregates are internalised into neuronal cells *via* macropinocytosis. Further understanding is also required around how these aggregates can gain access to the cytosol. It is likely that elucidating these mechanisms will provide rational therapeutic targets that could stop the spread of pathology and halt ALS and potentially other progressive neurodegenerative diseases in their tracks.

The overarching aim of this project is to investigate the roles of WT and mutant SOD1 in the macropinocytosis dependent propagation in ALS, through the use of the motor neuron-like

cell line, NSC-34, Human primary neurons and Human iPSC derived motor neuron cultures. Specifically, this project aims to:

1. Investigate the mechanism of uptake of SOD1 into neuronal cells, in particular to determine the mechanisms and processes involved in, and leading up to the uptake of SOD1 proteins in their soluble and aggregated form;
2. Examine the mechanisms of SOD1 aggregate release, uptake and propagation in NSC-34 motor neurons.
3. Determine whether exogenous recombinant SOD1 protein aggregates can induce and/or contribute to TDP-43 pathology, specifically its mislocalisation and aggregation and;
4. Determine if SOD1 aggregates can enter human neurons *via* the same mechanism of action using both iPSC derived motor neurons and primary neurons.

These aims will be addressed in Chapters 2-5, respectively.

Chapter 2

SOD1 PROTEIN AGGREGATES STIMULATE MACROPINOCYTOSIS IN NEURON-LIKE CELLS TO FACILITATE THEIR PROPAGATION

2.1 Background

The hallmark of Amyotrophic Lateral Sclerosis (ALS) is the selective death of upper and lower motor neurons in the motor cortex, brainstem and spinal cord, leading to loss of voluntary muscle control, muscle atrophy and invariably death. The specific causes of most cases of ALS are undefined, although approximately 10% are inherited. The best-studied familial ALS (fALS) cases are from families possessing mutations in the gene encoding copper/zinc superoxide dismutase (Cu/Zn SOD, *SOD1*) (Rosen et al., 1993). There is, however, a rapidly growing list of other genes in which mutations have been implicated in fALS. These include *ALS2*, *SETX*, *FUS*, *VAPB*, *ANG*, *TARDBP*, *OPTN*, *VCP*, *UBQLN2*, *PFN1, SQSTM1*, and a hexanucleotide repeat in a non-coding region of *C9ORF72* (Renton et al., 2014). Current clinical practices are such that by the time that a diagnosis is confirmed disease progression is well under way and as many as 50% of motor units may already have been affected (Aggarwal and Nicholson, 2002). There is now very strong evidence in humans that neurodegeneration in ALS begins focally and then spreads amongst adjacent motor neurons and neighbouring cells or through axonal pathways to other cells throughout the three dimensional anatomy of the central nervous system (CNS) (Brettschneider et al., 2014; Ravits and La Spada, 2009; Shaw, 2002). More detailed knowledge of the action of this spreading is crucial, as is identifying a means of early detection of the disease if we are to therapeutically slow disease progression.

In common with other neurodegenerative diseases, such as Alzheimer's Disease (AD) and Parkinson's Disease (PD) (Chiti and Dobson, 2006; Knowles et al., 2014), there is growing evidence that disruptions to proteostasis, protein misfolding and aggregation are the underlying mechanisms driving neurodegeneration in ALS (Pasinelli and Brown, 2006). Of particular interest is the fact that, although nucleation of protein aggregation appears to be a stochastic process (Abdolvahabi et al., 2016; Hortschansky et al., 2005), suggesting that

protein aggregation should cause a random pattern of cell death, cell death in ALS occurs in an ordered and progressive manner. One way to explain this ordered progression is the prion-like propagation of protein misfolding and aggregation between adjacent cells. In addition, recent work has indicated that secondary processes, notably nucleation (Cohen et al., 2013; Knowles et al., 2009; Knowles et al., 2011), takes place on the surface of aggregates, and along with other diffusional or active transport of protein aggregates between cells can give rise to cell-to-cell propagation of the type that is often defined as prion-like behaviour.

Clues to understanding the entry of aggregates into cells comes from studies that show uptake of aggregates of SOD1 can be blocked with EIPA, wortmannin, IPA-3 (Munch et al., 2011) and rottlerin (Grad et al., 2014; Sundaramoorthy et al., 2013), which inhibit Na^+/H^+ exchangers, phosphoinositide 3-kinases (PI3K), P21 protein (Cdc42/Rac)-activated kinase 1 (PAK-1) and protein kinase C (PKC), respectively (suppressing signalling events that promote actin rearrangement and pinosome closure), findings to date that suggest the involvement of fluid phase pinocytosis, possibly macropinocytosis, in the aggregate uptake process.

Macropinocytosis is a form of non-selective endocytosis used by cells to engulf large amounts of solute macromolecules (fluid phase) or particles too large for other forms of endocytosis. Macropinocytosis is typically defined as a transient, externally induced, actin-dependent endocytic process associated with vigorous perturbations, such as ruffles and blebs, in the plasma membrane (Swanson and Watts, 1995). The activation of this process results in a transient increase in receptor-independent fluid phase endocytosis in large vesicles or vacuoles (0.5-10 μm) termed macropinosomes (Mercer and Helenius, 2009; Swanson and Watts, 1995). Macropinosomes do not have a coat to guide their formation and are heterogeneous in size and shape. Macropinocytosis provides non-phagocytic cells with the ability to take up large particles, but the process must be triggered by an external

stimulus. Bacteria, viruses, apoptotic bodies and necrotic cells have all been shown to induce the ruffling behaviour typical of macropinocytosis resulting in their uptake along with fluid (Swanson and Watts, 1995).

There is emerging evidence that prions and prion-like proteins may also enter cells *via* macropinocytosis allowing the propagation of their aggregation (Grad et al., 2014; Holmes et al., 2013; Munch et al., 2011; Sundaramoorthy et al., 2013; Wadia et al., 2008). However, the small molecule inhibitors utilized to define macropinocytosis, such as EIPA, are not specific to a single cellular event and depending on the cell type can prevent various forms of endocytosis (Ivanov, 2008). However, whether SOD1 aggregates stimulate macropinocytosis in neuronal cells has not been reported.

2.1.1 Aims

Recent evidence suggests a role for SOD1 in ALS disease progression through a prion-like propagation of protein misfolding and aggregation between neighbouring cells (Münch et al., 2011; Zeineddine and Yerbury, 2015). Given the potential role for SOD1 in mediating disease progression in ALS, this work initially aimed to further investigate the mechanism of uptake of SOD1 into neuronal cells. In particular, the current study aimed to investigate the mechanism(s) involved in the uptake of SOD1 in both its soluble and aggregated form.

2.2 Methods

2.2.1 Reagents and Antibodies

DMEM/F-12 medium, DMEM/F-12 without phenol red, 0.05% trypsin-EDTA, GlutaMAX, SuperSignal West Pico Chemiluminescent Substrate, SYTOX Red dead cell stain, FM® 1-43FX, fixable analog of FM® 1-43 membrane stain, 10 kDa 647-dextran, Image-iT ™ LIVE Red caspase detection kit and Lab-Tek chambered coverglass 8 well with cover were purchased from ThermoFisher Scientific (Waltham, USA). Any kD Mini-PROTEAN TGX Precast Protein Gels and Precision Plus Protein dual color protein standard were from Bio-Rad (California, USA). Foetal Bovine Serum (heat-inactivated prior to addition in media; FBS) was from Bovogen Biologicals (East Keilor, Australia). Amersham Hyperfilm was obtained from GE Healthcare (Little Chalfont, Buckinghamshire, UK). RedDot 2 was from Biotium (Hayward, CA). Sterile cell culture plates were form Greiner Bio-One (Frickenhausen, Germany). Casein (heat denatured before use; HDC), dimethyl sulfoxide (DMSO), bovine serum albumin (BSA), β-mercaptoethanol, Brilliant blue R concentrate, paraformaldehyde (PFA), biotinamidohexanoic acid 3-sulfo-N-hydroxysuccinimide ester sodium salt, Bicinchoninic Acid Kit, Glutaraldehyde solution (50% in H2O), Propidium iodide, Osmium tetroxide solution (4 WT. % in H2O) and dithiothreitol (DTT) were from Sigma-Aldrich (St. Louis, MO). Ethylenediaminetetraacetic acid (EDTA) was from Amresco (Solon, USA). Uranyl acetate and 19 mm glass coverslips were from ProSciTech (Kirwan, Australia). Protease inhibitor cocktail tablets (complete, Mini, EDTA-free) was from Roche Diagnostics (Penzberg, Germany). RAC1 G-LISA Activation Assay Kit (Colorimetric Based) was purchased from Cytoskeleton (Denver, CO). All other reagents including salts, powders and chemicals were from Amresco, Sigma-Aldrich or Astral Scientific (Gymea, Australia). All reagents used were endotoxin free. Antibodies (Abs) and inhibitor compounds and their

respective manufacturing companies used in this current study are listed in Table 2.1 and Table 2.2 respectively.

Table 2.1 Antibodies used in this study to investigate the effect of SOD1 proteins on TDP-43 pathology

Host species (clonality)[1]	Anti-body target (Immunogen)[2]	Conjugate	Manufacturer (product number)[3]
Mouse (mAb)	Beta Actin [AC-15]	-	Abcam (ab8226)
Rabbit (pAb)	Vimentin	-	Abcam (ab137321)
Sheep (pAB)	SOD1	-	ThermoFisher Scientific (PAI-30817)
Mouse (mAb)	RAC1	-	Cytoskeleton (ARC03)
Goat (pAB)	Mouse IgG	Alexa Fluor 488	ThermoFisher Scientific A-(11001)
Goat (pAB)	Rabbit IgG	Alexa Fluor 488	ThermoFisher Scientific (A-11008)
Donkey (pAb)	Sheep IgG	Alexa Fluor 488	Abcam (150177)
Goat (pAb)	Mouse IgG	Alexa Fluor 633	ThermoFisher Scientific (A-21052)
Donkey (pAb)	Sheep IgG	HRP	Abcam (97125)
Goat (pAb)	Mouse IgG	HRP	Merck Millipore (12-349)

[1] pAb, polyclonal anti-body, mAb, monoclonal anti-body; [3] Abcam, Cambridge, USA; ThermoFisher Scientific (Waltham,MA, USA); BD Biosciences San Jose, CA, USA; Merck Millipore, Billerica, Massachusetts, USA; Cytoskeleton (Denver, CO,USA)

Table 2.2 Pharmacological inhibitors used in this study to investigate the mechanisms of SOD1 uptake

Compound	Manufacturer (product number)[1]
5-N-ethyl-N-isopropyl-amiloride (EIPA)	Sigma (A3085)
Chlorpromazine hydrochloride (Chlorp HCL)-	Sigma (C8138)
Genistein (Gen)	Sigma (G6649)
Rottlerin (Rot)-	Sigma (R5648)
RAC1 inhibitor W56	Tocris Bioscience (2221)

[1]Sigma, (St. Louis, MO, USA), Tocris Bioscience (Avonmouth, Bristol,UK)

2.2.2 Cell Lines

The mouse neuroblastoma x spinal cord hybrid cell line (NSC-34 cells) (Cashman et al., 1992) were routinely cultured in DMEM/F12 supplemented with 10% (v/v) FBS and 2 mM GlutaMAX. Cells were maintained in an incubator at 37°C under a humidified atmosphere containing 5% (v/v) CO_2.

2.2.3 Aggregation and biotinylation of WT and mutant G93A SOD1 proteins

WT and G93A SOD1 were expressed and purified from *E.coli* as previously outlined (Lindberg et al., 2002; Roberts et al., 2013). SOD1 aggregation was performed *in vivo* as previously described (Roberts et al., 2013). Briefly, solutions of purified WT or G93A mutant SOD1 protein (1 mg/ml) in PBS were co-incubated with 20 mM dithiothreitol (DTT) and 5 mM ethylenediaminetetraacetic acid (EDTA) for 72 h at 37 °C with shaking using a orbital shaker (universal IKA® MS 3, 230 V) (Sigma, St. Louis, MO). The aggregated SOD1 was then labelled with biotin amidohexanoic acid 3-sulfo-N-hydroxysuccinimide ester sodium salt (40 mg/ml) in DMSO for 2 h at RT. The unconjugated biotin was then separated from the aggregates by centrifugation (21 000 *x g* for 30 min) and washed three times with PBS (300 *x g* for 5 min). The purified aggregates free of unconjugated biotin were then resuspended in PBS (1 mg/ml). A bicinchoninic acid (BCA) protein assay was performed to determine the amount of protein in solution.

2.2.4 SOD1 protein Immunoblotting

Purified SOD1 proteins in their soluble and aggregate form (1 µg protein/lane) were separated under reducing conditions (5% β-mercaptoethanol) using Any kD Mini-PROTEAN TGX Stain-Free™ Precast Gels (Bio-Rad, Hercules, CA). Proteins were then transferred onto nitrocellulose membranes using the Trans-Blot Turbo Transfer System (Bio-Rad).

Membranes were blocked with heat denatured casein (HDC) in for 1 h at 37°C. To confirm immunoreactivity of SOD1 and confirm the aggregation and biotinylation of the SOD1 proteins, sheep anti-SOD1 pAb (1:500) and streptavidin−peroxidase (1:400) (Sigma, St. Louis, MO) diluted in HDC/PBS was incubated with membranes for 1 h at 37°C, to detect SOD1 soluble and biotinylated-aggregated protein respectively. The following day, the membrane containing soluble proteins was washed three times over 15 min with PBS containing 0.1% Triton X-100. The membrane was then incubated with peroxidase-conjugated to anti-sheep IgG Ab (1:1000) for 1 h at 37°C. Membranes were washed three times over 30 min with PBS containing 0.1% Triton X-100 and membranes were visualised using chemiluminescent substrate and Amersham Hyperfilm ECL (GE Healthcare). The processing of films was achieved using GBX Developer and Replenisher and GBX Fixer and Replenisher (Kodak Australiasia, Collingwood, Victoria Australia). Images of the films were collected using a GS-800 Calibrated Densitometer (Bio-Rad).

2.2.5 Transmission electron microscopy of SOD1 aggregates

Negative staining transmission electron microscopy (TEM) was performed using substrate carbon-coated nickel grids (Proscitech Kirwan, Australia). Initially, 2 µl aliquots of SOD1 WT and G93A proteins (1 mg/ml) were loaded onto carbon-coated nickel grids (Proscitech Kirwan, Australia) for 1 min at RT. Grids were washed 3 times with filtered Milli-Q water. Grids were then negatively stained using 2% (w/v) uranyl acetate (ProsciTech Kirwan, Australia) diluted in Milli-Q water for 2 min at RT. Grids were then dried using filter paper blotting and then left at RT for 5 min, until processing. Protein structure and morphology was then analysed using a JEOL 2011 TEM (Tokyo, Japan) operated at 200kV. Images were taken using a Gatan Microscopy Suite (Version 2.30.542.0) (California, USA).

2.2.6 Internalisation of SOD1 by flow cytometry

NSC-34 cells were incubated with 20 μg/ml of aggregated SOD1 or PBS (no protein; negative control) for 60 min at 4°C. Cells were then washed twice in PBS, harvested using 5 mM EDTA (5 min, 37°C) and then washed again using centrifugation (300 *x g* for 5 min). Cells were fixed with 4% PFA in PBS for 20 min at RT, and then washed again using centrifugation (300 *x g* for 5 min). Cells were washed once with ice-cold PBS and then incubated with Triton X-100 for 30 min at 4°C. Cells were washed again in ice cold PBS (300 *x g* for 5 min) and incubated with blocking solution (5% FCS, 1% BSA and 0.3% Triton X-100) for 20 min at RT. Cells were incubated with anti- SOD1 IgG Ab (1:500; diluted in 4% BSA and 0.1% Triton X-100) for 30 min at 4°C. Cells were washed again in ice cold PBS (300 *x g* for 5 min) and incubated with anti-sheep IgG conjugated to Alexa Fluor 488 (1:500 diluted in 1% BSA and 0.1% Triton X-100) for 30 min at 4°C protected from light. Cellular events were collected using a LSR II flow cytometer (BD Biosciences) (Excitation 488 nm, emission collected with 515/20 band-pass filter). The live cells were analysed using gating methods with forward and side scatter parameters. Mean fluorescence intensity (MFI) was then determined using FlowJo software (Tree Star, Ashland, OR).

2.2.7 Detection of internalised SOD1 aggregates by immunoblotting

In separate experiments, NSC-34 cells were treated with biotin conjugated-SOD1 aggregates as previously outlined above. Post incubation, cells were washed (300 *x g* for 5 min) twice with PBS and harvested using 0.05% trypsin-EDTA (5 min, 37°C) and then washed again using centrifugation (300 *x g* for 5 min). Cells were lysed (1.5×10^6 - 1.5×10^8 cells/ml) over 15 min at 4°C in ice-cold lysis buffer (10 mM Tris, 150 mM NaCl, 5 mM EDTA, 1% Triton X-100 and protease inhibitor cocktail, pH 7.0). Cell debris was then cleared (21,000 × *g* at 4°C for 30 min) and supernatants (75 μg protein/lane) were collected and separated under

reducing conditions (5% β-mercaptoethanol) using Any kD Mini-PROTEAN TGX Stain-Free Gels (Bio-Rad, Hercules, CA). Proteins were then transferred to nitrocellulose membranes using a Trans-Blot Turbo Transfer System (Bio-Rad). The membrane was blocked with heat denatured casein (HDC) in for 1 h at 37°C. The nitrocellulose membrane was then incubated with mouse anti-actin mAb (1:5000), diluted in HDC/PBS for 1 h at 37°C. The membrane was washed three times over 15 min with PBS containing 0.1% Triton-X-100. The membrane was then incubated with peroxidase-conjugated anti-streptavidin (1:400) (Sigma, St. Louis, MO) and goat anti-mouse IgG Ab-HRP diluted in HDC/PBS for 1 h at 37°C for aggregates and actin respectively, and then washed as above. Internalised SOD1 aggregates were visualised using chemiluminescent substrate and Amersham Hyperfilm ECL (GE Healthcare). Images of films were collected using a GS-800 Calibrated Densitometer (Bio-Rad). Actin was used as a loading control.

2.2.8 Rapid detection of aggregated SOD1 by flow cytometry

NSC-34 cells were incubated with 20 μg/ml of soluble and aggregated SOD1, GST or PBS (no protein, control) for 30 min at 37°C/5% CO_2. Cells were then washed twice in ice-cold PBS, harvested using 5 mM EDTA (5 min, 37°C) and then washed again using centrifugation (300 *x g* for 5 min). Cells were fixed with 4% PFA for 20 min at RT, and then washed again (300 *x g* for 5 min) with ice-cold PBS. Cells were then incubated with Triton X-100 for 30 min at 4°C. Cells were washed again in ice cold PBS (300 *x g* for 5 min) and incubated with blocking solution (5% FCS, 1% BSA and 0.3% Triton X-100) for 20 min at 4°C. Cells were then incubated anti-SOD1 IgG Ab (1:500 diluted in 4% BSA and 0.1% Triton X-100) for 30 min at 4°C. Cells were washed again in ice cold PBS (300 *x g* for 5 min) and incubated with anti-sheep IgG conjugated to Alexa Fluor 488 (1:500 diluted in 1% BSA and 0.1% Triton X-100) for 30 min at 4°C protected from light. Cellular events were collected using a LSR II

flow cytometer (BD Biosciences) (Excitation 488 nm, emission collected with 515/20 band-pass filter). The live cells were analysed using gating methods with forward and side scatter parameters. Mean fluorescence intensity (MFI) of these cells was then determined using FlowJo software (Tree Star, Ashland, OR).

2.2.9 Rapid detection of aggregated SOD1 by confocal microscopy

NSC-34 cells (2–3 x 10^4 cells/0.2 ml/chamber) were cultured in chamber slides at 37°C/5% CO_2 overnight. Cells were incubated with 20 μg/ml of aggregated SOD1 or PBS (no protein control) for 30 min at 4°C to slow endocytosis. Cells were fixed with 4% PFA in PBS for 20 min at RT and washed twice with ice cold PBS over 5 min. Cells were then incubated with Triton X-100 for 30 min at 4°C. Cells incubated with blocking solution (5% FCS, 1% BSA and 0.3% Triton X-100) for 20 min at RT. Cells were incubated with anti- SOD1 IgG Ab (1:500 diluted in 4% BSA and 0.1% Triton X-100) for 30 min at 4°C. Cells were washed again in ice cold PBS and incubated with anti-sheep IgG conjugated to Alexa Fluor 488 (1:500 diluted in 1% BSA and 0.1% Triton X-100) for 30 min at 4°C protected from light. An inverted microscope (DM IBRE) and a Leica TCS SP confocal imaging system were used to visualise and image cells (excitation 488, emission collected at 520-545). Fluorescence, bright field (differential interference contrast; DIC) and merged images were captured using Leica confocal software.

2.2.10 Permeabilisation of NSC-34 cells

NSC-34 cells were incubated in chamber slides with 20 μg/ml of aggregated-biotin conjugated SOD1 for 60 min at 4°C. Cells were fixed with 4% PFA in PBS for 20 min at RT and washed twice with ice cold PBS over 5 min. Cells were then incubated with Triton X-100 (permeabilised) or PBS (not permeabilised) for 30 min at 4°C. Cells were incubated with blocking solution (5% FCS and 1% BSA) for 20 min at RT. Cells were incubated in 1 μg/ml

Alexa Fluor 488 streptavidin (diluted in 1% BSA and 0.1% Triton X-100) for 1 hr at RT protected from light. An inverted microscope (DM IBRE) and a Leica TCS SP confocal imaging system were used to visualise and image cells (excitation 488, emission collected at 520-545). Fluorescence, bright field (differential interference contrast; DIC) and merged images were captured using Leica confocal software.

2.2.11 Treatment with trypsin

NSC-34 cells (2–3 x 10^4 cells/0.2 mL/chamber) were cultured in chamber slides at 37°C/5% CO_2 overnight. Cells were incubated with 20 μg/ml labelled aggregated SOD1 for 1 h at 37°C/5% CO_2. Cells were incubated with 0.25% trypsin or PBS (control) for 5 min at 37°C/5% CO_2. Cells were washed (300 *x g* for 5 min) and the resulting suspended cells were re-cultured in complete DMEM culture medium for a total of 6 h at 37°C/5% CO_2 to allow cells to recover. Cells were then immediately fixed with 4% PFA in PBS for 20 min at RT and washed twice with PBS over 5 min. Cells incubated with 0.5% Triton X-100 for 30 min at 4°C. Cells were then incubated with blocking solution (5% FCS, 1% BSA and 0.3% Triton X-100) for 20 min at RT. Cells were then incubated with Alexa Fluor 488 streptavidin (1:1000 diluted in 1% BSA and 0.1% Triton X-100) for 1 h at RT. Sytox Red (5 μM) was used as a counter stain, and incubated with cells for 10 at RT. An inverted microscope (DM IBRE) and a Leica TCS SP confocal imaging system were used to visualise and image cells (excitation 488, emission collected at 520-545 and excitation 633, emission collected at 635-650). Fluorescence, bright field (differential interference contrast; DIC) and merged images were captures using Leica confocal software. Mean fluorescence intensities (MFI) per cell of SOD1 aggregate uptake were quantified from confocal images using ImageJ software (Version 1.48) (National Institutes of health, Bethesda, MD).

2.2.12 Pre-treatment of NSC-34 cells with trypsin

NSC-34 cells were harvested using either 5 mM EDTA (control) or 0.25% trypsin-EDTA (10 min, 37°C) and then washed again using centrifugation (300 *x g* for 5 min). Cells were then incubated with 20 µg/ml of aggregated SOD1 or PBS (no protein, control) for 30 min at 37°C/5% CO_2. Cells were then washed twice in ice-cold PBS (300 *x g* for 5 min), and fixed with 4% PFA for 20 min at RT, then washed again with ice-cold PBS using centrifugation (300 *x g* for 5 min). Cells were then incubated with Triton X-100 for 30 min at 4°C. Cells were washed again in ice cold PBS (300 *x g* for 5 min), incubated in solution (5% FCS, 1% BSA and 0.3% Triton X-100) for blocking for 20 min at RT. Cells were incubated with anti-SOD1 IgG Ab (1:500 diluted in 4% BSA and 0.1% Triton X-100) for 30 min at 4°C. Cells were washed again in ice cold PBS (300 *x g* for 5 min) and incubated with anti-sheep IgG conjugated to Alexa Fluor 488 (1:500 diluted in 1% BSA and 0.1% Triton X-100) for 30 min at 4°C protected from light. Cellular events were collected using a LSR II flow cytometer as described above.

2.2.13 Inhibition of SOD1 uptake - confocal microscopy

Internalisation of aggregated SOD1 was measured in the presence or absence of a range of compounds that inhibit various internalisation mechanisms. NSC-34 cells (4 x 10^4 cells/.35 ml/well) were incubated in 24-well culture plates fitted with sterile 19 mm glass coverslips (1.5 ml/ well) and incubated at 37°C/5% CO_2 overnight to allow time to adhere. Cells were pre-treated with various endocytic inhibitors including 100 µM 5-N-ethyl-N-isopropyl-amiloride (EIPA), 5 µM chlorpromazine hydrochloride (Chlorp HCl), 10 µM genistein (Gen) or 3 µM rottlerin (Rot) diluted in 1% BSA/PBS or PBS (no inhibitor, diluted in 0.1% DMSO or 20% acetonitrile in water) for 30 min at 37°C/5% CO_2. Cells were then co-incubated with by 20 µg/ml soluble or aggregated SOD1 for an additional 30 min at 37°C/5% CO_2. Cells

were immediately fixed with 4% PFA in PBS for 20 min at RT and washed twice with PBS over 5 min. Cells were incubated with Triton X-100 for 30 min at 4°C. Cells were then incubated with blocking solution (5% FCS, 1% BSA and 0.3% Triton X-100) for 20 min at RT. Cells were incubated with anti-SOD1 IgG Ab (1:500 diluted in 4% BSA and 0.1% Triton X-100) for overnight at 4°C. Cells were subsequently washed again in PBS and incubated with anti-sheep IgG conjugated to Alexa Fluor 488 (1:500 diluted in 1% BSA and 0.1% Triton X-100) for soluble proteins and with Alexa Fluor 488 streptavidin (1:1000 diluted in 1% BSA and 0.1% Triton X-100) for 1 h at RT. Sytox Red (5 nM) was used as a counter stain, and incubated with cells for 10 min at RT. An inverted microscope (DM IBRE) and a Leica TCS SP confocal imaging system were used to visualise and image cells (excitation 488, emission collected at 520-545). Fluorescence, bright field (differential interference contrast; DIC) and merged images were captured using Leica confocal software.

2.2.14 Inhibition of SOD1 uptake - flow cytometry

Cells were harvested using 5 mM EDTA (5 min, 37°C) and then washed again using centrifugation (300 *x g* for 5 min). Cells were pre-treated with various endocytic inhibitors including 100 µM EIPA, 5 µM Chlorp HCl, 10 µM Gen, 3 µM Rot or RAC1 inhibitor W56 (200 µM) diluted in 1% BSA/PBS or PBS (no inhibitor, diluted in 0.1% DMSO or 20% acetonitrile in water) for 30 min at 37°C/5% CO_2. Cells were then washed twice in PBS (300 *x g* for 5 min) and then co-incubated with by 20 µg/ml soluble or aggregated WTSOD1 for an additional 30 min at 37°C/5% CO_2. Cells were then washed twice in PBS (300 *x g* for 5 min) and immediately fixed with 4% PFA in PBS for 20 min at RT. Cells were then washed twice in PBS (300 *x g* for 5 min) and then incubated with Triton X-100 for 30 min at 4°C. Cells were washed twice in PBS (300 *x g* for 5 min) and incubated with blocking solution (5% FCS, 1% BSA and 0.3% Triton X-100) for 20 min at RT. Cells were then washed twice in PBS (300 *x g* for 5 min) and incubated with anti-SOD1 IgG Ab (1:500 diluted in 4% BSA

and 0.1% Triton X-100) for 30 min at 4°C for 1 h at RT. Cells were washed again (300 *x g* for 5 min) in PBS and incubated with anti-sheep IgG conjugated to Alexa Fluor 488 (1:500 diluted in 1% BSA and 0.1% Triton X-100) for soluble proteins and with Alexa Fluor 488 streptavidin (1:1000 diluted in 1% BSA and 0.1% Triton X-100) for 1 h at RT. Cells were then washed twice in PBS (300 *x g* for 5 min). Cellular events were collected using a LSR II flow cytometer (excitation 488 nm, emission collected at 515/20 nm) and the MFI of relative SOD1 uptake into NSC-34 cells was determined using FlowJo software. Results are the average of at least five independent experiments.

2.2.15 Field emission scanning electron microscopy (FESEM)

Detached NSC-34 cells ($7x10^4$ cells/ml/well) were incubated in 24-well culture plates fitted with sterile 19 mm glass coverslips (1.5 ml/well) and incubated at 37°C/5% CO_2 overnight to allow time to adhere. Cells were then serum starved in DMEM F12 phenol red free culture medium for 24 h at 37°C/5% CO_2. Cells were then washed once with PBS and incubated with 20 µg/ml soluble or aggregated proteins in PBS or PBS containing 200 nM phorbol 12-myristate 13-acetate (PMA) for 2 h at 37°C/5% CO_2. Post incubation, cells were washed three times in PBS then fixed in 2.5% glutaraldehyde/4% PFA in 0.1 M phosphate buffer for 3 h at 4°C. Cells were then washed three times in phosphate buffer and postfixed in 2% OsO_4/water at RT for 1 h. After washing with water, the cells were dehydrated using a gradient of ethanol at 30%, 50%, 70%, 80%, 90% and 100% (30 min per incubation) at RT. The cells were then critical point dried for 2 h using a LEICA CPD030 (Vienna, Austria) and coated with graphite-gold in a sputter coater. Cellular structures were visualised with a JEOL 6490LV SEM (Tokyo, Japan) microscope operated at 10 kV at a 10 mm working distance and a spot size setting of 35.

2.2.16 Membrane activity quantification

NSC-34 cells (2–3 x 10^4 cells/0.2 ml/chamber) were cultured in 8-well chamber slides in DMEM/F12 media supplemented with 10% FCS and were incubated overnight at 37°C/5%CO_2. Cells were incubated with 20 µg/ml of SOD1 proteins, PBS alone, or PMA (200 nM) in PBS for 1 h at 37°C/5% CO_2. Cells were then washed twice in PBS and incubated with 10 µM of FM 1-43FX membrane stain diluted in PBS for 7 min at 37°C/5% CO_2. Excess dye was removed by several washes in PBS and cells were returned to the incubator (37°C/5% CO_2) for 4 min. This procedure was repeated to give a total of 8 min of incubation in PBS. Post incubation, ice-cold PBS was added to stop endocytosis and prepare cells for fixation in 4% PFA in PBS for 20 min at 4°C. Post fixation, cells were washed twice in PBS and incubated with 1x Red Dot 2 for 10 min at RT.

2.2.17 Fluid phase uptake - confocal microscopy

Pinocytosis involves uptake of solutes from the extracellular medium. One well established solute is dextran. To quantify the amount of fluid phase solute uptake NSC-34 cells (2–3 x 10^4 cells/0.2 ml/chamber) were incubated in chamber slides with 20 µg/ml of SOD1 proteins in PBS alone or PMA (200 nM) for 30 min at 37°C/5%CO_2. Prior to harvesting or fixation, cells were then co-incubated for 15 min with 0.5 mg/ml 10 kDa dextran conjugated to Alexa Fluor 647 at 37°C/5% CO_2. The cells were then placed on ice to stop dextran uptake and cells were washed three times with ice cold PBS and once with low pH buffer (0.1 M sodium acetate, 0.05 M NaCl, pH 5.5) for 10 min. The cells were then incubated with anti-SOD1 IgG Ab (1:500 diluted in 4% BSA and 0.1% Triton X-100) overnight at 4°C. Cells were washed again in PBS and incubated with anti-sheep IgG conjugated to Alexa Fluor 488 (1:500 diluted in 1% BSA and 0.1% Triton X-100) for soluble proteins and Alexa Fluor 488 streptavidin (1:1000 diluted in 1% BSA and 0.1% Triton X-100) for 1 h at RT. An inverted microscope

(DM IBRE) and a Leica TCS SP confocal imaging system were used to visualise and image cells (excitation 488, emission collected at 495-515 and 650-668). Fluorescence, bright field (differential interference contrast; DIC) and merged images were captured using Leica confocal software.

2.2.18 Fluid phase uptake - flow cytometry

NSC-34 cells (5 x 10^4 cells/0.5 ml/well) were incubated with 20 µg/ml of SOD1 proteins in PBS alone or PMA (200 nM) for 30 min at 37°C/5% CO_2. Cells were co-incubated with 0.5 mg/ml 10 kDa dextran conjugated to Alexa Fluor 647 for 15 min at 37°C/5% CO_2. The cells were then placed on ice to supress dextran uptake and cells were washed three times with ice cold PBS (300 *x g* for 5 min) and once with low pH buffer (300 *x g* for 5 min) (0.1 M sodium acetate, 0.05 M NaCl, pH 5.5) for 10 min. The cells were then incubated with anti-SOD1 IgG Ab (1:500 diluted in 4% BSA and 0.1% Triton X-100) for 1 h at RT. Cells were washed again (300 *x g* for 5 min) in PBS and incubated with anti-sheep IgG conjugated to Alexa Fluor 488 (1:500 diluted in 1% BSA and 0.1% Triton X-100) for soluble proteins and Alexa Fluor 488 streptavidin (1:1000 diluted in 1% BSA and 0.1% Triton X-100) for 1 h at RT. Cellular events were collected using a LSR II flow cytometer as described above.

2.2.19 Inhibition of PMA induced dextran uptake

NSC-34 cells (5 x 10^4 cells/0.5 ml/well) were serum starved for 24 h. Cells were pre-treated with various endocytic inhibitors including 100 µM EIPA, 5 µM chlorpromazine hydrochloride (Chlorp HCL), 10 µM Gen and 3 µM Rot diluted in 1% BSA/PBS or PBS (0.1% DMSO) for 30 min at 37°C/5% CO_2. Cells were co-incubated with 200 nM PMA for an additional 30 min at 37°C/5% CO_2. Cells were co-incubated with 0.5 mg/ml 10 kDa dextran conjugated to Alexa Fluor 647 for 15 min at 37°C/5% CO_2. The cells were then placed on ice to supress dextran uptake and cells were washed three times with ice cold PBS

(300 *x g* for 5 min) and once with low pH buffer (300 *x g* for 5 min) (0.1 M sodium acetate, 0.05 M NaCl, pH 5.5) for 10 min. Cellular events were collected using a LSR II flow cytometer (BD Biosciences) as outlined above.

2.2.20 RAC1 activation ELISA assay

NSC-34 cells were incubated in sterile 12-well culture plates (2 ml/well) and incubated at 37°C/5% CO_2 overnight. Cells were then serum starved in phenol red free culture medium for 24 h at 37°C/5% CO_2. Cells were then washed once with ice cold PBS and incubated with 20 µg/ml of soluble and aggregated SOD1 proteins for 30 min at 37°C/5% CO_2. Cells were washed twice with ice-cold PBS and harvested by treatment with 0.05% trypsin for 10 min at 37°C. Cells were washed again (300 *x g* for 5 min) in PBS. RAC1 activation was measured using a G-LISA activation kit (Kit #BK128 Cytoskeleton, Inc. Denver, USA) as per the manufacturer's recommendations. Absorbance values of wells were recorded with a SpectraMax Plus 384 Microplate Reader and SoftMax Pro software (Molecular Devices, Silicon Valley, CA) (490nm).

2.2.21 RAC1 inhibition and membrane activity

NSC-34 cells (2–3 x 10^4 cells/0.2 ml/chamber) were cultured in 8-well chamber slides in complete culture medium and were incubated overnight at 37°C/5% CO_2. Cells were pre-incubated with RAC1 inhibitor W56 or PBS (in 20% acetonitrile in water) diluted in 1% BSA/PBS for 1 h at 37°C/5% CO_2. Cells were then co-incubated with PMA (200 nM) in PBS for an additional 30 min at 37°C/5% CO_2. Cells were then washed twice in PBS and incubated with 10 µM of FM 1-43FX membrane stain diluted in PBS for 7 min at 37°C/5% CO_2. Excess dye was removed by several washes in PBS and cells were returned to the incubator (37°C/5% CO_2) for 4 min. This procedure was repeated to give a total of 8 min of incubation in PBS. Post incubation, ice-cold PBS was added to stop endocytosis and prepare

cells for fixation in 4% PFA in PBS for 20 min at 4°C. Post fixation, cells were washed twice in PBS and incubated with 1x Red Dot 2 for 10 min at RT for imaging with confocal microscopy.

2.2.22 Etoposide Assay

To confirm cell blebbing is not apoptosis related, a Caspase Detection kit was used according to manufacturer's instructions. Detached NSC-34 cells ($10x10^4$ cells/ml/well) were incubated in 12-well culture plates fitted with sterile 19 mm glass coverslips (1 ml/well) and incubated at 37°C/5%CO_2 overnight to allow time to adhere. Cells were incubated with either 20 µg/ml soluble and labelled aggregated SOD1 or 100 µM Etoposide for 2 h at 37°C/5% CO_2. Cells were incubated with 1X FLICA reagent for 60 min at 37°C/5% CO_2, protected from light. Cells were washed gently with cell-culture medium (DMEM F12 phenol red free). Cells were then incubated with SYTOX Green stain (5 µM) for 8 min at 37°C/5% CO_2. The cells were then washed with 2 ml of 1X wash buffer and coverslips were mounted on slides using one drop of apoptosis fixative solution in 1X wash buffer according to manufacturer's instructions. An inverted microscope (DM IBRE) and a Leica TCS SP confocal imaging system were used to visualise and image cells (excitation 488, emission collected at 495-515 and 650-668). Fluorescence, bright field (differential interference contrast; DIC) and merged images were captures using Leica confocal software.

2.2.23 Presentation of data and statistical analyses

Data is presented as the mean ± SD. ANOVA paired with Tukey's HSD multiple comparison post-test tests were used to analyse and compare differences between multiple treatments. Unpaired student's t-tests were performed for single treatment comparisons. Prism 5 for Windows (Version 5.01) (GraphPad Software, San Diego, CA) was used to generate these statistical analyses. Differences were defined as significant for $P < 0.05$.

2.3 Results

2.3.1 SOD1 aggregates associate with the cellular surface and internalise into neuronal cells *via* membrane proteins

2.3.1.1 Aggregating WT and G93A SOD1 proteins

Given the identification of SOD1-positive lewy-body like hylaline inclusions and skein like inclusions in surviving motor neurons derived from spinal cords of SOD1-related fALS patients (Piao et al., 2003) it is now generally accepted that pathogenic mutations in SOD1 increases the propensity of SOD1 to aggregate (Bruijn et al., 1998), and that SOD1 misfolding and aggregation contribute to the underlying cause for pathology in SOD1 fALS cases (Furukawa and O'Halloran, 2005). To investigate the effects of properly folded soluble SOD1 and aggregated proteins on motor-neuron like cell lines, recombinantly produced, properly folded (soluble SOD1) and dimeric human WT and G93A SOD1 was purified and subsequently aggregated *in vivo* to form fibrillar structures, as previously described (Yerbury et al., 2013). To investigate the morphology of these aggregates, negative staining TEM was performed. Representative TEM images of endpoint aggregates for both the WT and G93A SOD1 proteins displayed short fibril-like structures, similar to those seen in human fALS cases (Figure 2.1)

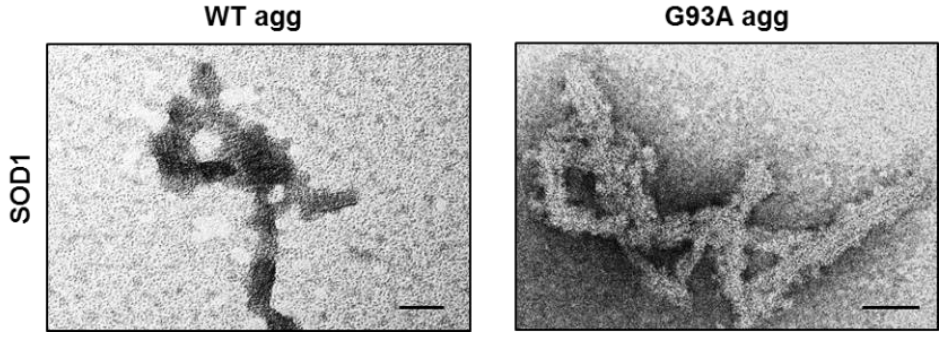

Figure 2.1 SOD1 proteins aggregate in to fibril-like structures. Representative TEM image of endpoint aggregates. WT and G93A (1 mg/ml) protein samples (2 µl) were loaded onto carbon-coated nickel grids for 1 min at RT and negatively stained using 2% uranyl acetate for 2 min at RT. Bars represent 20 nm.

2.3.1.2 Applying exogenous recombinant SOD1 aggregates to the extracellular environment of NSC-34 mouse motor neuron like cells

Our group and others have previously shown that aggregated human SOD1 can be taken up by neuronal cells (Grad et al., 2014; Münch et al., 2011; Sundaramoorthy et al., 2013). To confirm these results and further investigate entry, preformed SOD1 aggregates were added to the media of NSC-34 cells (Figure 2.2). Following incubation of the cells with the SOD1 aggregates for 60 min, the aggregates could be detected in association with the cells by flow cytometry Figure 2.2A). Next, to further investigate whether the SOD1 aggregates had entered into NSC-34 cells, cells were incubated with SOD1 aggregates for 60 min and lysed. Immunoblotting of cell lysates resulted in bands corresponding to the size of SOD1, including SDS resistant high molecular weight (HMW) species (Figure 2.2B).

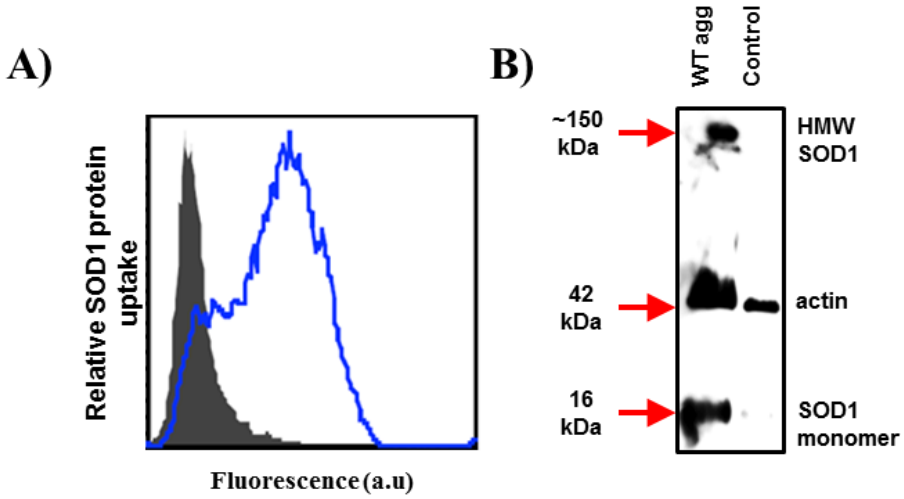

Figure 2.2 SOD1 protein aggregates are internalised into NSC-34 cells. (A) NSC-34 cells were incubated with 20 µg/ml of SOD1 aggregates (blue line) or PBS alone (no protein, gray line) for 60 min at 4°C. Cells were harvested, labelled with anti-sheep IgG conjugated to Alexa Fluor 488. (B) *(Right panel)* Western blot of cell lysates detecting human SOD1 (and actin as a loading control). Lysates from NSC-34 cells were treated with SOD1 aggregates or PBS (control) for 60 min at 4°C and were separated by SDS-PAGE under non-reducing conditions, transferred to nitrocellulose membrane and probed with streptavidin-peroxidase and mouse anti-actin mAb. Arrows indicate approximate size of each band. Results are representative of at least 2 independent experiments.

2.3.1.3 Uptake into NSC-34 cells is specific for SOD1 and occurs rapidly

To further characterise the entry of SOD1 aggregates into NSC-34 cells, putative uptake of SOD1 was investigated (Figure 2.3). NSC-34 cells were incubated with soluble SOD1 or

aggregates for 30 min and immediately examined by flow cytometry (Figure 2.3A). Incubation with the soluble (properly folded) WT SOD1 and non-aggregated ALS associated mutant G93A SOD1 resulted in a significant increase in fluorescence compared to control cells in the absence of protein. Similarly, aggregated WT SOD1 also associated with cells when compared to the cells incubated in the absence of protein. In contrast, there was no statistically significant increase in immunofluorescence after incubation with an unrelated control protein GST suggesting that the uptake of both soluble and aggregated forms of SOD1 is relatively specific. Next, to examine whether these aggregates enter cells efficiently and rapidly, cells were incubated with SOD1 aggregates at 4ºC for 30 min. SOD1 aggregates were found associated with the surface of NSC-34 cells after the 30 min incubation (Figure 2.3B), suggesting that interaction occurs relatively rapidly, given that endocytosis is slowed and or inhibited by ice cold temperatures. To show that the observed SOD1 aggregates associated with the cell surface are taken up by NSC-34 cells, cells were incubated with the aggregates and treated with Triton X-100 detergent which non-selectively permeabilises membranes. Similar to the flow cytometry observations described above, SOD1 aggregates were no longer detected on the cell surface at 60 min (Figure 2.3C nevertheless they were detected following permeabilisation of cells with Triton X-100, consistent with their internalisation (Figure 2.3D).

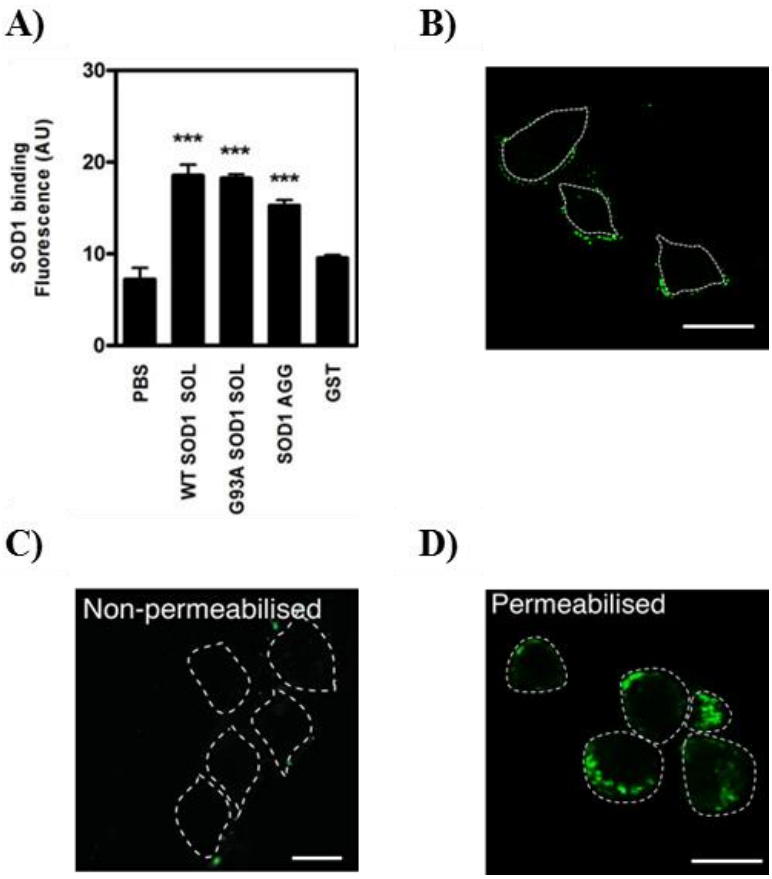

Figure 2.3 SOD1 protein aggregate are internalised rapidly into NSC-34 cells. (A) NSC-34 cells treated with 20 µg/ml of soluble and aggregated WT SOD1, GST or PBS (no protein, control) for 30 min at 37°C, fixed with 4% PFA, permeabilised and labelled with Alexa Fluor 488 streptavidin. Uptake of proteins was determined by flow cytometry and results shown as means ± SE, $n = 3$, $^{***}P < 0.001$ compared to corresponding control. (B) NSC-34 cells treated with 20 µg/ml of aggregated SOD1 for 30 min at 4°C, fixed with 4% PFA, and labelled with Alexa Fluor 488 streptavidin. Slides were analysed by confocal microscopy. Bars represent 20 µm. (C-D) NSC-34 cells treated with 20 µg/ml of aggregated SOD1 for 60 min at 4°C, fixed with 4% PFA, permeabilised (or not) and labelled with Alexa Fluor 488 streptavidin. Slides were analysed by confocal microscopy. Outline of cells from transmission images are indicated with white dashed lines. Bars represent 20 µm. Results are representative of at least 3 independent experiments.

2.3.1.4 SOD1 protein aggregates are not solely bound to the cells surface

Next, the possibility that WT and G93A SOD1 aggregates were bound primarily to the cell surface was investigated. Previous work has used trypsin digestion to remove surface-bound proteins (Wu et al., 2013). Incubation with 0.25% trypsin post treatment with SOD1 aggregates induced no significant differences in SOD1 signal, with similar levels of WT and G93A SOD1 aggregate uptake in the presence or absence of trypsin, indicating that signal observed in the flow cytometry experiments was not solely due to SOD1 aggregates associated with the cell membrane, rather SOD1 aggregates were inside cells (Figure 2.4A and B).

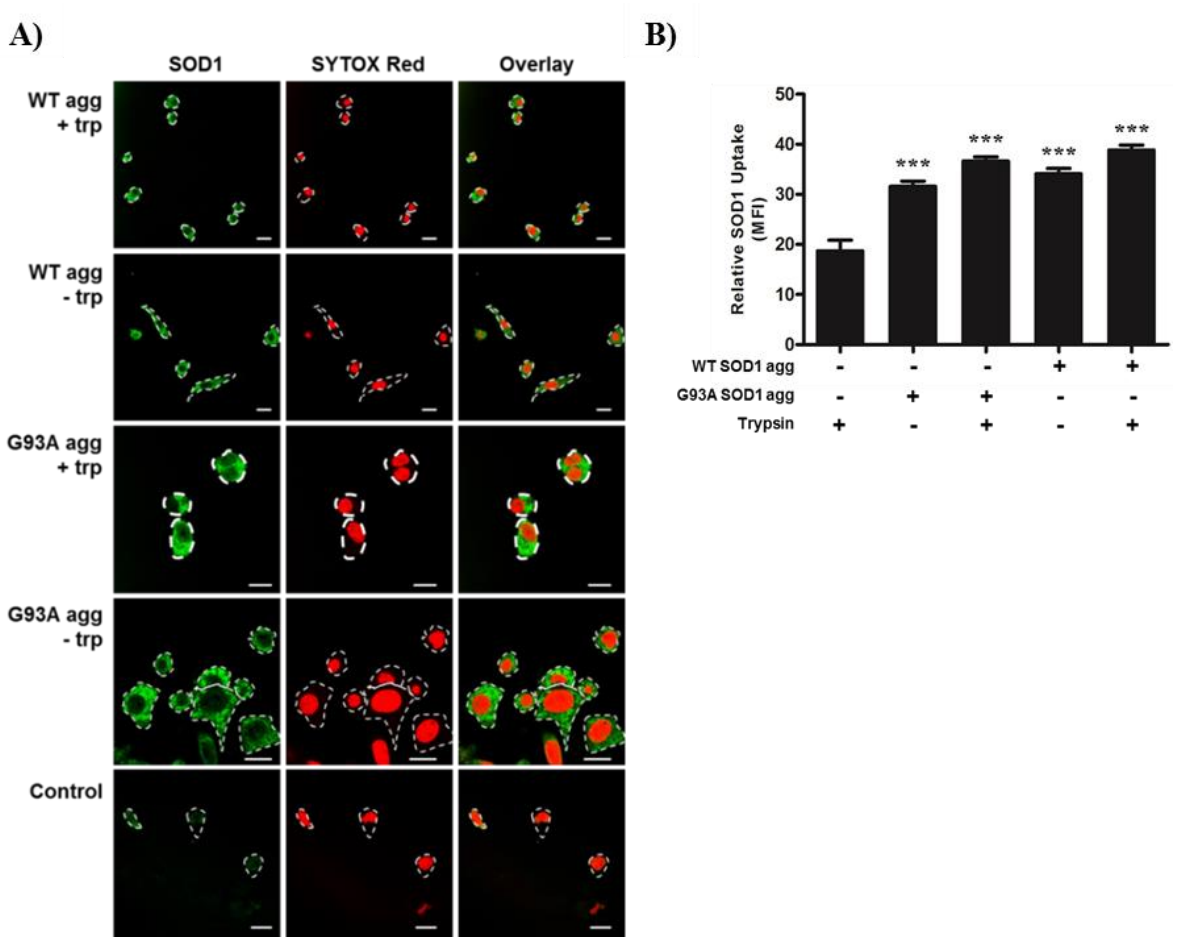

Figure 2.4 SOD1 aggregates are detected inside in NSC-34 cells. Adherent NSC-34 cells were incubated with 20 µg/ml of aggregated SOD1 or PBS (no protein, control) for 1 h at 37°C. Cells were then incubated with 0.25% trypsin or PBS (control) for 5 min at 37°C. Suspended cells were re-plated for 6 h at 37°C before fixation and immunocytochemistry. Biotinylated aggregates were detected with streptavidin-Alexa488. Sytox Red (5 µM) was used as a counter stain (10 min at RT). Outline of cells from transmission images are indicated with white dashed lines. Bars represent 20 µm. Mean fluorescence intensities (MFI) of SOD1 aggregate uptake were quantified from these images using ImageJ software (Version 1.48) (National Institutes of health, Bethesda, MD). Results shown as mean cellular fluorescence intensity means ± SD, $n > 3$, $^{***}P < 0.001$ compared to corresponding control (no protein treatment).

2.3.1.5 Digestion of membrane proteins by trypsin inhibits SOD1 uptake

Since SOD1 aggregate uptake had been observed and quantified, the possible role of membrane proteins in the uptake into NSC-34 cells was next investigated. To investigate whether an association between SOD1 aggregate uptake and membrane proteins exists, cells were pre-treated with trypsin prior to the addition of SOD1 aggregates (Figure 2.5). In the absence of a pre-incubation step with trypsin, a significantly higher fluorescence intensity was measured for both WT and G93A protein aggregate treatments, compared to cells pre-incubated with trypsin. This indicates that digestion of plasma membrane associated proteins

result in significant inhibition of aggregate association with cells, suggesting that the uptake of SOD1 aggregates is dependent upon cell surface proteins.

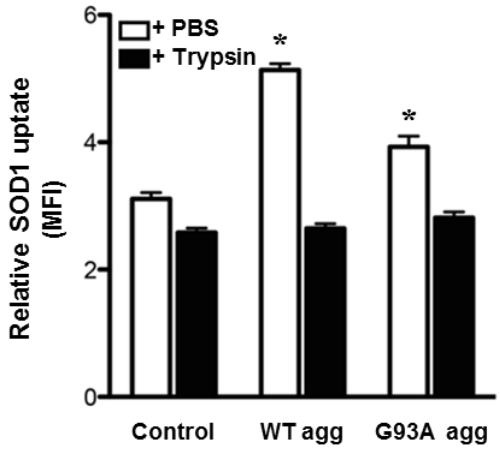

Figure 2.5 SOD1 protein aggregates associate with NSC-34 cells *via* membrane proteins. Internalisation of aggregated WT and G93A SOD1 (20 µg/ml) proteins for 30 min at 37oC, in the absence (control) or presence of a pre-incubation step with 0.05% trypsin for 10 min at 37°C. MFI of 10 kDa dextran conjugated to Alexa Fluor 647 uptake was measured using flow cytometry. Results shown as geometric means ± SD, $n = 6$. Results shown as mean cellular fluorescence intensity means ± SD, $n > 30$, $^{*}P < 0.05$ compared to corresponding control (no protein treatment).

2.3.2 SOD1 aggregates are internalised *via* macropinocytosis pathways in NSC-34 cells

2.3.2.1 Pharmacological inhibitors of Macropinocytosis reduce SOD1 aggregate uptake in NSC-34 cells

Previous studies have shown that small molecules that inhibit actin rearrangement, Na^+/H^+ exchangers, Pak-1, PI3K, and PKC suppress aggregate uptake (Grad et al., 2014; Munch et al., 2011; Sundaramoorthy et al., 2013), consistent with macropinocytosis. However, it remains to be shown whether SOD1 triggers macropinocytosis through an interaction with cells or whether aggregates are taken up by a constitutive process. To investigate the involvement of macropinocytosis-like pathways in the uptake of SOD1 aggregates into NSC-34 cells, cells were firstly incubated in the absence or presence of EIPA (an inhibitor of the Na^+/H^+ exchanger and subsequent endocytosis) and rottlerin (an inhibitor of PKC), as reported previously (Grad et al., 2014; Munch et al., 2011; Sundaramoorthy et al., 2013), and assessed by confocal microscopy and the mean fluorescence intensity for SOD1 uptake determined by flow cytometry (Figure 2.6).

Similar to previous experiments (Grad et al., 2014; Münch et al., 2011; Sundaramoorthy et al., 2013), incubation with rottlerin and EIPA resulted in a significant reduction in the uptake of SOD1 aggregates by (37±5% and 76±4%, Figure 2.6B) and (49±1% and 44±1%, Figure 2.6D for the WT and G93A aggregate treated cells respectively, compared to cells incubated in the absence of inhibitors. However, inhibitors of clathrin (chlorpromazine) or caveolin (genistein) dependent endocytosis had no significant effect on the uptake process. Therefore, similar results were found regardless of whether or not the aggregates were WT or mutant G93A SOD1. When soluble (non-aggregated) WT SOD1 (Figure 2.6C) was applied to cells (Figure 2.6A) pre-incubated with EIPA, a significant reduction in SOD1 uptake was also observed (48±8%). Similarly, pre-incubation with rottlerin suppressed WT SOD1 uptake by (50±9%), however, this was not statistically significant. Although rotterlin (44±6%), EIPA (50±9%) as well as genistein (43±6%) had some effect on reducing the uptake of G93A SOD1 proteins into cells, pre-incubation with chlorpromazine hydrochloride was able to significantly suppress uptake by (65±0.5%). Likewise, immunocytochemical analyses confirmed these flow cytometry results, whereby lower signals of immunofluorescence are indicative of reduced uptake of SOD1 proteins.

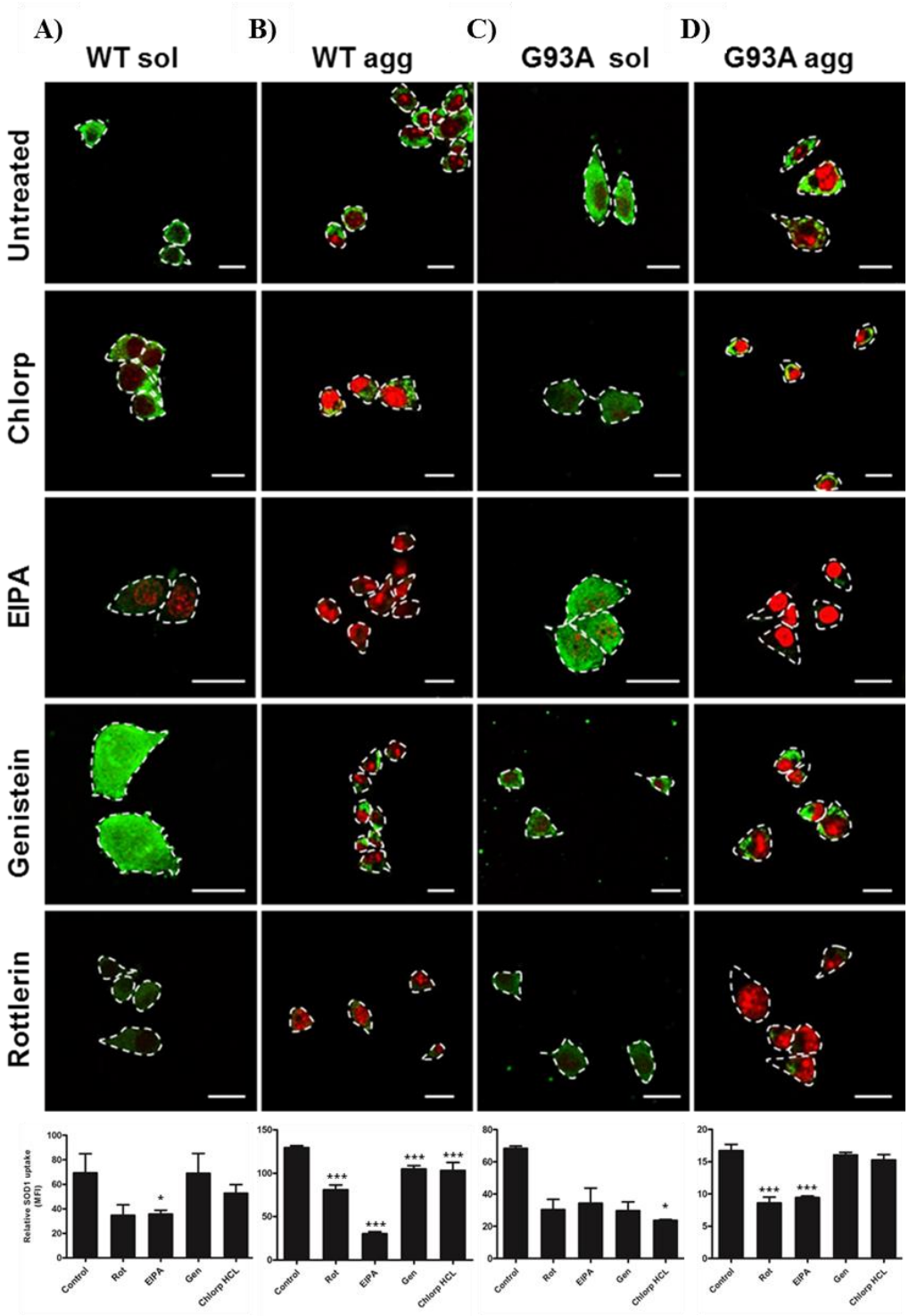

Figure 2.6 Small molecule inhibitors block SOD1 uptake. NSC-34 cells treated with 20 µg/ml of (A-C) soluble or (B-D) aggregated SOD1 proteins (20 µg/ml) for 30 min at 37°C, in the absence (control) or presence of a pre-incubation step with either rottlerin (3 µM) a PAK-1 and PKC inhibitor, EIPA (100 µM) a Na+/H+ exchange inhibitor, genistein (10 µM) a caveolin mediated uptake inhibitor or chlorpromazine hydrochloride (Chlorp HCL) (5 mM) a clathrin mediated endocytosis inhibitor, fixed with 4% PFA, permeabilised and labelled with either (A-C) anti-human SOD1 Ab (soluble) or (B-D) Alexa Fluor 488 streptavidin. Slides were analysed by confocal microscopy. Outline of cells are indicated with white dashed lines. Bars represent 20 µm. Results are representative of at least $n = 3$. Uptake of proteins under the same conditions were determined by flow cytometry and results shown as mean fluorescence intensity ± SD, $n = 6$, $^{***}P < 0.001$ or $^{*}P < 0.05$ compared to corresponding control.

2.3.3 SOD1 aggregates trigger cell surface ruffling and activate RAC1 in NSC-34 cells allowing the exploitation of macropinocytosis as a route of entry into cells

2.3.3.1 SOD1 aggregates induce cell surface ruffles and blebs in the membrane to enter into NSC-34 cells

Actin cytoskeleton restructuring and the formation of ruffles and blebs in the cellular surface are required for macropinocytosis and are generally formed upon an external stimuli such as growth factors but can be triggered by a variety of other particles such as bacteria, apoptotic bodies, necrotic cells and viruses (Swanson and Watts, 1995; Mercer and Helenius, 2012). Since macropinocytosis has been implicated in SOD1 uptake (Münch et al., 2011; Sundaramoorthy et al., 2013), the possible role of SOD1 aggregates in stimulating cellular ruffles and blebs was investigated. To test whether there were any perturbations to the cell surface membrane caused by incubation with SOD1, cells were treated with either PMA (positive control) or SOD1 (aggregated and non-aggregated), for 2 h and then the detailed morphology of cells was examined by field emission scanning electron microscopy (FESEM) (Figure 2.7). In the absence of protein treatment, little to no membrane perturbations were observed (Figure 2.7A), however, incubation with 200 nM PMA resulted in an obvious increase in membrane perturbations, including ruffles and blebs (Figure 2.7B), consistent with an activation of macropinocytosis. Incubation with soluble WT (Figure 2.7C) and G93A SOD1 (Figure 2.7D) did not induce such membrane perturbations. In contrast, incubation with aggregated WT (Figure 2.7E) and G93A SOD1 (Figure 2.7F) induced pronounced membrane ruffling and blebbing consistent with stimulated macropinocytosis. Subsequent quantifiable investigations into membrane perturbations induced by SOD1 were therefore carried out.

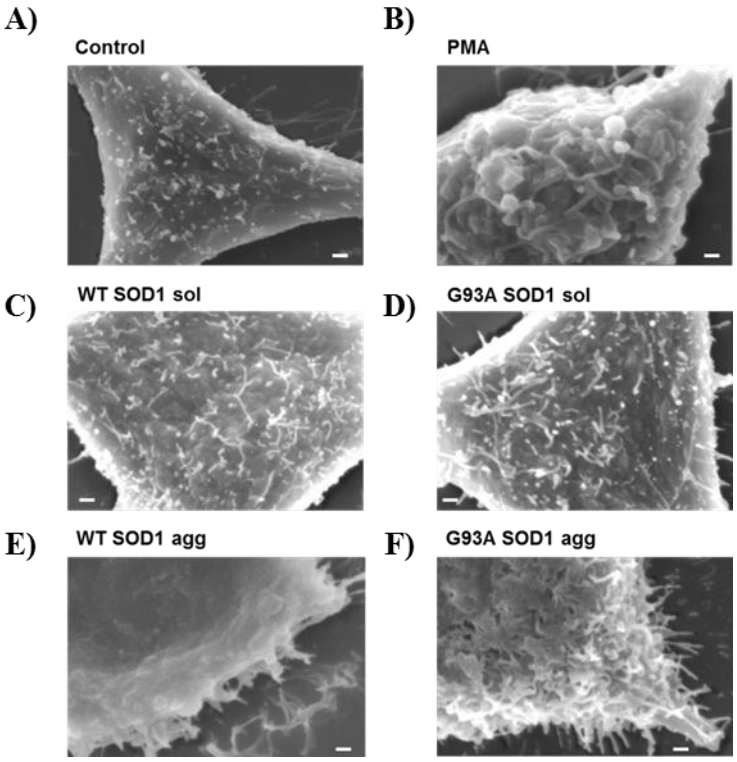

Figure 2.7 Aggregated SOD1 induces ruffles in the plasma membrane of NSC-34 cells. NSC-34 cells were serum starved for 24 h and were incubated with (A) PBS (control, no protein), (B) PBS containing 200 nm PMA or 20 µg/ml of (C-D) soluble (non-aggregated) and (E-F) aggregated SOD1, for 2 h, fixed with 2.5% glutaraldehyde/4% PFA in 0.1 M phosphate buffer for 3 h, postfixed in 2% OsO4/ water, dehydrated using a gradient of ethanol (30-100%, 30 min per treatment), critical point dried for 2 h and coated with graphite-gold. Increases in membrane perturbations can be observed, such as ruffles and blebs. Slides were analysed by field emission scanning electron microscopy. Bars represent 1 µm. Results are representative of n = 2.

2.3.3.2 SOD1 protein aggregates induce significant membrane perturbations in the cellular surface of NSC-34 cells

To visualise and quantify the extent of observed SOD1 aggregate-induced membrane perturbation to the cellular surface of NSC-34 cells, cells were treated with either PMA or SOD1 (aggregated and non-aggregated), prior to incubation with the membrane dye FM 1-43FX (Figure 2.8). FM1-43FX has been used in previously for studies of membrane perturbation during growth cone ruffling (Kolpak et al., 2009). Fluorescence images of NSC-34 cells were then acquired (Figure 2.8A) and quantified (Figure 2.8B). In cells treated with PMA, a significant increase in membrane dye fluorescence was observed (57±2) compared to cells incubated in the absence of protein (30± 0.7). Similarly, incubation with WT (63±1) and G93A (69±3) soluble SOD1 also resulted in a significant increase in fluorescence.

Nevertheless, there was a three-fold higher mean fluorescence intensity for membrane fluorescence in cells incubated with WT (97±6) and G93A (93±3) SOD1 aggregates, consistent with an increase in membrane perturbation.

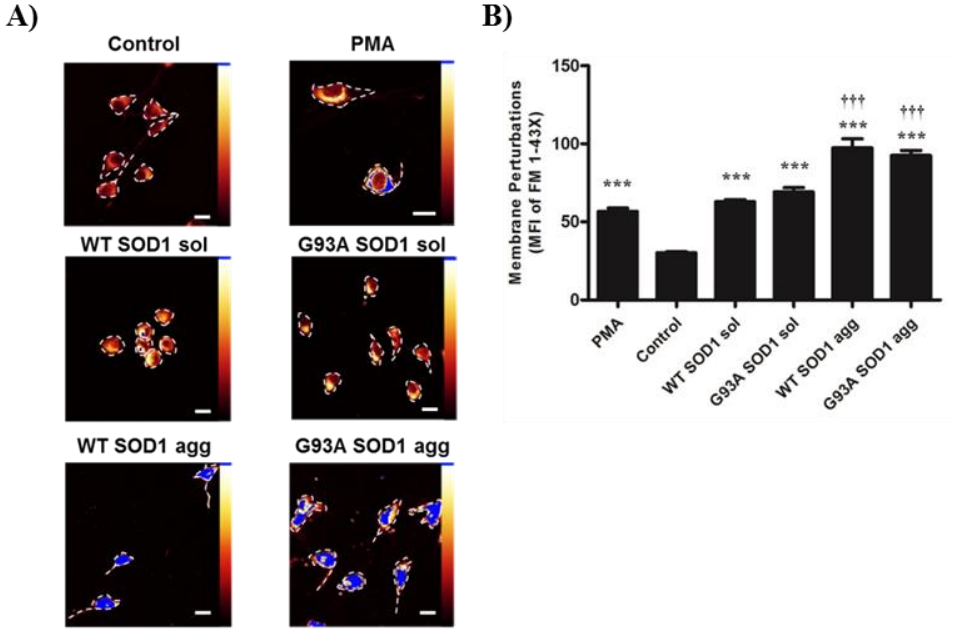

Figure 2.8 SOD1 aggregates induce membrane perturbations in the cell surface of NSC-34 cells (A) NSC-34 cells were incubated with PBS alone, 200 nM PMA or 20 µg/ml of aggregated SOD1for 60 min at 37°C, incubated with the membrane dye FM1-43FX and fixed with 4% PFA. Outline of cells are indicated with white dashed lines. Bars represent 20 µm. (B) Mean fluorescence intensities (MFI) of membrane dye per cell were quantified from these images using ImageJ software (Version 1.48) (National Institutes of health, Bethesda, MD). A minimum of 200 cells were scored per treatment. Results shown as mean cellular fluorescence intensity means ± SD, n = 3, $^{***}P$ <0.001 compared to corresponding control (no protein treatment); $^{†††}P$ < 0.001 compared to corresponding soluble protein.

2.3.3.3 SOD1 aggregates interact with the cell surface to trigger fluid phase uptake

Macropinocytosis is a form of fluid phase endocytosis that engulfs solutes at whatever concentrations they are found in the extracellular medium, rather than concentrating ligands at the cell surface. Thus, activation of macropinocytosis is well known to induce a transient increase in dextran, a fluid phase marker (Kerr and Teasdale, 2009). To investigate whether the interaction of SOD1 aggregates with cells triggers an increase in fluid phase uptake, NSC-34 cells were incubated in the presence of both SOD1 and 10 kDa dextran conjugated to Alexa Fluor 647 and assessed by both confocal microscopy (Figure 2.9A) and flow cytometry (Figure 2.9B). Firstly, cells incubated in the presence of both WT and G93A SOD1 aggregates displayed an increase in fluid uptake compared to the untreated cells, with little to

no difference observed for the cells treated with soluble SOD1. Next, cells were then analysed by flow cytometry. Again, incubation with both WT (16±0.1%) and G93A (18±0.3%) SOD1 aggregates triggered a significant increase in dextran uptake compared to that in the absence of treatment (9±0.2%) or following incubation with WT (13±0.2%) and G93A (13±0.1%) soluble SOD1. Whilst there was a small increase in dextran uptake in cells treated with the soluble SOD1 compared to those not treated, it was concluded that this was thus not attributable to stimulated macropinocytosis as it occurred in the absence of membrane ruffling (see above).

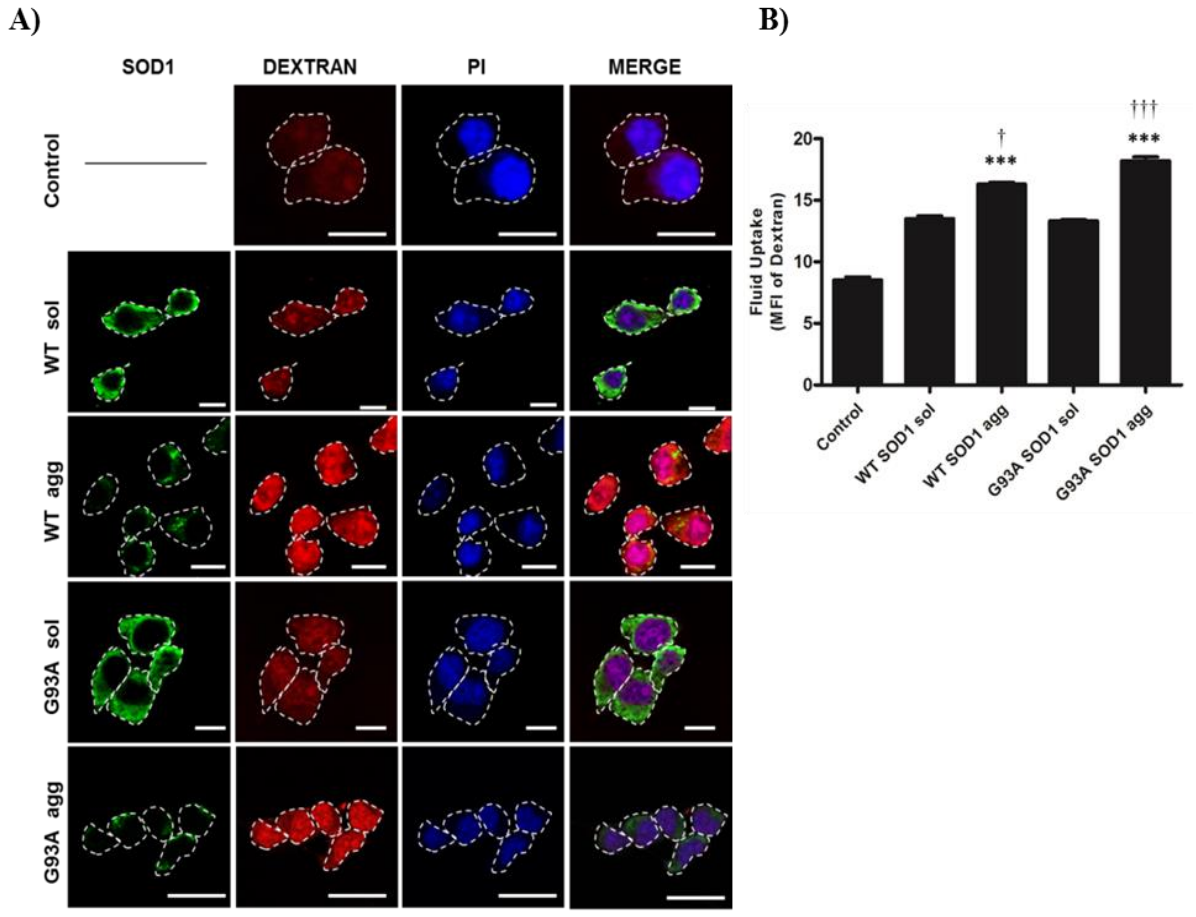

Figure 2.9 SOD1 aggregates trigger fluid phase uptake using fluorescently labelled dextran. NSC-34 cells were incubated with PBS alone (control) or 20 µg/ml of soluble and aggregated SOD1 for 30 min at 37°C, co-incubated with dextran Alexa-647 for 15 min, fixed with 4% PFA, permeabilised and labelled with either anti-human SOD1 Ab (non-aggregated/ soluble) or Alexa Fluor 488 streptavidin. Slides were analysed by (A) confocal microscopy. Outline of cells are indicated with white dashed lines. Bars represent 10 µm. Results are representative of at least $n = 3$. (B) Cells were firstly gated on forward (FSC) and side (SSC) scatter to exclude dead cells and the mean fluorescence intensities (MFI) of dextran Alexa-647 in NSC-34 cells was determined by flow cytometry. Results shown as means ± SD, $n = 6$; $^{***}P < 0.001$ compared to corresponding control; $^{†††}P < 0.001$ or $^{†}P < 0.05$ compared to corresponding soluble treatment.

2.3.3.4 Pharmacological Inhibitors of Macropinocytosis also inhibit dextran uptake into NSC-34 cells

To confirm that inhibitors of macropinocytosis can suppress dextran uptake into NSC-34 cells, cells were pre-incubated in the absence (PMA) or presence of pharmacological inhibitors of macropinocytosis or in the absence of PMA and inhibitors (mock) (Figure 2.10). As above (Figure 2.6) EIPA and rottlerin inhibited fluid phase uptake (quantified as uptake of 10 kDa dextran conjugated to Alexa647) stimulated by PMA treatment of NSC-34 cells, but genistein and chlorpromazine did not, demonstrating the specificity of the inhibitors to PKC-dependent fluid phase uptake.

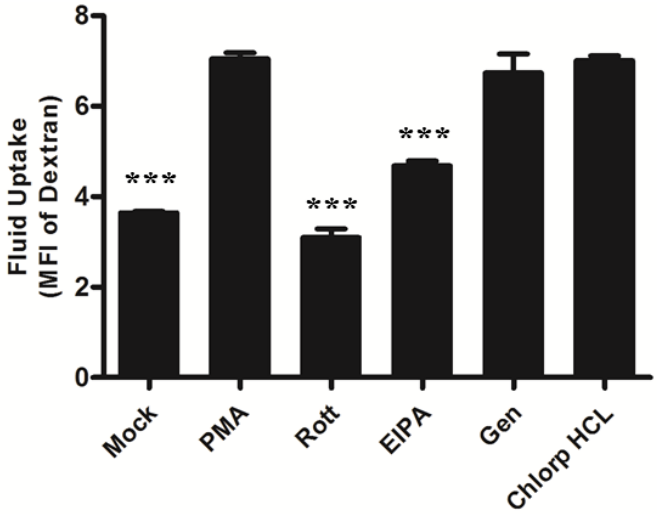

Figure 2.10 PMA induced dextran uptake is suppressed by inhibitors of macropinocytosis. The induction of fluid phase uptake was measured using fluorescently labelled dextran. NSC-34 cells were serum starved for 24 h and co-incubated with 200 nM PMA for 30 min, in the absence (PMA) or presence of a pre-incubation step with either rottlerin (3 µM), EIPA (100 µM), genistein (10 µM) or in the absence of PMA and inhibitors (mock) for 30 min, and co-incubated with dextran Alexa-647 for 15 min. Induced fluid uptake was determined by flow cytometry and results shown as mean cellular fluorescence intensity means. Cells were firstly gated on forward (FSC) and side (SSC) scatter to exclude dead cells and the mean fluorescence intensities (MFI) of dextran Alexa-647 in NSC-34 cells was determined by flow cytometry. Results shown as means ± SD, $n = 6$; $^{***}P < 0.001$ compared to corresponding PMA treatment.

2.3.4 RAC1-GTPase activation is required for SOD1 aggregate uptake into NSC-34 cells

2.3.4.1 SOD1 aggregates trigger RAC1 activation to enter into NSC-34 cells

To further characterise the role of SOD1 protein aggregates in stimulating macropinocytosis, additional events downstream of macropinocytosis activation were investigated. This included activation of the Rho GTPase RAC1, which is involved in triggering membrane

ruffling on the cell surface (Ridley et al., 1992). To investigate the activation status of RAC1 during entry of SOD1 aggregates into NSC-34 cells, cells were incubated with SOD1 and RAC1 activation was probed for using a G-LISA based assay (Figure 2.11). Incubation of cells with soluble SOD1 and aggregated WT SOD1 had no significant effect on RAC1 activation. While incubation with G93A SOD1 aggregates resulted in an almost one and a half–fold significant increase in the amount of activated RAC1 (RAC1-GTP) in NSC-34 cells.

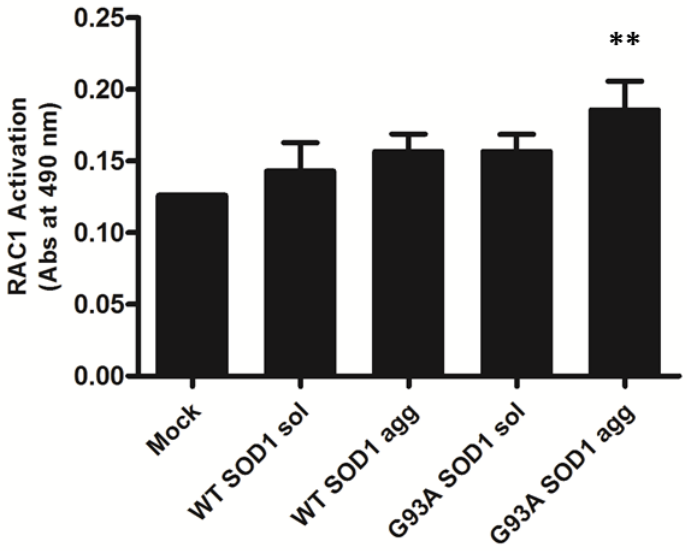

Figure 2.11 RAC1 has an important role in SOD1 aggregate entry into NSC-34 cells. NSC-34 cells were serum starved 24 h, incubated with PBS alone (mock) or 20 μg/ml of soluble and aggregated SOD1 for 30 min at 37°C and lysed. RAC1 activation was measured using a RAC1 activation G-LISA kit activation assay that probes for RAC1-GDP. Absorbance values of anti- RAC1 HRP at 490 nm were determined by spectrometry and results are shown as mean absorbances (490 nm) ± SD of 6 experiments, $^{**}P < 0.01$ compared to corresponding mock.

2.3.4.2 Addition of RAC1 inhibitor reduces SOD1 uptake.

To further examine the role of RAC1 in the uptake of SOD1 aggregates, the effect of the RAC1 inhibitor W56 on SOD1 aggregate uptake was investigated (Figure 2.12). Significant WT (19±0.4%) and G93A (21±0.4%) SOD1 aggregate uptake was observed in cells incubated in the absence of W56. However, pre-treatment with W56 significantly suppressed the uptake of WT (12±0.1%) and G93A (17±0.2%) SOD1 aggregates into NSC-34 cells.

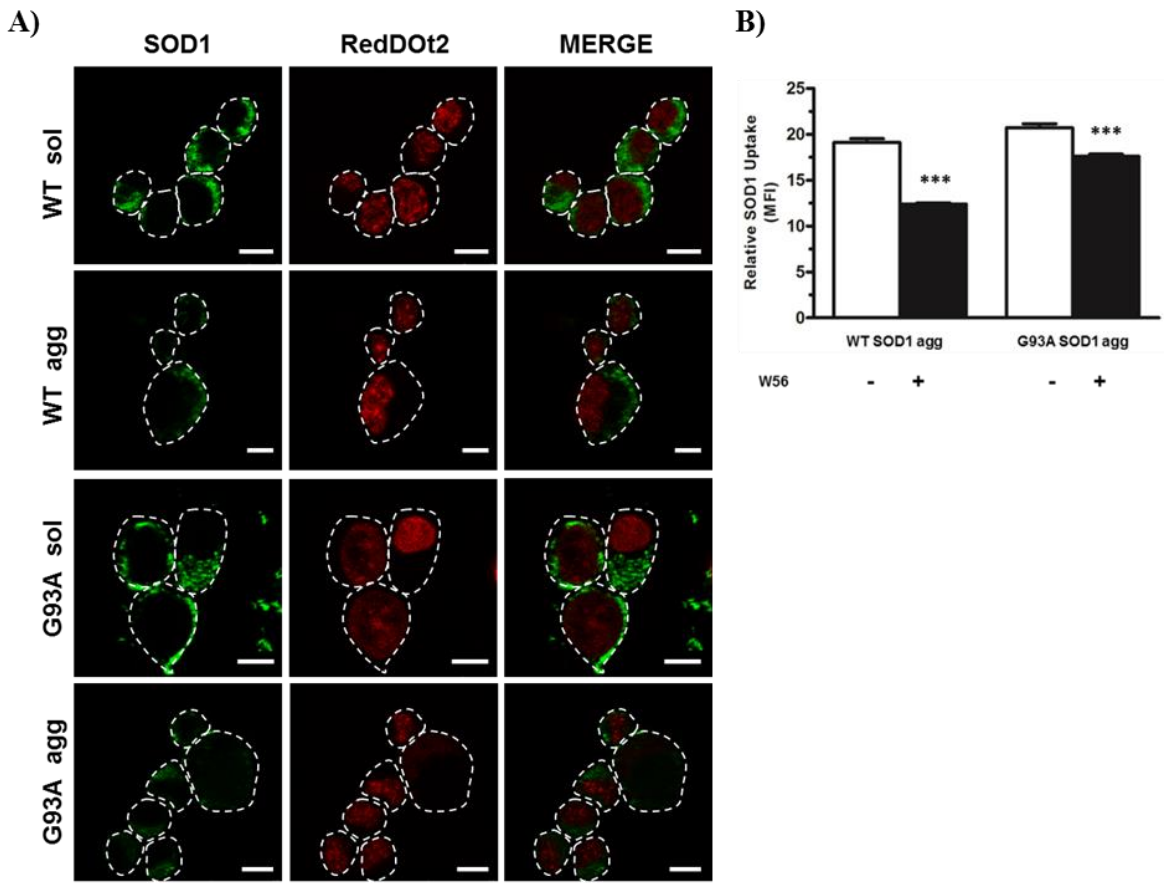

Figure 2.12 RAC1 inhibitor W56 suppresses the uptake of SOD1 aggregates. NSC-34 cells treated with 20 µg/ml of aggregated SOD1 proteins (20 µg/ml) for 30 min, in the absence (control) or presence of a pre-incubation step with RAC1 inhibitor W56 (200 µM) for 1 hr, fixed with 4% PFA, permeabilised and labelled with either anti-human SOD1 Ab (non-aggregated/ soluble) or Alexa Fluor 488 streptavidin. (A) Slides were analysed by confocal microscopy. Outline of cells are indicated with white dashed lines. Bars represent 10 µm. (B) Mean fluorescence intensities (MFI) per cell of a minimum of 100 cells were quantified from these images using ImageJ software (Version 1.48) (National Institutes of health, Bethesda, MD). Results shown as mean cellular fluorescence intensity means ± SD, n = 3, $^{***}P$ <0.001 compared to corresponding control (absence of RAC1 inhibitor).

2.3.4.3 RAC1 inhibitor W56 suppresses the formation of Ruffles in the cell surface in NSC-34 cells

Lastly, the effect of the W56 on ruffle formation in NSC-34 was investigated. Cells were incubated with PMA in the presence or absence of pre-treatment with W56 and then examined for membrane perturbations using membrane dye FM1-43FX (Figure 2.13). PMA induced ruffle formation (112±1%) was significantly inhibited upon incubation with W56 (72±2%). Collectively, these results confirm that RAC1 activation is upstream of membrane

ruffling, which in turn is required for macropinosome formation and entry of SOD1 aggregates into NSC-34 cells.

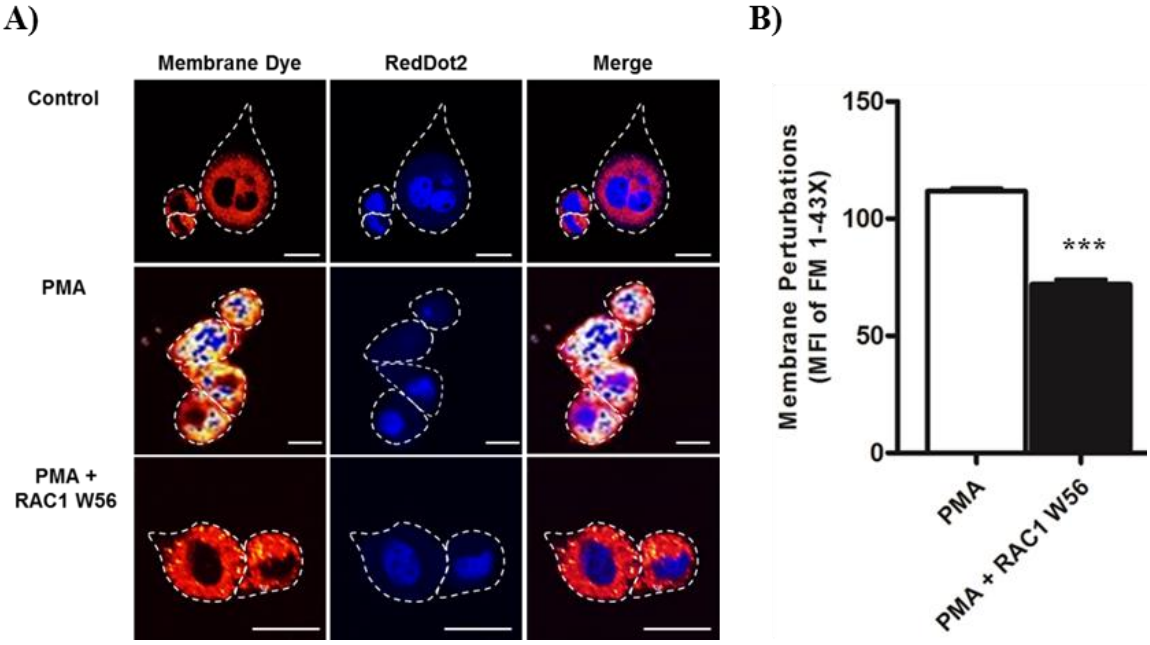

Figure 2.13 RAC1 activation is upstream of membrane ruffling. (A) NSC-34 cells treated with 200 nM PMA for 30 min, in the absence (PMA) or presence of a pre-incubation step with RAC1 inhibitor W56 (200 µM) or absence of PMA and inhibitor (control) for 1 hr, incubated with the membrane dye FM1-43FX for 7 min and fixed with 4% PFA. 1X RedDot2 was used as a counter stain (10 min, RT). Outline of cells are indicated with white dashed lines. Bars represent 10 µm. (B) Mean fluorescence intensities (MFI) of membrane dye per cell were quantified from these images using ImageJ software (Version 1.48) (National Institutes of health, Bethesda, MD). A minimum of 200 cells were scored per treatment. Results shown as mean cellular fluorescence intensity means ± SD, n = 6, $^{***}P < 0.001$ compared to corresponding control (no protein treatment); $^{\dagger\dagger\dagger}P < 0.001$ compared to corresponding soluble protein.

2.3.5 SOD1 induced macropinocytosis activation is not associated with cell death under experimental conditions, in NSC-34 cells

Membrane perturbations in the form of ruffling and blebbing are required for entry of particles and macromolecules to enter cells *via* macropinocytosis. However, protrusions of the plasma membrane in the form of blebs can also be found in association with cell injury, including apoptosis (Trump et al., 1997). To exclude the possibility that cells were blebbing due to apoptosis, cells were firstly incubated in the absence or presence of SOD1 proteins or the positive control etoposide (Schonn et al., 2010), and then the cells were examined for levels of activated caspase-3 over the 2 h time period of the experiment (Figure 2.14).

Incubation with SOD1 proteins; WT (25±1%) and G93A (20±2%) soluble (non-aggregated) and WT (9±0.3%) and G93A (10±1%) aggregates did not induce caspase 3 activation in cells above basal (22±0.5%) levels (PBS treated) in the timeframe of this experiment.

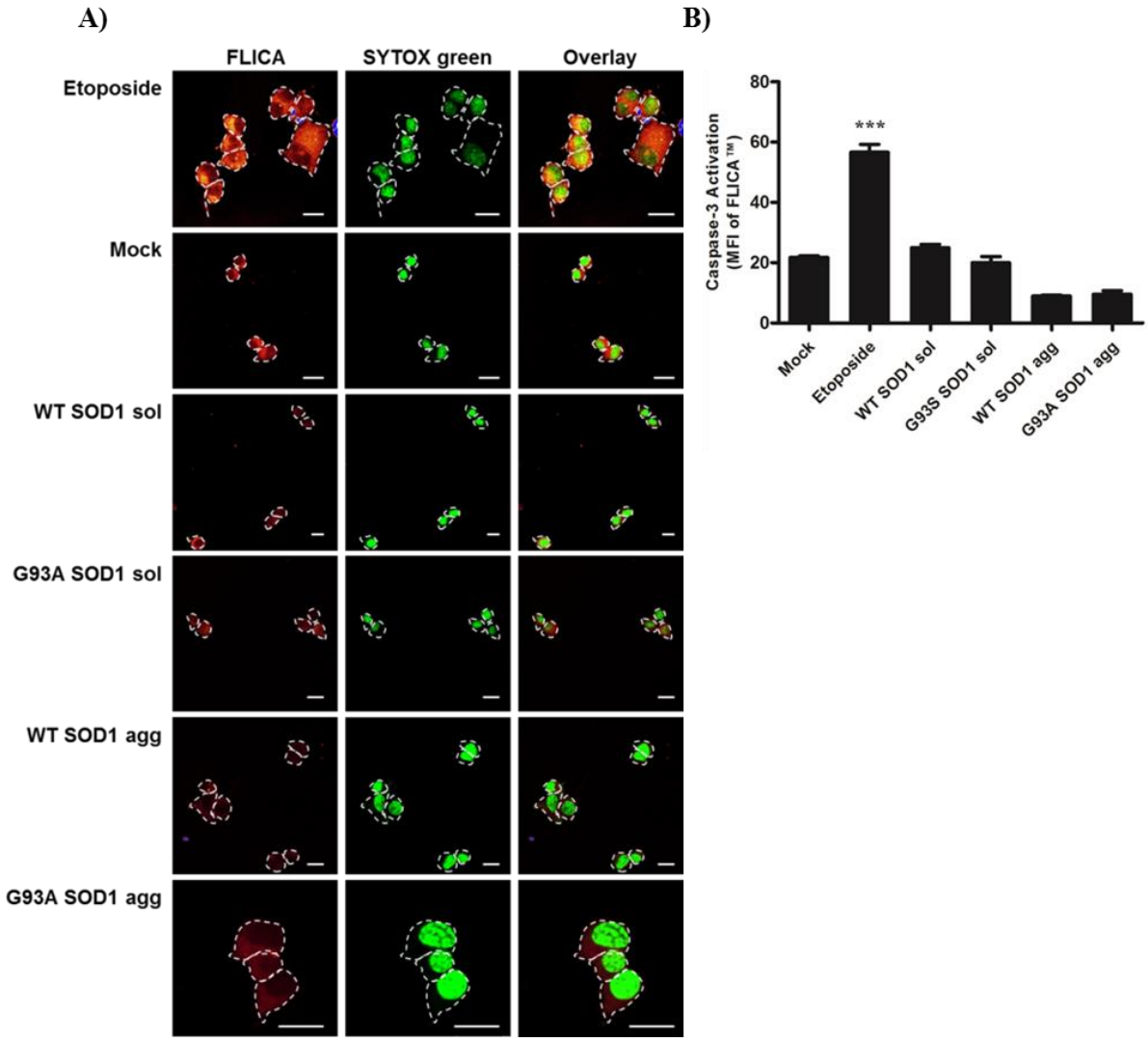

Figure 2.14 Addition of SOD1 does not induce rapid apoptosis. (A) NSC-34 cells were incubated with PBS alone (mock), 100µM etoposide or 20 µg/ml of aggregated SOD1 for 2 h at 37°C, followed by incubation with FLICA reagent and fixed with apoptosis fixative solution. The levels of activated caspase-3 were tested using Image-IT kit. Outline of cells are indicated with white dashed lines. Bars represent 20 µm. (B) Mean fluorescence intensities (MFI) of FLICA reagent per cell were quantified from these images using ImageJ software (Version 1.48) (National Institutes of health, Bethesda, MD). Results shown as mean cellular fluorescence intensity means ± SD, n = 3, $^{***}P$ <0.001 compared to corresponding control (no protein treatment).

2.4 Discussion

The current study confirms a role for stimulated macropinocytosis in the uptake of SOD1 aggregates into NSC-34 cells. The morphology of SOD1 aggregates were assessed in the current study and these short fibrillar aggregates were found to associate with NSC-34 cells *via* membrane proteins and efficiently internalise into cells. In addition, the addition of pharmacological inhibitors of macropinocytosis including EIPA, rottlerin and W56 disrupted the uptake of SOD1 aggregates into cells. Furthermore, this study demonstrated for the first time that aggregates of SOD1 trigger activation of the Rho GTPase RAC1, leading to the formation of membrane ruffles on the cell surface and fluid phase uptake that defines macropinocytosis. Collectively, this suggests that SOD1 aggregates are capable of stimulating macropinocytosis to facilitate their entry into NSC-34 cells. This process would facilitate further seeding of SOD1 aggregates similar to what is suggested to occur during progression of disease in SOD1 ALS.

It has been suggested that extracellular misfolded or aggregated SOD1 plays an active role in the spread of pathology among motor neurons (Grad et al., 2014; Münch et al., 2011), contributing to disease progression *via* interactions with both the cell surface and internalisation into cells in both fALS and sALS (Sundaramoorthy et al., 2013). In the current study, exogenously applied WT and mutant G93A SOD1 fibril-like aggregates were taken up efficiently by naïve motor neuron-like cells. Similarly, the uptake of extracellular WT SOD1 aggregates, recombinantly produced or derived from conditioned media has previously been observed (Grad et al., 2014; Sundaramoorthy et al., 2013). The morphology of human recombinant SOD1 proteins were amlyloid-like in structure, consistent with another study which suggest SOD1 positive inclusions derived from fALS patients do not stain with amyloid dyes (Kerman et al., 2010). Furthermore, the work presented here demonstrated that uptake of SOD1 was selective and rapid. Incubation with the soluble (properly folded) WT

SOD1 and non-aggregated ALS associated mutant G93A SOD1 resulted in their uptake into cells, to a similar extent to that of WT SOD1 aggregates. In contrast, there was no statistically significant increase in immunofluorescence after incubation with an unrelated control protein GST, suggesting that the uptake of both soluble and aggregated forms of SOD1 is relatively specific. Other studies have also utilised recombinant soluble SOD1 proteins and similarly demonstrated the uptake of soluble WT and mutant SOD1 (Sundaramoorthy et al., 2013). This may reflect the proposed role of non-classically secreted SOD1 in signal transduction (Damiano et al., 2013; Turner et al., 2005).

In the current study, SOD1 aggregates were shown to associate with the neuronal cell surface after 30 min incubation and after 60 min are no longer detected on the surface but instead are only detected following permeabilisation of cells with Triton X-100, suggesting these entered into cells with remarkable efficiency, consistent with reports from previous studies (Münch et al., 2011). Furthermore, this current study suggests that uptake of aggregates is dependent upon cell surface membrane proteins, since trypsinisation of potential endocytosis receptor proteins prior to treatment with aggregates significantly inhibited aggregate association with cells. This is consistent with another study which shows treatment of the cell surface with trypsin, inhibited the uptake of α-synuclein (Sung et al., 2001).

A role for macropinocytosis in the uptake of extracellular native and aggregated WT and mutant SOD1 into neuronal cells has been previously suggested (Grad et al., 2014; Münch et al., 2011; Sundaramoorthy et al., 2013). In these studies, the addition of small molecules that inhibit actin rearrangement, Na^+/H^+ exchangers, Pak-1, PI3K, and PKC was reported to impair the uptake of SOD1 aggregates (Grad et al., 2014; Munch et al., 2011; Sundaramoorthy et al., 2013), consistent with macropinocytosis. In the current study, EIPA (an inhibitor of the Na^+/H^+ exchanger and subsequent endocytosis) and rottlerin (an inhibitor of PKC), as reported previously (Grad et al., 2014; Munch et al., 2011; Sundaramoorthy et

al., 2013), were used to confirm the involvement of macropinocytosis-like pathways in the uptake of SOD1 aggregates into NSC-34 cells. EIPA and rottlerin inhibited the uptake of SOD1 aggregates, however, inhibitors of clathrin (chlorpromazine) or caveolin (genistein) dependent endocytosis had no significant effect on this process. Furthermore, this process differs from that responsible for the uptake of soluble SOD1 proteins, which occurs presumably *via* a constitutive form of pinocytosis in the case of the WTSOD1 and potentially *via* a range of mechanisms in the case of soluble G93A SOD1. Thus, these results suggest a primary role for macropinocytosis in the uptake of SOD1 aggregates

While previous work demonstrated a role for macropinocytosis in the uptake of SOD1 aggregates into neuronal cells, it had been unclear whether macropinocytosis is triggered through an interaction of SOD1 with cells or whether aggregates are taken up by some other constitutive process. SOD1 aggregate-mediated *activation* of macropinocytosis and subsequent internalisation into NSC-34 cells was confirmed in the current study. Triggering the activation of macropinocytosis leads to the entry of large amounts of solute macromolecules or particles too large for other forms of endocytosis across the plasma membrane (Swanson and Watts, 1995). Activation of macropinocytosis has been reported to induce a number of downstream signaling events including the activation of a Rho GTPase, RAC1 (Ridley et al., 1992), which contributes to the modulation of ruffle formation, macropinosome closure and membrane trafficking (Lanzetti et al., 2004).

Activated RAC1, has been identified as an important and central player in triggering membrane ruffles and blebbing in the form of lamellipodia, circular-shaped membrane extensions (ruffles) and large plasma membrane extrusions (blebs) (Mercer and Helenius, 2009), associated with virus entry into cells and has been found to do so by activating downstream effectors of actin polymerisation (Sanchez et al., 2012). While the precise role of PKC in virus entry is still unclear, its activation with PMA (as used in this current study) can

induce ruffling and fluid uptake in the absence of ligands that bind the cell surface (Swanson, 1989). The activation of RAC1 and subsequent membrane ruffling was supported in the current study. Similarly, intracellular mutant SOD1 has been found to interact with and activate RAC1 (Harraz et al., 2008). Of note, inhibition of RAC1, supressed the uptake of SOD1 aggregates, thus implicating these membrane perturbations in SOD1 entry. As expected, incubation with SOD1 aggregates induced increased membrane perturbations, including ruffles (retracting) and blebs, consistent with the formation of large vacuoles (macropinosomes) at the plasma membrane, thus further supporting uptake of SOD1 aggregates occurs as part of the activation of macropinocytosis process. Of note, the current study confirmed that activation of RAC1 activation is upstream of membrane ruffling.

Macropinocytosis is a form of fluid phase endocytosis that engulfs fluids and solutes at whatever concentrations they are found in the extracellular medium, rather than concentrating ligands at the cell surface. The data presented here shows that the activation of macropinocytosis mediated by SOD1 aggregates induced fluid uptake, coinciding with the formation of membrane ruffling, attributable to stimulated macropinocytosis. EIPA and rottlerin inhibited fluid phase uptake (quantified as 10 kDa dextran conjugated to Alexa Fluor 647uptake) stimulated by phorbol 12-myristate 13-acetate (PMA) treatment of NSC-34 cells, but genistein and chlorpromazine did not, demonstrating the specificity of the inhibitors to PKC-dependent fluid phase uptake.

In addition to SOD1 aggregates, various viruses, such as the vaccinia virus, adenovirus 3, herpes simplex virus 1 and HIV, utilize macropinocytosis to gain entry to cells. This phenomenon is likely to be due to the fact that macropinosomes are not restricted in size, enabling even large virions to be internalised, and that many cell types, not just professional phagocytes (such as macrophages), have the ability to activate the macropinocytosis

pathways (Swanson and Watts, 1995). Indeed, macropinocytosis can be activated in neurons by interactions with large viral particles (Kalia et al., 2013).

While it was not confirmed in this study whether addition of recombinant SOD1 induced stress, previous studies have found that addition of extracellular recombinant mutant and/or aggregated SOD1 to naïve neuronal cells induce ER stress (Sundaramoorthy et al., 2013). In the current study, NSC-34 cell death was not observed following incubation with SOD1 aggregates in the short timeframe of the experiment, as apoptosis is likely to occur at a much longer incubation period (least 10 hours). Collectively, this suggests that SOD1 aggregates are capable of mediating macropinocytosis, independent of cell death.

In conclusion, the current study represents the first findings of SOD1 aggregate mediated activation of macropinocytosis pathways, similar to those utilized by virions, in neuronal cells, in the specific context of ALS. While, this was not demonstrated *in vivo*, it is likely that the activation of macropinocytosis occurs potentially alongside other pathways. Indeed, future studies investigating whether macropinocytosis occurs *in vivo* is warranted. Collectively, this suggests that extracellular SOD1 aggregates together with the activation of macropinocytosis are key components of ALS progression. Thus, future investigations into the role of SOD1-induced activation of macropinocytosis during disease progression in SOD1-ALS *in vivo* are warranted.

Chapter 3

SOD1 AGGREGATES PROPAGATE IN A PRION-LIKE MANNER

3.1 Background

Amyotrophic lateral sclerosis (ALS) is a fatal and rapidly progressing neurodegenerative disorder, affecting both upper and lower motor neurons. ALS is characterised by a focal onset of motor neuron degeneration, followed by outward neurospatial spreading of disease pathology, to neighbouring neurons and to distant regions *via* axonal pathways (Braak et al., 2013). One potential explanation for the progressive spread of pathology is the prion-like propagation of protein misfolding. Evidence is mounting that ALS associated proteins, such as SOD1, may play an active role in the systematic spread of disease pathology (Ayers et al., 2016; Grad et al., 2014; Münch et al., 2011; Zeineddine and Yerbury, 2015).

For propagation of aggregation to occur, the newly formed intracellular aggregates must initially be released into the extracellular space. The secretion or release of SOD1 by neuronal cells has been suggested to occur *via* both active mechanisms such as the secretion of proteins from cells *via* exosomes and passive mechanisms such as cell death, as previously demonstrated *in vivo* (Gomes et al., 2007; Grad et al., 2014; Urushitani et al., 2006). Both human wild type (WT) and mutant SOD1 proteins have been observed in association with vesicles, particularly exosomes (Gomes et al., 2007; Grad et al., 2014; Silverman et al., 2016) or released as free aggregates as a result of cell death (Grad et al., 2014). SOD1 has also been detected in the cerebrospinal fluid of ALS patients with and without SOD1 mutations and in animals, implying its release *via* non-classical mechanisms (Jacobsson et al., 2001; Winer et al., 2013; Zetterstrom et al., 2011). Given that SOD1lacks an ER signal peptide, this suggests that the secretion of pathogenic SOD1 from affected cells may occur *via* similar mechanisms *in vivo* and *in vitro*; however the exact triggers and mechanisms of secretion *in vivo* are yet to be established.

Soluble and aggregated SOD1 have previously been shown to be taken up by neuroblastoma cells (mouse NSC-34 and human SHSY5Y) *via* macropinocytosis (Grad et al., 2014; Sundaramoorthy et al., 2013) (reviewed in Chapter 1). Once SOD1 internalises into cells, it accumulates in cytosolic inclusions (Sundaramoorthy et al., 2013). In addition, the uptake of extracellular misfolded WT or mutant SOD1 inhibits protein transport between the ER-Golgi apparatus, leading to Golgi fragmentation, induction of ER stress and apoptotic cell death, (Sundaramoorthy et al., 2013), similar to ER-stress related neurodegenerative pathways observed in ALS pathology (Atkin et al., 2008; Saxena et al., 2009).

For intracellular spread of pathological proteins to occur, after exogenous misfolded SOD1 is internalised into neighbouring naïve cells, the SOD1 misfolding competent seeds need to escape the vesicular lumen and gain access to the cytosol to further nucleate the aggregation of soluble endogenous SOD1. Examples of protein aggregates escaping membrane vesicles is that amyloid fibrils have previously been shown to induce membrane damage, thus causing the rupture of membrane vesicles leading to cellular toxicity (Milanesi et al., 2012). In addition, particles such as virions, including those of the vaccinia virus, Japanese encephalitis and adenovirus species (Mercer and Helenius, 2012), have been shown to hijack macropinocytosis pathways to enter the cytoplasm of cells, including neurons (Kalia et al., 2013). A lack of physical structure of the macropinosome is thought to leave it vulnerable to a loss of integrity and may explain why particles (e.g. bacteria and virions) can efficiently escape macropinosomes and reach the cytosol (Conner and Schmid, 2003).

Previous work has shown that exogenously applied mutant SOD1 aggregates induce a self-perpetuating seeding of aggregation of native SOD1 (Grad et al., 2014; Munch et al., 2011). Importantly, recent work shows that injection of spinal cord homogenates from symptomatic G93A SOD1 mice into the sciatic nerve of mice expressing G85R SOD1-YFP has been shown to kindle protein aggregation and subsequently induce an ALS-like phenotype (Ayers

et al., 2014). In addition, using human embryonic kidney HEK-293 or human WT SOD1-expressing murine primary spinal cord cultures, it has been reported that uptake and self-perpetuating propagation of SOD1 misfolding is dependent upon the passage of misfolded SOD1 (either WT or mutant) from cell-to-cell, a process that can be neutralised by antibodies reactive with misfolded SOD1 epitopes (Grad et al., 2014). However, the precise mechanism by which SOD1 aggregates reached the cytosol to seed endogenous SOD1 was not determined in these studies. Presumably, the newly formed aggregates must then be secreted or released into the extracellular space to reinitiate the propagation cycle.

3.1.1 Aims

SOD1 aggregates have been shown to be released, associated with cell death, and internalised by naïve cells to seed the aggregation of native soluble proteins (Grad et al., 2014; Münch et al., 2011). Thus, this study aimed to investigate the mechanisms of SOD1 aggregate uptake in to naïve cells, and more importantly identify and quantify seeding activity between donor and recipient cells expressing SOD1 using a novel technique for quantifying inclusions; flow cytometric characterisation of inclusions and trafficking (FloIT).

3.2 Methods

3.2.1 Reagents and antibodies

DMEM/F-12 medium, DMEM/F-12 without phenol red, 0.05% trypsin-EDTA, GlutaMAX, SuperSignal West Pico Chemiluminescent Substrate, FM® 1-43FX, fixable analog of FM® 1-43 membrane stain, LysoTracker Red DND-99, Lipofectamine 2000, Lipofectamine 3000, SuperSignal West Pico Chemiluminescent Substrate, Subcellular Protein Fractionation Kit for Cultured Cells, CellTrace CFSE Cell Proliferation Kit, restriction endonucleases *Bam*HI and *Hind*III, Ez- link- NHS- Biotin and SYTOX Red dead cell stain were purchased from ThermoFisher Scientific. Cell culture 8-chamber μ-slides were purchased from Ibidi, (Planegg-Martinsried, Germany). Any kD Mini-PROTEAN TGX Precast Protein Gels and Precision Plus Protein dual color protein standard were from Bio-Rad (California, USA). Foetal Bovine Serum (heat-inactivated prior to addition in media; FBS) was from Bovogen Biologicals (East Keilor, Australia). Amersham Hyperfilm and cellulose acetate membrane (0.2 μm) was obtained from GE Healthcare (Little Chalfont, Buckinghamshire, UK). RedDot 2 was from Biotium (Hayward, CA). Sterile cell culture plates were form Greiner Bio-One (Frickenhausen, Germany). Casein (heat denatured before use; HDC), dimethyl sulfoxide (DMSO), bovine serum albumin (BSA), β-mercaptoethanol, Brilliant blue R concentrate, paraformaldehyde (PFA), biotinamidohexanoic acid 3-sulfo-N-hydroxysuccinimide ester sodium salt, Bicinchoninic Acid Kit, Propidium iodide, Osmium tetroxide solution (4 WT. % in H_2O), ethidium bromide, Deoxyribonuclease I from bovine pancreas and dithiothreitol (DTT) were from Sigma-Aldrich (St. Louis, MO). Ethylenediaminetetraacetic acid (EDTA) was from Amresco (Solon, USA). Digitonin, High Purity was from Calbiochem was from San Diego, CA, USA. Glass coverslips (19 mm) were from ProSciTech (Kirwan, Australia). Protease inhibitor cocktail tablets (complete, Mini, EDTA-free) was from Roche Diagnostics (Penzberg, Germany). All other reagents including salts, powders and chemicals were from

Amresco, Sigma-Aldrich or Astral Scientific (Gymea, Australia). All reagents used were endotoxin free. Antibodies (Abs) and inhibitor compounds and their respective manufacturing companies used in this current study are listed in **Table 3.1**.

Table 3.1 Antibodies used in this study to investigate the effect of SOD1 proteins on TDP-43 pathology

Host species (clonality)[1]	Anti-body target (Immunogen)[2]	Conjugate	Manufacturer (product number)[3]
Mouse (mAb)	Beta Actin [AC-15]	-	Abcam (ab8226)
Rabbit (pAb)	Vimentin	-	Abcam (ab137321)
Rabbit (pAb)	EEA1	-	Abcam (ab2900)
Mouse (mAb)	LAMP1 [H4A3]	-	Abcam (25630)
Mouse (mAb)	beta III Tubulin [2G10]	-	Abcam (78078)
Rabbit (pAb)	Green fluorescent protein	-	Abcam (ab6556)
Mouse (mAb)	BiP/GRP78	-	BD Biosciences (610978)
Sheep (pAb)	SOD1	-	ThermoFisher Scientific (PAI-30817)
Goat (pAb)	Transferrin	-	Sigma-Aldrich (T2027)
Mouse (pAb)	GST	-	Sigma-Aldrich (ge27-4577-01)
Mouse (mAb)	Galectin 3	-	Abcam (A3A12)
Goat (pAB)	Mouse IgG	Alexa Fluor 488	ThermoFisher Scientific A-(11001)
Goat (pAb)	Rabbit IgG	Alexa Fluor 488	ThermoFisher Scientific (A-11008)
Donkey (pAb)	Sheep IgG	Alexa Fluor 488	Abcam (150177)
Goat (pAb)	Mouse IgG	Alexa Fluor 633	ThermoFisher Scientific (A-21052)
Donkey (pAb)	Sheep IgG	HRP	Abcam (97125)
Goat (pAb)	Mouse IgG	HRP	Merck Millipore (12-349)

[1] pAb, polyclonal anti-body, mAb, monoclonal anti-body; [3] Abcam, Cambridge, USA; ThermoFisher Scientific (Waltham,MA, USA); BD Biosciences San Jose, CA, USA; Merck Millipore, Billerica, Massachusetts, USA; Cytoskeleton (Denver, CO,USA) ; Sigma-Aldrich (St. Louis, MO)

3.2.2 Cell Lines

The mouse neuroblastoma x spinal cord hybrid cell line (NSC-34 cells) (Cashman et al., 1992) were routinely cultured in DMEM/F12 supplemented with 10% (v/v) FBS and 2 mM GlutaMAX. Cells were maintained in an incubator at 37°C under a humidified atmosphere containing 5% (v/v) CO_2.

3.2.3 Cell Transfections

3.2.3.1 Plasmid purification

pEGFP-N1 expression vectors containing $SOD1^{WT}$, $SOD1^{G93A}$ and $SOD1^{A4V}$ cDNAs were provided by Bradley Turner (University of Melbourne, Melbourne, Australia) (Turner et al., 2005a). pFUW expression vectors containing $SOD1^{G127X}$ cDNAs were kindly provided by Edward Pokrishevsky (University of British Columbia, Vancouver, Canada) (Grad et al., 2011). SOD1-tomato red (TdTomato) constructs were created by replacing the EGFP sequences with tdTomato from pcDNA3.1(+)Luc2tdT by GenScript (Piscataway, NJ). pCAG-RFP expression vectors containing TDP-43^{WT} cDNA was obtained from Addgene, provided by Zuoshang Xu (University of Massachusetts Medical School, Worcester, Massachusetts, USA)(Yang et al., 2010). Chemically competent DH5α *Escherichia coli* cells were provided by Jason McArthur (University of Wollongong, Wollongong, Australia). Cells were transformed with the TDP-43 and SOD1 containing plasmids as per manufacturer's instructions, using the heat shock (42 ºC) method. Transformed cells were then transferred onto lysogeny broth (10% w/v tryptone, 10% w/v NaCl, and 5% w/v yeast; LB) agar plates with 50 µg/ml kanamycin sulphate and incubated overnight at 37°C. Single-transformed bacterial colonies were selected and inoculated into sterile LB media containing 50 µg/ml kanamycin sulphate to prepare starter cultures. Plasmid DNA was then extracted from bacterial cells using the CompactPrep Plasmic Maxi Kit (Qiageb, Hilden, Germany), as per manufacturer's instructions.

The purity (260/280 ratio) and concentration of extracted DNA was measured using the NanoDrop 2000c dual-mode UV-Vis Spectrophotometer (ThermoFisher Scientific, Waltham, USA). To further confirm the purity of the extracted DNA samples, a restriction digestion was carried out at 37ºC for 1 h using enzymes HindIII and BamHI that correspond to specific

restriction sites in the plasmids. Digested DNA samples were separated on a 1% agarose gel in tris-acetate-EDTA (TAE) buffer (1 mM ethylenediaminetetraacetic acid (EDTA) disodium salt, 40 mM Tris and 20 mM acetic acid). The resulting gel was then stained with ethidium bromide overnight and visualised using the GS-800 Calibrated Densitometer (Bio-Rad).

3.2.3.2 Transfecting cells with Lipofectamine 2000

NSC-34 cells were maintained in DMEM/F12 medium supplemented with 10% FBS and 2 mM GlutaMAX (complete culture medium) at 37°C under a humidified atmosphere containing 5% (v/v) CO_2 unless otherwise stated. To transfect, cells previously seeded at (6 x 10^5 cells/mL) were incubated in DMEM/F-12, in the absence of serum, containing 2 µg plasmid DNA and Lipofectamine 2000 for 5 h. Cells were then washed once with serum free DMEM/F12 media and replenished with complete culture medium for the duration of the experiment.

3.2.3.3 Transfecting cells with Lipofectamine 3000

NSC-34 cells were seeded in 8-well chamber slides at a density of 3-4 x 10^5 cells/ 200 µL/ chamber and were incubated overnight. Cells were then incubated in complete DMEM/F-12 culture medium containing 2 µg plasmid DNA, P3000 reagent and Lipofectamine 3000 (diluted in serum free DMEM/F-12 medium) for either 24 h, 48 h, or 72 h. For co-transfection assays, 1 µg of each plasmid was used for a total of 2 µg of DNA.

3.2.3.4 Collection and separation of transfected cells and conditioned media

To confirm transfection and determine sufficient transfection efficiency, cells were visualised by fluorescence microscopy using an Eclipse TE2000 inverted microscope (Nikon, Tokyo, Japan). Following transfection (2, 24, 48, or 72 h), conditioned media were collected from

respective treatments. Cells were harvested using 0.05% trypsin (5 min, 37°C) and conditioned media were processed and analysed as described below.

3.2.4 Aggregation and biotinylation of WT and mutant G93A SOD1

WT and G93A (mutant SOD1) SOD1 were expressed and purified from *E.coli* as previously outlined (Lindberg et al., 2002; Roberts et al., 2013). SOD1 aggregation was performed *in vivo* as previously described (Roberts et al., 2013). Briefly, solutions of purified WT or mutant SOD1 (1 mg/ml) in PBS were incubated with 20 mM dithiothreitol (DTT) and 5 mM EDTA (Sigma, St. Louis, MO) for 72 h at 37 °C with shaking using a digital shaker (universal IKA® MS 3, 230 V). The aggregated SOD1 was then labelled with biotinamidohexanoic acid 3-sulfo-N-hydroxysuccinimide ester sodium salt (40 mg/ml) in DMSO for 2 h at RT. The unconjugated biotin was then separated from the aggregates by centrifugation (21 000 x g for 30 min) and washed three times with PBS (300 x g for 5 min). The purified aggregates free of unconjugated biotin were then resuspended in PBS (1 mg/ml). A bicinchoninic acid (BCA) protein assay was performed to determine the amount of protein remaining after labelling.

3.2.5 Aggregated SOD1 association with acidic compartments by confocal microscopy

NSC-34 cells (2–3 x 10^4 cells/200 µL/chamber) were cultured in chamber slides at 37°C overnight. Cells were pre-treated with Lysotracker Red (75 nM) for 2 h at 37°C as per the manufacturer's instructions. Cells were then washed and incubated with 20 µg/ml of aggregated WT and mutant SOD1 for either 10 min, 30 min or 60 min at 37°C. Cells were fixed at respective time points with 4% PFA in PBS for 20 min at RT and washed twice with PBS over 5 min. Cells were then incubated with Triton X-100 for 30 min at 4°C. Cells were incubated with blocking solution (5% FCS, 1% BSA and 0.3% Triton X-100) for 20 min at RT. Cells were incubated with anti- SOD1 IgG (1:500 diluted in 4% BSA and 0.1% Triton X-

100) overnight at 4°C. Cells were subsequently washed again in PBS and incubated with anti-sheep IgG conjugated to Alexa Fluor 488 (1:500 diluted in 1% BSA and 0.1% Triton X-100) protected from light for 1 h at RT. An inverted microscope (DM IBRE) and a Leica TCS SP confocal imaging system were used to visualise and image cells (excitation 488, emission collected at 520-540). Fluorescence, bright field (differential interference contrast; DIC) and merged images were captures using Leica confocal software.

3.2.6 Subcellular Fractionation assay of NSC-34 cells

NSC-34 cells were incubated with WT or mutant G93A SOD1 proteins in aggregated form (20 µg/mL) in PBS for 2 h at 37°C/5% CO_2. Post incubation, the cells were washed three times with PBS (300 x g for 5 min) harvested using 0.5% trypsin and 5 mM EDTA and washed (500 x g for 5 minutes). The cells were washed three times with ice cold PBS (500 x g for 3 minutes) for fractionation using a Subcellular Protein Fractionation Kit for Cultured Cells as per manufacturer's instructions (Thermo Fisher Scientific). Initially, NSC-34 cells (10 x 10^6 cells/mL) were incubated with cytoplasmic extraction buffer (CEB) containing protease inhibitors for 10 min rotating at 4°C. The supernatant (cytoplasmic fraction) was collected (500 × *g* for 5 minutes). The cell pellet was then incubated with membrane extraction buffer (MEB) containing protease inhibitors for 10 min rotating at 4°C. Post incubation, the supernatant (extracted membrane fraction) was collected (3000 × *g* for 5 minutes). Ice cold nuclear extraction buffer (NEB) containing protease inhibitors was added to the cell pellet for 30 min rotating at 4°C. The supernatant (extracted soluble nuclear fraction) was collected (5000 × *g* for 5 minutes). Chromatin-bound extraction buffer (NEB, 100 mM $CaCl_2$ and 300 units of Micrococcal Nuclease) was added to the pellet for 15 mins at RT. The supernatant (chromatin-bound nuclear extract) was collected (16,000 x g for 5 mins). Lastly, Pellet Extraction Buffer (PEB) containing protease inhibitors was added to the cell

pellet for 10 mins at RT. The supernatant (the cytoskeletal extract) was collected (16,000 x g for 5 mins).

Protein concentration was determined using the BCA method. Fractions (20 μg protein/lane) were separated under reducing conditions (5% β-mercaptoethanol) using Any kD Mini-PROTEAN TGX Stain-Free™ Precast Gels. Proteins were then transferred to nitrocellulose membranes using a Trans-Blot Turbo Transfer System (Bio-Rad). Total protein per lane was then imaged and measured with a Bio-Rad Criterion Stain Free Imager and Image Lab software. Membranes were blocked with heat denatured casein (HDC) in for 1 h at 37°C. To test the efficiency of the separation, rabbit anti-EEA1 pAb (1:500), rabbit anti-Vimentin pAb (1:500) and mouse anti-actin mAb (1:5000), diluted in HDC/PBS for 1 h at 37°C were used to probe the CE, ME, NE and PE fractions. Membranes were visualised using chemiluminescent substrate and Amersham Hyperfilm ECL (GE Healthcare). Images of films were collected using a GS-800 Calibrated Densitometer (Bio-Rad). The processing of films was achieved using GBX Developer and Replenisher and GBX Fixer and Replenisher (Kodak Australiasia, Collingwood, Victoria Australia). Images of the films were collected using a GS-800 Calibrated Densitometer (Bio-Rad).

3.2.7 Selective Permeabilisation of NSC-34 cells

NSC-34 cells were incubated in chamber slides with 20 μg/ml of soluble and biotin-conjugated aggregated WT and G93A SOD1 protein for either 60 or 120 min at 37°C. Cells were immediately fixed with 4% PFA in PBS for 20 min at RT and washed twice with PBS over 5 min. Cells were incubated with either Triton X-100 (0.5%) or digitonin (10 μM) for 30 min and 10 min at 4°C respectively. Cells were then incubated with blocking solution (5% FCS, 1% BSA and 0.3% Triton X-100) for 20 min at RT. Cells were incubated with anti-SOD1 IgG (1:500 diluted in 4% BSA and 0.1% Triton X-100) overnight at 4°C. Cells were

washed again in PBS and incubated with Alexa Fluor 488 streptavidin (1:1000 diluted in 1% BSA and 0.1% Triton X-100) for 1 h at RT. Cells were incubated with Sytox Red (5 nM) for 10 min at RT. An inverted microscope (DM IBRE) and a Leica TCS SP confocal imaging system were used to visualise and image cells (excitation 488, emission collected at 510-550). Fluorescence and merged images were captured using Leica confocal software.

3.2.7.1 Controls for selective permeabilisation

NSC-34 cells incubated in chamber slides for 24 h in complete culture media were fixed with 4% PFA in PBS at RT for 20 min at RT, and washed twice with PBS over 5 min. Cells were incubated with either Triton X-100 (0.5%) or digitonin (10 µM) for 30 min and 10 min at 4°C respectively. Cells were then incubated with blocking solution (5% FCS, 1% BSA and 0.3% Triton X-100) for 20 min at RT. Next, cells were incubated with mouse anti-LAMP1 (mAb) (0.3 µg/ 100µL), mouse anti-BiP/GRP78 (mAb) (0.5 µg/ 100µL), mouse anti-β-tubulin (mAb) (0.2 µg/ 100µL) and rabbit anti-EEA1 (pAb) (0.5 µg/ 100µL) overnight at 4°C. Cells were subsequently washed again in PBS and incubated with goat Alexa Fluor 488-conjugated goat anti-rabbit IgG Ab (0.3 µg/ 100 µL) and Alexa Fluor 488-conjugated goat anti-mouse IgG Ab (0.3 µg/ 100 µL) in PBS containing 1% BSA and 0.1% Triton X-100 protected from light for 1 h at RT. Cells were incubated with RedDot2 (1:200) for 10 min at RT. Imaging was performed as outlined above.

3.2.8 Membrane damage (haemolytic) assay

Fresh Human venous blood was kindly provided by Wollongong Hospital Pathology Unit; NSW, Wollongong, Australia (The University of Wollongong Human Ethics Approval H202/080). Firstly, human blood was incubated with 5 mM EDTA and protease inhibitor cocktail, pH 7.0 for 1 h at 4ºC. The next day, the blood samples were gently mixed by inversion and were washed three times in PBS (300 x g for 5 min) and harvested (1 x10^6

cells/mL/tube) by resuspension in phosphate/sodium acetate buffer (10 mM CH_3CO_2Na, 10mM Na_2HPO_4, 137 mM NaCl, 2.7 mM and 2 mM) pH 7.2. Clarified blood cells were incubated with 20 μg/ml of WT and G93A SOD1 soluble and aggregated protein or 0.1% Triton-x100 was used for total cell lysis for 2 h at 37°C. Following incubation, blood cells were washed twice in phosphate/sodium acetate buffer (300 x g for 5 min). Total Haemoglobin levels of the supernatant were determined *via* optical density (absorbance) measurements, a measure of lysed erythrocytes using a SpectraMax Plus 384 Microplate Reader and SoftMax Pro software (Molecular Devices, Silicon Valley, CA) (540 nm).

3.2.9 Preparation of Giant Unilamellar Vesicles

The rapid evaporation method was used to prepare giant unilamellar vesicles for confocal microscopy as described in (Milanesi et al., 2012). Briefly, soy L-α-phosphatidylcholine (Avanti Polar Lipids Inc) was dissolved in $CHCl_3$:MeOH (2:1) to give a phospholipid concentration of 5 mM. Liposome buffer (50 mM HEPES, 107 mM NaCl, 1 mM EDTA, 0.1 M sucrose, pH 7.4, 2.5 mL) was then added to the lipid/solvent solution in a 50 mL round bottom flask and the two phases mixed by vigorous pipetting. The organic solvent was removed by rotary evaporator under reduced pressure (final pressure 44 mbar) for 5 min at 37°C. The resulting liposome suspension was stored overnight at 4°C prior to confocal microscopy studies. The next day, liposomes were incubated with 20 μg/ml of aggregated SOD1 proteins for 2 h 37°C.

3.2.10 Galectin -3 as a marker of cell rupture

NSC-34 cells were incubated in chamber slides with 20 μg/ml of soluble and biotin-conjugated aggregated WT and G93A SOD1 protein for 2 h at 37°C. Cells were immediately fixed with 4% PFA in PBS for 20 min at RT and washed twice with PBS over 5 min. Cells were incubated with either Triton X-100 (0.5%, control) or digitonin (10 μM) for 30 min and

10 min at 4°C respectively. Cells were then incubated with blocking solution (5% FCS, 1% BSA and 0.3% Triton X-100) for 20 min at RT. Cells were incubated with anti-Galectin 3 IgG (0.5 µg/100 µL) overnight at 4°C. Cells were subsequently washed again in PBS and incubated with goat Alexa Fluor 488-conjugated goat anti-mouse IgG (0.3 µg/ 100 µL) in PBS containing 1% BSA and 0.1% Triton X-100 protected from light for 1 h at RT. Cells were incubated with RedDot2 (1x) for 10 min at RT. Imaging was performed as outlined above.

3.2.11 Release of SOD1 aggregates and filter trap assay

Following transfection (at 72 h), conditioned media from SOD1 transfected cells were collected and pre-incubated with 1 unit DNaseI per µg of transfected DNA for 10 min at RT and centrifuged for 30 min at 21,000 x *g* at 4°C into soluble and pelletable fractions. Pelletable fractions were incubated with an equal volume of phosphate-buffered saline (PBS) containing 1% SDS at RT for 15 min. Samples were analaysed using using filter trap analysis and SDS-PAGE. For filter trap analysis, pellatable fractions were added to the microfiltration apparatus and then SDS resistant protein were collected and separated onto a cellulose acetate membrane with 0.2 µm pores (GE Healthcare) using a Bio-Dot SF Microfiltration System (Bio-Rad) under vacuum pressure. The membrane was washed with PBS containing 1% SDS three times over 5 min, followed by PBS. In addition, pelletable fractions were separated under reducing conditions (5% β-mercaptoethanol) using Any kD Mini-PROTEAN TGX Stain-Free™ Precast Gels. Proteins were then transferred to nitrocellulose membranes using a Trans-Blot Turbo Transfer System (all Bio-Rad). The presence of EGFP-SOD1 aggregates were then detected by immunoblotting. The membranes were blocked with heat denatured casein (HDC) for 1 h at 37°C. The membranes were then incubated with at 4°C overnight with an anti-EGFP pAb (1:1000-1:10000). The following day, the membrane was washed

three times over 15 min with PBS containing 0.1% Triton X-100. The membrane was then incubated at room temperature for 1 h with peroxidise-conjugated anti-rabbit (1:1000) IgG Ab and then washed as above. Released SOD1 protein aggregates were visualised using chemiluminescent substrate and Amersham Hyperfilm ECL (GE Healthcare). Images of films were collected using a GS-800 Calibrated Densitometer (Bio-Rad. Relative EGFP and EGFP-SOD1 aggregates were quantified from these images using ImageJ software (Version 1.48) (National Institutes of Health, Bethesda, MD).

3.2.12 Released protein uptake assay by immunoblotting and confocal microscopy

Conditioned media from transfected cells were collected 72 h post-transfection and pre-incubated with 1 unit DNaseI per μg of transfected DNA for 10 min at RT and centrifuged for 30 min at 21,000 x g at 4°C into soluble and pelletable fractions. Pelletable fractions were washed and resuspended in complete culture media (500 μL) and added to adherent naïve NSC-34 cells plated in 12-well plates at (1.5×10^6 cells/ 0.4 mL/ well) 24 h prior to treatment with conditioned media for 2 h at 37°C/5% CO_2. Imaging was performed as outlined above (see section 3.2.5). NSC-34 cells were washed in three times in PBS and harvested using trypsin (0.5%) and washed (500 x g for 5 minutes). Cells were then lysed over 15 min at 4°C in ice-cold lysis buffer (10 mM Tris, 150 mM NaCl, 5 mM EDTA, 1% Triton X-100 and protease inhibitor cocktail, pH 7.0). Cell debris was then cleared (21,000 × *g* at 4°C for 30 min) and large SDS resistant protein aggregates in the supernatants (100 μg protein/slot) were trapped onto a cellulose acetate membrane with 0.2 μm pores (GE Healthcare) using a Bio-Dot SF Microfiltration System (Bio-Rad) under vacuum pressure. The membrane was washed with PBS containing 1% SDS three times over 5 min, followed by PBS. The presence of EGFP-SOD1 aggregates were then detected by immunoblotting as above. Internalised SOD1 protein aggregates in the supernatants were visualised using chemiluminescent

substrate and Amersham Hyperfilm ECL (GE Healthcare). Images of films were collected using a GS-800 Calibrated Densitometer (Bio-Rad).

3.2.13 Cell death assay

Following transfection (24 , 48 , and 72 h in total), NSC-34 cells expressing EGFP(control), $SOD1^{WT}$ and $SOD1^{G93A}$ -EGFP were washed twice in incomplete culture media (lacking FCS) and then harvested using 5 mM EDTA (5 min, 37°C) and then washed again using centrifugation (300 x g for 5 min). Cells (1 $x10^5$ cells/mL/tube) were resuspended in PBS and incubated with SYTOX Red dead cell stain (5 µM) immediately before analysis by flow cytometry. Cellular events were collected using a LSR II flow cytometer (excitation 488 nm, emission collected at 515/20 nm band pass filter; excitation 488nm, emission collected at 575/20 nm band pass filter) for EGFP and PI respectively. The percentage of dead cells was expressed as cells positive for PI as a proportion of total EGFP-positive cells and was determined FlowJo software. Results are the average of at least three independent experiments.

3.2.14 UV ablation assay by confocal microscopy

Adherent NSC-34 cells in 8-chamber well slides were transiently transfected with $TDP\text{-}43^{WT}$ and TDP^{G294A}-EGFP using Lipofectamine 3000 (see above). Following transient transfection of NSC-34 cells (48 h), a fluorescent cell with aggregates was identified and assessed as suitable for ablation. UV laser mediated cell selective destruction was performed on the nucleus of the cell for 20s using Leica Confocal Software. Live cell imaging was performed at 15 min time intervals and then fluorescent and bright-field images were captured for 24 h using a DM IBRE inverted microscope and TCS SP confocal imaging system (Leica, Germany) (excitation 488 nm, emission collected at 510-540 nm).

3.2.15 FloIT assay by flow cytometry

Adherent NSC-34 cells in 24-well plates (6×10^5 cells/ 0.5 mL/well) were transiently transfected separately (co-culture) or co-transfected with $SOD1^{WT}$ and $SOD1^{G93A}$ fused to either EGFP or tdTomato using Lipofectamine 3000 (see section 3.2.3.3). For the co-culture assay, following transient transfection (24 h), cells expressing $SOD1^{WT}$-tdTomato were washed three times in incomplete culture media, and cells expressing $SOD1^{G93A}$-EGFP were harvested using 0.5% trypsin and 5 mM EDTA and washed (500 x g for 5 minutes). The cells were then resuspended in complete culture media (500 µl) and were co-plated with adherent cells (at a ratio 1:1) expressing $SOD1^{WT}$-tdTomato for a total of 72 h (post co-culture). As an additional control, cells expressing $SOD1^{WT}$-tdTomato and $SOD1^{G93A}$-EGFP were cultured separately, and then mixed immediately before flow analysis (corresponding to the respective timepoint). For the co-transfection assay, NSC-34 cells were co-transfected with $SOD1^{WT}$-tdTomato and $SOD1^{G93A}$-EGFP (6 h prior to co-culturing) for a total of 72 h (corresponding to the time point of the co-culture experiment). For the seeding assays, cells expressing $SOD1^{WT}$-tdTomato were cultured in the presence of 20 µg/ml of with human recombinant mutant SOD1 (G93A) aggregates at the indicated time points. Following co-transfection, co-culturing or addition of recombinant SOD1 aggregates (at 24h, 48 h and 72h in total), cells were harvested using 5 mM EDTA (5 min, 37°C) and then washed again using centrifugation (300 x *g* for 5 min). Cells were then washed twice in PBS (300 x g for 5 min) and resuspended in PBS (0.5 mL/tube). An aliquot of cells were (2×10^5cells/0.15mL) collected then analysed for transfection efficiency (excitation 488 nm, emission collected with 525/50 nm band pass filters; excitation 561 nm and emission collected with 586/15 nm band pass filters for EGFP and tdTomato respectively) determined by flow cytometry. The remaining cells (2×10^5cells/0.35mL) were washed as above and lysed prior to analysis in lysis buffer

(0.5% Triton X-100 and Complete protease inhibitor in PBS). Cell lysates were then incubated with RedDot2 (1:1000) at RT for 2 min.

All events were collected using a LSRFortessa X-20 Cell Analyzer (BD Biosciences) (excitation 488 nm, emission collected with 525/50 band-pass filter and excitation 561, emission collected with 586/15 nm band-pass filter for EGFP and RedDot2, respectively; excitation 561 nm and emission collected with 586/15 nm band pass filters for tdTomato). All parameters were set to $\log^{10}$ during acquisition from cell lysates. The forward scatter threshold was set to the minimum value (200 AU) to minimize the exclusion of small protein inclusions. Nuclei were identified and enumerated based on RedDot2 fluorescence and forward scatter and then excluded from further analysis. The percentage of $EGFP^+$/$tdTomato^+$ particles was determined using quadrant markers in FlowJo software. The remaining particles were analysed for the presence of inclusions based on GFP/ tdTomato fluorescence, forward scatter and comparison lysates prepared from cells expressing only the corresponding fluorescent protein.

The number of inclusions in the population can be normalised to the number of nuclei, and reported as inclusions/1000 transfected cells (iFloIT) according to the equation:

$$i_{FloIT} = 100\left(\frac{n_i}{\gamma . n_{nuc}}\right)$$

where n_i represents the number of inclusions acquired, n_{nuc} is the number of nuclei acquired, and γ is the transfection efficiency.

Analysis of all events were performed using FlowJo software (Tree Star, Ashland, OR). A summary of the methods carried out for analysis of SOD1 propagation in NSC-34 cells is summarised (Figure 3.1) and described below.

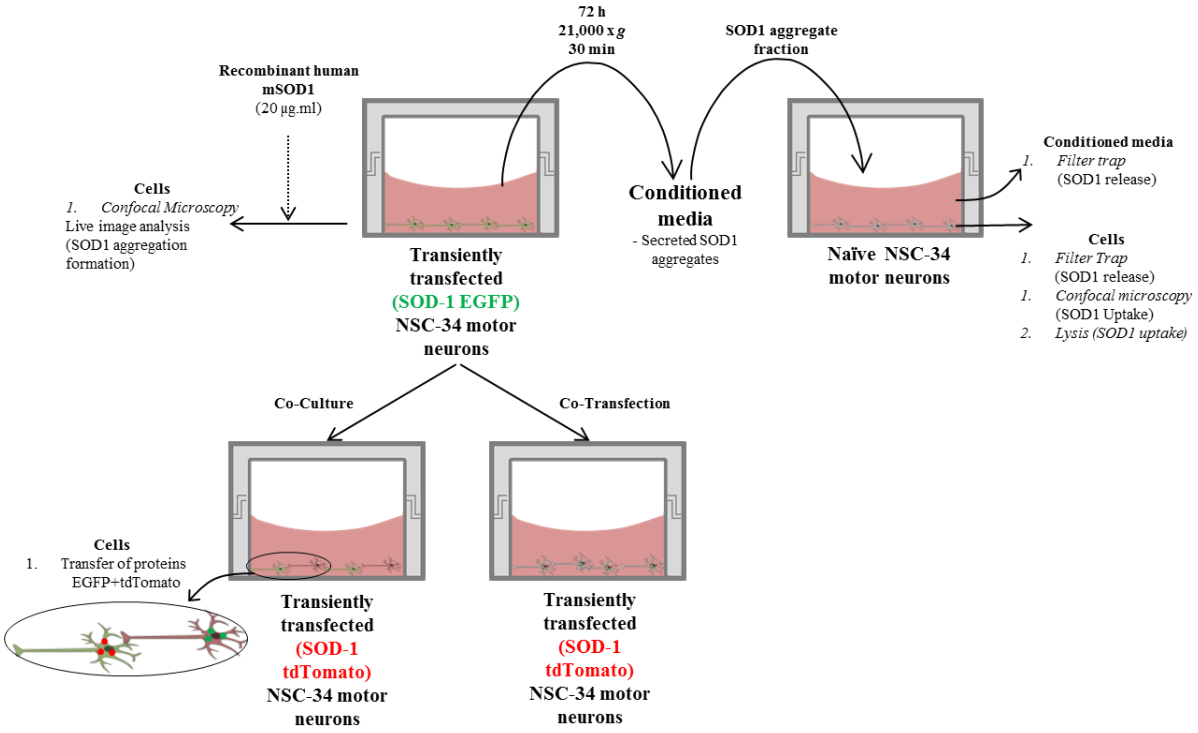

Figure 3.1 Summary of methods to investigate the prion-like propagation of SOD1 in NSC-34 motor neurons Following transfection (72 h), conditioned media from NSC-34 cells were collected and centrifuged (21,000 x g for 30 min) to remove cell debris, and analysed using filter trap. Naïve NSC- 34 cells were incubated with fractionated conditioned media for 2 h and then lysates were analysed by filter trap analysis. In other experiments, SOD1 aggregate formation (in the absence or presence of recombinant human mutant SOD1 aggregates) was visualised by confocal microscopy. Transiently transfected NSC-34 cells were either co-cultured or co-transfected with SOD1-EGFP or SOD1 tdTomato for 72 h and assessed by flow cytometry to identify transfer events.

3.3 Results

3.3.1 Transient expression of mutant SOD1 can induce cell death in NSC-34 motor neurons over time

SOD1 proteins have been shown to have spontaneous fibrilisation activity *in vivo* (Chia et al., 2010; Furukawa et al., 2008). Therefore, the presence of inclusion bodies containing SOD1 aggregates indicative of spontaneous aggregation was investigated. To investigate the number of SOD1 positive inclusions in NSC-34 motor neurons, cells were transfected with $SOD1^{WT}$ tdTomato and $SOD1^{G93A}$ GFP for 48 and 72 h and the number of inclusions were quantified using flow cytometric characterisation of inclusions and trafficking (FloIT) technique (Figure 3.2A). Initially, the lysates of NSC-34 cells containing large particles were gated (nuclei and inclusions). After nucleus removal, particles were analysed for green or red fluorescence to identify inclusions positive for EGFP or tdTomato (Figure 3.2B). A significantly greater number of inclusion bodies were identified in cells expressing mutant $SOD1^{G93A}$ and $SOD1^{WT}$ compared to cells expressing EGFP or tdTomato alone (Figure 3.2C). Furthermore, a significantly greater number of inclusions were measured between cells expressing mutant $SOD1^{G93A}$ and $SOD1^{WT}$. However, there was no statistical difference in the number of inclusions between tdTomato and EGFP controls.

Next, the relationship between timing of SOD1 aggregate formation and cell death was investigated. NSC-34 motor neurons were transfected with $SOD1^{WT}$ and $SOD1^{G93A}$-EGFP for 48 and 72h, treated with SYTOX red dead cell stain and assessed by flow cytometry (Figure 3.2D). Cell death is expressed as the total of dying and dead cells (red dot exclusion) that are positive for EGFP. A significantly greater amount of cell death was observed for the cells expressing $SOD1^{WT}$-EGFP at 48 h relative to cells expressing EGFP alone although this increase was only ~1% of GFP positive cells. At 72 h however, the percentage of cell death

between these treatments was similar. A significantly higher percentage of total cell death was however observed for cells expressing SOD1^{G93A}-EGFP relative to cells transiently expressing EGFP alone, and this increased two-fold at 72 h. Furthermore, cell death was significantly higher from 48-72 h in cells expressing SOD1^{G93A}-EGFP compared to cells transfected with SOD1^{WT}-EGFP, consistent with reports of mutant SOD1 induced toxicity to cells (Brotherton et al., 2013). These findings suggest a relationship between SOD1-inclusion body formation and cell death in NSC-34 cells.

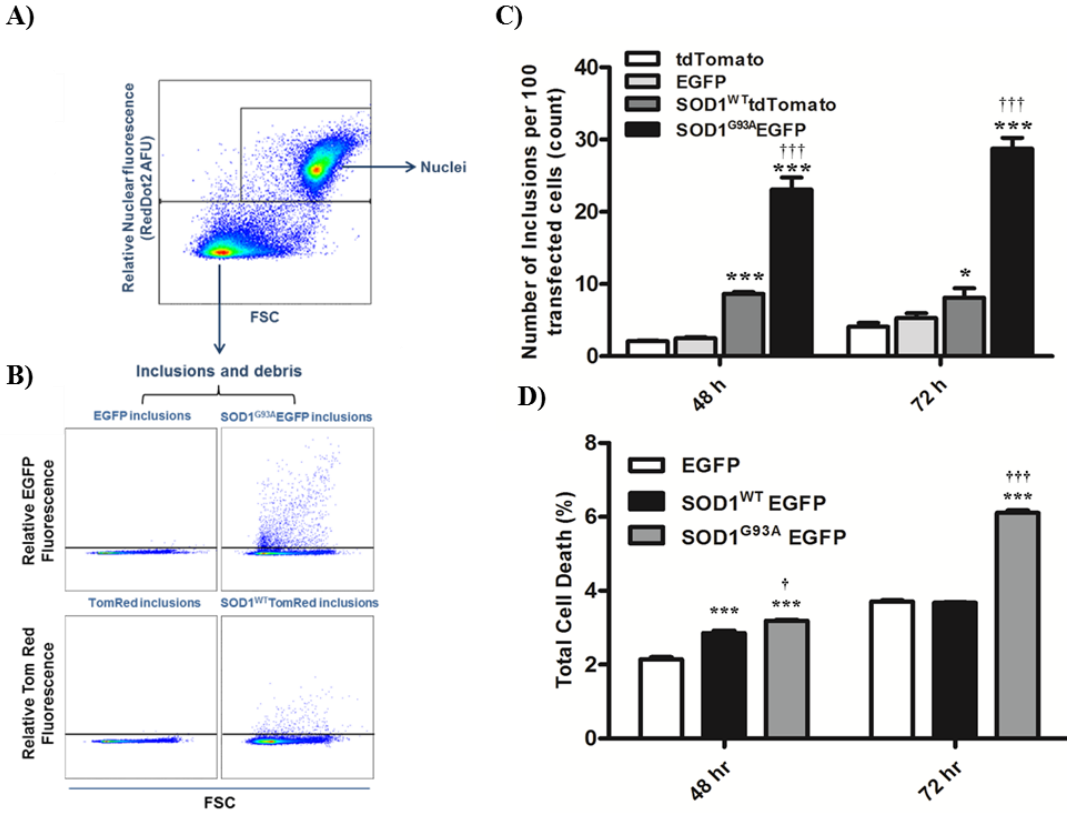

Figure 3.2 Spontaneous aggregation of SOD1 and cell death of EGFP-positive cells after 72 h post transfection was examined by flow cytometry. Following transfection, using Lipofectamine 3000, NSC-34 transiently transfected with SOD1^{WT} tdTomato, SOD1^{G93A}-EGFP, tdTomato or EGFP were cultured separately for 48 and 72 h. (A) Cell lysates were firstly gated on forward scatter (FSC) and RedDot2 fluorescence to identify nuclei and then (B) the number of EGFP and tdTomato positive- inclusions were identified from the non-nuclei gated population determined by flow cytometry. (C) Results shown as mean number of inclusions per 100 transfected cells ± SEM, n = 3; $^{***}P < 0.001$ and $^{*}P < 0.05$ compared to controls (fluorescent tags); $^{\dagger\dagger\dagger}P < 0.001$ compared to corresponding SOD1^{WT} tdTomato. (D) Following transfection at 48 h, and 72 h, using lipofectamine 2000 adherent NSC-34 cells in complete DMEM medium expressing EGFP (control), SOD1^{WT} and SOD1^{G93A} EGFP were harvested and incubated with propidium iodide (1 mg/mL). Cells were gated on forward and side scatter to exclude doublets and cell debris and then the percentage of cells positive for EGFP and SYTOX Red dead cell stain were determined by flow cytometry. Results shown as total percentage of cell death in EGFP expressing cells ± SD, n = 3; $^{***}P < 0.001$ or $^{*}P < 0.05$ compared to corresponding EGFP control; $^{\dagger\dagger\dagger}P < 0.001$ and $^{\dagger}P < 0.05$ compared to corresponding SOD1^{WT}-EGFP.

3.3.2 Intracellular SOD1 aggregates are released from NSC-34 motor neurons

Intracellular SOD1 protein aggregates have been previously been reported to be secreted *via* active mechanisms and released by passive means (Gomes et al., 2007; Grad et al., 2014). Filter trap analysis and immunoblotting is a conventional method to study protein aggregates (Juenemann et al., 2015), including SOD1 aggregate detection in conditioned media (Grad et al., 2014), thus this technique was used to observe and quantify the profile of secreted WT and a series of mutant SOD1 proteins in conditioned media (Figure 3.3). To determine whether a range of SOD1 aggregates can be released from NSC-34 motor neurons, cells were transfected with EGFP or WT and mutant SOD1- EGFP variants including $SOD1^{WT}$ and mutant SOD1 variants including $SOD1^{G93A,}$ $SOD1^{A4V}$ and $SOD1^{G127X}$ for 72 h. Total conditioned media was then collected from these cells and separated by centrifugation.

Pelletable fractions were examined by immunoblotting, and the relative amount of SOD1-EGFP quantified (Figure 3.3A). Little to no EGFP was detected in the fraction derived from conditioned medium of cells transfected with EGFP. In comparison, filter trap analysis identified small but significant amounts of SDS-resistant material that was anti-EGFP reactive and larger than the 0.2 μm pore size of the membrane in conditioned media from cells expressing $SOD1^{WT}$. A significantly greater amount of SDS-resistant material positive for EGFP was identified in conditioned medium from NSC-34 cells expressing $SOD1^{G93A}$, $SOD1^{A4V}$ and $SOD1^{G127X}$ –EGFP (Figure 3.3A).

To further characterise these SOD1 aggregates released from NSC-34 cells, the conditioned medium was analysed by SDS PAGE separation and immunoblotting (Figure 3.3B). Again, no EGFP was identified in the fraction obtained from conditioned medium of cells transfected with EGFP. In comparison, anti-EGFP bands with an approximate molecular size of 35 kDa and 50 kDa consistent with the molecular weight of SOD1-EGFP monomer and

dimer respectively (Turner et al., 2005), were identified in conditioned media from cells expressing $SOD1^{WT}$, expressing $SOD1^{G93A}$, $SOD1^{A4V}$ and $SOD1^{G127X}$ –EGFP. In addition, high molecular weight, SDS-resistant oligomeric species were detected in these respective fractions, ranging in molecular size from 150 kDa to above 250 kDa. This is consistent with above filter trap analysis data.

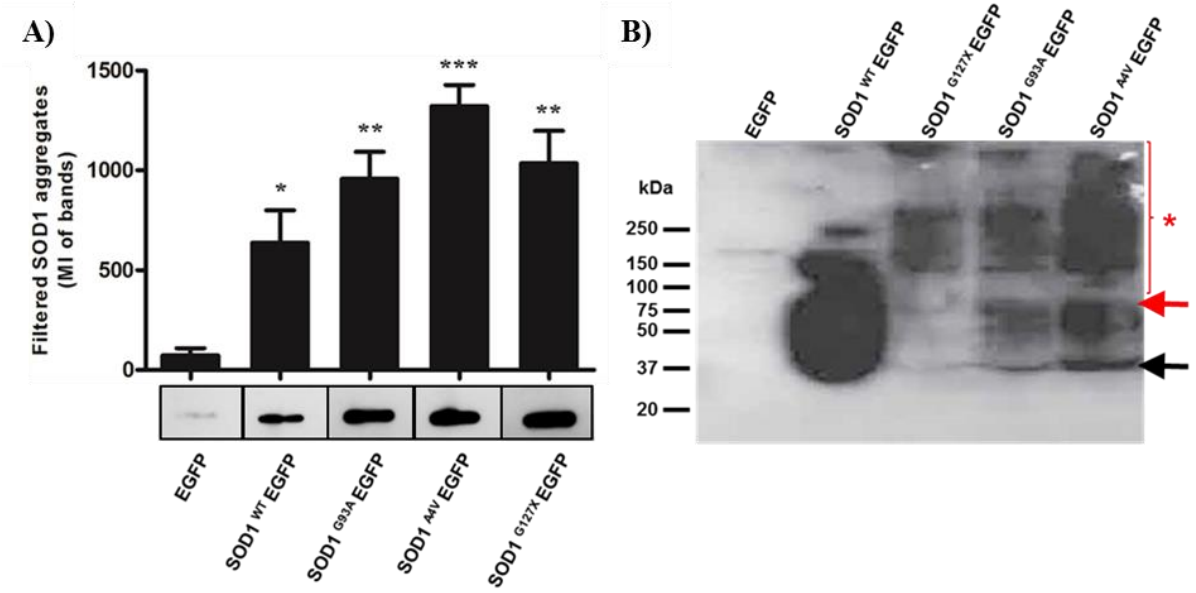

Figure 3.3 Wild type and mutant SOD1 proteins can be detected in conditioned media of NSC-34 motor neurons (A) Following transfection (at 72 h) using lipofectamine 2000, conditioned media were collected and incubated 250 units of DNase for 10 min at RT, fractionated into pelletable fractions by centrifugation and incubated with 1% SDS in PBS. SDS resistant proteins were separated onto cellulose acetate membrane (0.2µM) in a filter trap apparatus, and then incubated with anti-EGFP Ab. Results shown as mean band density relative to EGFP ± SD, $n = 6$; $^{***}P < 0.001$, $^{**}P < 0.01$ or $^{*}P < 0.05$ compared to corresponding EGFP control. (B) Conditioned media were fractionated into pelletable and soluble fractions by centrifugation. Pelletable fractions were then separated by SDS-PAGE under reducing conditions and transferred to a nitrocellulose membrane. The membrane was then incubated with anti-EGFP Ab. The black arrow indicates SOD1–EGFP monomer whereas the red arrow indicates SOD1–EGFP dimer. The area indicated by an asterisk represents SDS-resistant oligomeric SOD1 species. The slot-blot presented is representative of bands cut horizontally, and displaying $n = 1$.

3.3.3 Released SOD1 aggregates are capable of entering into Naïve NSC-34 motor neurons

Next, to investigate whether released SOD1 aggregates are capable of entering into naïve NSC-34 motor neurons, naïve cells were incubated with pelleted fractions derived from conditioned medium of NSC-34 cells transfected with $SOD1^{WT}$ and mutant SOD1 variants including $SOD1^{G93A,}$ $SOD1^{A4V}$ and $SOD1^{G127X}$ for 2 h (Figure 3.4). Following incubation, conditioned media was then collected from these cells and separated by centrifugation

(Figure 3.4A). Cells were incubated in conditioned media and visualised by microscopy to identify SOD1-EGFP inclusions inside the cells (Figure 3.4B), and then whole lysates were probed with anti-EGFP pAb. SOD1 or EGFP in pelletable fractions derived from conditioned media was then examined by immunoblotting with an anti-EGFP pAb (Figure 3.4C).

Similar to above data, no SDS-resistant material was identified in the fraction derived from conditioned medium of cells transfected with EGFP. However, a substantial amount of SDS-resistant material, larger than the 0.2 μm pore size that was anti-EGFP reactive in conditioned media from cells expressing $SOD1^{WT}$and $SOD1^{G93A}$, $SOD1^{A4V}$ and $SOD1^{G127X}$ –EGFP. Similarly, large SDS resistant material was present in the respective fractions obtained from whole lysates of cells expressing WT and mutant variants of SOD1, however these were present at a much lower intensity. Prior to lysis, cells were assessed by microscopy, cells incubated with conditioned media from cells expressing SOD1-EGFP displayed discrete and diffuse fluorescence, characteristic of SOD1 inclusions.

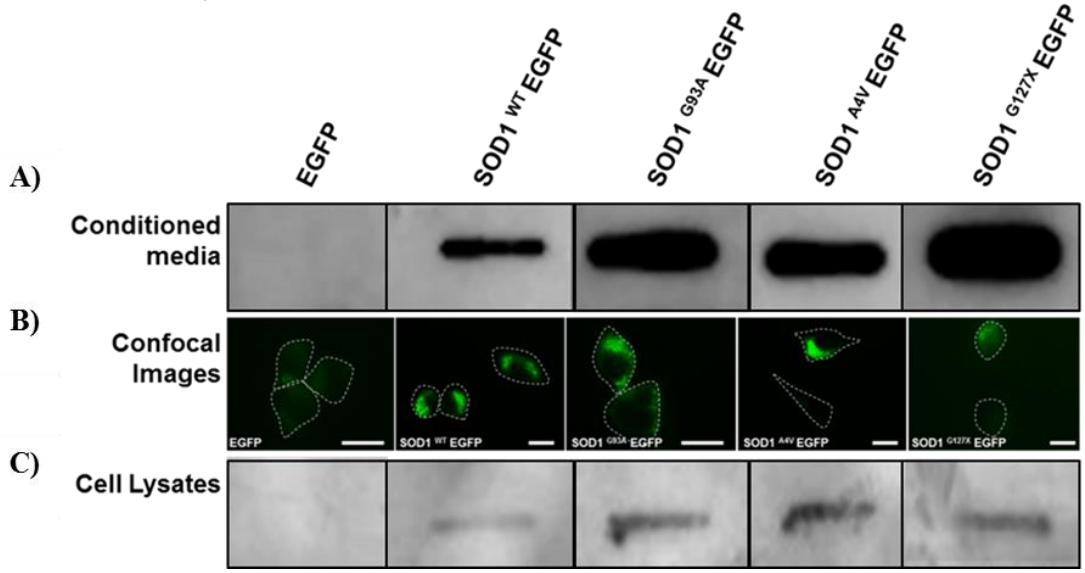

Figure 3.4 Wild type and mutant SOD1 proteins can be detected in conditioned media of NSC-34 motor neurons transiently transfected with SOD1 and these can transmit to naïve NSC-34 cells (A) After identifying the presence of aggregates using filter trap analysis (72 h) (B) conditioned media was collected and treated with 250 units of Dnase for 10 min at RT, centrifuged and pelletable fraction added onto adherent naïve NSC-34 cells for 2 h and were visualised by confocal microscopy to observe for internalised extracellular SOD1 protein aggregates. Bars represent 10 μm and results are representative of n=2 (C) Cells were lysed and a pelletable fractions were obtained by centrifugation. Pelletable fractions were then separated onto cellulose acetate membrane (0.2μM) in a filter trap apparatus, and then incubated with anti-EGFP Ab.

3.3.4 SOD1 aggregates can transfer from cell to cell

Given the ability for naïve cells to take up aggregates from conditioned media, the ability of aggregate transfer from cell-to-cell was next examined. Prior to analysis, fluorescence compensation was performed to account for spectral overlap into the GFP channel **(**Figure 3.5A). Cells were either transfected with GFP or tdTomato separately and then cell populations mixed, any acceptor cells with both red and green after the incubation period was deemed a SOD1 transfer event. Next, transfer events were quantified as the percentage of transfected acceptor cells positive for both EGFP/tdTomato using the gating strategy outlined in Figure 3.5B. Two cell populations transiently expressing $SOD1^{WT}$ tdTomato or $SOD1^{G93A}$-EGFP proteins were co-cultured at a ratio of 1:1 and analysed using flow cytometry **(**Figure 3.5C). Control cells were also transfected separately, however they were mixed immediately prior to flow cytometry analysis. Similar to previous cell to cell in culture findings (Grad et al., 2014), approximately 2.7 ± 1% at 24 h, 1.2 ± 0.1% at 48 h and 5.2 ± 0.6% at 72 h acceptor NSC-34 cells were found to contain significantly greater amount of both $SOD1^{WT}$ tdTomato and $SOD1^{G93A}$-EGFP from donor cells, and were scored as EGFP/tdTomato red double-positive, compared to the controls. These results therefore indicate that that either or both $SOD1^{WT}$ tdTomato and $SOD1^{G93A}$-EGFP can release from NSC-34 donor cells into the conditioned media, into which they are then taken up by other neighbouring transiently transfected NSC-34 acceptor cells. This therefore demonstrated cell to cell transfer of SOD1 between donor and acceptor cells.

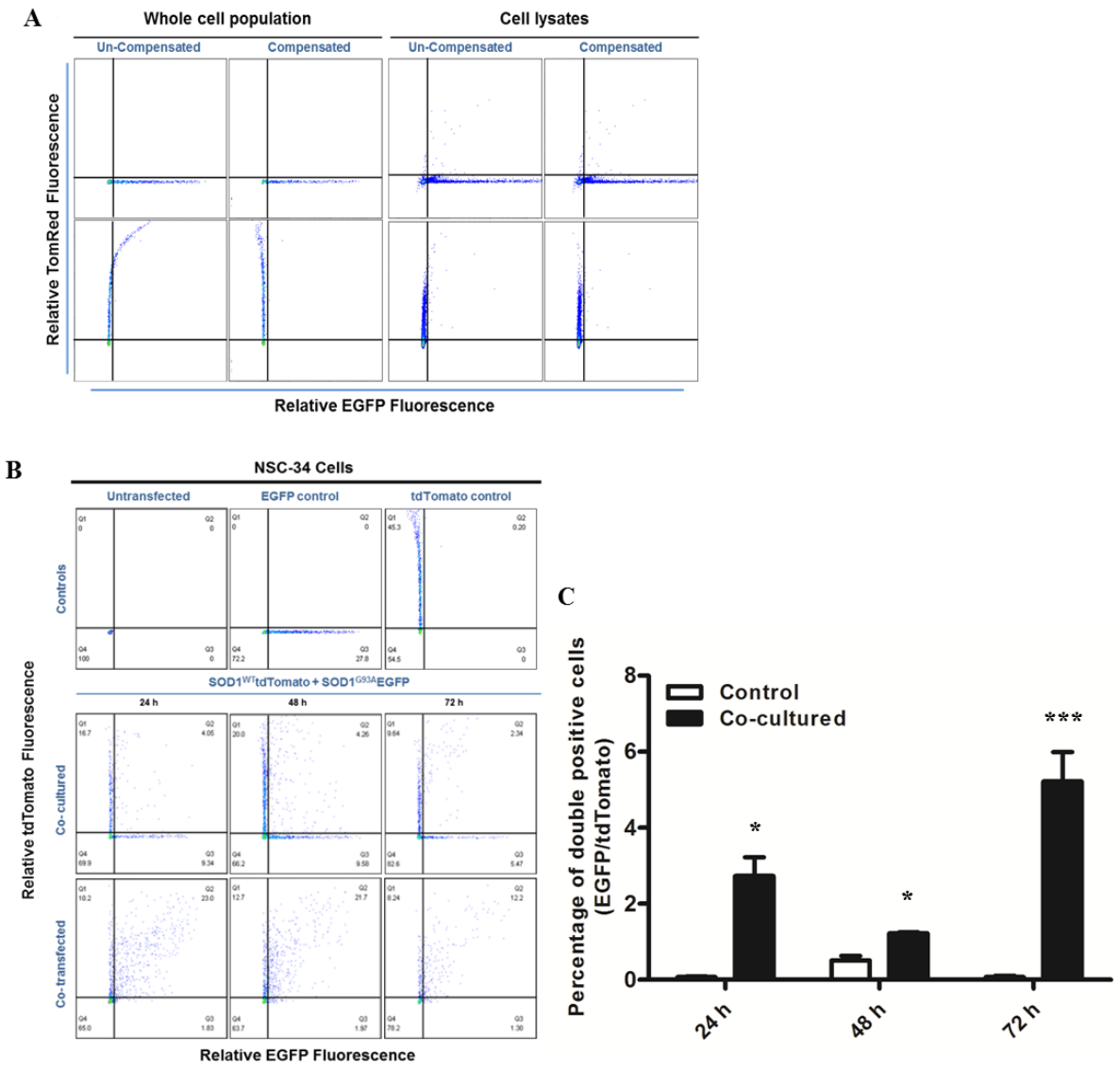

Figure 3.5 SOD1WT tdTomato and SOD1G93A-EGFP proteins can transfer between co-cultured NSC-34 motor neurons. Following transfection, using Lipofectamine 3000, NSC-34 transiently transfected with $SOD1^{WT}$ tdTomato, $SOD1^{G93A}$-EGFP, tdTomato or EGFP were either co-cultured or cultured separately for 24, 48 and 72 h. NSC-34 cells cultured separately were mixed prior to analysis (control) (A) $SOD1^{WT}$ tdTomato compensation to account for spectral overlap into the GFP channel (B) Results shown as dot plots of one representative set of data demonstrating the quadrant markers (C) mean percentage of cells ± SEM, $n = 3$; $^{***}P < 0.001$ or $^{*}P < 0.05$ compared to control (mixed population of cells).

3.3.5 SOD1 aggregates escape the endocytic pathway by damaging or rupturing the membrane of vesicles to gain access to the cytosol in NSC-34 motor neurons.

3.3.5.1SOD1 aggregates escape the endolysosomal system and enter into cytosol

The data presented in Chapter 2 demonstrated that SOD1 aggregates are indeed able to enter NSC-34 cells via stimulated macropinocytosis. However, the mechanism by which exogenously applied SOD1 aggregates induce the formation of cytoplasmic inclusions containing intracellular SOD1 has not yet been established. Given that this likely involves the escape of SOD1 from membrane bound endolysosomes, the ability of SOD1 aggregates to escape from endolysosomal compartments following its uptake was first investigated (Figure 3.6). NSC-34 cells were incubated with SOD1 aggregates at 37°C and imaged following incubation at incremental time intervals as indicated. Cells were then probed for SOD1 aggregates (using biotin-SA), and for lysosomes using Lysotracker red and images were captured with confocal microscopy. Exogenously added WT SOD1 aggregates entirely co-localised with Lysotracker dye, until 30 minutes, after which low levels of SOD1 could be observed outside the acidic endo-lysosomal system (Figure 3.6A) as indicated by the arrows. Similarly, G93A SOD1 aggregates were predominately observed in association with the lysotracker at 10 min and 30 min, however at 60 min aggregates were detected outside the acidic vesicles (Figure 3.6B) as indicated by the arrows.

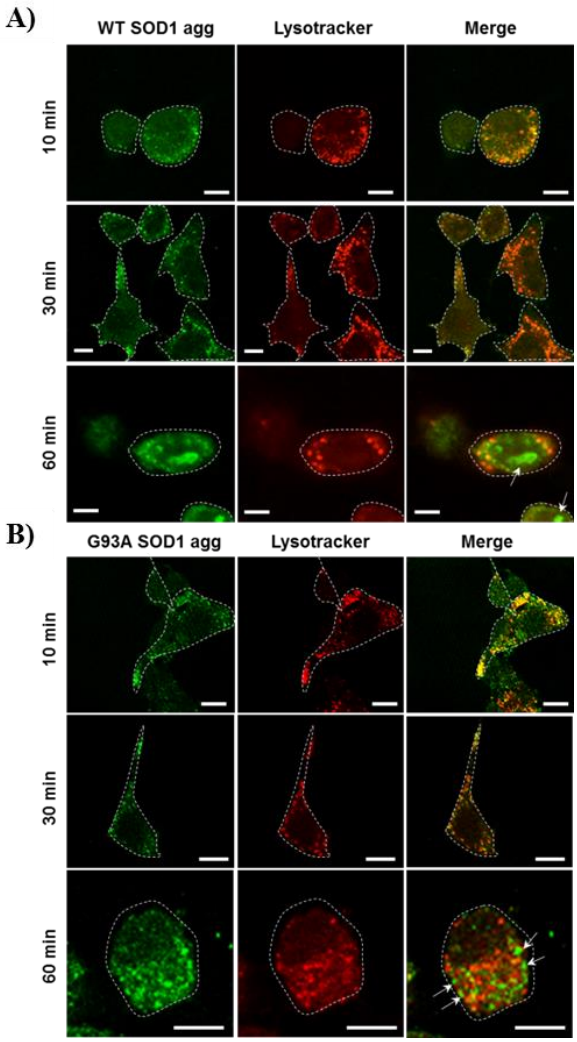

Figure 3.6 Internalised SOD1 aggregates entering *via* the endocytic pathway escape from the endosomes to the cytosol. Representative confocal images of NSC-34 cells pre-treated with Lysotracker Red for 2 h followed by treatment with 20 µg/ml of aggregated (A) WT SOD1 or (B) G93A SOD1 for either 10 min, 30 min or 60 min at 37°C, fixed with 4% PFA, permeabilised and labelled with an anti-human SOD1 pAB and anti-sheep IgG conjugated to Alexa Fluor 488. Slides were analysed by confocal microscopy. Representative confocal images are shown. Outline of cells are indicated with white dashed lines. Bars represent 10 µm. Results are representative of at least $n = 3$.

These data suggest that SOD1 aggregates can escape the endolysosomal system (Figure 3.6). However, to confirm whether SOD1 aggregates had entered the cytosol, NSC-34 cells were incubated with WT and G93A SOD1 aggregates and their location within the cell was then investigated by immunoblotting of cytosolic, membrane (ER/Golgi), nuclear and cytoskeletal supernatant fractions (Figure 3.7). In the WT SOD1 treated fractions (Figure 3.7A), WT SOD1 aggregates predominantly fractionated with the cytoskeleton (PE) fraction presenting as a high molecular weight smear ranging from 50 to over 160 kDa in size. An additional band in the cytoplasmic (CE) fraction was detected, with an approximate size of 16 kDa,

corresponding to human SOD1 monomer likely separated from larger aggregates. Similarly, treatment with G93A SOD1 aggregates (Figure 3.7B) resulted in the detection of high molecular weight smear ranging from approximately 60 to over 150 kDa in size in the cytoskeleton (PE) fraction. In addition, minor smearing of high molecular weight bands was observed in the cytoplasmic (CE) fraction ranging from approximately 50-160 kDa in size and a band at 16 kDa; the predicted size of human SOD1 monomer. Non-specific Ab binding was also observed, predominantly in the G93A blot. To further confirm the efficiency of the fractionation, the fractions were immunoblotted using an anti-actin, anti-EEA1 and anti-vimentin Ab (Figure 3.7C). Confirming the success of the fractionation vimentin (54 kDa) was predominantly found in the PE fraction and EEA1 (180 kDa) was primarily detected in the ME fraction. Actin was found in all fractions. Furthermore, proteins remaining in the endolysosomal system would be present in the membrane extract (ME) fraction, and therefore absence of these proteins in the ME fraction support above findings.

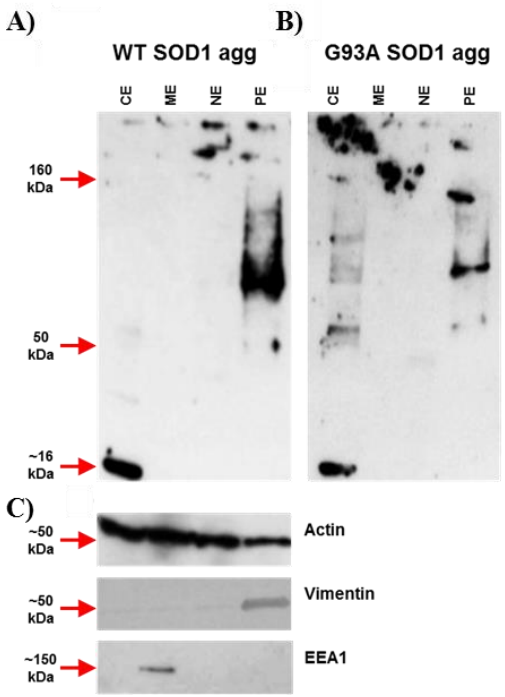

Figure 3.7 Internalised aggregates are detected in the cytoplasm of NSC-34 cells. Cytoplasmic extract (CE), membrane extract (ER/Golgi) (ME), nuclear extract (NE) and pellet extract (cytoskeleton) (PE) fractions by centrifugation from NSC-34 cells treated with either (A) WT or (B) G93A SOD1 aggregates (20 µg/mL) or (C) PBS alone and were separated by SDS PAGE under reducing conditions, transferred to nitrocellulose membrane and incubated with streptavidin-HRP, anti-actin, anti-EEA1 or anti-vimentin Abs (as indicated). Results show one experiment and are representative of two experiments.

To further investigate the presence of SOD1 aggregate uptake into membrane bound vesicles and their subsequent escape to the cytosol, a selective permeabilisation assay was performed (Figure 3.8). Selective permeabilisation involves the use of Triton X-100 detergent, which disrupts all cellular membranes, or the glycoside digitonin which selectively permeabilises the plasma membrane leaving only intracellular, nuclear, ER and Golgi membranes intact (Figure 3.8A) (Nizard et al., 2007). Firstly, the assay conditions were optimised to confirm adequate and selective permeabilisation of NSC-34 cells. Cells were incubated with either Triton X-100 (0.5%) or digitonin (10 μM) for 30 min and 10 min at 4°C respectively, and immunolabelled with Abs specific for lysosomal associated membrane protein 1, LAMP1; Binding immunoglobulin protein, BiP; Early endosome antigen 1, EEA1; and cytosolic protein, β-Tubulin and analysed by confocal microscopy (Figure 3.8B). LAMP1, BIP and EEA1 were detected upon treatment with Triton-X 100 only, and no protein signal was observed upon treatment with digitonin, consistent with their location in membrane enclosed vesicles. However, β-Tubulin was detected after treatment with both Triton-X100 and digitonin consistent with its presence in the cytoplasm. This indicated that the Triton-X100/digitonin method under these conditions, and in NSC-34 cells, provides satisfactory selective permeabilisation.

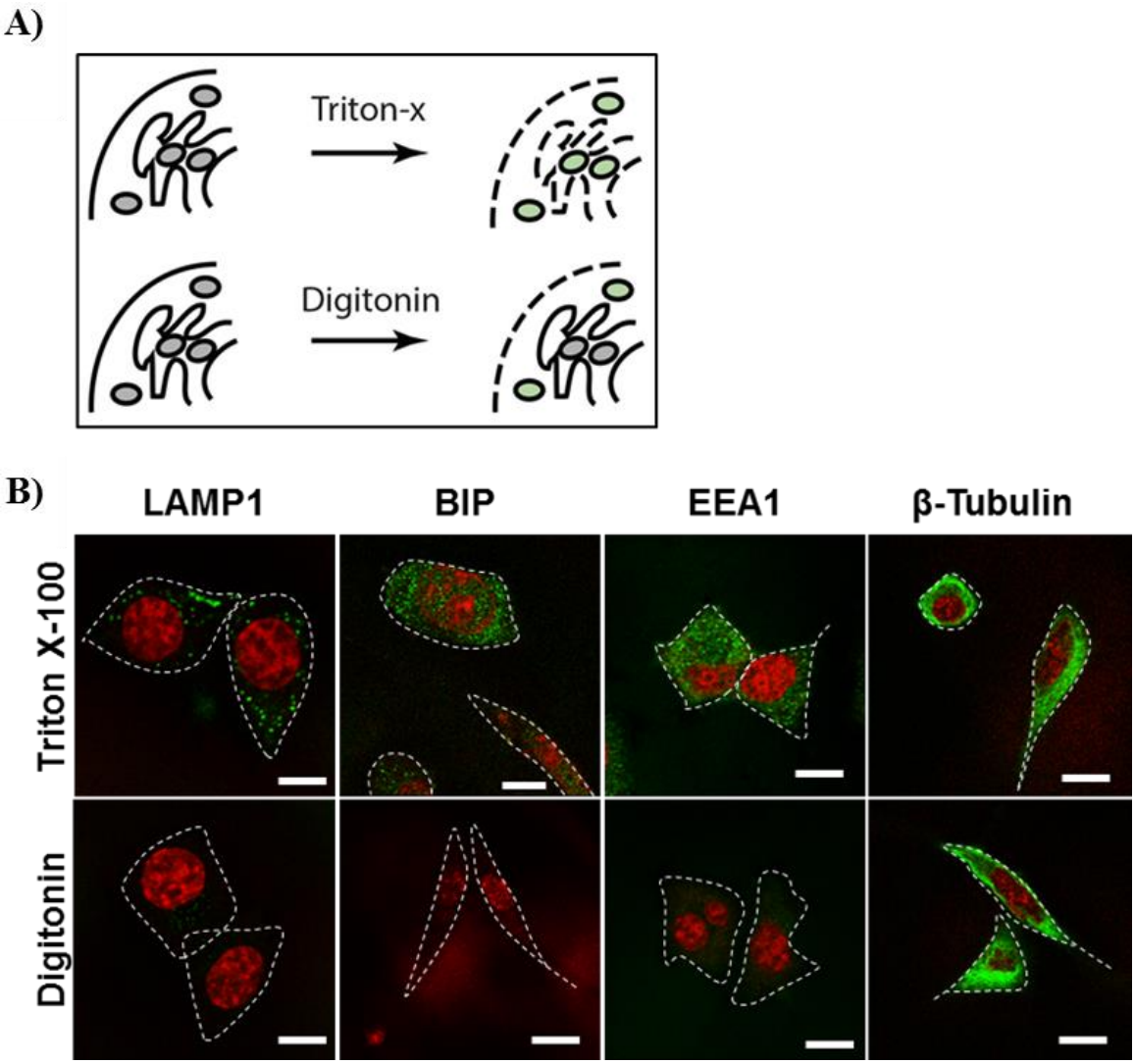

Figure 3.8 Digitonin selectively permeabilises the plasma membrane of NSC-34 cells. Adherent NSC-34 cells were incubated in complete culture media for 24 h. min at 37°C, fixed with 4% paraformaldehyde, permeabilised with either triton-x 100 or digitonin. Cells were labelled with anti-LAMP1 mAb, anti-BiP/GRP78 mAb, anti-β-tubulin mAb and anti-EEA1 pAb followed by Alexa Fluor 488-conjugated anti- rabbit and mouse Ab and analysed by confocal microscopy. RedDot2 (1X) was used as a counter stain (10 min at RT). Representative confocal images are shown. Outline of cells are indicated with white dashed lines. Bars represent 10 µm. Results are representative of at least $n = 2$.

Next, to confirm that aggregates were present outside any membrane enclosed compartments, cells were incubated with aggregated or soluble SOD1 and treated either with Triton X-100 or digitonin, immunolabelled with a specific Ab and analysed by confocal microscopy (Figure 3.9). At the 60 min time-point, SOD1 aggregates were detected only after Triton X-100 permeabilisation in NSC-34 cells treated with WT (Figure 3.9A) and mutant G93A SOD1 aggregates (Figure 3.9B), with no detectable fluorescence signal in cells treated with digitonin.

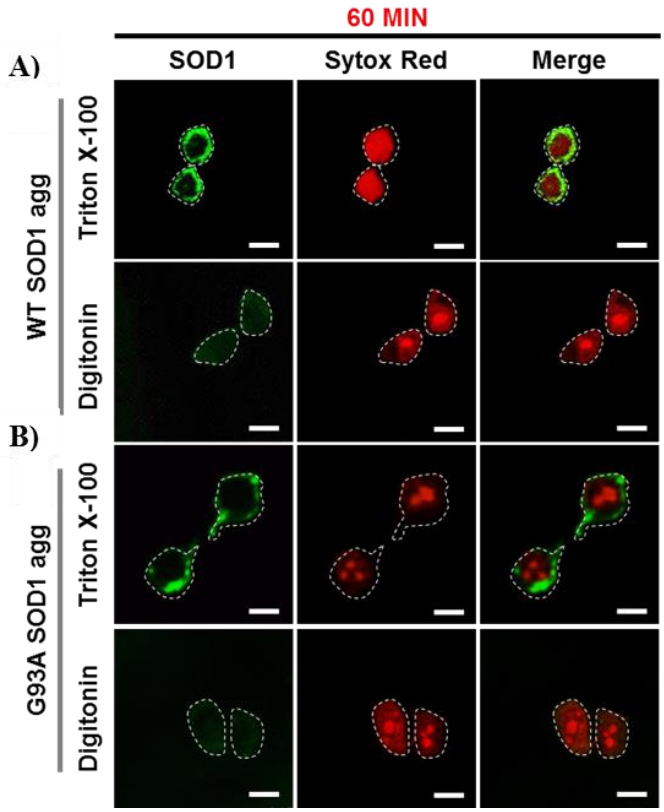

Figure 3.9 Internalised SOD1 aggregates are not detected in the cytoplasm of NSC-34 cells at 60 min Adherent NSC-34 cells were incubated with 20 µg/ml of aggregated (A) WT or (B) G93A SOD1 for 60 min at 37°C, fixed with 4% paraformaldehyde, permeabilised with either triton-x 100 or digitonin and labelled with Alexa Fluor 488 streptavidin for biotinylated aggregates. Sytox Red (5 µM) was used as a counter stain (10 min at RT). Slides were analysed by confocal microscopy. Representative confocal images are shown. Outline of cells are indicated with white dashed lines. Bars represent 10 µm. Results are representative of at least $n = 3$.

While it had been observed that SOD1 aggregates appear to escape the endolysosomal system after 60 min incubation, the above data suggest that aggregates remain within membrane bounded compartments at 60 min of incubation (Figure 3.9)**.** Thus, the release of SOD1 aggregates from membrane bound vesicles was further investigated after the 60 min time-point in NSC-34 cells (Figure 3.10). Cells were incubated with SOD1 aggregates for an extended period of 120 min and then treated with either Triton-X 100 or digitonin as above. Interestingly, both WT (Figure 3.10A) and G93A (Figure 3.10B) SOD1 aggregates were now detected after permeabilization by digitonin, suggesting that SOD1 aggregates are present in the cytosol at 120 min. To demonstrate the specificity of the assay, NSC-34 cells were incubated with the control protein RAP-GST for 120 min (Figure 3.10C). After 120 min

RAP-GST was detected after Triton-X 100 permeabilisation but not after digitonin permeablisation, consistent with its maintenance in a membrane bound vesicle.

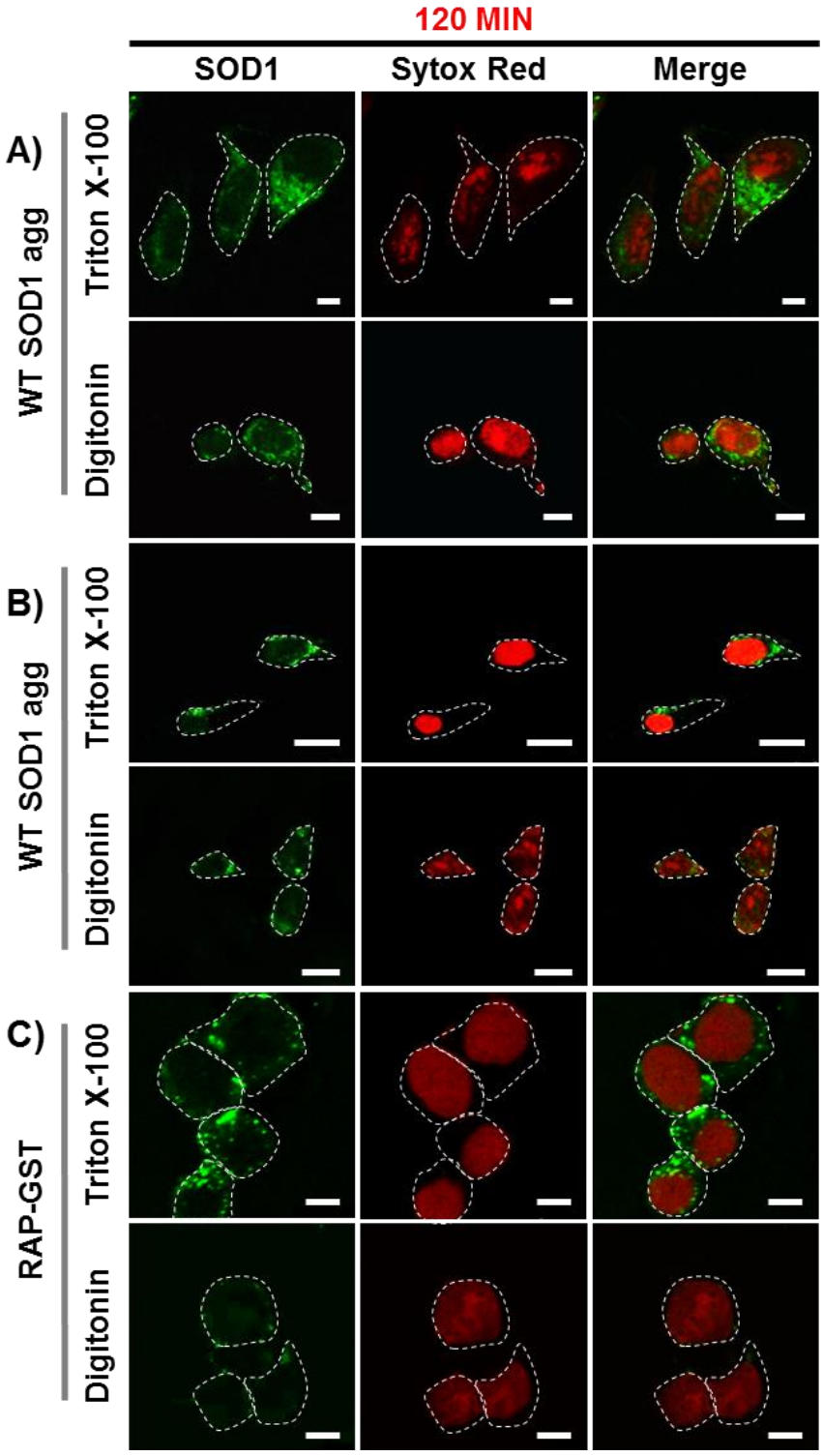

Figure 3.10 Internalised SOD1 aggregates are detected in the cytoplasm of NSC-34 cells at 120 min Adherent NSC-34 cells were incubated with 20 µg/ml of aggregated SOD1 for 120 min at 37°C, fixed with 4% paraformaldehyde, permeabilised with either triton-x 100 or digitonin. Biotinylated aggregates were detected with Alexa Fluor 488 streptavidin or anti-RAP Ab. Sytox Red (5 µM) was used as a counter stain (10 min at RT). Representative confocal images are shown. Outline of cells are indicated with white dashed lines. Bars represent 10 µm. Results are representative of at least $n = 3$.

3.3.5.2 SOD1 aggregates induce the rupture of endocytic vesicles in NSC-34 motor neurons

Exogenous human SOD1 aggregates have been shown to enter into NSC-34 cells *via* stimulated macropinocytosis, thus are transported intracellularly in macropinosomes (Chapter 1) which are thought to be 'leaky' due to their lack of a physical or rigid structure (Conner and Schmid, 2003). Since the redistribution of Galectin-3 has been used as a tool to identify and measure vesicle rupture in studies of bacteria and viruses (Maier et al., 2012; Ray et al., 2010), here the redistribution of galectin-3 was used to examine if extracellularly applied SOD1 aggregates could rupture vesicles (Figure 3.11). Galectin-3 is a cytosolic protein that binds strongly to structures on the luminal side of the endosome, thus upon rupture a redistribution of galectin-3 occurs. To examine whether SOD1 aggregates lead to the accumulation of galectin-3, cells were incubated with SOD1 aggregates for 2 h and specifically permeabilised with digitonin, stained for galectin-3 and then examined by confocal microscopy (Figure 3.11A). Galectin-3 staining was quantified from these images (Figure 3.11B). Cells permeabilised by digitonin and treated with PBS alone (negative control) presented with very little accumulated galectin-3 staining compared to cells permeabilised with triton x-100 which presented with significantly higher galectin-3 staining. This is consistent with a large fraction of galectin-3 being bound on the inside of endosomal compartments (Schneider et al., 2010). Similarly, incubation with WT and G93A SOD1 aggregates and mutant SOD1 soluble protein induced a significant increase galectin-3 staining and pronounced intracellular and punctate structures. This is consistent with endosome rupture and accumulation of galectin-3.

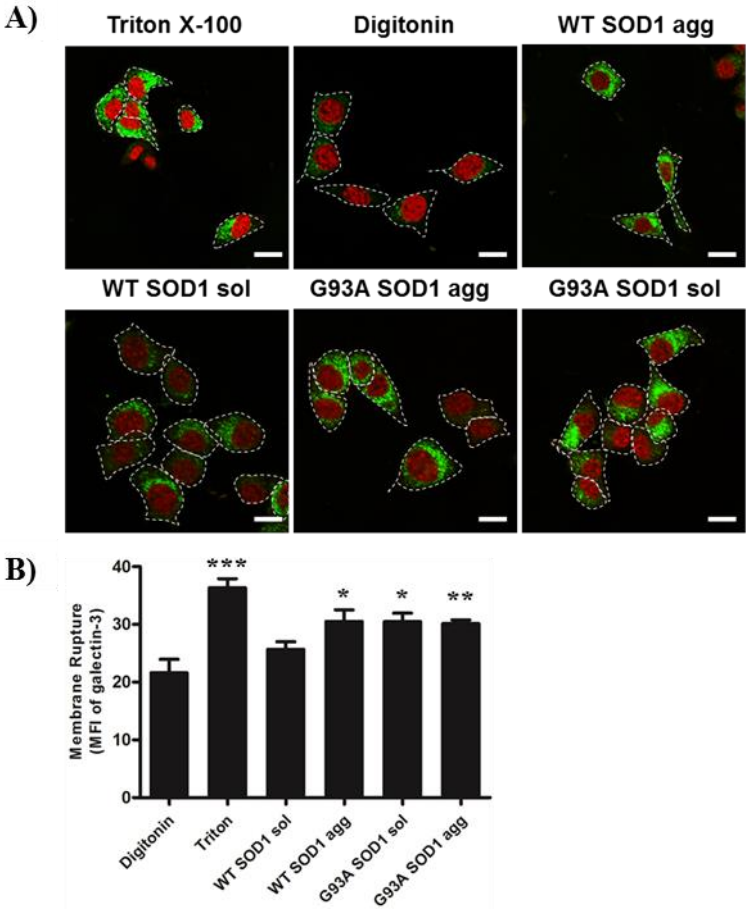

Figure 3.11 SOD1 aggregates and mutant SOD1 soluble proteins induce discrete Galectin-3 puncta immunofluorescence (A) Adherent NSC-34 cells were incubated with 20 µg/ml of soluble and aggregated WT and G93A SOD1 for 2 h at 37°C, fixed with 4% paraformaldehyde, permeabilised with either triton-x 100 (control only) or digitonin (all samples). Cells were labelled with anti-Galectin 3 mAb followed by Alexa Fluor 488-conjugated anti- mouse Ab and analysed by confocal microscopy. RedDot2 (1X) was used as a counter stain (10 min at RT). Representative confocal images are shown. Outline of cells are indicated with white dashed lines. Bars represent 10 µm. (B) Mean fluorescence intensities (MFI) of Galectin-3 per cell were quantified from these images using ImageJ software (Version 1.48) (National Institutes of health, Bethesda, MD). A minimum of 200 cells were scored per treatment. Results shown as mean cellular fluorescence intensity means ± SD, n = 3, $^{***}P$ <0.001, $^{**}P$ < 0.01 or $^{*}P$ < 0.05 compared to corresponding control (no protein treatment).

3.3.5.3 SOD1 aggregates induce significant changes in biological membrane structures

To further characterise the ability of exogenous human SOD1 aggregates to rupture membranes, human red blood cells and liposomes were obtained and examined for interactions with SOD1 aggregates (Figure 3.12). First, purified human red blood cells were incubated for 2 h in the presence of SOD1 aggregates and then the amount of membrane disruption was measured by total amount of free hemoglobin in the supernatants (Figure 3.12A). Very little hemoglobin was detected in the supernatants of cells treated with PBS

only; however, a significantly higher amount of hemoglobin was measured in the supernatants of red blood cells treated with Triton-X100. Incubation with soluble mutant G93A SOD1 and aggregated SOD1 proteins significantly increased the amount of free hemoglobin consistent with an ability to damage biological membranes. Similar to red blood cells, SOD1 aggregates altered the morphology liposomes, deforming their structures (Figure 3.12B). Collectively, this suggests that SOD1 aggregates are capable of inducing damage to biological membranes and thus allowing their escape in to the cytosol.

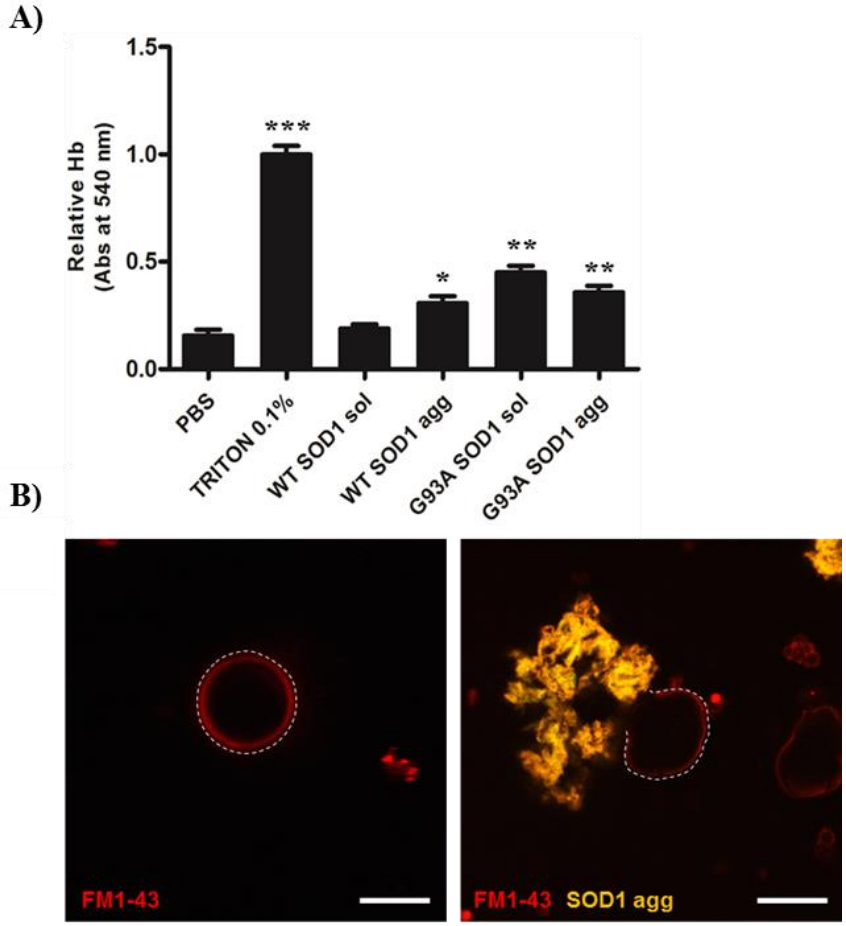

Figure 3.12 Mutant SOD1 and SOD1 protein aggregates damage biological membranes. (A) Clarified human blood cells were incubated with 20 µg/ml of WT and G93A SOD1 soluble and aggregated proteins or 0.1% Triton-x100 for 2 h at 37°C. Absorbance of haemoglobin (A540nm) was determined by spectrometry and results shown as means A540 nm ± SD, $n = 6$; $^{***}P < 0.001$, $^{**}P < 0.01$ or $^{*}P < 0.05$ compared to corresponding control (PBS). (B) Unilamellar vesicles were formed from L-α-phosphatidylcholine and incubated with 20 µg/ml of SOD1 aggregates for 2 h at 37°C as indicated. Slides were analysed by confocal microscopy. Bars represent 10µM. Results are representative of one experiment.

3.3.6 SOD1^{G93A} –EGFP can induce aggregation of SOD1^{WT} tdTomato protein in co-cultured NSC-34 motor neurons

The above data indicates that SOD1 proteins can transfer between co-cultured NSC-34 motor neurons and that SOD1 aggregates can escape membrane bound vesicles. Thus, the ability of mutant SOD1 aggregates to induce aggregation of WT SOD1 was next characterised in NSC-34 cells. Given that SOD1^{WT} tdTomato produces cells with very few aggregates it was used as a marker for seeding by SOD1^{G93A}-EGFP (Figure 3.13). Initially, the lysates of NSC-34 cells containing large particles were gated (nuclei and inclusions) and after nucleus removal, particles were analysed for green or red fluorescence to identify inclusions made by EGFP or tdTomato (see Figure 3.2). Using FloIT, the number of SOD1^{WT} inclusions was then investigated to identify and measure seeding activity induced by mutant SOD1^{G93A}-EGFP. To calculate the average number of inclusions per 100 transfected cells in the populations analysed, the number of inclusions acquired is simply divided by the transfection efficiency (separately determined by flow cytometry) of the sample, which is then multiplied by the corresponding number of cell nuclei enumerated. An increase in the amount of SOD1^{WT} tdTomato inclusion formation in the co-cultured treatment was observed from 24 to 72 h. However, a statistical significance was only measured at 72 h compared to the corresponding control, indicative of mutant SOD1^{G93A}-EGFP induced seeding of SOD1^{WT}. However, the control treatment which is transfected NSC-34 cells cultured separately and mixed prior to analysis; presented with significantly high amounts of inclusions overtime, potentially due to differences in toxicity or an effect of seeding reactions.

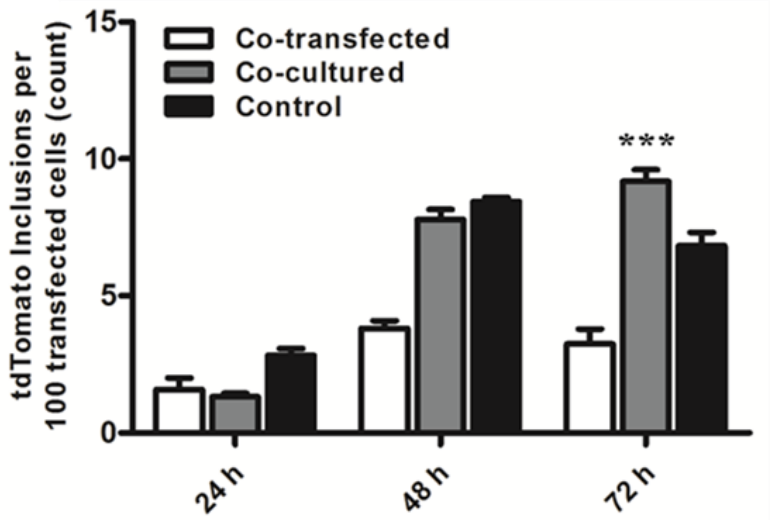

Figure 3.13 Co-culture with SOD1G93A increases WT SOD1 aggregation. Following transfection, NSC-34 cells expressing $SOD1^{WT}$ tdTomato or $SOD1^{G93A}$-EGFP were subsequently co-cultured, co-transfected or cultured separately together for 24, 48 and 72 h. The number of WT SOD1 inclusions obtained were enumerated by the FloIT method; means ± SEM, $n = 3$; $^{***}P < 0.001$ compared to corresponding treatment at 24 h.

3.3.7 Recombinant mutant SOD1 can seed aggregation and induce inclusion formation in NSC-34 cells expressing $SOD1^{WT}$ tdTomato protein

It has previously been observed that mutant SOD1 aggregates in conditioned media can induce the aggregation of soluble intracellular mutant SOD1 (Münch et al., 2011). Furthermore, other studies have shown that mutant SOD1 induces the misfolding of human $SOD1^{WT}$ when transfected in human mesenchymal and neural cell lines (Grad et al., 2011). In addition, the above data indicates that there is a significant increase in the number of inclusions identified in transfected NSC-34 motor neurons from co-cultured with cells expressing SOD1G93A at 72 h. Thus, the seeding behaviour of protein only aggregates of SOD1 was further investigated at 72 h. To assess whether non-vesicular mutant SOD1 aggregates induce the aggregation of endogenous SOD1 proteins in NSC-34 motor neurons, cells were transiently transfected with $SOD1^{WT}$ tdTomato protein and incubated with human recombinant G93A mutant SOD1 aggregates for 72 h (Figure 3.14). As previously described above, the number of inclusions per transfected cell was determined by flow cytometry using the FLoIT technique. Incubation with mutant SOD1 aggregates at 72 h, induced a significantly higher number of inclusions (75 ± 3) in comparison to cells incubated in the

absence of mutant SOD1 aggregates (32 ± 3). This suggests that mutant SOD1 aggregates can induce aggregation of $SOD1^{WT}$ tdTomato in NSC-34 cells.

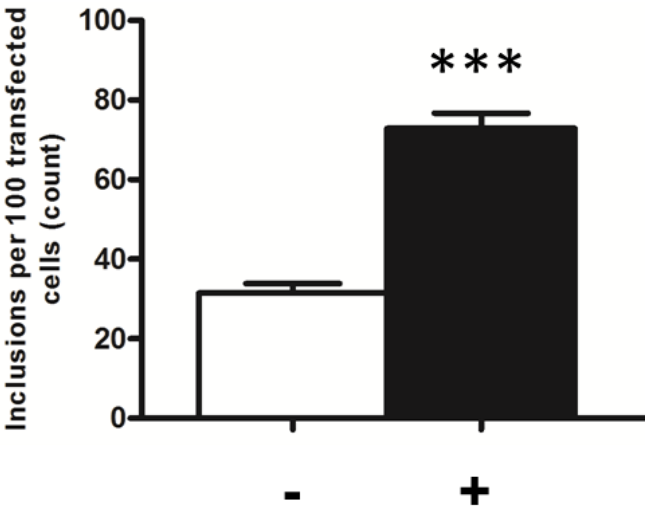

Figure 3.14 Recombinant human mutant SOD1 aggregates induce the aggregation of SOD1WT tdTomato in NSC-34 motor neurons. Following transfection, using Lipofectamine 3000, NSC-34 cells expressing $SOD1^{WT}$ tdTomato, were incubated with 20 µg/mL of human recombinant protein only; G93A mutant SOD1 for 72 h. The number of inclusions obtained were enumerated by FloIT method means ± SEM, $n = 3$; $^{***}P < 0.001$ compared to corresponding control (absence of mutant SOD1 aggregates). (+) refers to the presence of recombinant mutant SOD1 aggregates, (-) refers to the absence of recombinant mutant SOD1 aggregates.

3.4 Discussion

The current study demonstrated that WT and mutant G93A SOD1 proteins can form spontaneous aggregates in cells and their appearance coincides with an increase in cell death. The current study also demonstrated and confirmed that SOD1 aggregates can be released from transiently transfected NSC-34 motor neurons potentially from dying or dead cells. Furthermore, extracellular released SOD1 aggregates derived from conditioned media were shown associated with naïve cells and their internalisation was confirmed. The transfer of SOD1 between NSC-34 cells was also confirmed in this study. Upon endocytosis by NSC-34 motor neurons, soluble and aggregated SOD1 escapes the endolysosome system to be deposited in the cytosol. Lastly, using the novel FLoIT method which is a tool to accurately measure and quantify inclusions, demonstrated increased inclusion formation of WT SOD1 induced by co culture with cells expressing mutant SOD1. Seeding by protein only human recombinant exogenous aggregates was also demonstrated, supporting these results. The results presented here suggest that SOD1 aggregates rupture macropinosomes and escape into the cytosol where they can induce aggregation of SOD1, consistent with reports of exogenous mutant SOD1 aggregates identified in the cytosolic compartment of mammalian cells (Münch et al., 2011). Collectively, this supports a role for SOD1 in the infectious prion-like spread of protein aggregation in neuronal cells.

Previous studies have suggested that WT and mutant forms of SOD1 can spontaneously form aggregates and fibrils given the right conditions *in vivo* (Chia et al., 2010) and *in vivo* where human WT SOD1 has been shown to spontaneously aggregate in G93A Gurney strains of mice (Prudencio et al., 2010). Similar to these observations, spontaneous SOD1 aggregate formation in NSC-34 cells was confirmed in the current study. In addition, NSC-34 cells expressing mutant $SOD1^{G93A}$ formed significantly greater numbers of inclusions compared to

the $SOD1^{WT}$ expressing cells. Inclusion formation has been reported to inversely correlate to the number of motor neurons found in ALS spinal cord tissue, suggesting that inclusion formation is toxic and leads to cell death (Giordana et al., 2010). Similarly, a previous study has reported that cytoplasmic mislocalisation and aggregation of mutant SOD1 induces cell death in WT and mutant G93A SOD1 mouse primary neurons and astrocytes (Lee et al., 2015). Supporting this notion, a significant increase in cell death was observed over the 72 h transfection period in NSC-34 cells expressing $SOD1^{G93A}$EGFP. Cell death was also apparent for NSC-34 cells expressing $SOD1^{WT}$-EGFP to a lesser extent. Although misfolded wild-type and mutant SOD1 have been reported to activate the same neurotoxic mechanism and share an aberrant conformation (Bosco et al., 2010), mutants possess a higher inherent propensity to aggregate, thus may be more toxic to cells (Prudencio et al., 2009b; Valentine and Hart, 2003). Recently, a study was able to show that different mutant SOD1 variants have differential aggregation propensities in NSC-34 cells (McAlary et al., 2016). This study also reported that cellular aggregation correlates with cell loss and that the major predictor for cellular aggregation of SOD1 variants is the abundance of destabilized SOD1 states which differs between different mutants. However, although a strong correlation exists between cellular aggregation and cell loss, translating this to severity of human disease is limited, given that one of the variants ($SOD1^{G37R}$) reported in this study is toxic in cells and has a high propensity to aggregate, however has a mean disease duration of 17 years (McAlary et al., 2016).

While there is now good evidence that both soluble and aggregated SOD1 can be taken up by neurons and neuron like cells, there is little work describing the release of SOD1 aggregates. Soluble SOD1 secretion into the culture medium has previously been shown using human hepatocyte, fibroblast, neuroblastoma, and thymic-derived cell lines (Cimini et al., 2002; Mondola et al., 1996). In the current study, the release of WT and mutant SOD1 variants

including G93A, A4V and G127X from NSC-34 motor neurons was initially observed 72 h following transfection. The release of SOD1 from transiently transfected cells has previously been attributed to cell death (Grad et al., 2014). While other studies have reported SOD1 release is mediated *via* constitutive mechanisms such as calcium dependant release and chromaginin mediated secretion of SOD1 (Santillo et al., 2007; Urushitani et al., 2006), the current study suggests that SOD1 release coincides with toxicity, under the conditions used for the filter trap assay.

The work presented here cannot rule out that $SOD1^{G93A}$-EGFP released from cells was secreted either *via* exosomes, microvesicles or neurosecretory vesicles or a combination of these. In support of this idea, the active release of SOD1 as part of exosomes and microvesicles from NSC-34 and neuroblastoma cells respectively, has been previously reported (Gomes et al., 2007; Grad et al., 2014; Mondola et al., 2003). Further supporting this notion, ALS pathology spreads from region to region in a spatiotemporal manner (Ravits and Spada, 2009) prior to obvious cell death, suggesting an active release process in the early stages of the disease. In addition, mutant SOD1 can interact with chromogranins which promote their secretion from neurosecretory vesicles (Urushitani et al., 2006). Consistent with this, mutant SOD1 has shown to translocate from the cytosol to the ER-Golgi pathway (Urushitani et al., 2008), and the secretion of mutant SOD1 from NSC-34 can be reduced upon incubation with a secretion inhibitor (Turner et al., 2005). In addition, it is suggested that less mutant SOD1 is secreted when compared to WT SOD1, and this impaired secretion coincides with intracellular formation of inclusions thus toxicity (Gomes et al., 2007; Turner et al., 2005).

Recent lines of evidence implicate the transmission of extracellular SOD1 in the progression of disease in ALS *via* a prion-like mechanism, involving pathological interactions with the

cell surface and internalisation into neuronal and non-neuronal neighbouring cells. A toxic role for SOD1 was suggested by a previous study, which found secreted SOD1 from astrocytes derived from post-mortem spinal cord tissues from sALS and SOD1-related fALS induced motor neurons cell death (Haidet-Phillips et al., 2011). The uptake of SOD1 has previously been thought to be mediated by non-specific endocytosis, specifically macropinocytosis (see Chapter 1) (Münch et al., 2011; Sundaramoorthy et al., 2013). Furthermore, both WT and mutant SOD1 can be detected in the cerebrospinal fluid of fALS patients and healthy controls (Zetterstrom et al., 2011). In the current study, both WT and mutant SOD1 variants released into conditioned media were found to internalise into naïve NSC-34 cells. This transmission was unaffected by DNase digestion of conditioned media, ruling out a role for residual plasmid in recipient culture media. The uptake of secreted SOD1 from conditioned media was also reported in other studies (Grad et al., 2014; Münch et al., 2011; Sundaramoorthy et al., 2013). While experiments in chapter 2 showed that uptake of SOD1 was relatively specific (i.e. GST was not taken up), here we could not rule out a non-specific uptake of GFP given no measurable amount of EGFP was detected in the conditioned media. Moreover, consistent with observations presented here, media-to-cell transfer of protein aggregates has been previously reported for α-synuclein (Desplats et al., 2009), polyglutamine peptides and Huntingtin protein aggregates associated with Huntington's disease (Ren et al., 2009; Yang et al., 2002).

Cell-to-cell transmission is a characteristic of mammalian prions. The spreading of pathology through neuronal pathways has previously been suggested to involve the cell-to-cell transmission of toxic protein species in ALS. Recent work has identified transmission of protein misfolding in the case of both WT and mutant SOD1 (Grad et al., 2014; Münch et al., 2011). However, the exact mechanisms involved in this transfer are not yet understood. In the current study, SOD1 released into co-culture conditioned medium from cells expressing

SOD1^{WT}-EGFP and SOD1^{G93A}-EGFP were found to be taken up into acceptor cells. This suggests that these proteins were able to transfer from cell-to-cell, consistent with reports from others (Grad et al., 2014; Münch et al., 2011). The percentage of co-cultured cells containing dual fluorescence, that is containing both WT SOD1-tdTomato and G93A SOD1-EGFP was around 1-2% for the first 48 h after which the numbers of dual coloured cells increased to around 5 % at 72 h. This suggests that at a time point when both aggregation and toxicity is increased so too is transfer of protein. This further supports the idea that motor neurons may be dying, releasing their content and transferring from cell to cell during disease propagation.

The autophagic-lysosomal pathway has been shown to play major roles in the removal of intracellular protein aggregates, however, previous reports suggest that certain infectious protein aggregates can escape these intracellular vesicles to enter into the cytosol (Freeman et al., 2013; Frost et al., 2009; Ren et al., 2009). Furthermore, propagation of aggregation in SOD1-ALS has been suggested to involve the escape of SOD1 aggregates from membrane bound endolysosomes (Münch et al., 2011). In the current study, recombinant WT and G93A SOD1 aggregates co-localised with acidic compartments until 30 min after which SOD1 aggregates were detected in the cytosol at 60 min. Thus, this suggests that SOD1 aggregates are initially compartmentalised to acidic compartments but rapidly escape these.

It has been identified previously that aggregates that enter cells somehow escape endocytic vesicles to interact with cytosolic protein. As described in Chapter 2 and other studies suggest that SOD1 aggregates are entering *via* macropinocytosis, thus these SOD1 aggregates are likely trafficked through large macropinosomes once internalised and the subsequent fate of macropinosomes varies depending on the cell type (Meier and Greber, 2003; Swanson and Watts, 1995). Macropinosomes are known to be leaky due to their lack of physical structure

and the resulting relatively easy loss of integrity of the macropinosome membrane (Conner and Schmid, 2003). This fact is often exploited by certain viruses to reach the cytosol (Kalia et al., 2013; Mercer and Helenius, 2009; 2012). Thus, it is suggested that the rigid structure of the SOD1 aggregates promote their escape from membrane bound vesicles, as a result of the destabilisation of the lipid bilayer (Holmes et al., 2013).

Consistent with the current study, protein aggregates made from other proteins, including α-synuclein associated with Parkinson's disease, enters cells *via* macropinocytosis and then the newly formed macropinosomes undergo traditional maturation and fuse with the lysosome (Nara et al., 2012). However, α-synuclein aggregates were then shown to induce the rupture of lysosomes following endocytosis into SH-SY5Y cells (Freeman et al., 2013). In addition, amyloid plaques, which are associated with Alzheimer's disease, are shown to contain active lysosomal hydrolases, which implies that plaques may originate from lysosomal rupture (Nixon et al., 2000). Moreover, protein aggregates are not the only infectious particle that enter the cytosol *via* rupture of endosomes, other infectious particles such as the Adenovirus protein type 5 enter the cytosol *via* this mechanism (McGuire et al., 2011). In the current study, SOD1 aggregates and mutant SOD1 G93A soluble protein induced membrane damage and rupture in human red blood cells, further supporting the notion that aggregated or misfolded SOD1 can interact with and destabilize membranes through exposed hydrophobic surfaces, therefore this suggests that the G93A soluble protein may have been in its unfolded state. Consistent with this idea, fibrillar β_2-microglobulin amyloid fibrils caused pronounced distortions to the membrane of liposomes (Milanesi et al., 2012). Further evidence of protein aggregate rupture of vesicles is the fact that non-monomeric forms α-synuclein induced the relocalisation of galectin-3 and the rupture of vesicles in the neuronal cell lines N27 and SH-SY5Y (Freeman et al., 2013). Similarly, in the current study, SOD1 aggregates and mutant SOD1 soluble proteins were shown to be able to disrupt the integrity of vesicular membranes

resulting in the relocation of galectin-3. Previous studies have shown that ROS generation is induced upon vesicular rupture (Freeman et al., 2013; Halle et al., 2008; McGuire et al., 2011), therefore making cells more susceptible to cell death. While it was not a line of investigation in the current study, it will be an interesting future direction to determine whether SOD1 induced rupture of lysosomes corresponds with an increase in cellular reactive oxygen species (ROS) and cell dysfunction and death in neurons, possibly contributing to disease progression.

Work presented here shows that both WT and G93A SOD1 aggregates were localised to the cytoplasmic and cytoskeleton fractions 2 h post-incubation. These results are consistent with SOD1 aggregates having a density comparable to cytoskeleton elements and, in addition, is consistent with cytosolic exposure of SOD1 aggregates. There was also a very small amount of high molecular weight WT SOD1 detected associated with the nuclear fraction, again consistent with cytosolic exposure (outside of the endo-lysosome system). However, in confocal microscopy experiments, aggregates were not observed within the nucleus suggesting aggregated material either bound the external portion of the nuclear membrane or pelleted at a similar density to the nuclear fraction. Nevertheless, this is consistent with other reports (Münch et al., 2011).

Selective permeabilisation using digitonin and Triton-X 100 (Nizard et al., 2007) confirmed that SOD1 aggregates were present outside any membrane-enclosed compartments. Specifically, imaging after plasma membrane permeabilisation with digitonin suggested that SOD1 aggregates could only be detected in cells after 120 min incubation with aggregates. This work suggests that SOD1 aggregates were within membrane bound organelles at 60 min, after which time the membrane of vesicles were ruptured by recombinant SOD1 aggregates. In comparison, RAP-GST, which is well-established to be internalised by receptor mediated endocytosis because of the recognition of RAP by LRP (Caetano-Pinto et al., 2016), was not

detected after digitonin permeabilsation at 120 min, indicating the maintenance of RAP-GST in endosomal-lysosomal compartment and suggesting that rupture of intracellular vesicles and/or escape of SOD1 is specific to SOD1.

A role for misfolded or aggregated SOD1 in seeding the aggregation of intracellular native SOD1 in a fashion similar to that of prions has been suggested by a number of recent studies (Chia et al., 2010; Grad et al., 2014; Münch et al., 2011; Pokrishevsky et al., 2012). It is well established that misfolded protein alone is sufficient to induce further misfolding in native proteins (Prusiner, 1982), and that newly formed misfolded protein may propagate misfolding pathology either through template-directed misfolding or nucleated polymerisation (Horwich and Weissman, 1997). In the current study, mutant SOD1 expressed in one population of cells was shown to induce the aggregation of intracellular WT SOD1 in another population of cells in a mechanism that must involve cell-to-cell transfer. Given that the methods used identified both dual coloured NSC-34 cell populations and also measured increases in intracellular WT SOD1 associated aggregates, this indicates that the transfer of mutant SOD1 seeded the aggregation of intracellular WT SOD1 proteins. Furthermore, the addition of human recombinant mutant SOD1 G39A protein aggregates to cells expressing $SOD1^{WT}$-EGFP enhanced the average number of WT SOD1 inclusions measured following incubation at 72 h, suggesting that mutant SOD1 aggregates are capable of inducing the misfolding and aggregation of human WT SOD1 in NSC-34 cells in a manner similar to prion template misfolding. Furthermore, this observation is consistent with another study that observed the conversion of native WT SOD1 to misfolded SOD1 in both a cellular context and in a cell-free system by mutant conformers (Grad et al., 2011). Although the exact mechanisms were not investigated in this current study, previous studies suggest that inducing the misfolding of human WT SOD1 is limited by the exposure of a single amino acid residue, a tryptophan (Trp) at position 32 (Grad et al., 2011). The seeding behaviour observed in the current study

is therefore similar to that of prion-activity, and consistent with the hypothesis that the propagation of protein aggregates between cells is responsible for the orderly progression of disease pathology observed in some neurological disorders (Clavaguera et al., 2009; Desplats et al., 2009; Jucker and Walker, 2013; Li et al., 2008; Ren et al., 2009; Volpicelli-Daley et al., 2011).

In conclusion, expression of WT and mutant SOD1 induced spontaneous aggregation of these proteins and cell death in NSC-34 cells. The release of SOD1 aggregates and their subsequent uptake in to naïve cells occurred at a time point that corresponded to a significant increase in cell death. It is therefore likely that aggregates are released *via* cell death however active release *via* exosomes cannot be ruled out. Furthermore, there are likely other pathways mediating the secretion of SOD1 *in vivo* and a range of mechanisms of SOD1 release, maybe potentially working in conjunction *in vivo*. The internalisation of both WT and mutant SOD1 protein aggregates induced the rupture of endocytic vesicles to gain access to the cytosol. The ability of these aggregates to induce damage and rupture in vesicles and biological membranes was confirmed and thus may play a role in cellular dysfunction. The underlying mechanisms by which misfolding propagation exerts toxic effects, whether it be inducing the misfolding of endogenous proteins through template directed misfolding or through secondary nucleation in the recipient cell is yet to be determined. The similarities observed between both WT and mutant SOD1 may explain the clinically indistinguishable nature of sALS and fALS.

Chapter 4

THE MISLOCALISATION AND AGGREGATION OF THE PRION-LIKE PROTEIN TDP-43

4.1 Background

Amyotrophic lateral sclerosis (ALS) is an incurable neurodegenerative disorder characterized by the loss of both the upper and lower motor neurons in the brain and spinal cord respectively, resulting in the progressive paralysis of the muscles of speech, limbs, swallowing and respiration, due to the progressive degeneration of innervating motor neurons (Cleveland and Rothstein, 2001).

The neuropathology of all cases of ALS are characterised by disease-specific proteins, mutant and wild type alike; mislocalised and abnormally accumulated as misfolded, insoluble aggregates in the cytoplasm of afflicted motor neurons (Bosco et al., 2010; Leigh et al., 1991; Ross and Poirier, 2004). Proteinaceous inclusions, containing misfolded aggregated proteins, peptides and fragments, also occur in many other neurodegenerative disorders including Alzheimer's disease (AD), Parkinson's disease (PD), frontotemporal dementia (FTLD), Huntington's disease (HD) (Forman et al., 2004); and prion diseases, such as Creutzfeldt-Jakob disease, Kuru and fatal familial insomnia diseases (Prusiner, 1982; Prusiner, 1984).

Mutations in several genes cause familial ALS (fALS) which account for 5-10% of total ALS cases and contribute to the development of sporadic ALS (sALS, 90% of ALS cases) (Andersen and Al-Chalabi, 2011). In fALS, mutations in the gene encoding the Cu/Zn superoxide dismutase (SOD1), a ubiquitously-expressed homodimeric enzyme, results in the misfolding and aggregation of this normally stable protein (Banci et al., 2009) found in patients carrying SOD1 mutations and in mutant SOD1 rodent disease models (Bruijn et al., 1997; Wang et al., 2002). However, recently misfolded SOD1 species have been increasingly identified in non-SOD1 fALS and sALS cases (Bosco et al., 2010; Forsberg et al., 2010), suggesting that misfolded SOD1 may play a pathological role in all types of ALS (Pokrishevsky et al., 2012).

In addition to SOD1, TAR DNA binding protein (TDP-43) has been identified as a major component of cytoplasmic inclusions in sALS, SOD1-negative fALS and ALS with dementia; as well as most common pathological subtype of frontotemporal lobar dementia (FTLD) with ubiquitinated inclusions (Arai et al., 2006; Cairns et al., 2007; Davidson et al., 2007; Mackenzie et al., 2010; Neumann et al., 2007; Neumann et al., 2006). Clinical and pathological overlap of these diseases has suggested a pathogenic mechanistic-link between these disorders and has prompted their reclassification as TDP-43-proteinopathies. These diseases exhibit the same pathological features in cells containing neuronal cytoplasmic inclusions (NCIs) including; loss of the normal nuclear TDP-43, co-localisation of TDP-43 and ubiquitin, ubiquitinated and hyperphosphorylated TDP-43 proteins and lastly formation of abnormal fragments of TDP-43 in post-mortem tissue (Neumann et al., 2007; Nonaka et al., 2009a; Zhang et al., 2009). Of interest, AD associated Aβ has been implicated in triggering the phosphorylation and cytosolic accumulation of pathogenic TDP-43 in rodent models and in brain autopsies from AD patients, similar to other observations in ALS-FTLD (Herman et al., 2011). This may explain the presence of TDP-43 pathology in a proportion of AD cases (Wilson et al., 2011).

TDP-43 is a conserved heterogeneous ribonucleoprotein that is ubiquitously expressed. TDP-43 has two RNA recognition motifs and a glycine rich C-terminal domain (Ayala et al., 2008; Buratti and Baralle, 2001) and functions as a regulator of transcription (Ou et al., 1995) and alternative splicing (Buratti et al., 2001; Mercado et al., 2005), respectively. TDP-43 is also involved in nucleocytoplasmic shuttling of messenger RNA (Ayala et al., 2008) and participates in nuclear body formation (Buratti and Baralle, 2008; Ou et al., 1995). Of interest, the C-terminal region of TDP-43 contains a prion-like domain which is predicted to be prone to misfolding and aggregation (Mousavi and Hotta, 2005). In addition, the C-

terminal fragments can bind with full-length TDP-43 to possibly facilitate the aggregation of full length TDP-43 (Nonaka et al., 2009b; Zhang et al., 2009).

Furthermore, a number of dominant mutations in the gene encoding TDP-43 have been associated with fALS and FTLD, confirming the importance of the role TDP-43 in disease pathogenesis (Daoud et al., 2009; Gitcho et al., 2008; Kabashi et al., 2008; Sreedharan et al., 2008; Van Deerlin et al., 2008; Yokoseki et al., 2008). Of note, TDP-43 pathology is not present in cases with SOD1 mutations, thus demonstrating TDP-43 inclusions are not required to initiate ALS (Lagier-Tourenne et al., 2010; Mackenzie et al., 2007).

TDP-43 is largely restricted to the nucleus in healthy cells (Ayala et al., 2008). However, in afflicted cells in ALS, abnormal cellular distribution and post-translational modification(s) of TDP-43, result in the mislocalisation and subsequent deposition in the cytoplasm as insoluble misfolded aggregates (Arai et al., 2006; Gregory et al., 2012; Li et al., 2015; Neumann et al., 2006). In TDP-43-positive cytoplasmic inclusions, TDP-43 is abnormally phosphorylated, unbiquitinated and truncated, resulting in the accumulation of both full-length TDP-43 and toxic TDP-43 fragments (Li et al., 2015). These fragments have been identified as a 25-kDa C-terminal fragment (CTF25) and a 35-kDa (CTF35) C-terminal fragment, in addition to other minor CTFs, in cytoplasmic aggregates (Li et al., 2015). Overexpression of full length TDP-43 in cultured cells and animals has been found to result in the production of CTF25, with current understanding suggesting that TDP-43 is capable of inducing the misfolding of SOD1 upon accumulation in the cytosol (Li et al., 2015).

It is well established that TDP-43 redistributes and deposits as insoluble TDP-43 aggregates in the cytoplasm of affected motor neurons in the majority of cases of ALS. It has also been shown that TDP-43 pathology causes misfolding of WT SOD1 (Pokrishevsky et al., 2012), and separately shown that WT SOD1 misfolding can be propagated cell to cell (Grad et al.,

2014). While previous work has shown that uptake of wild type SOD1 aggregates can cause endoplasmic reticulum (ER) stress (Sundaramoorthy et al., 2013), whether uptake of SOD1 aggregates influence TDP-43 pathology is yet to be established.

The presence of aberrant protein aggregates in affected neurons are characteristic of most neurodegenerative diseases, however, the mechanisms that underlie pathology are not yet completely understood. An increasing number of recent studies now support the prion-like propagation of a range of aggregated proteins associated with various neurodegenerative diseases (reviewed in Marciniuk et al., 2013). In addition to SOD1, the propagation of TDP-43 aggregation has been likened to a prion-like seeding mechanism, with evidence of regional spreading of pathology occurring in a sequential pattern through the neuroaxis (Brettschneider et al., 2013). Recent evidence suggests that phosphorylated and ubiquitinated TDP-43 aggregates may propagate from cell to cell in cultured neuroblastoma cells and induce TDP-43 aggregation in the cells expressing human TDP-43 in a self-templating fashion (Nonaka et al., 2013). An additional study presented evidence to suggest that TDP-43 can transfer between cells and induce the seeding of endogenous TDP-43 in a prion like manner (Feiler et al., 2015). More recently, it was observed that TDP-43 fibrils triggered the seed-dependant aggregation of WT TDP-43 or TDP-43 lacking a nuclear localisation signal and similar to prions, different peptides sequences of TDP-43 produce fibrils that induces different TDP-43 associated pathologies (Shimonaka et al., 2016).

In the current study, we aimed to investigate whether exogenous recombinant SOD1 protein aggregates can induce and/or contribute to TDP-43 pathology, specifically its mislocalisation and aggregation. Upon incubation with large recombinantly formed SOD1 aggregates with cells we detected mislocalised WT TDP-43 in the cytoplasm of both mouse neuronal-like cells and human embryonic kidney cells. We also demonstrate that, upon addition of the

SOD1 aggregates, fragments of TDP-43 can be observed in the cytoplasm of NSC-34 cells. Thus, we conclude that addition of recombinant SOD1 aggregates to the extracellular environment of neuron like cells results in TDP-43 mislocalisation, aggregation and fragmentation.

4.2 Methods

4.2.1 Reagents and Antibodies

DMEM/F-12 medium, DMEM/F-12 without phenol red, 0.05% trypsin-EDTA, GlutaMAX, Lipofectamine 2000, Lipofectamine 3000, SuperSignal West Pico Chemiluminescent Substrate, Subcellular Protein Fractionation Kit for Cultured Cells, restriction endonucleases *Bam*HI and *Hind*III, Ez- link- NHS- Biotin, SYTOX Red dead cell stain and Lab-Tek chambered coverglass 8 well with cover were purchased from ThermoFisher Scientific (Waltham, USA). Any kD Mini-PROTEAN TGX Precast Protein Gels and Precision Plus Protein dual color protein standard were from Bio-Rad (California, USA). Foetal Bovine Serum (heat-inactivated prior to addition in media; FBS) was from Bovogen Biologicals (East Keilor, Australia). Amersham Hyperfilm was obtained from GE Healthcare (Little Chalfont, Buckinghamshire, UK). Agar, Mg132, Ethidium Bromide, Casein (heat denatured before use; HDC), dimethyl sulfoxide (DMSO), bovine serum albumin (BSA), β-mercaptoethanol, Brilliant blue R concentrate, paraformaldehyde (PFA) and dithiothreitol (DTT) were from Sigma-Aldrich (St. Louis, MO). Ethylenediaminetetraacetic acid (EDTA) was from Amresco (Solon, USA). All other reagents including salts, powders and chemicals were from Amresco, Sigma-Aldrich or Astral Scientific (Gymea, Australia). All reagents used were endotoxin free. Antibodies (Abs) and their respective manufacturing companies used in this current study are listed in Table 4.1.

Table 4.1 Antibodies used in this study to investigate the effect of SOD1 proteins on TDP-43 pathology

Host species (clonality)[1]	Antibody target (Immunogen)[2]	Conjugate	Manufacturer (product number)[3]
Mouse (mAb)	Beta Actin [AC-15]	-	Abcam (ab6276)
Rabbit (pAb)	Vimentin	-	Abcam (ab137321)
Rabbit (pAb)	EEA1	-	Abcam (ab2900)
Mouse (mAb)	TARDBP (K1B8)	-	Saphire Bioscience
Goat (pAb)	Rabbit IgG	HRP	Bio-Rad (1706515)
Goat (pAb)	Mouse (IgM, IgG, IgA)	HRP	Merck Millipore (AP501P)
Sheep (pAb)	SOD1	-	Pierce (PAI-30817)

[1] pAb, polyclonal antibody, mAb, monoclonal antibody; [2]Ig, immunoglobulin; [3] Abcam, Cambridge, USA; Saphire Biosciences (Redfern, Australia), Bio-Rad (California, USA); Merck Millipore, Billerica, Massachusetts, USA.

4.2.2 Cell Lines

The mouse neuroblastoma x spinal cord hybrid cell line (NSC-34 cells (Cashman et al., 1992a) were routinely cultured in DMEM/F-12 supplemented with 10% (v/v) FBS and 2 mM GlutaMAX. Cells were maintained in an incubator at 37°C under a humidified atmosphere containing 5% (v/v) CO_2. Human embryonic kidney (HEK)-293 cells were from the American Type Culture Collection (Manassas, VA). HEK-293 cells were cultured in DMEM/F-12 medium supplemented with 10% FBS and 2 mM GlutaMAX, in an incubator at 37°C under a humidified atmosphere containing 5% (v/v) CO_2.

4.2.3 Aggregation and biotinylation of WT and mutant G93A SOD1 proteins

WT and G93A SOD1 were expressed and purified from *E.coli* as previously outlined (Lindberg et al., 2002; Roberts et al., 2013). SOD1 aggregation was performed *in vivo* as previously described (Roberts et al., 2013). Briefly, solutions of purified WT or G93A mutant SOD1 protein (1 mg/mL) in PBS was co-incubated with 20 mM DTT and 5 mM EDTA for 72 h at 37°C with shaking using a digital shaker (universal IKA® MS 3, 230 V) (Sigma, St.

Louis, MO). The aggregated SOD1 was then labelled with biotinamidohexanoic acid 3-sulfo-N-hydroxysuccinimide ester sodium salt (40 mg/mL) in DMSO for 2 h at RT. The unconjugated biotin was then separated from the aggregates by centrifugation (21 000 *x g* for 30 min) and washed three times with PBS (300 *x g* for 5 min). The purified aggregates free of unconjugated biotin were then resuspended in PBS (1 mg/ml). A bicinchoninic acid (BCA) protein assay was performed to determine the amount of protein in solution.

4.2.4 Cell Transfections

4.2.4.1 Plasmid purification

pCAG-RFP expression vectors containing WT TDP-43 cDNA was obtained from Addgene, provided by Zuoshang Xu (University of Massachusetts Medical School, Worcester, Massachusetts, USA)(Yang et al., 2010). pCMV6-AC-GFP expression vector containing WT TDP-43 cDNA was obtained from Origene. pCMV6-AC-EGFP expression vector containing TDP-43^{WT} cDNA was obtained from Origene. TDP-tomato red (TdTomato) constructs were created by replacing the EGFP sequences in the SOD1-EGFP plasmids with tdTomato (by Genscript, USA) and site directed mutagenesis was also performed by Genscript (Piscataway, NJ) to create the G124A mutant. Chemically competent DH5α *Escherichia coli* cells were provided by Jason McArthur (University of Wollongong, Wollongong, Australia). Cells were transformed with the TDP-43 containing plasmids as per manufacturer's instructions, using the heat shock (42 ºC) method. Transformed cells were then transferred onto lysogeny broth (10% w/v tryptone, 10% w/v NaCl, and 5% w/v yeast; LB) agar plates with 50 µg/ml kanamycin sulphate and incubated overnight at 37°C under a humidified atmosphere containing 5% (v/v) CO_2. Single-transformed bacterial colonies were selected and inoculated into sterile LB media containing 50 µg/ml kanamycin sulphate to prepare starter cultures. Plasmid DNA was then extracted from bacterial cells using the CompactPrep Plasmic Maxi

Kit (Qiageb, Hilden, Germany), as per manufacturer's instructions. The purity (260/280 ratio) and concentration of extracted DNA was measured using the NanoDrop 2000c dual-mode UV-Vis Spectrophotometer (ThermoFisher Scientific, Waltham, USA). To further confirm the purity of the extracted DNA samples, a restriction digestion was carried out at 37ºC for 1 h using enzymes HindIII and BamHI that correspond to specific restriction sites in the plasmids. Digested DNA samples were separated on a 1% agarose gel in tris-acetate-EDTA (TAE) buffer (1 mM ethylenediaminetetraacetic acid disodium salt, 40 mM Tris and 20 mM acetic acid). The resulting gel was them stained with ethidium bromide overnight and visualised using the GS-800 Calibrated Densitometer (Bio-Rad).

4.2.4.2 Transfecting cells with Lipofectamine 2000

NSC-34 cells (2 – 3 x 10^4 cells/ 0.2 mL/ chamber) were cultured in 8-well chamber slides in complete culture medium and were incubated overnight at 37°C under a humidified atmosphere containing 5% (v/v) CO2. Cells were then incubated in DMEM-F-12 serum-free culture medium containing 2 μg WT TDP tomato red (TR) plasmid DNA and Lipofectamine 2000 for 5 h at 37°C under a humidified atmosphere containing 5% (v/v) CO_2. Cells were then washed once with serum free media and replenished with complete culture medium. Cells were then incubated for a longer period of time either for 19 h, 43 h or 67 h (24 h, 48 h, and 72 h in total, respectively).

4.2.4.3 Transfecting cells with Lipofectamine 3000

Hek-293 cells (3 – 4 x cells/ 0.2 mL/ chamber) were cultured in 8-well chamber slides and were incubated overnight at 37°C/5% CO2. Cells were then incubated in complete DMEM/F-12 culture medium containing 2 μg WT TDP GFP plasmid DNA, P3000 reagent and Lipofectamine 3000 (diluted in serum free DMEM/F-12 medium) for 24 h at 37°C/CO_2.

Cells were then incubated for a longer period of time for either 19 h, 43 h or 67 h (24 h, 48 h, and 72 h in total, respectively).

4.2.5 Treatment of transfected NSC-34 cells with SOD1

Cells were visualised prior to experimentation using an Eclipse TE2000 inverted microscope (Nikon, Tokyo, Japan) to confirm transfection and determine transfection efficiency. NSC-34 cells were incubated with labelled biotinylated aggregates, or soluble (non-aggregated) WT and mutant G93A SOD1 proteins (20 µg/mL) or no protein as a control at 37°C/CO_2, for either 2 h or 72 h. Post incubation, cells were immediately fixed with 4% PFA in PBS for 20 min at RT and washed twice with PBS over 5 min. Cells were incubated with Triton-X 100 for 30 min at 4°C. Cells were incubated with blocking solution (5% FCS, 1% BSA and 0.3% triton-x100) for 20 min at RT. The cells were then probed with Alexa Fluor 488 streptavidin (1:1000 diluted in 1% BSA and 0.1% triton-x100) for the aggregates or sheep anti-SOD1 (1:500 diluted in 4% BSA and 0.1% Triton-x100) for for 1 h at RT or overnight at 4°C respectively. Cells were then incubated with anti-sheep IgG conjugated to Alexa Fluor 488 (1:500 diluted in 1% BSA and 0.1% Triton-x100) for 1 hr at RT for soluble proteins.

4.2.6 Treatment of transfected HEK-293 cells with SOD1 proteins

The medium was then replaced, and the transfected HEK-293 cells were incubated with labelled biotinylated aggregates of WT and mutant G93A SOD1 proteins (20 µg/mL) at 37°C/CO_2, or no protein as a control or MG132 (10 µM) for 24 h and imaged under live cell condition. Imaging was repeated at 48 h and 72 h. Post 72 h incubation, the cells were fixed with 4% PFA in PBS for 20 min at RT and washed twice with PBS over 5 min. Cells were incubated with Triton-X 100 for 30 min at 4°C. Cells were incubated with blocking solution (5% FCS, 1% BSA and 0.3% triton-x100) for 20 min at RT. The cells were then probed with

Alexa Fluor 488 streptavidin (1:1000 diluted in 1% BSA and 0.1% triton-x100) for the aggregates for 1 h at RT.

4.2.7 TDP-43 Pathology by Confocal microscopy

An inverted microscope (DM IBRE) and a Leica TCS SP confocal imaging system were used to visualise and image transfected dual colour NSC-34 cells (excitation 488, emission collected at 495-515 and 561 nm, emission collected at 590-630 nm) and HEK-293 cells (excitation 488, emission collected at 475-515). Fluorescence, bright field (differential interference contrast; DIC) and merged images were captures using Leica confocal software.

4.2.8 Subcellular Fractionation assay of NSC-34 cells

NSC-34 cells were incubated with WT SOD1 in soluble and aggregated form (20 µg/mL) in PBS for 2 h at 37°C/5% CO_2. Post incubation, the cells were washed three times with PBS (300 *x g* for 5 min) harvested using 0.5% trypsin and 5 mM EDTA and washed (500 *x g* for 5 minutes). The cells were washed three times with ice cold PBS (500 x *g* for 3 minutes) for fractionation using a Subcellular Protein Fractionation Kit for Cultured Cells as per manufacturer's instructions (Thermo Fisher Scientific). Initially, NSC-34 cells (10 x 10^6 cells/mL) were incubated with cytoplasmic extraction buffer (CEB) containing protease inhibitors for 10 min rotating at 4°C. The supernatant (cytoplasmic fraction) was collected (500 × *g* for 5 minutes). The cell pellet was then incubated with membrane extraction buffer (MEB) containing protease inhibitors for 10 min rotating at 4°C. Post incubation, the supernatant (extracted membrane fraction) was collected (3000 × *g* for 5 minutes). Ice cold nuclear extraction buffer (NEB) containing protease inhibitors was added to the cell pellet for 30 min rotating at 4°C. The supernatant (extracted soluble nuclear fraction) was collected (5000 × *g* for 5 minutes). Chromatin-bound extraction buffer (NEB, 100mM CaCl2 and 300 units of Micrococcal Nuclease) was added to the pellet for 15 mins at RT. The supernatant

(chromatin-bound nuclear extract) was collected (16,000 x *g* for 5 mins). Lastly, Pellet Extraction Buffer (PEB) containing protease inhibitors was added to the cell pellet for 10 mins at RT. The supernatant (the cytoskeletal extract) was collected (16,000 x *g* for 5 mins).

Protein concentration was determined using the BCA method. Supernatants (20 µg protein/lane) were separated under reducing conditions (5% β-mercaptoethanol) using Any kD Mini-PROTEAN TGX Stain-Free™ Precast Gels. Proteins were then transferred to nitrocellulose membranes using a Trans-Blot Turbo Transfer System (Bio-Rad,). Total protein per lane was then imaged and measured with a Bio-Rad Criterion Stain Free Imager and Image Lab software. Membranes were blocked with heat denatured casein (HDC) in for 1 h at 37°C. To test the purity of the separation, mouse anti-TDP-43 mAb (1:200); rabbit anti-EEA1 pAb (1:500), rabbit anti-Vimentin pAb (1:500) and mouse anti-actin mAb (1:5000), diluted in HDC/PBS for 1 h at 37°C were used to probe the CE, ME, NE and PE fractions. Membranes were visualised using chemiluminescent substrate and Amersham Hyperfilm ECL (GE Healthcare). Images of films were collected using a GS-800 Calibrated Densitometer (Bio-Rad). The processing of films was achieved using GBX Developer and Replenisher and GBX Fixer and Replenisher (Kodak Australiasia, Collingwood, Victoria Australia). Images of the films were collected using a GS-800 Calibrated Densitometer (Bio-Rad).

4.2.9 Presentation of data and statistical analyses

Data is presented as the mean ± SD. ANOVA paired with Tukey's HSD multiple comparison post-test tests were used to analyse and compare differences between multiple treatments. Unpaired student's t-tests were performed for single treatment comparisons. Prism 5 for Windows (Version 5.01) (GraphPad Software, San Diego, CA) was used to generate these statistical analyses. Differences were defined as significant for $P < 0.05$.

4.2.10 FloIT assay by flow cytometry

The FloIT assay was performed as outlined in section 3.2.15. Briefly, NSC-34 cells were transiently transfected with TDP-43 (TDP-43^{WT} tdtomato and TDP-43^{G124A}-EGFP) using Lipofectamine 3000 (see above). Following transient transfection at 24h, 48 h and 72h in total, cells were harvested and then washed again using centrifugation. Cells were then washed twice and resuspended in PBS (0.5 mL/tube). An aliquot of cells (2 x 10^5cells/0.15mL) were collected then analysed for transfection efficiency. The remaining cells (4 x 10^5cells/0.35mL) were washed as above and lysed prior to analysis in lysis buffer. Cell lysates were then incubated with RedDot2 (1:1000) at RT for 2 min. Events were collected using a LSRFortessa X-20 Cell Analyzer (BD Biosciences) (excitation 488 nm, emission collected with 525/50 band-pass filter and excitation 561, emission collected with 586/15 nm band-pass filter for EGFP and RedDot2, respectively). Lysates were firstly gated on forward and side scatter and then the fluorescence from RedDot2 were determined by flow cytometry. All parameters were set to $\log^{10}$ during acquisition from cell lysates. The forward scatter threshold was set to the minimum value (200 AU) to minimise the exclusion of small protein inclusions. Nuclei were identified and enumerated based on RedDot2 fluorescence and forward scatter and then excluded from further analysis. The remaining particles were analysed for the presence of inclusions based on GFP/ tdTomato fluorescence, forward

scatter and comparison lysates prepared from cells expressing only the corresponding fluorescent protein. The number of inclusions in the population can be normalised to the number of nuclei, and reported as inclusions/100 transfected cells (iFloIT) according to the equation outlined in section 0. Analysis of all events was determined using FlowJo software (Tree Star, Ashland, OR).

4.3 Results

4.3.1 Transient expression of TDP-43 proteins induces endogenous TDP-43 aggregation and inclusion formation in NSC-34 motor neurons over time.

TDP-43 is localised mostly in the nucleus where it can perform its normal functions including RNA processing (Buratti and Baralle, 2001; Lee et al., 2012). Under non-physiological and disease conditions however, TDP-43 is known to mislocalise to the cytosol and form insoluble aggregates (Neumann et al., 2006), although the mechanisms underlying TDP-43 mislocalisation and aggregation are not completely understood. However, a previous study has reported that TDP-43 is intrinsically aggregation-prone and thus can spontaneously form aggregates; a property attributed to the C-terminal domain (Johnson et al., 2009). Here, the presence of inclusion bodies containing TDP-43 aggregates was initially investigated over time. To investigate the number of TDP-43 positive inclusions in murine NSC-34 cells, cells were transfected with TDP-43^{WT} and TDP-43^{G124A} for 24, 48 and 72 h and the number of inclusions were quantified using flow cytometric characterisation of inclusions and trafficking (FloIT) (Figure 4.1) as outlined in section 3.2.15. A significant amount of inclusions of both TDP-43^{WT} and TDP-43^{G124A} were observed in cells expressing EGFP fusion proteins. Consistent with mutant TDP-43 being aggregation prone a significantly greater number of inclusion bodies were identified in cells expressing mutant TDP-43^{G124A} compared to cells expressing TDP-43^{WT}. However, there was a significant decrease in the number of cells containing TDP-43^{G124A} inclusions measured at 72 h, possibly due to cell toxicity and death in cells containing inclusions. This is consistent with previous reports which demonstrate that ALS-linked TDP-43 mutations in the TDP-43 gene increase the number of TDP-43 aggregates and promote toxicity *in vivo* (Johnson et al., 2009).

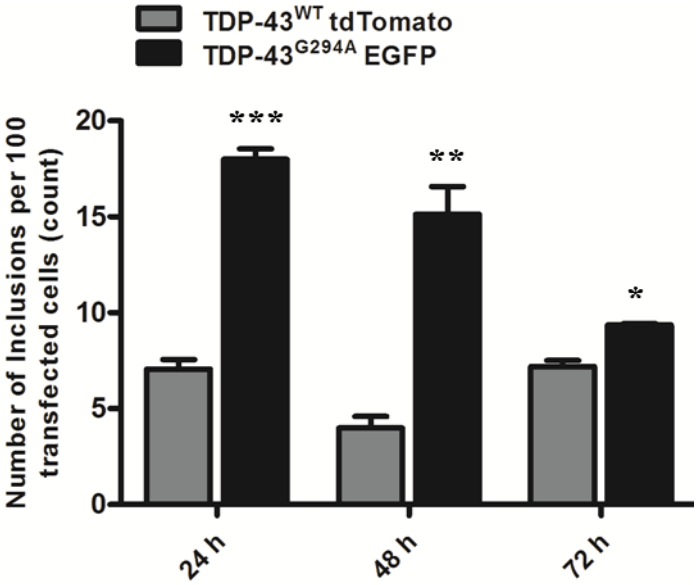

Figure 4.1 Spontaneous aggregation of TDP-43 was examined by flow cytometry. Following transfection, using Lipofectamine 3000, NSC-34 transiently transfected with either TDP-43^{WT} or TDP-43^{G124A} for 24, 48 and 72 h and analysed using flow cytometry. Results shown as mean number of inclusions per 100 transfected cells ± SEM, $n = 3$; $^{***}P < 0.001$, $^{**}P < 0.01$ and $^{*}P < 0.05$ compared to TDP-43^{WT}.

4.3.2 TDP-43 aggregates can transfer from cell to cell

Next, the ability of TDP-43 to transfer from cell-to-cell in culture was examined. Transfer events were quantified as the percentage of transfected cells positive for both EGFP/tdTomato using the gating strategy outlined in Figure 3.5. Two cell populations transiently expressing either TDP-43^{WT} tdTomato or TDP-43^{G124A} EGFP proteins were co-cultured at a ratio of 1:1 and analysed using flow cytometry (Figure 4.2). Control cells were also transfected separately, however, they were mixed immediately prior to flow cytometry analysis. Similar to previous findings for SOD1 (Figure 3.5), approximately 3.4 ± 0.3% at 24 h and 3.1 ± 0.3% at 48 h acceptor NSC-34 cells were found to contain significant amounts of both TDP-43^{WT} tdTomato and TDP-43^{G124A} EGFP presumably from donor cells, and were scored as EGFP/tdTomato red double-positive (dual fluorescence). These results suggest that TDP-43 is capable of transferring between cells in culture. However at 72 h, the percentage of dual fluorescent cells significantly decreased, compared to 24 h and 48 h time points. This is likely due to cellular toxicity associated with the presence of aggregates.

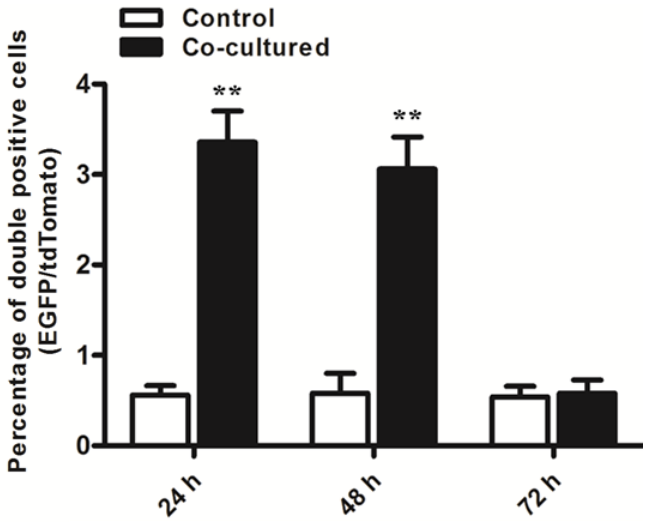

Figure 4.2 TDP-43WT or TDP-43G124A proteins can transfer from donor to recipient NSC-34 motor neurons. Following transfection, using Lipofectamine 3000, NSC-34 transiently transfected with TDP-43^{WT} tdTomato or TDP-43^{G124A} EGFP were either co-cultured or cultured separately for 24, 48 and 72 h. NSC-34 cells cultured separately were mixed prior to analysis (control). Results shown as mean percentage of cells ± SEM, $n = 3$; $^{**}P < 0.01$ compared to control (mixed population of cells).

4.3.2.1 TDP-43^{G124A} GFP can induce aggregation of TDP-43^{WT} tdTomato protein in co-cultured NSC-34 motor neurons

The above data implies that TDP-43 or more likely TDP-43 protein aggregates can transfer between co-cultured NSC-34 motor neurons. Thus, whether mutant TDP-43 aggregates can induce the aggregation of TDP-43^{WT} in a manner that could be described as seeding behaviour was next investigated (Figure 4.3). To test this, cells were either co-transfected with TDP-43^{WT} tdTomato and TDP-43^{G124A} EGFP or transfected separately and populations mixed or not (control), cells were lysed and aggregates counted by FLoIT. In particular, the number of TDP-43^{WT} inclusions were counted to identify and measure seeding activity induced by mutant TDP-43^{G124A} EGFP. To calculate the average number of inclusions per 100 transfected cells in the populations analysed, the number of inclusions acquired is simply divided by the transfection efficiency (separately determined by flow cytometry) of the sample, which is then multiplied by the corresponding number of cell nuclei enumerated. An almost two-fold significant increase in the amount of TDP-43^{WT} tdTomato inclusions detected in the co-transfected treatment compared to the corresponding control was observed from 48

to 72 h. This suggests that within individual cells mutant TDP-43^{G124A} induced the aggregation of TDP-43^{WT}. Interestingly, the control treatment (in which separately transfected populations are mixed just prior to analysis) showed an increase in inclusions through time likely indicative of cellular stress. Importantly, co-culture of cells expressing TDP-43^{G124A} induced cells with TDP-43^{WT} to significantly increase the number of inclusions formed compared to controls consistent with a cell-to-cell propagation of misfolding and aggregation.

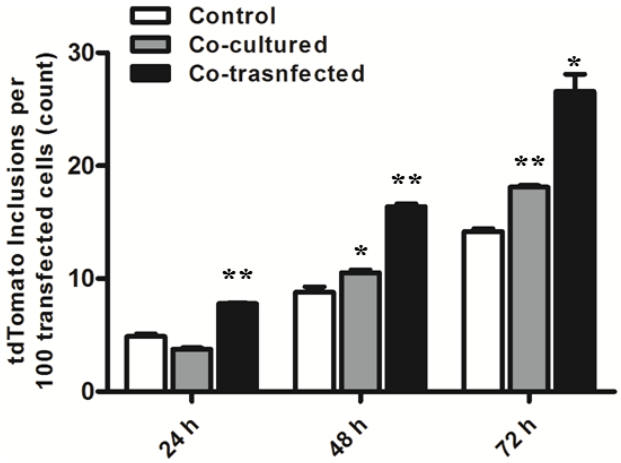

Figure 4.3 FloIT detects inclusions containing dual fluorescence from NSC-34 cells Following transfection, using Lipofectamine 3000, NSC-34 cells expressing TDP-43^{WT} tdTomato or TDP-43^{G124A} EGFP were subsequently co-cultured, co-transfected or cultured separately together for 24, 48 and 72. The number of inclusions obtained were enumerated by FloIT method means ± SEM, $n = 3$; $^{**}P < 0.01$ or $^{*}P < 0.05$ compared to corresponding treatment.

4.3.3 Transiently expressed TDP-43^{WT} is observed deposited in the cytosol of NSC-34 cells upon treatment with recombinant SOD1 protein aggregates

TDP-43 redistribution and aggregation is observed in the cytoplasm of affected cells in a diverse set of neurodegenerative diseases. However, the contributing factors responsible for TDP-43 mislocalisation and aggregation remain ambiguous. Both SOD1 and TDP-43 have been implicated in fALS and sALS pathogenesis, although whether SOD1 aggregates contribute to TDP-43 pathology is yet to be established. Thus the presence of SOD1 aggregates and deposition of TDP-43 proteins in the cytosol of NSC-34 cells was thus investigated. (Figure 4.5). To confirm whether exogenously added SOD1 aggregates have an effect on TDP-43 cytosolic mislocalisation and aggregation, purified human WT TDP-43-

tomato red (TDP-43^{WT} tdTomato) plasmid DNA was used to transiently transfect NSC-34 cells (Figure 4.4A). Post transfection, cells were incubated with either WT or mutant G93A SOD1 in both their aggregated and soluble state (Figure 4.4B). The percentage of cells containing mislocalised TDP-43 into foci that measured >1µm per treatment was determined by confocal microscopy (Figure 4.5A and B). Mislocalised TDP-43 by this definition included both TDP-43^{WT} cleared from the nucleus and TDP-43 that had accumulated in the cytosol even though some nuclear TDP-43^{WT} remained. A summary of the methods is outlined in Figure 4.4.

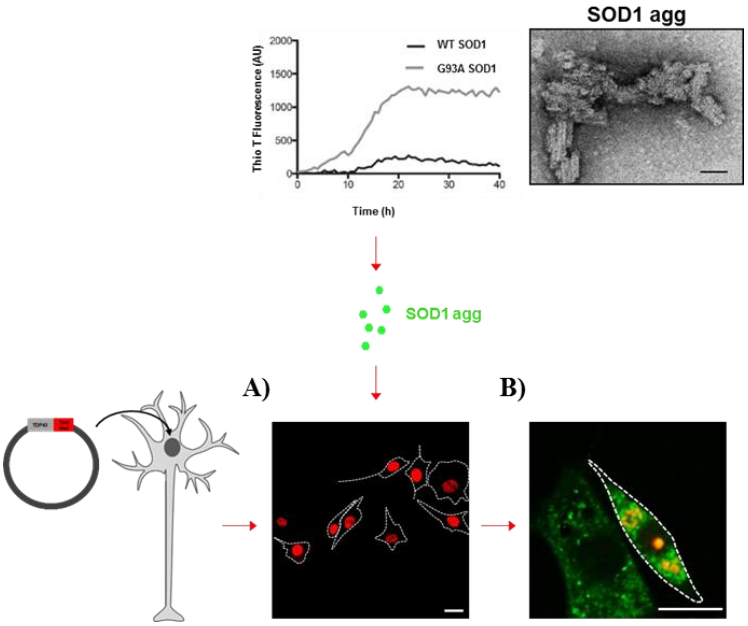

Figure 4.4 Treatment of NSC-34 cells with large SOD1 protein aggregates induces TDP-43 mislocalisation and aggregation. Immunofluorescence labelling of SOD1 (green) and TDP-43^{WT} (red) neuronal cytoplasmic inclusions (NCIs) in NSC-34 cells. Confocal microscopy of transfected NSC-34 cells expressing TDP-43^{WT} TR were incubated in complete DMEM medium in the (A) absence (control) or (B) presence of WT or G93A SOD1 proteins in their aggregated or soluble form (20 µg/mL) for 72 h. Bars represent 10 µm. Outline of cells are indicated with white dashed lines. TEM bar represents 50 nm.

Confocal microscopy and quantitative analysis was performed (Figure 4.5). The addition of SOD1 protein aggregates to NSC-34 cells resulted in a rapid and significant increase in percentage of cells that contained mislocalised TDP-43^{WT} (Figure 4.5A) when treated with either WT (23±5%) or G93A SOD1 (25±4%) aggregates compared to the control cells (absence of protein treatment; % cells with aggregates). In contrast, while there was a significant increase in cells displaying mislocalised TDP-43^{WT} when incubated with soluble

G93A SOD1 (16±3%) there was no significant difference between control cells and those treated with soluble WT SOD1 (10±2%) of transfected cells with mislocalised TDP-43^{WT}. Furthermore, little to no cells were observed to contain TDP-43^{WT} positive cytoplasmic inclusions without protein treatment at 2h. While cells incubated with aggregated G93A SOD1 aggregates had more TDP-43^{WT} inclusions than those incubated with soluble G93A, no significant differences were detected between them. In contrast, cells treated with WT SOD1 aggregates had significantly more TDP-43^{WT} aggregates when compared to soluble SOD1 protein (Figure 4. 5B).

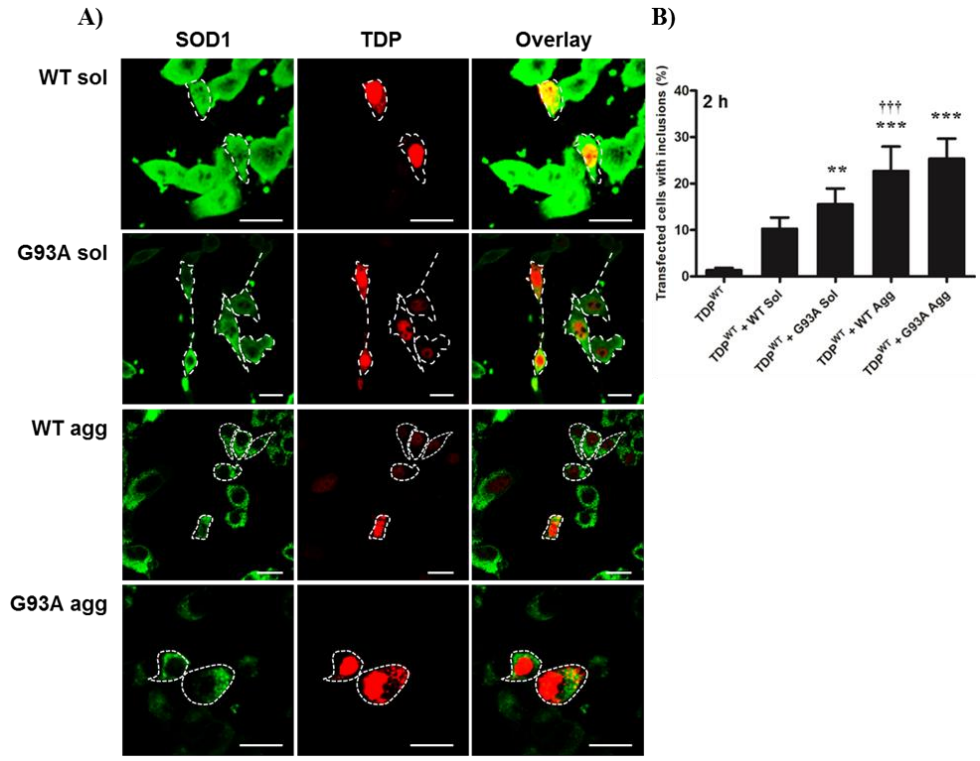

Figure 4.5 Cytosolic mislocalisation and aggregation of TDP-43^{WT} in NSC-34 cells is observed upon addition of the recombinant SOD1 protein aggregates at 2h. Immunofluorescence labelling of SOD1 (green) and TDP-43^{WT} (red) neuronal cytoplasmic inclusions (NCIs) in NSC-34 cells. (A) Confocal microscopy of transfected NSC-34 cells expressing TDP-43^{WT} tdTomato were incubated in complete DMEM medium in presence of WT or G93A SOD1 proteins in their aggregated or soluble form (20 µg/mL) for 2h. Bars represent 20 µm. Outline of cells are indicated with white dashed lines. (B) The percentage of NSC-34 cells containing TDP-43^{WT} positive aggregates was assessed by the number of cells containing mislocalised TDP-43^{WT} into foci that measured >1µm per treatment including both TDP-43^{WT} cleared from the nucleus and TDP-43^{WT} that had accumulated in the cytosol even though some nuclear TDP-43^{WT} remained, as determined by Image J**.** Results shown as means ± SD, n = 3; $^{***}P < 0.001$ and $^{**}P < 0.01$ compared to corresponding control (TDP-43^{WT} tdTomato), $^{†††}P < 0.001$ compared to corresponding soluble protein form.

Given TDP-43 translocation can be a rapid response to stress (Zhang et al., 2014) that can be reversible (Liu-Yesucevitz et al., 2010), we next tested whether the TDP-43^{WT} mislocalisation associated with SOD1 aggregate treatment persisted for 72 h (Figure 4.6). After the extended incubation with SOD1 aggregates, a large number of cells still exhibited mislocalised TDP-43^{WT}, which appeared as larger clusters of aggregates or inclusion bodies, when assessed by confocal microscopy (Figure 4.6A).

Incubation of aggregated SOD1, both WT and G93A, resulted in a significantly higher percentage of transfected cells with miscolcalised TDP-43^{WT} compared to the control cells (Figure 4.6B). Although, no significant difference was detected in the percentage of transfected cells with mislocalised TDP-43^{WT} when treated with the WT (24±7%) and G93A (27±7%) soluble proteins compared to the control cells, some cells were observed to contain large TDP-43^{WT} positive inclusions in the cytosol of the soluble G93A treated cells (as shown in Figure 4.5).

In contrast to the 2 h experiment, a significant difference was found to exist between the cells that were treated with the soluble and the aggregated form of the mutant G93A protein. Thus, incubating the cells with the aggregated form of SOD1 had a significant effect on TDP-43^{WT} extranuclear accumulation in NSC-34 cells. However, it is important to note that complete loss of normal nuclear staining was still not observed. Addition of SOD1 aggregates leads to a variety of aggregation states outlined in Figure 4.7.

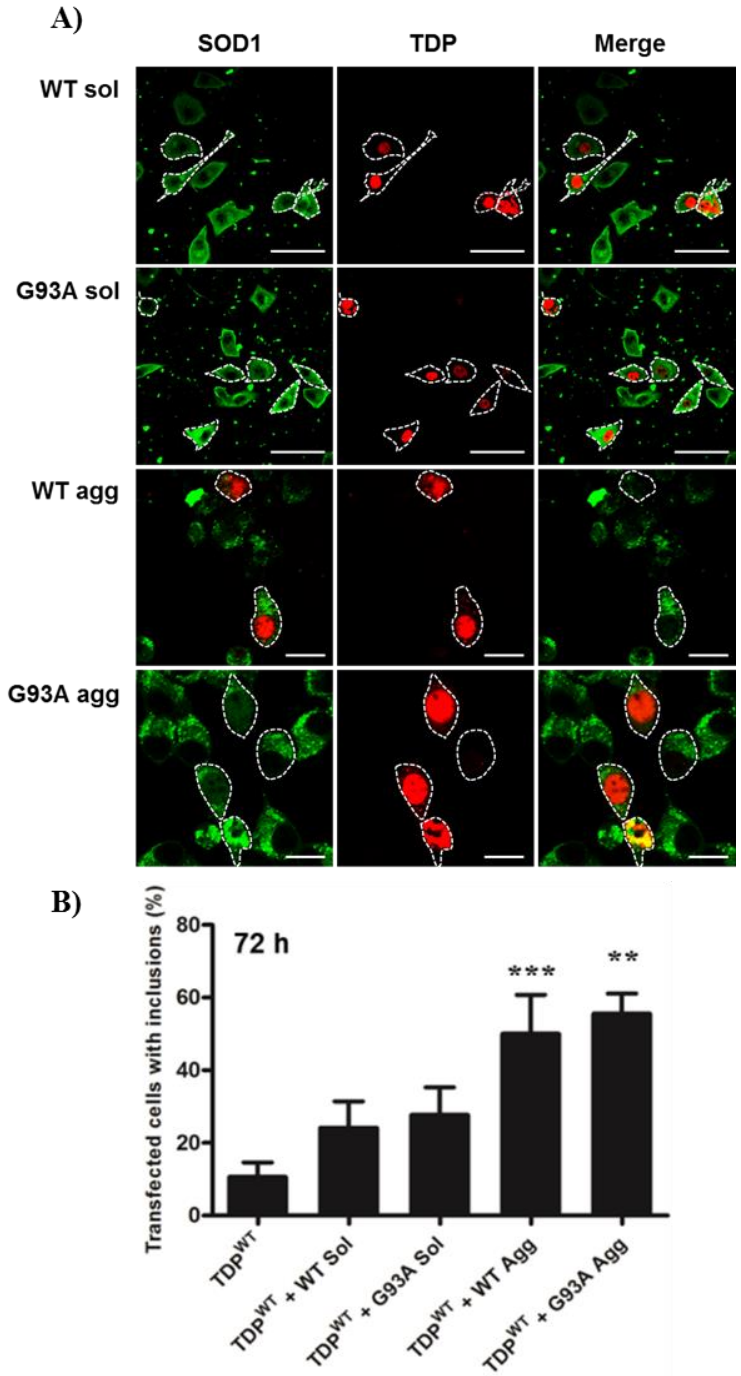

Figure 4.6 Cytosolic mislocalisation and aggregation of TDP-43 in NSC-34 cells is observed upon treatment with recombinant SOD1 protein aggregates at 72 hr. Immunofluorescence labelling of SOD1 (green) and TDP-43^{WT} (red) NCIs in NSC-34 cells. (A) Confocal microscopy of transfected NSC-34 cells expressing TDP-43^{WT} TR were incubated in complete DMEM medium in the absence (control) or presence of WT or G93A SOD1 proteins in their aggregated or soluble form (20 µg/mL) for 72 h. Bars represent 20 µm. Outline of cells are indicated with white dashed lines. (B) The percentage of NSC-34 cells containing TDP-43^{WT} positive aggregates was assessed by the number of cells containing mislocalised TDP-43^{WT} into foci that measured >1µm per treatment including both TDP-43^{WT} cleared from the nucleus and TDP-43^{WT} that had accumulated in the cytosol even though some nuclear TDP-43^{WT} remained, as determined by Image J. Results shown as means ± SD, n = 3; $^{***}P < 0.001$ or $^{**}P < 0.01$ compared to corresponding control (TDP-43^{WT} TR), compared to corresponding soluble protein form.

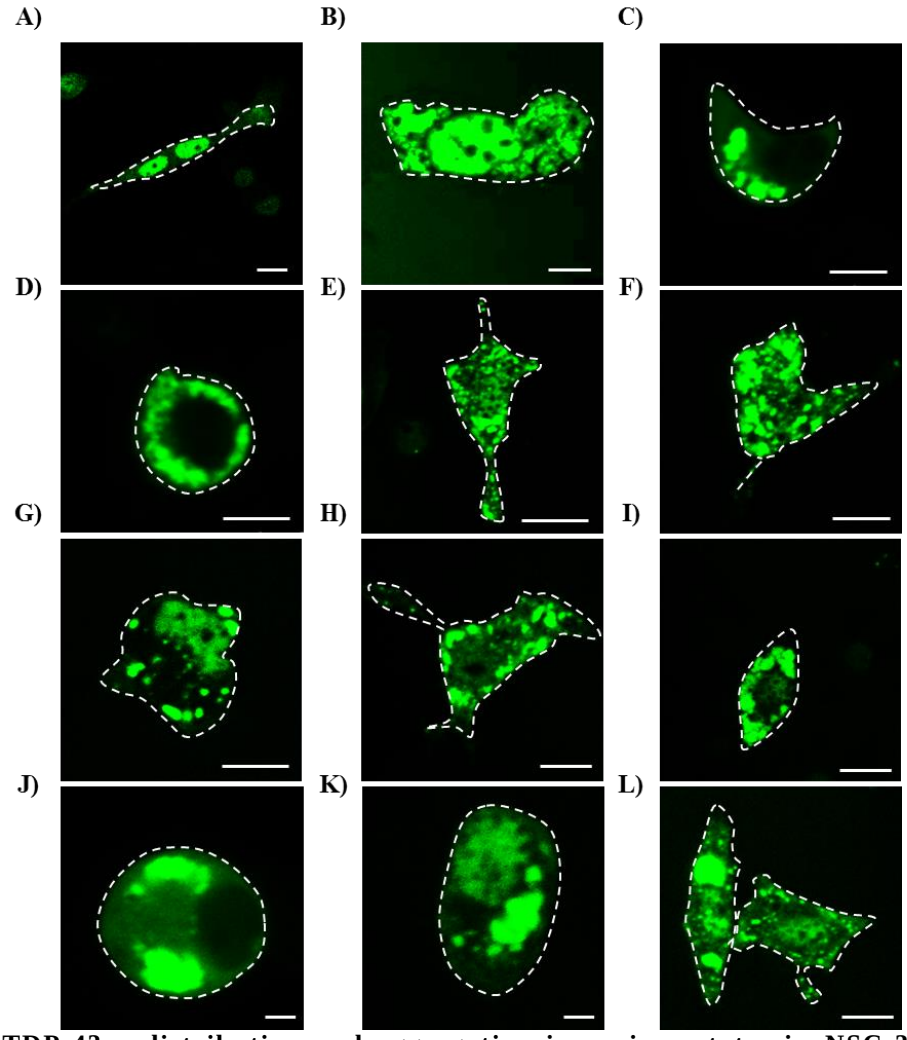

Figure 4.7 TDP-43 redistribution and aggregation in various states in NSC-34 cells. (A) Under normal conditions, TDP-43 localisation is limited to the nucleus. (B) Under temporary cellular stress conditions, TDP-43 can be mislocalised from the nucleus, however some TDP-43 may remain in the nucleus. (C-D) Under abnormal conditions, complete loss of nuclear TDP-43 is observed, and large inclusions bodies positive for TDP-43 are observed in the cytoplasm. (E-F) Inclusion bodies, containing TDP-43 can also be present diffusely throughout the cell under pathological conditions. (G-I) Distinct inclusions bodies can also be found diffusely surrounding the nucleus. (J-L) Large distinct clusters of TDP-43 positive inclusions can accumulate in the cytoplasm (foci > 20µm). These images are examples of the scoring system for mislocalisaed and aggregated TDP-43. Bars represent 10 µm

4.3.4 Recombinant mutant SOD1 can seed aggregation and induce inclusion formation in NSC-34 cells expressing TDP-43^{WT} tdTomato protein

Given that the above data demonstrates that the addition of SOD1 protein aggregates to NSC-34 cells resulted in a rapid and significant increase in percentage of cells that contained mislocalised TDP-43^{WT}, FloIT was next employed to confirm seeding behaviour and quantify these findings. To investigate whether mutant SOD1 aggregates can induce the aggregation of TDP-43^{WT} in NSC-34 motor neurons, cells were transiently transfected with TDP-43^{WT} tdTomato protein and incubated with human recombinant G93A mutant SOD1 aggregates for

either 24, 48 or 72 h (Figure 4.8). As outlined above, the number of inclusions per transfected cell was determined by flow cytometry using the FLoIT technique. A significant increase in the number of TDP-43^{WT} inclusions were identified from 24 to 72 h in cells incubated in the presence of mutant SOD1 aggregates compared to the corresponding cells in the absence of mutant SOD1 aggregates. This increase in inclusion formation was almost five fold from 24 to 72 h. This is therefore indicative of significant seeding events associated with mutant TDP-43 induced aggregation of SOD1^{WT} tdTomato in NSC-34 cells.

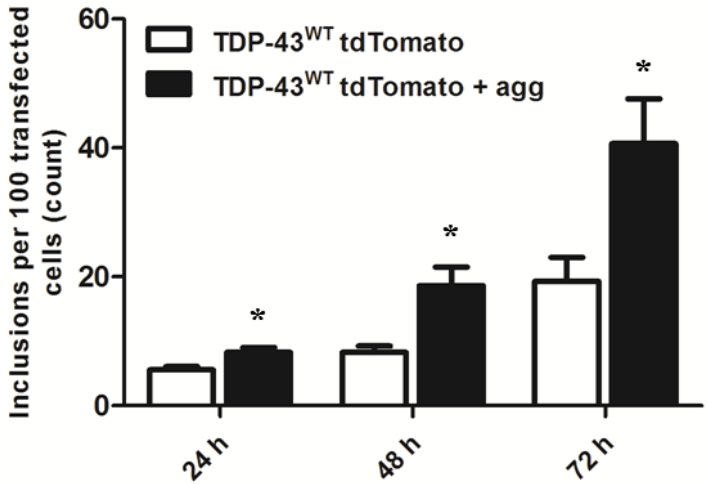

Figure 4.8 SOD1 aggregates are capable of inducing significant aggregation in TDP-43WT expressing NSC-34 cells using the Flo-it method. Following transfection (24 , 48 and 72 h) using lipofectamine 3000, adherent NSC-34 cells transiently transfected with TDP-43^{WT} were co-cultured with 20 µg/ml and aggregated G93A SOD1 at indicated time intervals at 37°C. Cells were harvested for supernatant analysis and then lysed. Cell lysates were incubated with RedDot2 for 2 min at RT. Transfection efficiencies, the number of inclusions and nuclei were determined by flow cytometry and results means ± SD, n = 3, $^{*}P$ < 0.05 compared to corresponding control (no protein treatment).

4.3.5 TDP-43^{WT} cytosolic mislocalisation and aggregation induced by exogenous SOD1 recombinant proteins is not limited to the NSC-34 cell line

The work presented above suggests that exogenously added SOD1 proteins induce the mislocalisation of TDP-43^{WT} in the NSC-34 cell line. It was therefore of interest to examine if these effects are limited to the mouse motor neuron like cell line (NSC-34). Thus, human embryonic kidney (HEK-293) cells were used to further investigate the effect of exogenous SOD1 on cell produced TDP-43 (Figure 4.10). In this experiment, a plasmid encoding a human TDP-43^{WT} GFP fusion was used to transiently transfect HEK-293 cells and SOD1

aggregates were used unlabelled. Post transfection, cells were incubated with either aggregated WT or mutant G93A SOD1 for either 24, 48 and 72 h, or the same time frames in the absence of protein as a control. In addition, MG132, an inhibitor of proteasome activity, which has been shown to induce TDP-43 aggregation (van Eersel et al., 2011) was used as a positive control. A summary of the methods is outlined in (Figure 4.9).

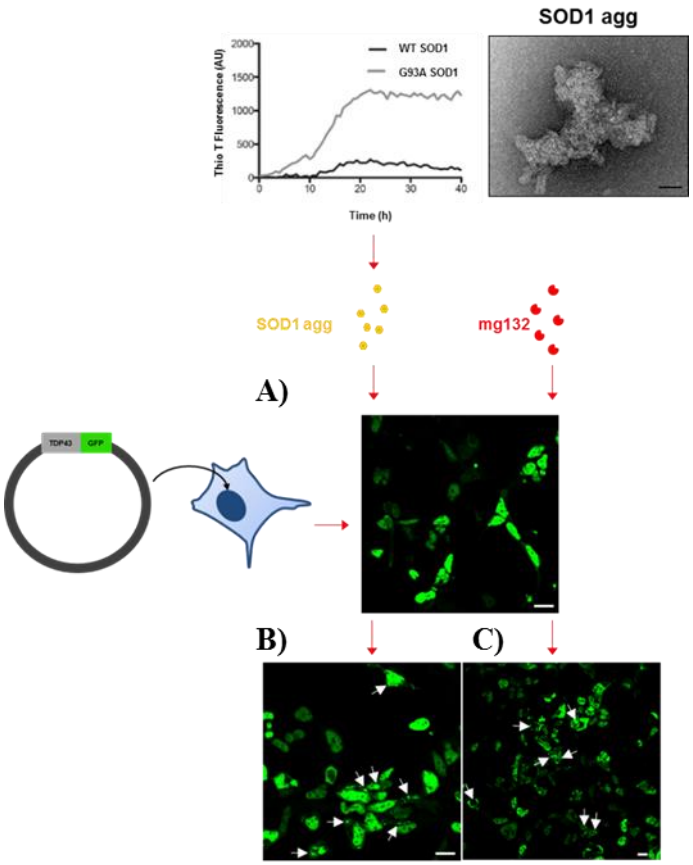

Figure 4.9 Recombinant SOD1 aggregates induce aggregation in HEK293 cells. Immunofluorescence labelling of TDP-43^{WT} (green) neuronal cytoplasmic inclusions (NCIs) in HEK293 cells. Transfected HEK-293 cells in culture medium expressing TDP-43^{WT} eGFP were incubated in (A) the absence (control) or (B) presence of protein aggregates (20 µg/mL) for 72 h or (C) mg132 (10 µM). Arrows represent area of TDP-43 aggregates. Bars represent 10 µm. Outline of cells are indicated with white dashed lines. TEM bar represents 50 nm.

As shown in Figure 4.10, incubation with either the WT (34±4%) or G93A (32±3%) SOD1 protein aggregates resulted in a significantly higher percentage of cells containing mislocalised TDP-43^{WT} at 24 h, compared to the control (19±2%). Similarly, after 48 h SOD1 aggregate treatment resulted in an increase in the percentage of cells with mislocalised TDP-43^{WT} (G93A 38 ±3 %, WT 35± 3%) relative to the control (20±3%). However, at 72 h, although there was a significant difference in the percentage of cells containing mislocalised

TDP-43^{WT} when treated with G93A (38 ±2 %) SOD1 aggregates compared to the control, there was no difference in the percentage of cells when compared to the 48 h period. Interestingly, in cells incubated with aggregated WT SOD1 there was a 5% decrease between the 48 and 72 h time points suggesting cells were recovering or that cells with inclusions had died. The positive control, MG132, induced TDP-43^{WT} cytoplasmic inclusions in a time dependant manner with an almost two-fold increase in the percentage of cells containing mislocalised TDP-43^{WT} between the 24 and 72 h time points (from 23±2% to 59.08±5%).

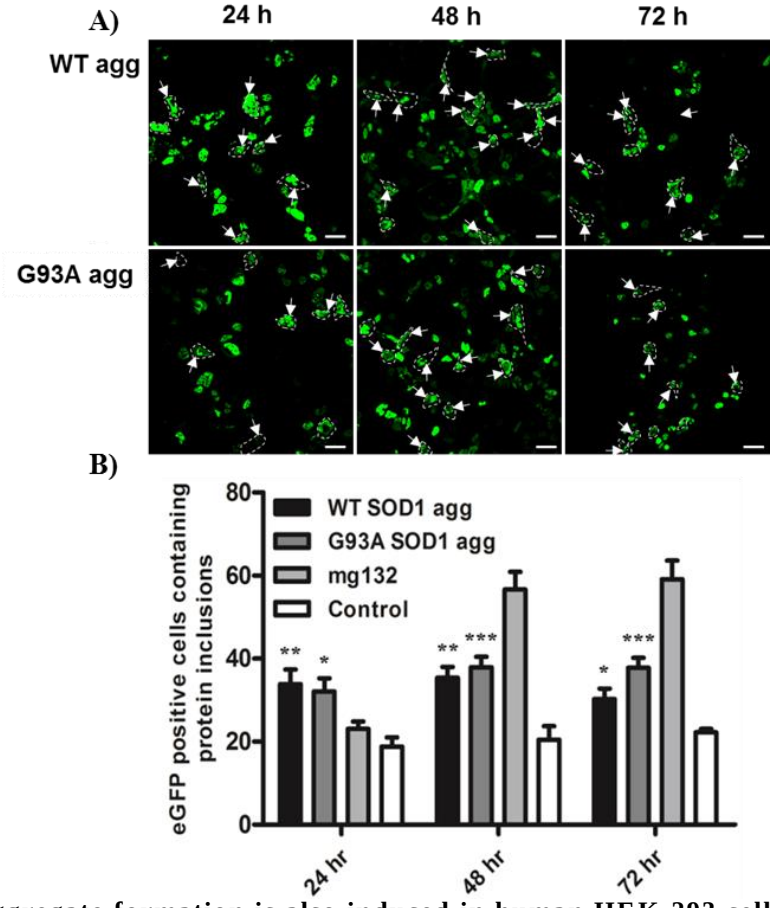

Figure 4.10 Aggregate formation is also induced in human HEK-293 cells expressing TDP-43WT GFP in the presence of recombinant SOD1 aggregates. (A) Transfected HEK-293 cells in DMEM/F12 expressing TDP-43^{WT} GFP were incubated in the absence (control) or presence of WT or mutant G93A SOD1 protein aggregates (20 µg/mL) for 24-72 h (as indicated). Bars represent 20 µm. Outline of cells are indicated with white dashed lines, arrows indicate TDP-43^{WT} positive inclusions. (B) The percentage of HEK-293 cells containing TDP-43-positive inclusions was assessed by the number of cells containing mislocalised TDP-43^{WT} into foci that measured >1µm per treatment including both TDP-43^{WT} cleared from the nucleus and TDP-43^{WT} that had accumulated in the cytosol, as determined by Image J. Results shown as means ± SD, $n = 3$; $^{***}P < 0.001$ or $^{**}P < 0.01$ or $^{*}P < 0.05$ compared to corresponding control (TDP-43^{WT} TR).

4.3.6 Exogenous recombinant SOD1 aggregates induce the cytosolic mislocalisation and fragmentation of endogenous TDP-43 in naive NSC-34 cells.

Current understanding suggests that the accumulation of the truncated TDP-43 fragment; CTF25 is a pathological feature detected in proteinopathies. Since this fragment has been suggested to play a critical role in ALS pathogenesis, we investigated whether adding aggregated SOD1 to NSC-34 cells had any effect on the formation of CTF25. We have previously shown that exogenously-added recombinant SOD1 proteins are capable of entering into NSC-34 cells and escaping into the cytosol (Zeineddine et al., 2015). To begin to investigate the effect of SOD1 aggregates on TDP-43 location and truncation, a subcellular fractionation assay and western blot was carried out on NSC-34 cell lysates (Figure 4.11). Given that the response of NSC-34 cells to WT and mutant G93A SOD1 proteins were similar, in the following experiment NSC-34 cells were treated with exogenous soluble and aggregated WT SOD1 for 2 h.

The presence of endogenous TDP-43 protein was then investigated by immunoblotting of the cytosolic, membrane (ER/Golgi), nuclear and cytoskeletal supernatant fractions. In the SOD1 aggregate-treated fractions (Figure 4. 11A), TDP-43 was detected as a range of bands but predominantly as distinct bands at 43 kDa and ~25 kDa. In contrast to the untreated controls where TDP-43 is found in the nuclear fraction (Figure 4.11C), after treatment with SOD1 aggregates TDP-43 is found in all the fractions. In the ME fraction additional bands were present at approximately 40 kDa and 18 kDa. The additional 40 kDa band was also present in the NE and PE supernatant fractions. Interestingly, the full length TDP-43 was predominantly cytosolic suggesting a rapid movement from the nucleus after SOD1 aggregate addition. In comparison, treatment with the WT SOD1 soluble protein (Figure 4.11B), resulted in the detection of only one band immunoreactive for endogenous TDP-43 in the NE fraction at

approximately 43 kDa similar to the untreated control with no evidence of bands at 25 kDa. To further confirm the purity of the supernatants, fractions were immunoblotted using an anti-actin, anti-EEA1 and anti-vimentin Ab (Figure 4.12D). These bands were detected in the ME fraction for EEA1 (180 kDa), vimentin (54 kDa) in the PE fraction and actin (42 kDa) as a loading control.

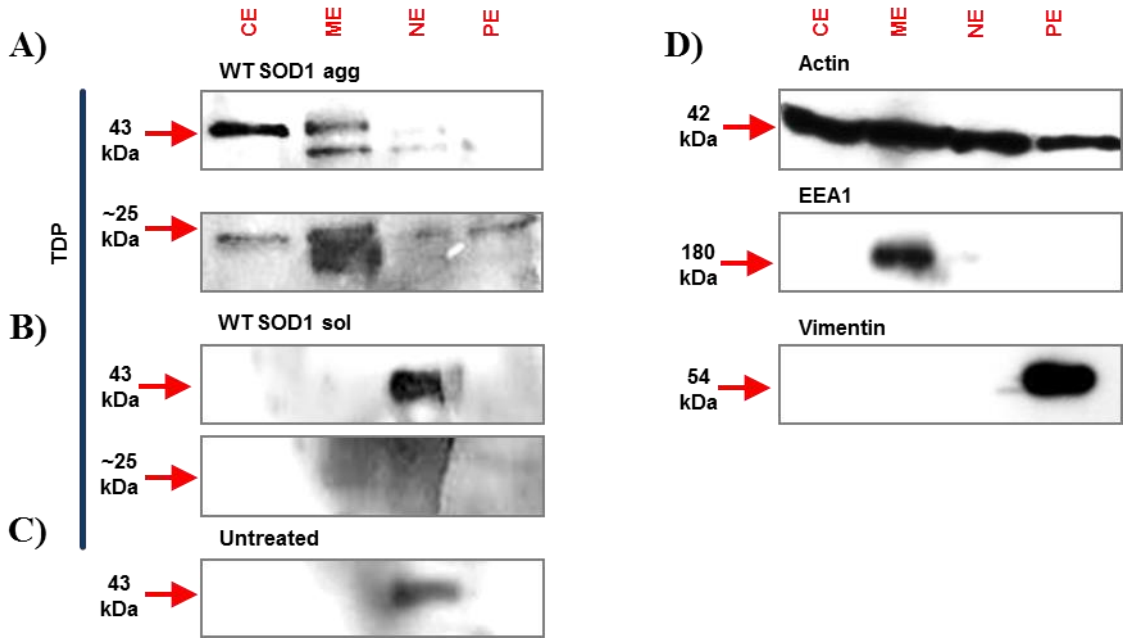

Figure 4.11 Exogenous recombinant SOD1 proteins induce TDP-43cytosolic mislocalisation in NSC-34 cells. Cytoplasmic extract (CE), membrane extract (ER/Golgi) (ME), nuclear extract (NE) and pellet extract (cytoskeleton) (PE) fractions by centrifugation from NSC-34 cells treated with either (A) WT SOD1 aggregates or (B) WT SOD1 soluble (20 µg/mL) or (C) no added protein were separated by SDS PAGE under reducing conditions, transferred to nitrocellulose membrane and incubated with anti-TDP-43 and (D) control Ab anti-actin, anti-EEA1 or anti-vimentin Abs (as indicated). Results are representative of at least 6 experiments.

4.4 Discussion

Mutations in the TDP-43 gene are found in sporadic and non-SOD1 familial ALS, implicating TDP-43 as a contributing factor to disease (Kabashi et al., 2008; Sreedharan et al., 2008). TDP-43 has previously been reported to spontaneously form aggregates that resemble TDP-43 deposits in degenerating neurons in ALS FTLD-U patients (Johnson et al., 2009). Furthermore, previous studies have reported that in the TDP-43 protein sequence, the C-terminal domain is critical for spontaneous aggregation and therefore TDP-43 is intrinsically aggregation prone (Ivanova et al., 2014; Johnson et al., 2009). In addition, previous work indicates that ALS associated mutations in TDP-43 can increase the number of discrete aggregates in the cytoplasm of yeast (Johnson et al., 2009) suggesting that ALS mutations increase the aggregation propensity of TDP-43. The work presented here is consistent with this; inclusions were detected in cells expressing WT and mutant TDP-43, with mutation increasing inclusion formation.

The *in vivo* cell-to-cell transmission of TDP-43 and induction of TDP-43 aggregation in recipient cells was observed in the current study. Similarly, the ability of TDP-43 to transfer between cultured SH-SY5Y (human neuroblastoma) cells in co-cultured experiments was demonstrated in another study, which found that phosphorylated TDP-43 aggregates could be released from donor cells and taken up into recipient cells (Nonaka et al., 2013). In addition, mutant TDP-43^{G124A} was shown to induce the aggregation of TDP-43^{WT} in NSC-34 motor neurons when co-cultured together. Similarly, conditioned media containing TDP-43–from cultured cells or lysates from ALS patient brain lysate have been shown to induce oligomerisation in recipient cells (Feiler et al., 2015). Furthermore, another study demonstrated that pathological TDP-43 aggregates from diseased brains exhibit prion-like properties when added to cultured cells containing plasmid-derived TDP-43 (Nonaka et al.,

2013). In the latter study, detergent-insoluble TDP-43 prepared from cells containing TDP-43 aggregates as well as seeds from brains were shown to induce the formation of self-templating intracellular TDP-43 aggregation in cultured cells (Nonaka et al., 2013). These findings together therefore support a role for the prion-like seeding of mutant TDP-43 induced aggregation of TDP-43^{WT}.

Consistent with misfolded SOD1 detected in sALS, previous work has demonstrated that WT SOD1 misfolding can be propagated cell to cell (Grad et al., 2014). Here we have shown that exogenously added large-SOD1 protein aggregates are capable of inducing the cytoplasmic mislocalisation and accumulation of cytosolic TDP-43 in both the motor neuron-like cell line (NSC-34) and in human embryonic kidney cells (HEK-293). Furthermore, the present study demonstrates that the addition of large SOD1 aggregates induces rapid fragmentation of TDP-43 in the cytoplasmic fraction of NSC-34 cells. Collectively, this suggests that exogenous SOD1 protein aggregates are capable of stimulating TDP-43 pathology through an unknown mechanism(s), resulting in their redistribution, fragmentation and aggregation, similar to what has been observed in most cases of ALS (Arai et al., 2010; Correia et al., 2015; Nonaka et al., 2009a; Pokrishevsky et al., 2012).

An association between misfolded and/or aggregated SOD1 and TDP-43 mislocalisation has been previously suggested. For example, a study has reported that TDP-43 cytoplasmic mislocalisation and deposition into ubiquitin immunoreactive inclusions were observed in lower motor neurons of end stage mutant SOD1 transgenic mice (Shan et al., 2009). In addition to this, misfolded human WT SOD1 has been observed in association with cytosolic accumulation of mutant TDP-43 in TDP-43-fALS and WT TDP-43 in sALS (Pokrishevsky et al., 2012). It has been suggested that mutant TDP-43 may indirectly induce the propagation of WT SOD1 misfolding in fALS and sALS (Pokrishevsky et al., 2012). Given that the

aggregation of TDP-43 and SOD1 appear to be distinct processes with structurally and morphologically discrete aggregates (Farrawell et al., 2015), it is unlikely that one will seed aggregation of the other in a conventional manner and therefore must be explained by an alternate mechanism, possibly through exerting stress.

The deposition of TDP-43 into the cytoplasm of NSC-34 cells was dependant on the length of time exposed to the SOD1 aggregates. The 2 h incubation with SOD1 aggregates was sufficient to induce aberrant TDP-43 mislocalisation in a proportion NSC-34 cells. Further, we have shown using a subcellular fractionation assay on NSC-34 cells at 2 h treated with SOD1 aggregates, that a distinct truncation product at ~25 kDa, was present in the cytoplasmic fraction as previously reported in sALS and SOD1-negative fALS (Kwong et al., 2008; Mackenzie et al., 2010; Neumann et al., 2006).

In contrast, after 72 h incubation with SOD1 aggregates TDP-43 mislocalisation was observed in a significantly higher percentage of cells; equating to an almost two fold increase for the WT SOD1 and the G93A aggregate treated cells from 2 to 72 h. This effect may be due to the stress imposed on cells by the uptake of SOD1 aggregates (Stieber et al., 2000), consistent with a direct relationship between SOD1 aggregates and cellular toxicity that has been previously reported (Bruijn et al., 2004; Cleveland and Rothstein, 2001). Similarly, incubation with SOD1 aggregates induced similar pathological features in HEK-293 cells. However, the effect was apparent at 24 h and changed little in over 72 h incubation period. The cell type specific differences may reflect differences in proteostasis capacity between different cell types; neurons have a relatively high threshold for inducing the heat shock response (Yerbury et al., 2016). Regardless, while there is a clear effect of SOD1 aggregate uptake on TDP-43 distribution the precise mechanism underlying this remains unclear.

Cytoplasmic accumulation of WT TDP-43 as a local response to injury or cell stress has been previously described in sporadic ALS (Liu-Yesucevitz et al., 2010). In addition to this, misfolded and aggregated WT and mutant SOD1 are well known to induce ER stress and dysfunction and stress granule formation in cell culture (Nishitoh et al., 2008), rodent ALS models at symptom onset and disease end stage and human ALS patients (Atkin et al., 2006; Atkin et al., 2008; Ilieva et al., 2007; Kaus and Sareen, 2015; Saxena et al., 2009).

There is evidence that the uptake of extracellular misfolded WT and mutant G93A SOD1 into human and mouse neuronal cells causes disruptions to protein transport between the ER and Golgi apparatus, resulting in ER stress, Golgi fragmentation, and subsequent apoptotic cell death (Sundaramoorthy et al., 2013). ER stress is activated when proteins accumulate within the ER lumen, thus triggering the unfolded protein response (UPR), which in turn may lead to cellular apoptosis if unresolved (Atkin et al., 2014). There is a strong link between ALS pathology and ER stress (Walker and Atkin, 2011) and it has been proposed that prolonged ER stress leads to motor neuron death in ALS (Walker and Atkin, 2011). While generally the unfolded protein response activated by ER stress is a protective response able to rescue cells from proteotoxicity, in the ALS context this can lead to further aggregation of ALS associated proteins such as TDP-43 (Suzuki et al., 2011). Taken together, these data are consistent with the idea that ER stress caused by uptake and maintenance of SOD1 aggregates may trigger TDP-43 mislocalisation and accumulation.

In fact, TDP-43 mislocalisation is a common response to a variety of stressors including oxidative stress (Colombrita et al., 2009), heat shock stress (Chang et al., 2013), and proteosomal stress (Scotter et al., 2014). Indeed extranuclear accumulation of WT TDP-43 has been shown to be a common pathology in sALS, FTLD and Alzheimer's disease, and therefore may be a general consequence of cellular stress (Wilson et al., 2011). Interestingly,

exogenously applied Aβ amyloid aggregates associated with Alzheimer's disease have also been shown to induce TDP-43 mislocalisation (Herman et al., 2011) suggesting that uptake of any aggregate regardless of which protein they are made from might be enough to trigger TDP-43 mislocalisation.

In conclusion, the work presented here demonstrates that TDP-43 can form aggregates spontaneously, transfer between cells in culture and induce the misfolding of their WT counterpart, similar to that reported for SOD1 and prions. In addition, the work presents findings to support the notion that aggregates made from SOD1 are able to induce TDP-43 mislocalisation and rapid fragmentation consistent with TDP pathology observed in sporadic disease. However, the exact mechanism(s) for this observation were not determined. It is likely that the stress induced by aggregate uptake was enough to trigger the mislocalisation of TDP-43. However, it should be noted that a high concentration (20 µg/ml) of large SOD1 protein aggregates were used in the current study to induce TDP-43 pathology, as demonstrated above. This concentration is higher than that used in a number of similar studies (Münch et al., 2011; Nonaka et al., 2013) and *in vivo*. Future investigations into the mechanism(s)/role of SOD1 aggregates on the formation of pathological TDP-43 are therefore warranted.

Chapter 5

THE ABILITY OF PROTEIN AGGREGATES TO TRIGGER MACROPINOCYTOSIS IS GENERIC

5.1 Background

Amyotrophic Lateral Sclerosis (ALS) is characterised by the selective death and degeneration of upper and lower motor neurons (Cleveland and Rothstein, 2001). There is now significant evidence that protein aggregation is linked closely to motor neuron death in ALS (Abdolvahabi et al., 2016; Sundaramoorthy et al., 2013; Walker et al., 2013). In addition, other common neurodegenerative diseases, including Alzheimer's, Tauopathies such as Frontotemporal Dementia, Parkinson's, Huntington's diseases, and transmissible spongiform encephalopathies (TSEs), have common pathological changes such as loss of neurons and the presence of pathological protein aggregates into either intracellular inclusions bodies or extracellular plaques. Although the peptides and proteins that aggregate are unrelated in terms of their native structure, often the resulting deposits are very similar, sharing a rope-like fibrillar morphology, a common cross-β core structure, and the ability to bind specific dyes such as thioflavin T and Congo red (Dobson, 2003). In addition, these common neurodegenerative diseases, including ALS, exhibit distinctive anatomical patterns of disease progression which are consistent with a spreading of pathology between nearby cells and remotely connected regions of the brain along axonal pathways (Brettschneider et al., 2015; Brundin et al., 2010). These patterns are consistent with the propagation of the protein misfolding, aggregation and spread reminiscent of those underpinning prion disease. (reviewed in Zeineddine and Yerbury, 2015). Furthermore, proteins known to aggregate in these disorders including β-amyloid, tau, α-synuclein and proteins with polyQ expansions are suggested to propagate the misfolding of their native soluble counterparts (see Aguzzi and Calella, 2009; Brundin et al., 2010). In addition, it has been shown that these protein aggregates can enter into cells, cross cellular membranes to transmit pathogenic proteins in a 'prion-like' manner through the triggering the misfolding of their normally structured counterparts in cells, tissues, and animal models (Brettschneider et al., 2015).

In order to facilitate the propagation of intracellular aggregation in neurodegenerative diseases, such as ALS, Parkinson's, Alzheimer's and Huntington's diseases, active aggregate nuclei or seeds must gain access to the cytosol of naïve cells. Active nuclei could be large aggregates such as those macroscopically visible accumulating in neurons (> 2 microns in size) or small soluble oligomeric aggregates that might diffuse between cells. Fibrillar aggregates are generally 1-20 nanometre across and can be hundreds of nm long and large aggregates that accumulate many fibrils in cells can be several micrometres in diameter. Thus, given that neurons are not professional phagocytes it would be reasonable to assume that endocytosis of protein aggregates by neurons would be almost impossible.

A role for macropinocytosis in the uptake of protein aggregates associated with various neurodegenerative diseases has been highlighted in several studies and the work presented in earlier chapters (Grad et al., 2014; Holmes et al., 2013; Münch et al., 2011; Sundaramoorthy et al., 2013). The study on the propagation of SOD1 aggregation by Münch et. al (2011) was the first to demonstrate that mutant SOD1 ALS protein aggregates enter into N2A cells *via* endocytic vesicles mediated by ATP and lipid raft dependent macropinocytosis (Münch et al., 2011). The study utilised a wide panel of inhibitors of a range of cellular functions to identify potential pathways of endocytosis specific for SOD1 (Münch et al., 2011). Subsequently, these results were confirmed by an additional study which showed that uptake of both extracellular wildtype and mutant SOD1 soluble forms into NSC-34 cells can be inhibited by small molecule inhibitors of macropinocytosis EIPA and rottlerin (Sundaramoorthy et al., 2013). Similarly, EIPA was shown to inhibit the uptake of human WT SOD1 aggregates into NSC-34 cells (Grad et al., 2014) consistent with macropinocytosis. EIPA (ethylisopropylamiloride) is an analogue of amiloride that is an inhibitor of Na^+/H^+ exchangers. EIPA is well-recognised as specific to macropinocytosis (compared to other

forms of endocytosis) as a result of the susceptibility of GTPases such as RAC1 to pH changes (Koivusalo et al., 2010).

More broadly, uptake and cell-to-cell transmission of α-synuclein into neurons has been shown to be mediated *via* an unconventional endocytosis (Desplats et al., 2009; Lee et al., 2008). Also, while initially synthetic polyQ fibrils were proposed to enter cells *via* direct penetration of the lipid bilayer (Ren et al., 2009) recently cell surfaces structures have been implicated in the binding and internalisation of both synthetic polyQ ($K_2Q_{44}K_2$) and huntingtin exon 1 Q_{44} (Htt $exon_1Q_{44}$) fibrils suggesting a role for endocytosis mediated uptake (Trevino et al., 2012). Further, exogenously added AD associated-recombinant Tau fibrils have also been shown to be taken up by cultured cells in a process consistent with pinocytosis suggested by the co-localisation of Tau aggregates with Dextran, a marker of fluid phase endocytosis (Frost et al., 2009). In support of these findings, a recent study was able to show that small misfolded Tau species are also internalised through the process of bulk endocytosis (Wu et al., 2013). Further to this, uptake of fibrillar Tau into C17.2 cells (mouse neural stem cells) could be inhibited by both amiloride and rottlerin consistent with macropinocytosis (Holmes et al., 2013). The same study demonstrates that Tau fibrils could be observed in vacuoles and invaginations with diameters of approximately 5 μm also consistent with macropinocytosis. Lastly, in a result that suggests stimulated macropinocytosis has been activated, the uptake of the fluid phase marker dextran was increased with increased doses of Tau fibrils (Holmes et al., 2013). This uptake could be inhibited by suppressing cell binding of Tau fibrils by blocking binding to heparan sulfate proteoglycans, indeed this also blocked uptake when aggregates were injected in to the brains of mice (Holmes et al., 2013). However, how the binding to heparan sulfate proteoglycans on the cell surface relate to activation of macropinocytosis remains unclear.

The fact that neurons can engulf large particles such as protein aggregates seems counterintuitive. Macropinocytosis of large particles is usually thought of as restricted to professional phagocytes such as macrophages and microglia. This endocytic pathway is useful for engulfment of viral particles, bacteria, and fragments of dying cells in order to degrade and remove them from the cell. Without extensive degradation machinery, such as in macrophages, neurons are seemingly left vulnerable with the ability to take up large particles whilst not built to remove them. Irrespective of the ability of neurons to perform such a function, it is unlikely that neurons have evolved to specifically endocytose pathogens and large protein aggregates. Although, several viruses are known to enter neurons *via* macropinocytosis (Hollidge et al., 2012; Kalia et al., 2013; Talekar et al., 2011), this is likely due to the hijacking of machinery involved in macropinocytosis evolved for other purposes.

Macropinocytosis, or closely related processes, are thought to regulate growth cone membrane recycling and is an integral part of growth cone collapse and axon retraction and turning during development and injury (Jurney et al., 2002; Kabayama et al., 2011; Kolpak et al., 2009; Tom et al., 2004). The membrane recycling process in growth cones is associated with actin-dependent membrane ruffles that fuse back on the plasma membrane creating large pinosomes dependent on PI3K and RAC1; all characteristic of macropinocytosis. Upon synaptogenesis this process is supressed, consistent with the idea that mature neurons do not undergo bulk changes in the membrane *via* macropinocytosis. However, axonal injury in *in vivo* and *in vitro* models triggers axonal remodelling in adult neurons that is associated with large amounts of fluid uptake (Tom et al., 2004) consistent with macropinocytosis. Interestingly, some disease associated mutations such as those in ALS2 (Amyotrophic lateral sclerosis) and γPKC (Spinocerebellar ataxia 14) result in dysregulation of macropinocytosis (Otomo et al., 2008; Yamamoto et al., 2014) suggesting dysfunction of these processes are detrimental to large neurons. In addition, a cell culture model of methamphetamine toxicity

suggested that meth induced over stimulation of macropinocytosis could lead to lysosomal exhaustion and cell death (Nara et al., 2012).

Most protein aggregation studies associated with these neurodegenerative disorders to date have been performed *in vivo* or *in vivo* using rodent models of ALS. However, given the unnatural (induced) nature of the ALS-like disease in rodents and differences between rodents and humans, there is a need for more applicable human models. Humanised models of ALS have been generated in the last few years, through the use of reprogramming biology and development of humanised models of ALS has been established. The generation of patient specific induced pluripotent stem cells (iPSCs) derived from reprogrammed somatic cells from a range familial and sporadic ALS patients now represent a more effective disease model of ALS (Hedges et al., 2016; Lee and Huang, 2015). A range of disease-relevant cell types including neurons and motor neurons can be differentiated from human induced pluripotent stem cells which can be used to study pathogenic mechanisms and elucidate specific drug targets.

4.1.1 Aims

Results presented in Chapter 2 indicate that SOD1 aggregates enter NSC-34 cells *via* macropinocytosis. Here, this work aimed to determine if activation of macropinocytosis by protein aggregates was a generic phenomenon. To test this, aggregates found to trigger macropinocytosis in cell lines were tested on human neurons, both iPSC derived motor neurons and primary neurons. In addition, given the generic role of protein aggregates associated with other neurodegenerative diseases in mediating disease progression, such as TDP-43, huntingtin and α-synuclein, this work aimed to further investigate the mechanisms of uptake and further characterise the activation of macropinocytosis by these protein aggregates into NSC-34 motor neurons. Lastly, this study aimed to confirm that activation of

macropinocytosis was not limited to specific disease associated protein species by using the non-disease protein α-lactalbumin in its amorphous and fibrillar aggregation state.

5.2 Methods

5.2.1 Reagents and Antibodies

DMEM/F-12 medium, DMEM/F-12 without phenol red, Neurobasal Medium, B-27 supplement, Glucose powder, 0.05% trypsin-EDTA, GlutaMAX, SuperSignal West Pico Chemiluminescent Substrate, SYTOX Red dead cell stain, FM® 1-43FX, fixable analog of FM® 1-43 membrane stain, 10 kDa 647-dextran, Image-iT ™ LIVE Red caspase detection kit Laminin, fibronectin and Lab-Tek chambered coverglass 8 well with cover were purchased from ThermoFisher Scientific (Waltham, USA). Any kD Mini-PROTEAN TGX Precast Protein Gels and Precision Plus Protein dual color protein standard were from Bio-Rad (California, USA). Foetal Bovine Serum (heat-inactivated prior to addition in media; FBS) was from Bovogen Biologicals (East Keilor, Australia). Amersham Hyperfilm was obtained from GE Healthcare (Buckinghamshire, UK)). RedDot 2 was from Biotium (Hayward, CA). Sterile cell culture plates were from Greiner Bio-One (Frickenhausen, Germany). Casein (heat denatured before use; HDC), dimethyl sulfoxide (DMSO), bovine serum albumin (BSA), β-mercaptoethanol, Brilliant blue R concentrate, paraformaldehyde (PFA), biotinamidohexanoic acid 3-sulfo-N-hydroxysuccinimide ester sodium salt, Bicinchoninic Acid Kit, Glutaraldehyde solution (50% in H_2O), Propidium iodide, Osmium tetroxide solution (4 WT. % in H_2O) and dithiothreitol (DTT) were from Sigma-Aldrich (St. Louis, MO). Ethylenediaminetetraacetic acid (EDTA) was from Amresco (Solon, USA). Digitonin, High Purity was from Calbiochem was from San Diego, CA, USA. Uranyl acetate and 19 mm glass coverslips were from ProSciTech (Kirwan, Australia). mRNA was purchased from Miltenyi Biotec Australia (Macquarie Park, Australia) (Protease inhibitor cocktail tablets (complete, Mini, EDTA-free) was from Roche Diagnostics (Penzberg, Germany). RAC1 G-LISA Activation Assay Kit (Colorimetric Based) was purchased from Cytoskeleton (Denver, CO). ISOLATE II RNA Mini Kit was purchased from Bioline (Alexandria, Australia).

Reagents for cDNA preparation were obtained from Promega (USA). All other reagents including salts, powders and chemicals were from Amresco, Sigma-Aldrich or Astral Scientific (Gymea, Australia). All reagents used were endotoxin free. Antibodies (Abs) and inhibitor compounds and their respective manufacturing companies used in this current study are listed in Table 5.1 and Table 5.2 respectively.

Table 5.1 Antibodies used in this study to investigate the effect of SOD1 proteins on TDP-43 pathology

Host species (clonality)[1]	Anti-body target (Immunogen)[2]	Conjugate	Manufacturer (product number)[3]
Sheep (pAB)	SOD1	-	ThermoFisher Scientific (PAI-30817)
Mouse (mAb)	RAC1	-	Cytoskeleton (ARC03)
Rabbit (mAb)	Islet 1	-	Abcam [EP4182] (ab109517)
Mouse (mAb)	SMI32	-	Abcam (ab73273)
Mouse (mAb)	Human OCT4	Alexa Fluor 488	STEMCELL Technologies Australia (3A2A20)
Goat (pAB)	Mouse IgG	Alexa Fluor 488	ThermoFisher Scientific A-(11001)
Goat (pAB)	Rabbit IgG	Alexa Fluor 488	ThermoFisher Scientific (A-11008)
Donkey (pAb)	Sheep IgG	Alexa Fluor 488	Abcam (150177)
Goat (pAb)	Mouse IgG	Alexa Fluor 633	ThermoFisher Scientific (A-21052)
Donkey (pAb)	Sheep IgG	HRP	Abcam (97125)
Goat (pAb)	Mouse IgG	HRP	Merck Millipore (12-349)

[1] pAb, polyclonal anti-body, mAb, monoclonal anti-body; [3] Abcam, Cambridge, USA; ThermoFisher Scientific (Waltham,MA, USA); BD Biosciences San Jose, CA, USA; Merck Millipore, Billerica, Massachusetts, USA; Cytoskeleton (Denver, CO,USA), STEMCELL Technologies Australia, Tullamarine, VIC, Australia.

Table 5.2 Pharmacological inhibitors used in this study to investigate the mechanisms of SOD1 uptake

Compound	Manufacturer (product number)[1]
5-N-ethyl-N-isopropyl-amiloride (EIPA)	Sigma (A3085)
Chlorpromazine hydrochloride (Chlorp HCL)	Sigma (C8138)
Genistein (Gen)	Sigma (G6649)
Rottlerin (Rot)	Sigma (R5648)
RAC1 inhibitor W56	Tocris Bioscience (2221)

[1]Sigma, (St. Louis, MO, USA), Tocris Bioscience (Avonmouth, Bristol,UK)

5.2.2 Cell Lines

The mouse neuroblastoma x spinal cord hybrid cell line (NSC-34 cells) (Cashman et al., 1992) were routinely cultured in DMEM/F12 supplemented with 10% (v/v) FBS and 2 mM GlutaMAX. Cells were maintained in an incubator at 37°C under a humidified atmosphere containing 5% (v/v) CO_2. Human primary neurons were cultured from 14 to 18 week foetal brains collected after therapeutic termination with informed consent and were prepared with the approval from Human Ethics Committees at the Universities of Sydney and New South Wales (Sydney, Australia), as previously described (Guillemin et al., 2005). Briefly, neurons were isolated from mixed foetal brain cells using a neuron isolation kit (Miltenyi Biotec, Australia). Human primary neurons were plated in culture flasks coated with Matrigel (BD Biosciences, CA) (1/20 in Neurobasal medium) for an hour at 37°C prior to seeding. Cells were maintained in neurobasal medium supplemented with 2% B-27 supplement, 2 mM Glutamax, and 5 mM glucose (complete medium) at 37^{o}C at 5% CO_2. Cells were cultured in complete medium for up to 10 weeks. The medium was changed once a week.

Human fibroblasts were sourced from non-ALS individuals (female aged 62 and male aged 59 at the time of collection) and reprogrammed into induced pluripotent stem cells using mRNA (Miltenyi Biotec, Australia). Pluripotency was confirmed by PluriTest Bioline RNA purification kit Genea and differentiation of the cells (Muller et al., 2011). Karyotyping was carried out in iPSCs, to ensure chromosomal abnormalities were not introduced during reprogramming and culture. Immunocytochemistry confirmed the expression of the pluripotency marker Oct4 (STEMCELL Tech). Differentiation of pluripotent stem cells into motor neurons was carried out as in (Bilican et al., 2014) and one clone from each line was used in experiments. Motor neurons (1.5 x 10^4 cells/ well) were plated onto laminin (20 µg/mL) and fibronectin (10 µg/mL) coated 13 mm coverslips. The timeline (Figure 5.1B) summarizes the differentiation stages and the growth factor conditions used during

differentiation. The morphological changes of each cell line were examined at each stage of the differentiation process.

Confirmation of motor neuron phenotype was carried out, including expression analysis by quantitative reverse transcription PCR and immunocytochemistry. The differentiated neurons expressed the motor neuron specific markers neurofilament heavy and islet 1. Immunocytochemistry identified the presence of extended dendrites ~100 μm in length. Quantitative reverse transcription PCR analysis identified the expression of the motor neuron specific gene *MNX1* (that encodes the transcription factor homeobox 9, HB9) (Arber et al., 1999). *MNX1* was specifically expressed in motor neurons and *MNX1* was silent in pluripotent stem cells. The cholinergic specific marker acetylcholine esterase (*ACHE* that encodes the enzyme responsible for the degradation of the neurotransmitter acetylcholine) was expressed in cholinergic motor neurons. The expression levels for both *MNX1* and *ACHE*, were normalized to the housekeeper gene *GAPDH*.

5.2.3 Fixed cell antibody staining of iPSCs.

The iPSCs were plated on matrigel-coated 8 mm coverslips at a density of 2.5x 10^4 cells/cm^2 and cultured for 3 days prior to staining. Cells were fixed with 4% PFA in PBS for 20 min at RT and washed twice with PBS over 5 min. Cells were washed once with ice-cold PBS and then incubated with 0.5% Triton-X 100 for 30 min at 4°C. Cells incubated with blocking solution (5% BSA) for 20 min at RT. The iPSC colonies were incubated with anti- Oct3/4 IgG Ab (1:500 diluted in 4% BSA and 0.1% Triton X-100) overnight at 4°C. Cells were washed again in ice cold PBS and incubated with anti-mouse IgG conjugated to Alexa Fluor 488 (1:1000 diluted in 1% BSA and 0.1% Triton X-100) for 1 h at RT protected from light. An inverted microscope (DM IBRE) and a Leica TCS SP confocal imaging system were used to visualise and image cells (excitation 488, emission collected at 520-545 nm).

Fluorescence, bright field (differential interference contrast; DIC) and merged images were captured using Leica confocal software.

5.2.4 Fixed cell antibody staining of motor neurons.

Cells were plated on coverslips coated with laminin (20 µg/mL) and fibronectin (10 µg/mL) at a density of 4.2 x 10^4 cells/cm^2. Cells were fixed with 4% PFA in PBS for 20 min at RT and washed twice with PBS over 5 min. Cells were washed once with ice-cold PBS and then incubated with 0.5% Triton-X 100 for 30 min at 4°C. Cells incubated with blocking solution (5% BSA) for 20 min at RT. Cells were incubated with anti- NFH (SMI32) IgG Ab (1:800 diluted in 4% BSA and 0.1% Triton X-100) overnight at 4°C. Cells were washed again in ice cold PBS and incubated with anti-mouse IgG conjugated to Alexa Fluor 488 (1:1000 diluted in 1% BSA and 0.1% Triton X-100) for 1 h at RT protected from light. An inverted microscope (DM IBRE) and a Leica TCS SP confocal imaging system were used to visualise and image cells (excitation 488, emission collected at 520-545). Fluorescence, bright field (differential interference contrast; DIC) and merged images were captured using Leica confocal software.

5.2.5 Quantitative RT-PCR

RNA was extracted and purified from differentiated cell using the ISOLATE II RNA Mini Kit (Bioline, USA), as per manufacturer's instructions. The purified RNA was quantified using NanoDrop 2000c dual-mode UV-Vis Spectrophotometer (ThermoFisher Scientific). RNA was reverse transcribed into complementary DNA (cDNA) for subsequent analysis. 5 µg of purified RNA was annealed to random primers (0.75 µg) and oligo dT primers (0.75 µg) by incubating at 65°C for 4 min, followed by 1 min incubation on ice. For reverse transcription, Moloney-murine leukaemia virus reverse transcriptase (M-MLV RTase) (150 U), 96 nmol dNTPs, RNasin (60 U) and 1x MMLV RTase Buffer were added to the reaction

mixture and then incubated at 37 ºC for 100 min. Primers used in Chapter 5 for qRT-PCR were obtained from Sigma Aldrich (USA) (unless stated otherwise) and sequences are outlined in Table 5.3.

Table 5.3 Primers used in Chapter 5 for qRT-PCR had the following sequences:

Gene	Forward	Reverse
Acetylcholinesterase (AChE)	5'-GGAACCGCTTCCTCCCCAAATTG-3'	5'-TGCTGTAGTGGTCGAACTGGTTCTTC-3'
Homeobox 9 (MNX1)	5'-GTTCAAGCTCAACAAGTACC-3'	5'-GGTTCTGGAACCAAATCTTC-3'
GFAP	5'-CTGGATCTGGAGAGGAAGATTGAGTCG-3'	5'-CTCATACTGCGTGCGGATCTCTTTCA-3'
glyceraldehyde 3-phosphate dehydrogenase GAPDH	5'-GAGCACAAGAGGAAGAGAGAGACCC-3'	5' GTTGAGCACAGGGTACTTTATTGATGGTACATG-3'

The final qRT-PCR reaction consisted of 10 µL of SYBR Select Master Mix, 800 nM of each forward and reverse primer, 2 µL of cDNA in a final reaction volume of 20 µL. Each reaction was run in duplicate and a negative control (water) and no reverse transcription (RNA) control was included as well as a positive control using cDNA of human putamen. The amplification consisted of 40 cycles, of 95ºC for 15 s (activation step), 58ºC for 15 s (annealing step) and 72ºC for 1 min. A melting curve analysis was conducted to confirm the presence of the appropriate amplified target. The acquired data was normalized against quantitative expression levels of the housekeeping gene GAPDH and analyzed using the comparative threshold cycle method.

5.2.6 Aggregation and biotinylation of SOD1, Htt_{ex1}46Q, α-synuclein, TDP-43, and α-lactalbumin aggregates

WT and G93A SOD1 were purified and labelled as outlined in section 2.3.3. Proteins α-synuclein and α-lactalbumin protein aggregates were kindly provided by Dr Heath Ecroyd (University of Wollongong, Wollongong, Australia). TDP-43 was produced by Melbourne Protein Production Unit (Monash University) and kindly provided by Natalie Farrawell. Monomeric Htt_{ex1}46Q-Cerulean-MBP fusion protein was kindly provided by Danny M. Hatters (The University of Melbourne, Melbourne, Australia). Monomeric Htt_{ex1}46Q-Cerulean-MBP fusion protein aggregation of Htt_{ex1}46Q was performed as previously described (Ramdzan et al., 2010). Briefly, Htt_{ex1}46Q-Cerulean-MBP was thawed from frozen stocks, diluted to 9 μM, and rapidly mixed with a 1/20 stock of TEV protease. After 15 min incubation at RT, the resulting cleaved fusion protein (Htt_{ex1}46Q-Cerulean) was diluted to 2 μM and divided into single use aliquots, snap frozen in liquid nitrogen and stored at -80°C for later use in experiments.

5.2.7 Transmission electron microscopy of Htt_{ex1}46Q, α-synuclein, TDP-43, and α-lactalbumin RCM and amorphous protein aggregates

Negative staining transmission electron microscopy (TEM) was performed as outlined in section 2.2.5. Briefly, 2 μl aliquots of Htt_{ex1}46Q, α-synuclein, TDP-43, and α-lactalbumin RCM and amorphous proteins (1 mg/ml) were loaded onto carbon-coated nickel grids for 1 min at RT, washed 3 times with filtered Milli-Q water and negatively stained using 2% (w/v) uranyl acetate diluted in Milli-Q water for 2 min at RT. Grids were then dried and stored until processing. Protein structure and morphology was then analysed using a JEOL 2011 TEM (Tokyo, Japan) operated at 200kV. Images were taken using Gatan Microscopy Suite (Version 2.30.542.0) (California, USA).

5.2.8 Htt_{ex1}46Q, α-synuclein, TDP-43, and α-lactalbumin RCM and amorphous aggregated protein detection in NSC-34 cells by confocal microscopy

NSC-34 cells (2–3 x 10^4 cells/0.2 ml/chamber) were cultured in chamber slides at 37°C/5%CO_2 overnight. Briefly, cells were incubated with 20 µg/ml of biotin-conjugated aggregates of Htt_{ex1}46Q, α-synuclein, TDP-43, α-lactalbumin RCM and amorphous proteins or PBS (no protein, control) for 2 h at 37°C. Cells were fixed with 4% PFA, incubated with Triton X-100 and blocked for detection with 1 µg/ml Alexa Fluor 488 streptavidin (diluted in 1% BSA and 0.1% Triton X-100) for 1 h at RT protected from light. An inverted microscope (DM IBRE) and a Leica TCS SP confocal imaging system were used to visualise and image cells (excitation 488, emission collected at 520-545 nm). Fluorescence, bright field (differential interference contrast; DIC) and merged images were captured using Leica confocal software.

5.2.9 Fluid phase uptake assays

Fluid phase uptake assay was performed as outlined in section 2.2.17. Briefly, NSC-34 cells (2–3 x 10^4 cells/0.2 ml/chamber) were incubated with 20 µg/ml of Htt_{ex1}46Q, α-synuclein, TDP-43, α-lactalbumin RCM and amorphous aggregates in PBS alone or a positive control, 200 nM PMA, for 30 min. Prior to harvesting or fixation, cells were then co-incubated for 15 min with 0.5 mg/ml 10 kDa dextran conjugated to Alexa Fluor 647 (10 kDa 647-dextran) at 37°C/5% CO_2. The cells were then placed on ice, washed three times with ice cold PBS and once with low pH buffer (0.1 M sodium acetate, 0.05 M NaCl, pH 5.5) for 10 min. The cells were then fixed with 4% PFA and permeabilised with 0.5% Triton-X 100. Cells were then incubated with anti-SOD1 IgG Ab overnight at 4°C. Cells were washed again in PBS and incubated with Alexa Fluor 488 streptavidin for 1 h at RT. This same assay was performed on human iPSC-derived and primary motor neurons incubated with 20 µg/ml of SOD1

aggregates. An inverted microscope (DM IBRE) and a Leica TCS SP confocal imaging system were used to visualise and image cells (excitation 488, emission collected at 495-515 and 650-668 nm). Fluorescence, bright field (differential interference contrast; DIC) and merged images were captured using Leica confocal software. In addition, cellular events were collected in a separate study using a LSR II flow cytometer as outlined in section 0.

5.2.10 Quantifying Inhibition of Htt_{ex1}46Q, α-synuclein, TDP-43, α-lactalbumin RCM and amorphous aggregated protein uptake

Inhibitor assays were performed as outlined in section 2.2.13. Briefly, NSC-34 cells were pre-treated with 100 µM 5-N-ethyl-N-isopropyl-amiloride (EIPA), 5 µM chlorpromazine hydrochloride (Chlorp HCl), 10 µM genistein (Gen) or 3 µM rottlerin (Rot) diluted in 1% BSA/PBS for 30 min. Cells were then co-incubated with by 20 µg/ml Htt_{ex1}46Q, α-synuclein, TDP-43, α-lactalbumin RCM and amorphous aggregated proteins for an additional 30 min. Aggregates were only incubated for 30 mins (shorter time) as uptake of aggregates is proposed to occur within this timeframe. Cells were immediately fixed with 4% PFA, washed twice with PBS and incubated with Triton X-100 for 30 min at 4°C. Cells were then incubated with blocking solution (5% FCS, 1% BSA and 0.3% Triton X-100) for 20 min. Cells were incubated with with Alexa Fluor 488 streptavidin for 1 h. Sytox Red (5 nM) was used as a counter stain, and incubated with cells for 10 min at RT. This same assay was performed on human iPSC-derived and primary motor neurons incubated with 20 µg/ml of SOD1 aggregates. An inverted microscope (DM IBRE) and a Leica TCS SP confocal imaging system were used to visualise and image cells (excitation 488, emission collected at 520-545). Fluorescence, bright field (differential interference contrast; DIC) and merged images were captured using Leica confocal software. In addition, cellular events were collected in a separate study using a LSR II flow cytometer as outlined in section 5.2.9.

5.2.11 Membrane activity quantification

Membrane dye uptake assay was performed as outlined in section 2.2.16. Briefly, human iPSC-derived motor neurons and human primary neurons were cultured as described above (see section 5.2.2). Cells were incubated with 20 µg/ml of SOD1, PBS alone, or PMA (200 nM) in PBS for 2 h at 37°C/5% CO_2. Cells were then washed, incubated with 10 µM of FM 1-43FX membrane stain diluted in PBS for 7 min and excess dye was removed by several washes in PBS and incubated in ice-cold PBS. Cells were then fixed in 4% PFA for 20 min at 4°C. Post fixation, cells were washed twice in PBS and incubated with 1x Red Dot 2 for 10 min at RT.

5.2.12 Field emission scanning electron microscopy (FESEM)

FESEM assay was performed as outlined in section 2.2.15. Briefly, NSC-34 cells were serum starved in phenol red free culture medium for 24 h and incubated with 20 µg/ml $Htt_{ex1}46Q$, α-synuclein, TDP-43, α-lactalbumin RCM and amorphous aggregated proteins in PBS or PBS containing 200 nM PMA for 2 h. Post incubation, cells were fixed in 2.5% glutaraldehyde/4% PFA in 0.1 M phosphate buffer for 3 h at 4°C. Cells were then washed and postfixed in 2% OsO_4/water at RT for 1 h. After washing with water, the cells were dehydrated using a gradient of ethanol, critical point dried for 2 h using a LEICA CPD030 and coated with graphite-gold in a sputter coater. This same assay was performed on human iPSC-derived and primary motor neurons incubated with 20 µg/ml of SOD1 aggregates Cellular structures were visualised with a JEOL 6490LV SEM (Tokyo, Japan) microscope operated at 10 kV at a 10 mm working distance and a spot size setting of 35.

5.2.13 RAC1 activation Elisa assays

RAC1 activation assay was performed as outlined in section 2.2.20. Briefly, NSC-34 cells serum starved in phenol red free culture medium for 24 h and incubated with 20 µg/ml of $Htt_{ex1}46Q$, α-synuclein, TDP-43, α-lactalbumin RCM and amorphous aggregated proteins for 30 min at 37°C/5% CO2. Cells were washed, harvested by treatment with 0.05% trypsin for 10 min and washed again (300 x g for 5 min) in PBS. RAC1 activation was measured using a G-LISA activation kit (Kit #BK128 Cytoskeleton, Inc. Denver, USA) as per the manufacturer's recommendations. Absorbance values of wells were recorded with a SpectraMax Plus 384 Microplate Reader and SoftMax Pro software (Molecular Devices, Silicon Valley, CA) (490nm).

5.3 Results

5.3.1 SOD1 aggregates are internalised *via* macropinocytosis pathways in iPSC-derived and primary human motor neurons

5.3.1.1 Characterisation of a motor neuron phenotype in iPSC-derived motor neurons

The results of investigations presented in detail in Chapter 2, demonstrate that SOD1 aggregates enter NSC-34 cells *via* macropinocytosis. To determine whether or not these findings extend to human neurons, SOD1 uptake pathways were next investigated in human cultured iPSC-derived motor neurons and human primary neurons. Prior to investigating the uptake pathways of SOD1 in human iPSC-derived motor neurons, the pluripotency and differentiation of the cells was characterised (Figure 5.1). Initially, karyotyping (StemCore, Australian Institute for Bioengineering and Nanotechnology, Australia) demonstrated that chromosomal abnormalities were not introduced during reprogramming and culture (data not shown). Immunocytochemistry confirmed the expression of the pluripotency marker Oct4 in iPSCs (Figure 5.1A). Differentiation of pluripotent stem cells into motor neurons was carried out as in (Bilican et al., 2014) and outlined in Figure 5.1B. The differentiated neurons expressed the motor neuron specific marker SMI32 (Figure 5.1C). Immunocytochemistry identified the presence of extended dendrites ~100 μm in length. Quantitative reverse transcription PCR analysis identified the expression of the motor neuron specific gene MNX1 (that encodes the transcription factor homeobox 9, HB9) (Arber et al., 1999). MNX1 was specifically expressed in motor neurons and MNX1 was silent in pluripotent stem cells. The cholinergic specific marker acetylcholine esterase (ACHE that encodes the enzyme responsible for the degradation of the neurotransmitter acetylcholine) was specifically expressed in cholinergic motor neurons. The expression levels for both MNX1 and ACHE, were normalized to the housekeeper gene GAPDH (Figure 5.1D).

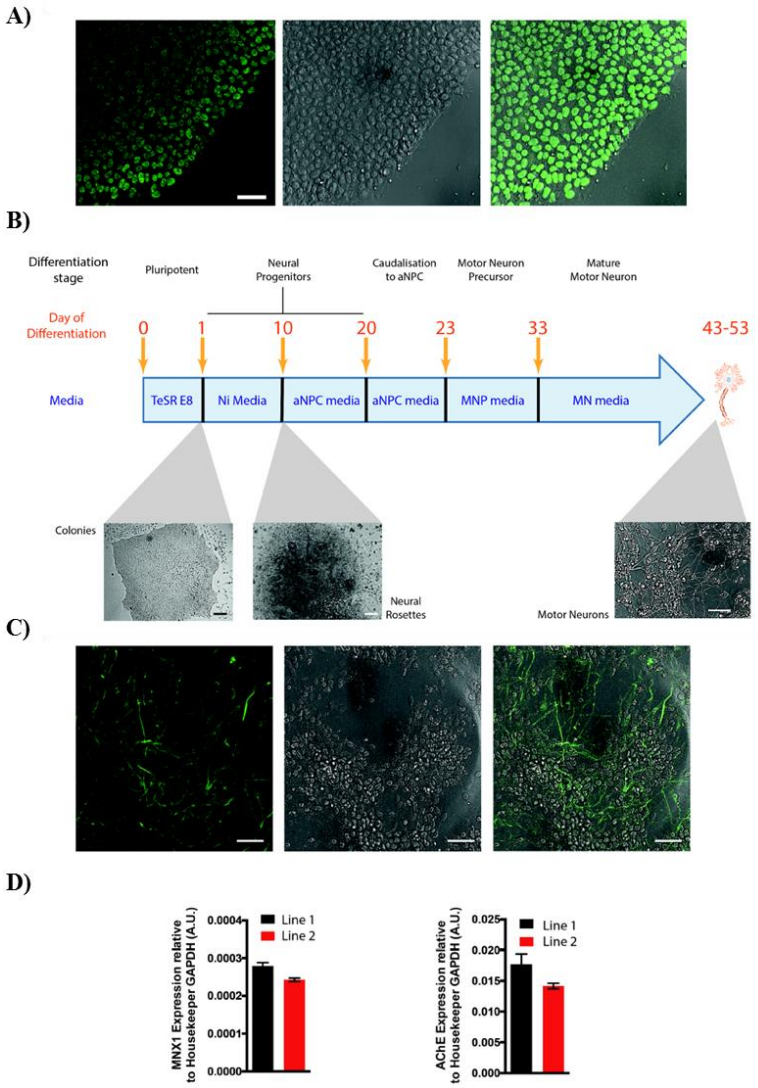

Figure 5.1 Characterisation of iPSC derived motor neurons. (A) Immunocytochemistry confirmed the expression of the pluripotency marker Oct4. Human induced pluripotent stem cells were cultured in TeSR-E8 on glass coverslips coated with Matrigel, fixed and stained with Alexa Fluor 488-conjugated Oct4 antibody. Confocal and brightfield images were taken on a Leica SP5 confocal microscope. Scale bar is 60 mm. (B) The timeline summarises the differentiation stages and the growth factor conditions used during differentiation (Billican et al.). Example images of cellular morphological changes during differentiation are shown. Scale bars are 100 mm, 50 mm, 50 mm respectively. (C) Motor neurons were cultured on glass coverslips coated with laminin, collagen and fibronectin. Immunocytochemistry confirmed the expression of the motor neuron marker SMI-32. Scale bars are 30 mm. (D) Expression of neuronal and cholinergic markers were quantified using quantitative RT-PCR. Data plotted as mean relative gene expression in motor neurons normalised to GAPDH (± SEM, n=3). MNX1 and ACHE expression was silent in pluripotent cells. This work was performed by Dzung Do-Ha, Monique Bax and Lezanne Ooi.

Next, the purity of the resulting motor neuron cultures was assessed by microscopy. Immunocytochemical analysis confirmed that the majority of the motor neuron cultures were positive (90.5 ± 1.4 %) for the motor neuronal marker SMI32 and 88.8 ± 1.4 % of cells were positive for neural stem cell marker Islet 1, with large cell bodies, consistent with a large proportion of the cells having a motor neuron morphology (Figure 5.2).

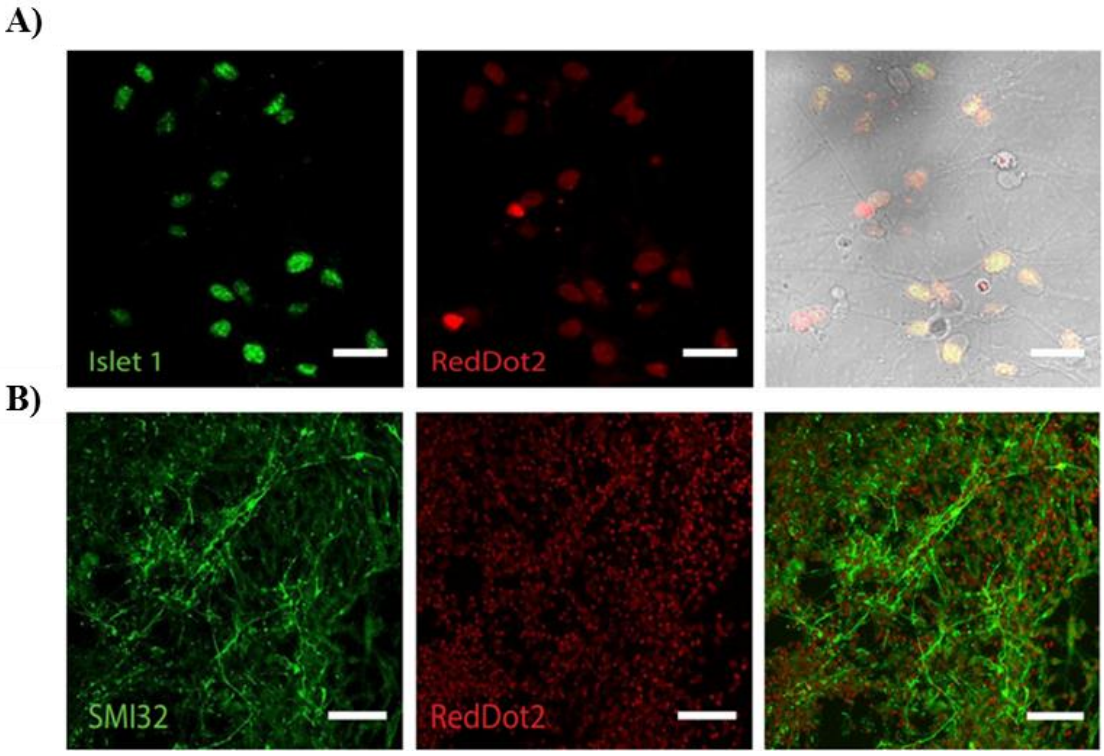

Figure 5.2 Characterisation of iPSC derived motor neurons. Quantification of Islet 1 (A) and SMI32 (B) positive cells was performed using immunocytochemistry and analysis using Image J software. Islet 1 and SMI32 positive cells were calculated as a percentage of the total number of cells (determined by nuclear stain) from motor neuron cultures generated from six donor cell lines, using 6-10 images from each technical replicate (separate differentiation experiments using 3 technical replicates for Islet 1 and 2 technical replicates for SMI32). The motor neuron cultures contained 90.5 ± 1.4 % SMI32-positive cells and 88.8 ± 1.4 % Islet 1-positive cells. Scale bars are (A) 100 mm and (B) 50 mm respectively. This work was performed by Dzung Do-Ha, Monique Bax and Lezanne Ooi.

5.3.1.2 Pharmacological inhibitors of Macropinocytosis reduce SOD1 aggregate uptake in human iPSC-derived and primary motor neurons

To examine the pathway of SOD1 uptake in human neurons, iPSC-derived motor neuron cultures (Figure 5.3A) and primary motor neurons (Figure 5.3B) were in pre-incubated in the absence or presence of the Na+/H+ exchange inhibitor; EIPA and the RAC1 inhibitor W56 which specifically inhibits RAC1 activity. Cells were firstly incubated with SOD1 aggregates in the absence or presence of EIPA and W56 and then the mean fluorescence intensity for the SOD1 aggregates was examined by confocal microscopy analysis. Relative SOD1 uptake was quantified from these images using ImageJ software.

Firstly, the uptake of WT and mutant SOD1 aggregates into human cultured iPSC-derived motor neurons and primary neurons was assessed. Similar to previous observations reported in Chapter 1, pre-incubation of human iPSC-derived motor neuron cells with 100 µM EIPA and 200 nM W56 significantly reduced WT SOD1 aggregate uptake by 17 ± 0.4% and 41 ± 0.5%, respectively. Similarly, incubation with EIPA and W56 significantly inhibited mutant G93A SOD1 aggregate uptake by 52 ± 0.7% and 58 ± 0.6%, respectively. In addition, human primary neurons were pre-incubated in the absence or presence of EIPA and W56 before addition of SOD1 aggregates. Incubation with EIPA and W56 significantly reduced WT SOD1 aggregate uptake by 56 ± 1% and 13 ± 0.9% and the uptake of mutant G93A SOD1 aggregate by 23 ± 1% and 35 ± 1%, respectively . Thus, given the large size of the aggregates and the ability of EIPA and W56 to modulate uptake, this suggests that macropinocytosis-like pathways play a role in the uptake of WT and mutant SOD1 aggregates in human neurons, similar to observations made in the mouse motor neuron-like (NSC-34) cell line (Chapter 1).

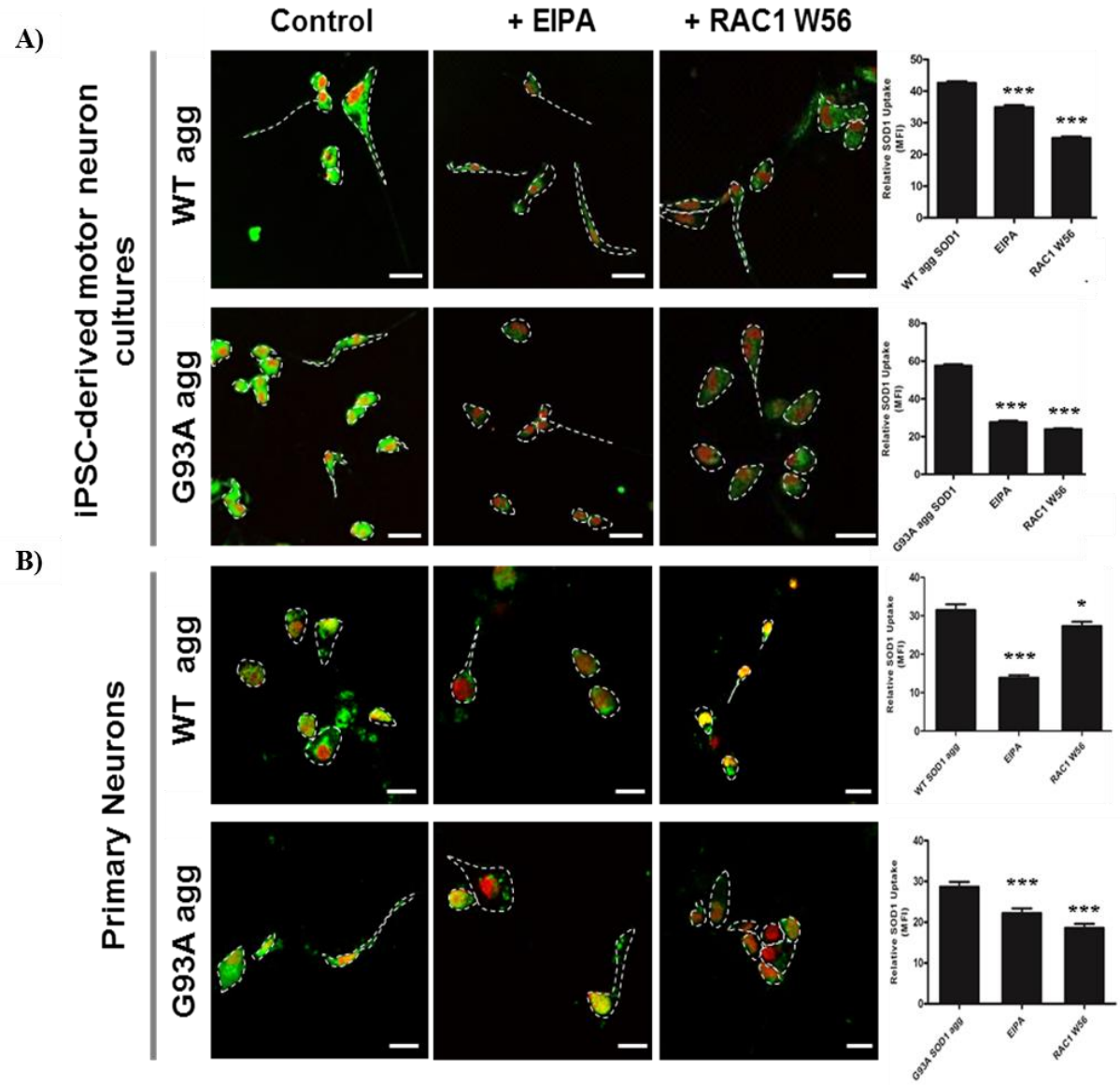

Figure 5.3 Small molecule inhibitors block macropinocytosis. (A) iPSC-derived and (B) primary human motor neurons were incubated with 20 µg/ml of aggregated SOD1 proteins (20 µg/ml) for 30 min at 37°C, in the absence (control) or presence of a pre-incubation step with either EIPA (100 µM) or RAC1W56 (200nm) inhibitor, fixed with 4% PFA, permeabilised and labelled with either anti-human SOD1 Ab (non-aggregated/ soluble) or Alexa Fluor 488 streptavidin. Slides were analysed by confocal microscopy. Outline of cells are indicated with white dashed lines. Bars represent 20 µm. Results are representative of at least $n = 3$. Uptake of proteins under the same conditions were determined by flow cytometry and results shown as mean fluorescence intensity ± SD, $n = 6$, $^{***}P < 0.001$ or $^{*}P < 0.05$ compared to corresponding control.

5.3.2 SOD1 aggregates trigger cell surface ruffling in human cultured iPSC-derived motor neurons and primary neurons

5.3.2.1 SOD1 aggregates induce cell surface ruffles and blebs in the membrane to enter into human cultured iPSC-derived motor neurons and primary motor neurons

Since membrane ruffling associated with macropinocytosis was implicated in SOD1 uptake into NSC-34 cells, the role of SOD1 aggregates in triggering actin-mediated membrane ruffling and blebbing in the plasma membrane of human cultured iPSC-derived motor neurons and primary neurons was tested. To investigate this, initially the detailed morphology of the cell surface was examined by field emission scanning electron microscopy (FESEM) (Figure 5.4). Incubation of human cultured iPSC-derived motor neurons (Figure 5.4A) with WT and mutant G93A SOD1 aggregates induced significant membrane perturbations in the form of systemic blebbing and lamellipodia-like membrane protrusions similar to that observed for cells treated with positive control; PMA. However, no obvious membrane perturbations were seen in cells incubated in the absence of protein treatment.

Similarly, primary neurons (Figure 5.4B) incubated in the presence of WT and mutant G93A SOD1 aggregates displayed lamellipodia- like ruffling and blebbing in the cell surface. These membrane perturbations were more prominent in cells treated with PMA, which present in the form of systemic blebbing and ruffling in the cell surface relative to the cells treated in the absence of protein.

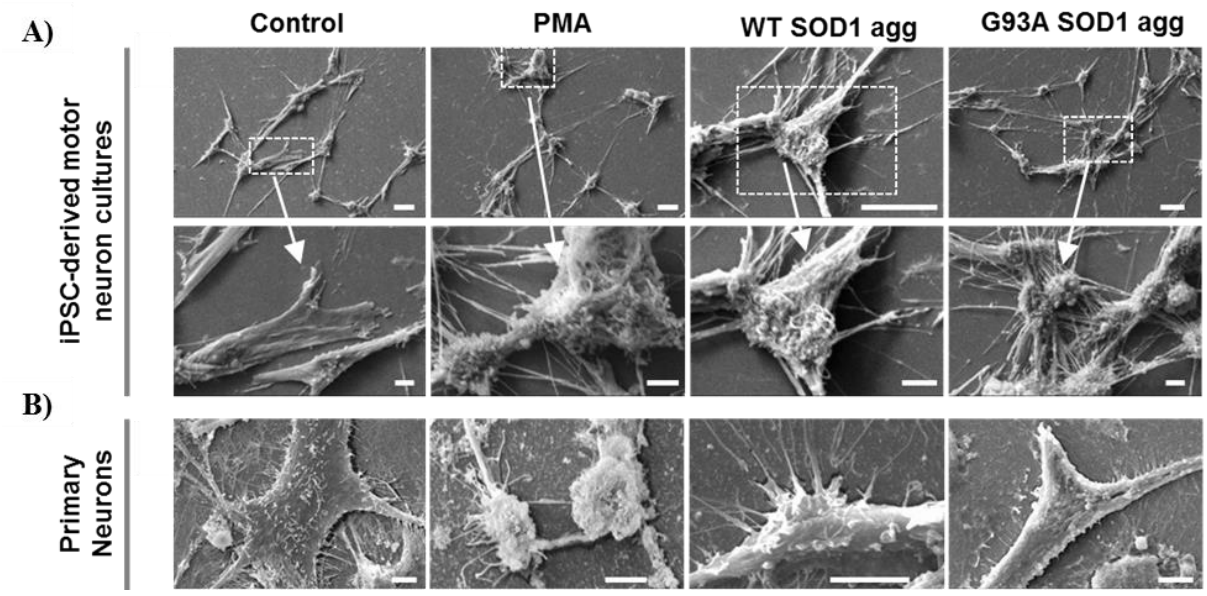

Figure 5.4 Aggregated SOD1-induced macropinocytosis involves ruffles in the plasma membrane of human iPSC-derived and primary motor neurons. (A) iPSC-derived and (B) primary human motor neurons were serum starved for 24 h and were incubated with PBS (control, no protein), PBS containing 200 nm phorbol 12-myristate 13-acetate (PMA) or 20 µg/ml of aggregated SOD1, for 2 h, fixed with 2.5% glutaraldehyde/4% PFA in 0.1 M phosphate buffer for 3 h, postfixed in 2% OsO_4/ water, dehydrated using a gradient of ethanol (30-100%, 30 min per treatment), critical point dried for 2 h and coated with graphite-gold. Increases in membrane perturbations can be observed, such as ruffles and blebs. Slides were analysed by field emission scanning electron microscopy. Bars represent 1 µm. Results are representative of n = 2.

Next, to quantify the extent of the observed membrane ruffling and blebbing in the plasma membrane, human cultured iPSC-derived motor neurons and primary neurons were pretreated with membrane dye FM 1-43FX, which has been used in previously for studies of membrane perturbation during growth cone ruffling (Kolpak et al., 2009). Cells were then incubated with SOD1 aggregates or PMA for 2 h (Figure 5.5). Incubation with SOD1 aggregates induced significantly higher membrane perturbations, as measured by an increase in cellular fluorescence compared to controls, in both human cultured iPSC-derived motor neurons (Figure 5.5A) and primary neurons Figure 5.5B). This finding reflected the FESEM data above and is consistent with increased ruffles and blebs at the cell surface.

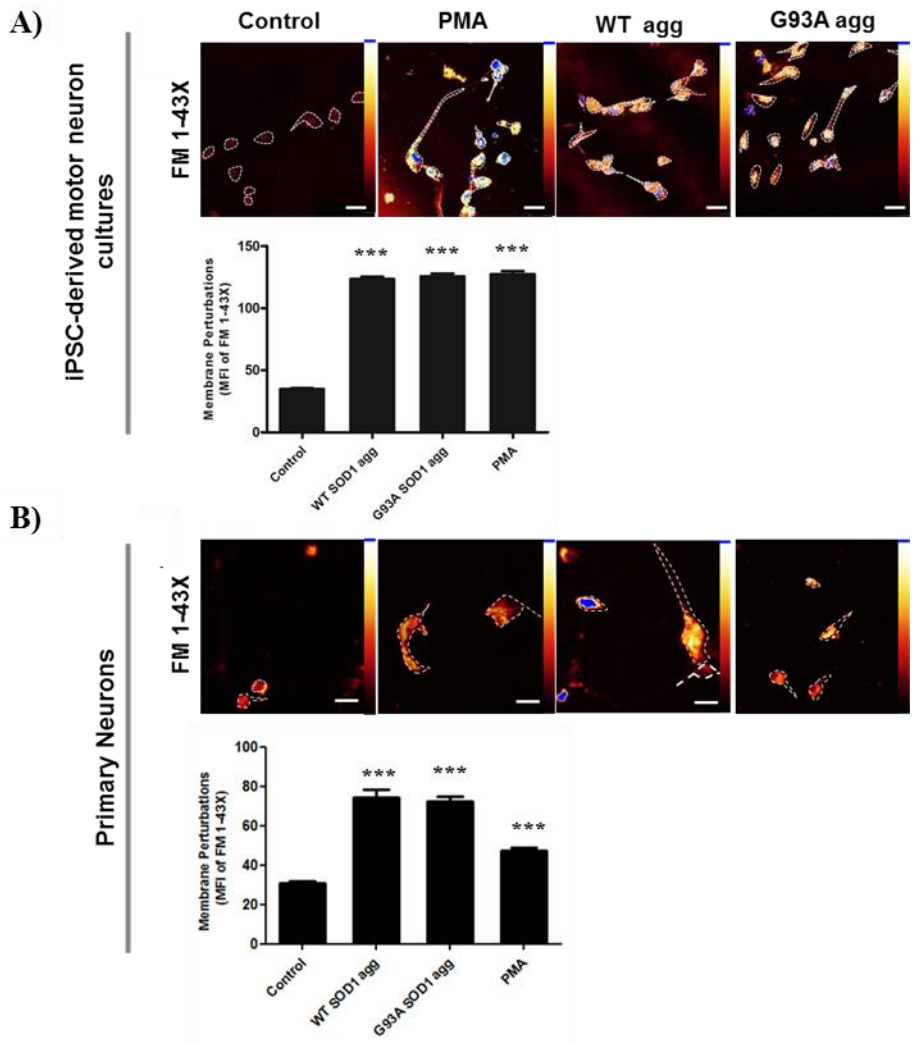

Figure 5.5 SOD1 aggregates induce membrane perutbations in the cell surface of iPSC-derived and primary human motor neurons (A) iPSC-derived and (B) primary human motor neurons were incubated with PBS alone, 200 nM PMA or 20 µg/ml of aggregated SOD1for 2 h at 37°C, incubated with the membrane dye FM1-43FX and fixed with 4% PFA. Outline of cells are indicated with white dashed lines. Bars represent 20 µm. Mean fluorescence intensities (MFI) of membrane dye per cell were quantified from these images using ImageJ software (Version 1.48) (National Institutes of health, Bethesda, MD). A minimum of 200 cells were scored per treatment. Results shown as mean cellular fluorescence intensity means ± SD, n = 3, $^{***}P$ <0.001 compared to corresponding control (no protein treatment).

5.3.2.2 SOD1 protein aggregates induce fluid uptake in human cultured iPSC-derived motor neurons and primary neuronal cells

One of the consequences of macropinocytosis is the non-selective internalisation of significant amounts of fluid and membrane (Swanson and Watts, 1995), thus fluid uptake into human cultured iPSC-derived motor neurons and primary neurons cells was next investigated (Figure 5.6). To investigate fluid uptake, internalization of fluorescently labeled dextran (a fluid-phase marker) into cells was assessed, as previously used in Chapter 2. In both human

cultured iPSC-derived motor neurons (Figure 5.6A) and primary neuron cells (Figure 5.6B), WT and mutant SOD1 aggregates induced a significantly higher uptake of 10 kDa 647-dextran compared to cells treated in the absence of protein, consistent with the triggering of macropinocytosis.

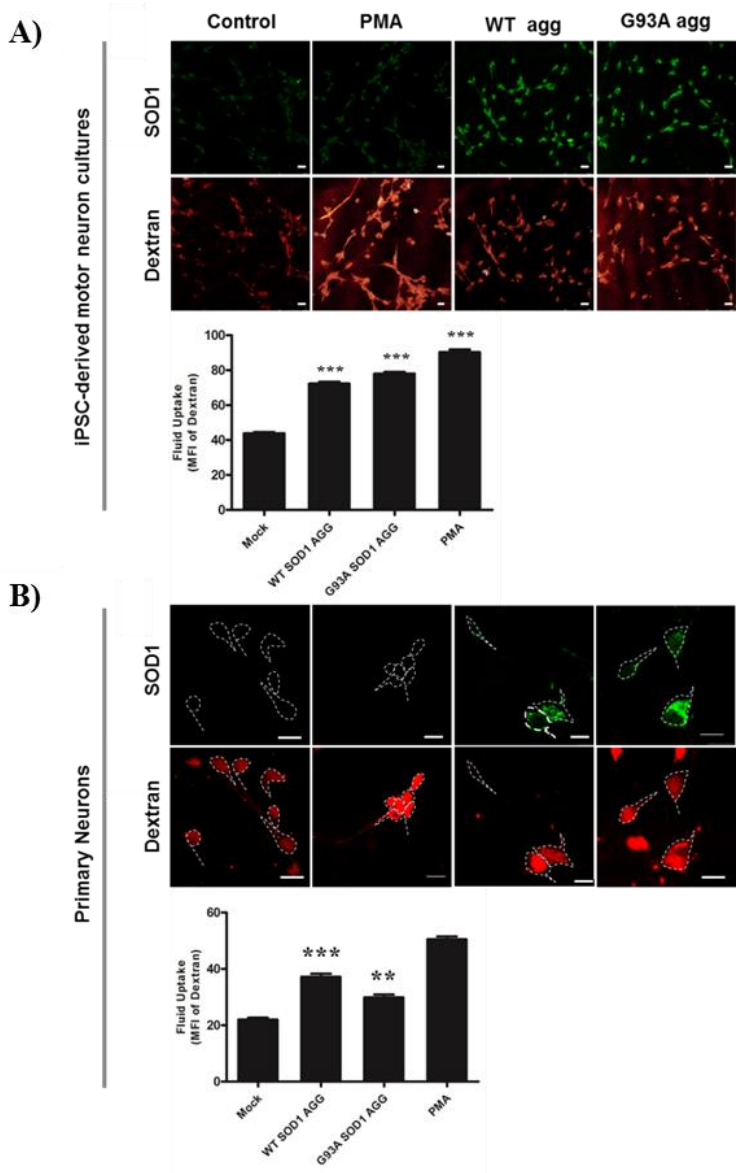

Figure 5.6 SOD1 aggregates trigger fluid phase uptake in iPSC-derived and primary human motor neurons using fluorescently labelled dextran. (A) iPSC-derived and (B) primary human motor neurons were incubated with PBS alone (mock) or 20 µg/ml of aggregated SOD1 for 30 min at 37°C, co-incubated with dextran Alexa-647 for 15 min, fixed with 4% PFA, permeabilised and labelled with Alexa Fluor 488 streptavidin. Slides were analysed by confocal microscopy. Outline of cells are indicated with white dashed lines. Bars represent 10 µm. Results are representative of at least $n = 3$, $^{***}P < 0.001$ or $^{**}P < 0.01$ compared to corresponding mock (no protein treatment);. Mean fluorescence intensities (MFI) per cell of dextran uptake were quantified from confocal images using ImageJ software (Version 1.48) (National Institutes of health, Bethesda, MD).

5.3.3 Activation of membrane ruffling is not restricted to SOD1 aggregates

There is now substantial evidence that SOD1 aggregates can enter into neuronal cells *via* macropinocytosis (Grad et al., 2014; Münch et al., 2011; Sundaramoorthy et al., 2013), with evidence from the study in Chapter 2 demonstrating that this process is not a passive one but that SOD1 aggregates can trigger the activation of membrane ruffling and entry *via* macropinocytosis. The possibility that the triggering of membrane ruffling is a generic cellular response to protein aggregates was then next investigated.

5.3.3.1 Purified Htt_{ex1}46Q, α-synuclein, TDP-43, and α-lactalbumin RCM and amorphous aggregates are heterogeneous in morphology

To determine the morphology of the purified recombinant Htt_{ex1}46Q, TDP-43, α-synuclein and the model proteins RCM induced fibrillar or amorphous α-lactalbumin protein aggregates, negative staining TEM was performed (Figure 5.7). Representative TEM images of endpoint aggregates for Htt_{ex1}46Q (Figure 5.7A), TDP-43 (Figure 5.7B), α-synuclein (Figure 5.7C), and the model protein α-lactalbumin RCM (Figure 5.7D) were found to consist of long fibril structures, similar to those seen in neurodegenerative diseases (reviewed in Brettschneider et al., 2015). The amorphous α-lactalbumin (Figure 5.7E) model protein was observed to have an amorphous structure but clumped together in large aggregates.

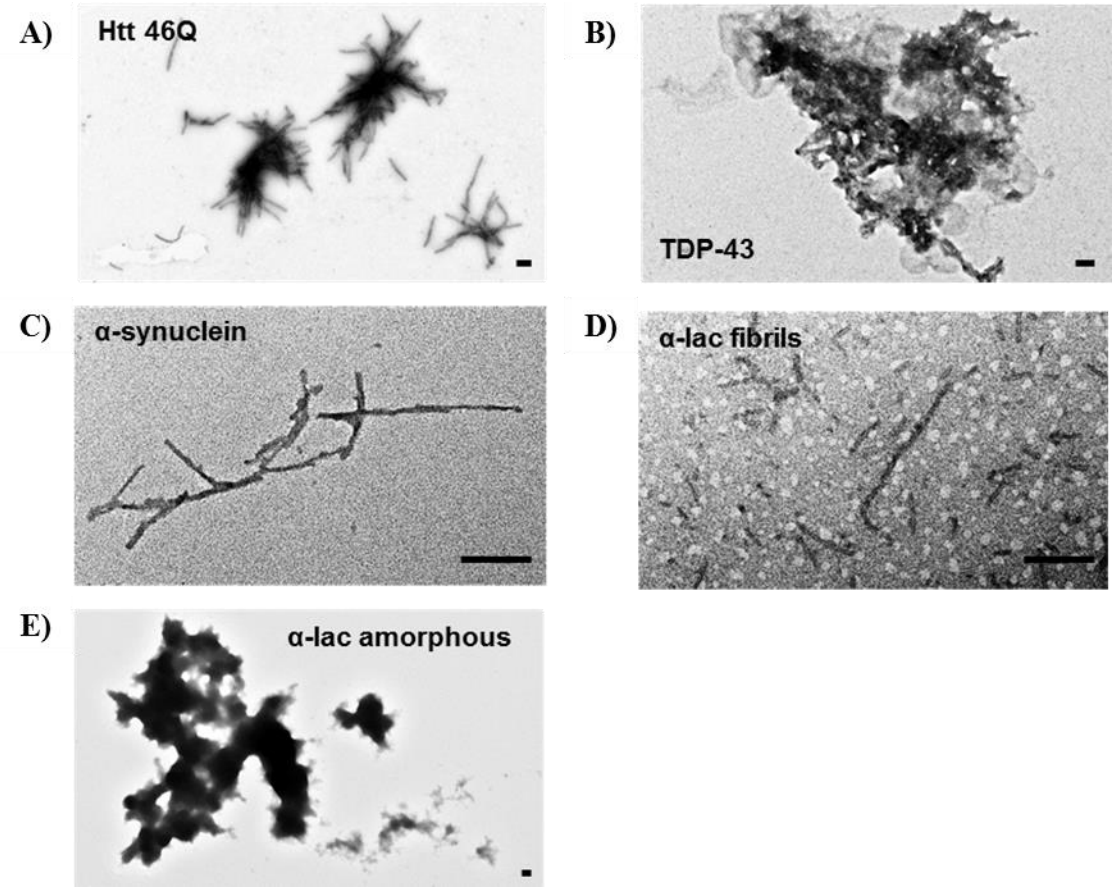

Figure 5.7 Fibrillar and amorphous Morphology of protein aggregates using TEM (A) Purified $Htt_{ex1}46Q$, (B) TDP-43, (C) α-synuclein, , and (D) α-lactalbumin RCM and (E) amorphous proteins (1 mg/ml). Representative TEM image of endpoint aggregates. Protein aggregate (1 mg/ml) samples (2_µl) were loaded onto carbon-coated nickel grids for 1 min at RT and negatively stained using 2% uranyl acetate for 2 min at RT. Bars represent 20nm.

5.3.3.2 Httex146Q, α-synuclein, TDP-43, and α-lactalbumin RCM and amorphous aggregates are detected in motor-neuron like NSC-34 cells

Next, the putative uptake of disease-associated fibrillar aggregates formed by $Htt_{ex1}46Q$ TDP-43, α-synuclein, and also of amorphous and fibrillar aggregates formed from the model protein α-lactalbumin (Kulig and Ecroyd, 2012) into NSC-34 cells was examined by confocal microscopy using Alexa Fluor 488 streptavidin (Figure 5.8). $Htt_{ex1}46Q$ (Figure 5.8A), TDP-43 (Figure 5.8B), α-synuclein (Figure 5.8C), and also both amorphous (Figure 5.8D) and RCM α-lactalbumin (Figure 5.8E) aggregates were observed to be internalised by NSC-34 cells after 2 h incubation.

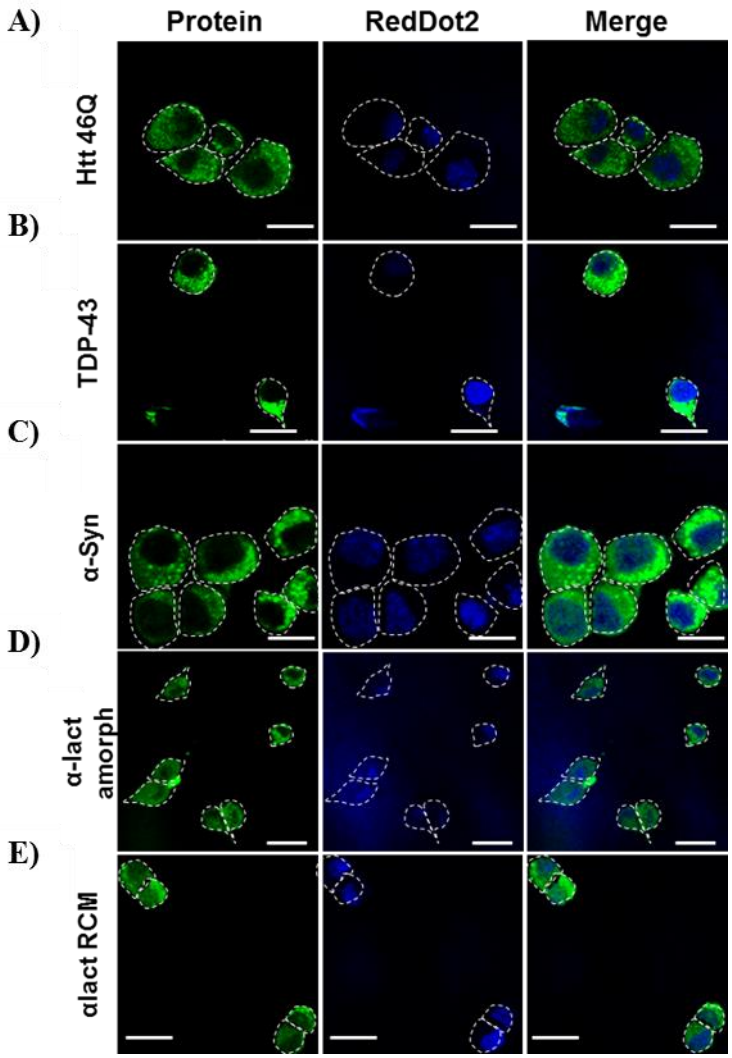

Figure 5.8 $Htt_{ex1}46Q$, α-synuclein, TDP-43, and α-lactalbumin RCM and amorphous aggregate protein aggregates enter into NSC-34. NSC-34 cells treated with 20 µg/ml of (A-E) aggregated proteins (20 µg/ml) for 2 h at 37°C, fixed with 4% PFA, permeabilised and labelled with Alexa Fluor 488 streptavidin. Chamber wells were analysed by confocal microscopy. Outline of cells are indicated with white dashed lines. Bars represent 20 µm. Results are representative of at least *n* = 2.

5.3.3.3 Pharmacological inhibitors of macropinocytosis reduce $Htt_{ex1}46Q$, α-synuclein, TDP-43, and α-lactalbumin RCM and amorphous aggregate uptake in to NSC-34 cells

Uptake of SOD1 aggregates into NSC-34 cells (Chapter 2) and in to human neurons (Figure 5.8) has been shown to be reduced in the presence of small molecule inhibitors of pathways involved in the regulation of macropinocytosis. Given that NSC-34 cells can efficiently take up of a variety of protein aggregates (Figure 5.8), it was next investigated whether small molecule inhibitors of macropinocytosis have an effect on the uptake of $Htt_{ex1}46Q$, TDP-43, α-synuclein, and amorphous and fibrillar α-lactalbumin aggregates (Figure 5.9). NSC-34 cells were firstly incubated with aggregates in the absence or presence of EIPA (an inhibitor of the

Na+/H+ pumps, essential for macropinocytosis) and then mean fluorescence intensity for uptake of protein aggregates uptake were examined by confocal microscopy (Figure 5.9A). Relative aggregate uptake was quantified from these images using ImageJ software (Figure 5.9B). Incubation with EIPA resulted in significant reductions in the uptake of $Htt_{ex1}46Q$ (51 ± 1.6%), TDP-43 (26 ± 1.3 %), α-lactalbumin amorphous (35 ± 1.3 %) and fibrillar (14 ± 1.9 %) aggregates. However, in contrast incubation with EIPA was not observed to inhibit the internalisation of α-synuclein

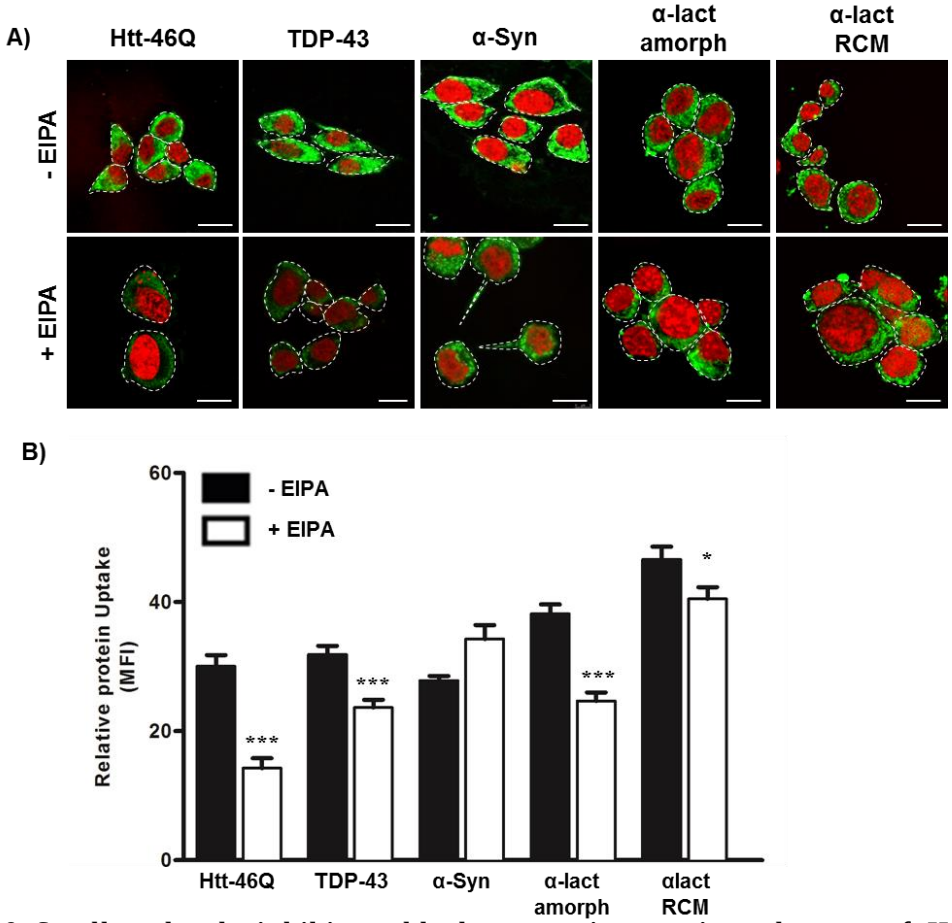

Figure 5.9 Small molecule inhibitors block macropinocytosis and entry of $Htt_{ex1}46Q$, TDP-43, α-lactalbumin RCM and amorphous aggregated proteins. (A) NSC-34 cells treated with 20 µg/ml $Htt_{ex1}46Q$, α-synuclein, TDP-43, α-lactalbumin RCM and amorphous aggregated protein for 30 min at 37°C, in the absence (control) or presence of a pre-incubation step with EIPA (100 µM) a Na+/H+ exchange inhibitor, fixed with 4% PFA, permeabilised and labelled with Alexa Fluor 488 streptavidin. Slides were analysed by confocal microscopy. Outline of cells are indicated with white dashed lines. Bars represent 20 µm. Results are representative of at least $n = 3$ (B) Uptake of proteins under the same conditions were determined by flow cytometry and results shown as mean fluorescence intensity ± SD, $n = 6$, $^{***}P < 0.001$ or $^{*}P < 0.05$ compared to corresponding control.

5.3.3.4 Htt_{ex1}46Q, α-synuclein, TDP-43, and α-lactalbumin fibrillar and amorphous aggregates trigger cell surface ruffling activation of RAC1 and fluid uptake in NSC-34 cells

Given that above data implicates a role for a more general role of macropinocytosis in the uptake of protein aggregates, the association of aggregates with induction of plasma membrane ruffling and/ or blebbing was next examined. To investigate whether there were any perturbations to the cell surface membrane caused by incubation with a variety of protein aggregates, cells were treated with either PMA or protein aggregates for 2 h and then the detailed morphology of cells was examined by FESEM (Figure 5.10). NSC-34 cells incubated with Htt_{ex1}46Q and TDP-43 aggregates displayed large planar lamellipodia-like ruffles. Similarly, α-synuclein induced cell-wide systemic blebbing and ruffles, similar to cells incubated with α-lactalbumin RCM. However, a small amount of membrane perturbations were observed for cells incubated with amorphous α-lactalbumin compared to the cells incubated in the absence of protein.

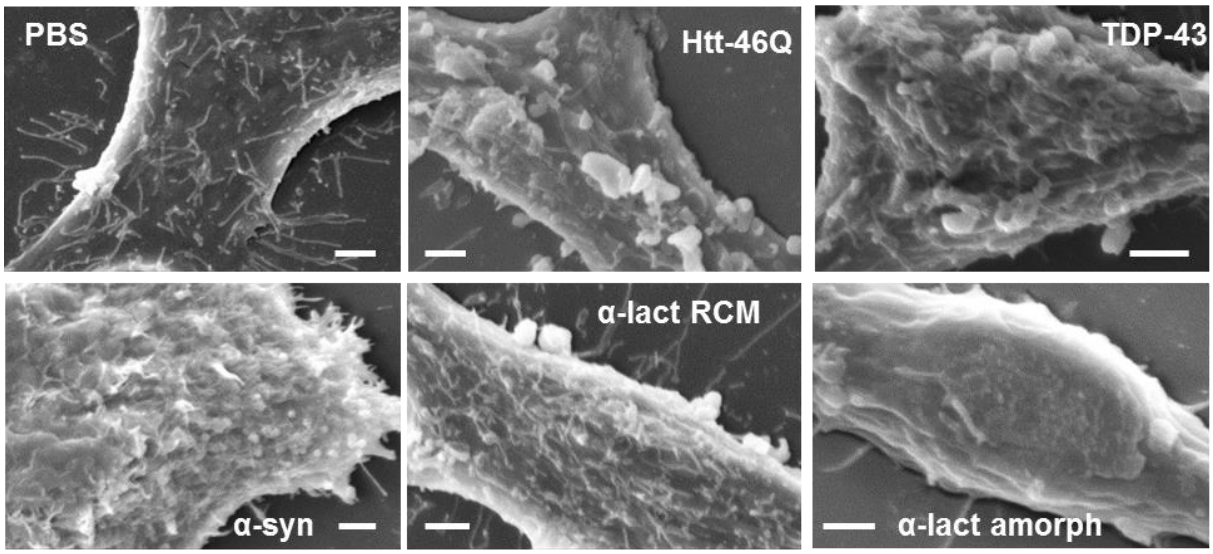

Figure 5.10 Aggregated Htt_{ex1}46Q, α-synuclein, TDP-43, α-lactalbumin RCM and amorphous proteins induce ruffles in the plasma membrane of NSC-34 cells. NSC-34 cells were serum starved for 24 h and were incubated with PBS (control, no protein) or 20 µg/ml of aggregated Htt_{ex1}46Q, α-synuclein, TDP-43, α-lactalbumin RCM and amorphous proteins for 2 h, fixed with 2.5% glutaraldehyde/4% PFA in 0.1 M phosphate buffer for 3 h, postfixed in 2% OsO_4/ water, dehydrated using a gradient of ethanol (30-100%, 30 min per treatment), critical point dried for 2 h and coated with graphite-gold. Increases in membrane perturbations can be observed, such as ruffles and blebs. Slides were analysed by field emission scanning electron microscopy. Bars represent 2 µm. Results are representative of $n = 2$.

Since activation of the Rho GTPase RAC1 is involved in regulating macropinocytosis, the activation of RAC1, *via* cellular interaction with protein aggregates was next assessed. To investigate whether Htt_{ex1}46Q, α-synuclein, and TDP-43 protein aggregates induce the activation of RAC1 upon entry into NSC-34 cells, cells were incubated with these aggregates and RAC1 activation was probed for using a G-LISA based assay (Figure 5.11). Compared to control cells, a significantly increased amount of activated RAC1 was detected in cells incubated with Htt_{ex1}46Q, α-synuclein, and TDP-43 aggregates. However, while the mean level of activated RAC1 was increased when cells were incubated with α-lactalbumin RCM and amorphous aggregates, this increase was not significant.

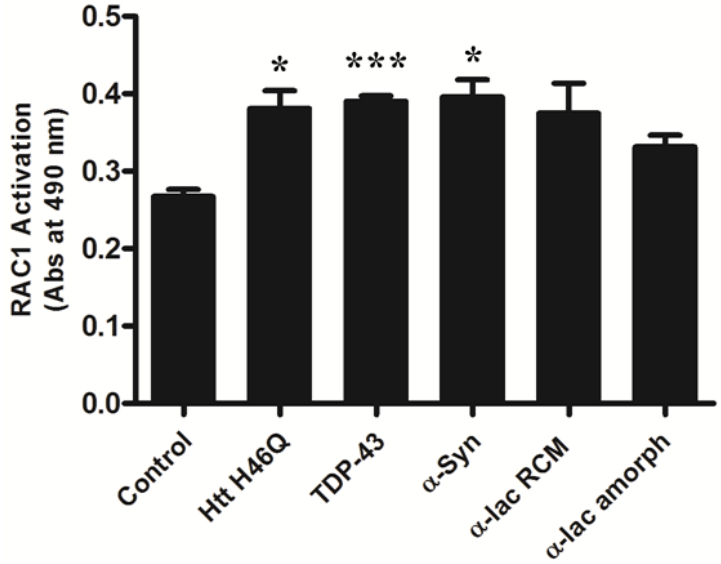

Figure 5.11 RAC1 also has an important role in Htt_{ex1}46Q, TDP-43, α-lactalbumin RCM and amorphous proteins entry into NSC-34 cells. NSC-34 cells were serum starved 24 h, incubated with PBS alone (control) or 20 μg/ml of Htt_{ex1}46Q, α-synuclein, TDP-43, α-lactalbumin RCM and amorphous proteins for 30 min at 37°C and lysed. RAC1 activation was measured using a RAC1 activation G-LISA kit activation assay that probes for RAC1-GDP. Absorbance values of anti- RAC1 HRP at 490 nm were determined by spectrometry and results are shown as mean absorbances (490 nm) ± SD of 6 experiments, $^{***}P < 0.001$ or $^{*}P < 0.05$, compared to corresponding control (mock).

Finally, to investigate whether the interaction of a variety of protein aggregates with cells triggers fluid phase uptake (Figure 5.12), NSC-34 cells were incubated in the presence of both Htt_{ex1}46Q, α-synuclein, α-lactalbumin, and TDP-43 with 10 kDa 647-dextran and assessed by confocal microscopy (Figure 5.12A) and flow cytometry (Figure 5.12B). Incubation with all protein aggregates including the model proteins α-lactalbumin fibrillar

and amorphous aggregates induced significant uptake of fluid (dextran- ALEXA-647), with significantly greater amounts of dextran detected in cells incubated with $Htt_{ex1}46Q$, TDP-43, α-lactalbumin and α-synuclein compared to cells compared to cells treated in the absence of protein aggregates.

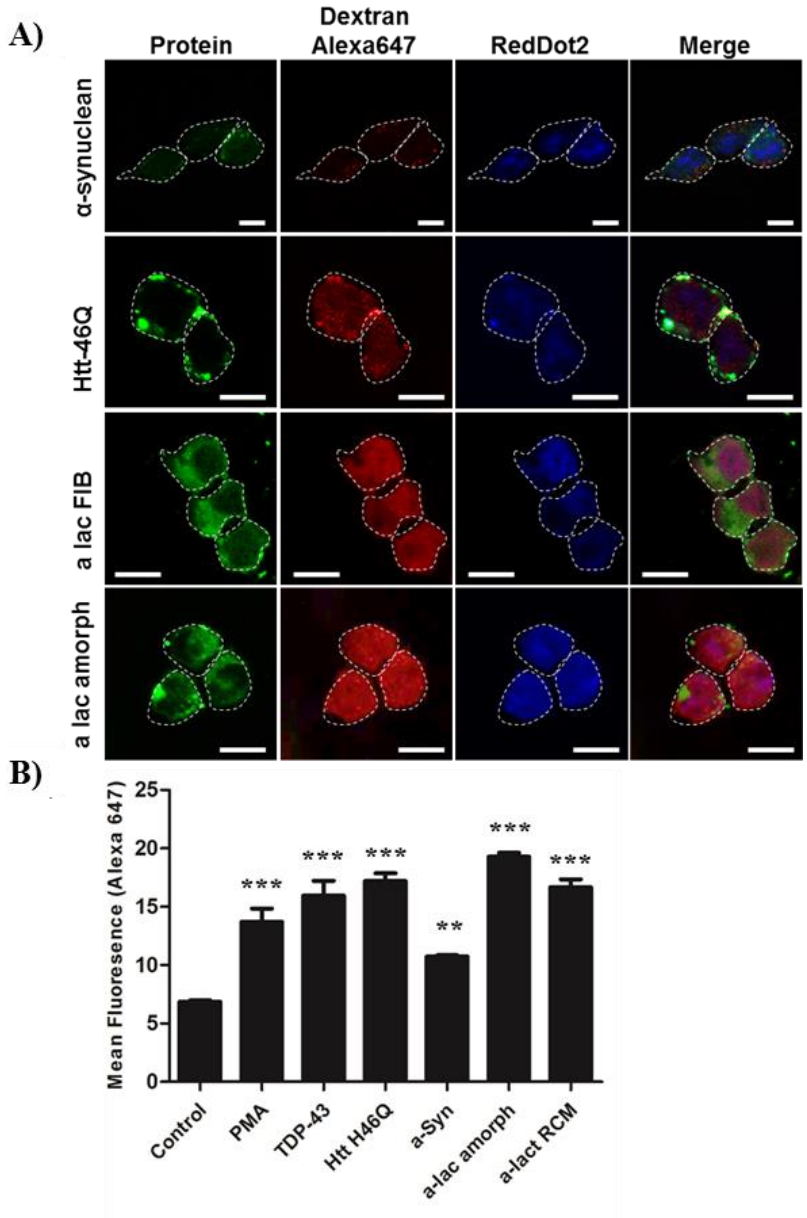

Figure 5.12 $Htt_{ex1}46Q$, α-synuclein, TDP-43, α-lactalbumin RCM and amorphous protein aggregates trigger fluid phase uptake using fluorescently labelled dextran. NSC-34 cells were incubated with PBS alone (mock) or 20 µg/ml of $Htt_{ex1}46Q$, α-synuclein, TDP-43, α-lactalbumin RCM and amorphous proteins for 30 min at 37°C, co-incubated with dextran Alexa-647 for 15 min, fixed with 4% PFA, permeabilised and labelled with Alexa Fluor 488 streptavidin. Slides were analysed by confocal microscopy. Outline of cells are indicated with white dashed lines. Bars represent 10 µm. Results are representative of at least $n = 3$. (B) Cells were firstly gated on forward (FSC) and side (SSC) scatter to exclude dead cells and the mean fluorescence intensities (MFI) of dextran Alexa-647 in NSC-34 cells was determined by flow cytometry. Results shown as means ± SD, $n = 6$; $^{***}P < 0.001$ or $^{**}P < 0.01$ compared to corresponding control.

5.4 Discussion

The current study demonstrates that SOD1 aggregates can be internalised *via* macropinocytosis-like pathways into human primary neurons and more importantly human motor neurons derived from iPSCs. The addition of pharmacological inhibitors of macropinocytosis including EIPA and W56 disrupted the uptake of SOD1 aggregates into these cells. SOD1-mediated activation of macropinocytosis-like pathways in these primary cells induced membrane perturbations in the forms of ruffles and blebs, and subsequent fluid uptake, which are characteristic of macropinocytosis. The current study also confirmed for the first time that other protein aggregates associated with ALS, Huntington's and Parkinson's diseases, including purified TDP-43, $Htt_{ex1}46Q$ and α-synuclein protein aggregates respectively, trigger the activation of the Rho GTPase RAC1. This results in the formation of membrane ruffles on the cell surface and fluid phase uptake in NSC-34 cells, facilitating the entry of large fibrillary or amorphous protein aggregates. Together, the current study indicates that SOD1 aggregates can stimulate macropinocytosis in human neurons and suggests a role for macropinocytosis in the uptake of a protein aggregates more generally.

Previous work had shown that exogenously applied misfolded mutant SOD1 could be taken up by cell lines and material found in conditioned media was shown to be internalised into human WT SOD1-expressing murine primary spinal cord cultures, derived from embryonic spinal cord of transgenic mice (Grad et al., 2014). In the work presented here, the ability of human neurons to take up SOD1 aggregates was observed for the first time, supporting previous observations which suggest that extracellular misfolded or aggregated SOD1 may have an active role in the spread of pathology among cells *in vitro* and motor neurons *in vivo* (Ayers et al., 2014). Thus, SOD1 aggregates may contribute to disease progression *via* interactions with both the cell surface and internalisation into cells, which may occur in both fALS and sALS (Grad et al., 2014; Münch et al., 2011; Sundaramoorthy et al., 2013).

Furthermore, the uptake of purified TDP-43, Huntington and α-synuclein aggregates into NSC-34 motor neuron cells was observed similar to uptake of SOD1 in Chapter 2. This is consistent with cellular uptake of TDP-43 into microfluidic neuronal cultures as reported by Feiler et al (Feiler et al., 2015). In the context of Parkinson's disease, cell culture studies have shown that extracellular α-synuclein in various forms (fibrils, oligomers, and monomers) can be internalised by cultured neuronal cells (Lee et al., 2008). Furthermore, α-synuclein is known to directly interact with lipids and membranes to facilitate its entry into neuronal cells (Lee et al., 2008). Similarly, in a Huntington's disease model, large polyglutamine aggregates were shown to internalise into cultured cells (Yang et al., 2002). However, the precise mechanisms for entry of these proteins into cells remain to be determined.

A role for macropinocytosis in the uptake of extracellular native and aggregated WT and mutant SOD1 into neuronal cells has been previously suggested (Grad et al., 2014; Münch et al., 2011; Sundaramoorthy et al., 2013). In these studies, cell lines were treated by the addition of small molecules that inhibit actin rearrangement, or Na^+/H^+ exchangers, Pak-1, PI3K, and PKC was reported to impair the uptake of SOD1 aggregates (Grad et al., 2014; Münch et al., 2011; Sundaramoorthy et al., 2013) consistent with macropinocytosis. In the current study, EIPA (inhibitor of Na+/H+ exchanger) which has previously been used as the main diagnostic test to identify macropinocytosis from other forms of endocytosis (West et al., 1989) and the RAC1 inhibitor W56 were used to confirm the involvement of macropinocytosis-like pathways in the uptake of SOD1 aggregates into human neurons. EIPA and RAC1 W56 inhibited the uptake of SOD1 aggregates into human iPSC derived motor neurons and primary neurons, similar to the study in Chapter 2 and previous observations (Grad et al., 2014; Münch et al., 2011; Sundaramoorthy et al., 2013). Similarly, the level of TDP-43 and $Htt_{ex1}46Q$ uptake into NSC-34 cells were significantly suppressed by EIPA. Other fibrils such as Tau associated with Alzheimer's disease have also been shown to enter

cells *via* macropinocytosis (Holmes et al., 2013). Taken together, these data suggest that SOD1, TDP-43 and Httex146Q and Tau are taken up by a similar mechanism, consistent with a generic mechanism of protein aggregate uptake. However, in the current study while α-synuclein aggregates triggered ruffling and fluid uptake, characteristic of macropinocytosis, the uptake of α-synuclein was not significantly affected by EIPA. This might suggest the involvement of distinct pathways, or it could suggest a higher concentration of EIPA is needed in this model, as α-synuclein aggregates are small in size and could potentially be interacting and internalising in a different manner. However, future investigations into the role of α-synuclein, and indeed Htt_{ex1}46Q, α-syn and TDP-43- aggregates in the induction of macropinocytosis is clearly warranted.

Triggering the activation of macropinocytosis leads to the entry of large amounts of solute, and because of the large size of macropinosomes macromolecules or particles too large for other forms of endocytosis are able to enter the cell (Swanson and Watts, 1995). Activation of macropinocytosis has been reported to induce a number of downstream signaling events including the activation of the Rho GTPase, RAC1 (Ridley et al., 1992), which contributes to the modulation of actin-mediated membrane ruffle formation in the form of lamellipodia, circular-shaped membrane extensions (ruffles) and large plasma membrane extrusions (blebs), macropinosome closure forming large intracellular vacuoles (0.5–10 μM) and membrane trafficking (Lanzetti et al., 2004; Mercer and Helenius, 2012). In the current study, SOD1, TDP-43, Htt_{ex1}46Q and α-synuclein aggregate-mediated activation of macropinocytosis thus internalisation into human primary neurons or NSC-34 cells respectively, was demonstrated. Incubation with SOD1, TDP-43, Htt_{ex1}46Q and α-synuclein aggregates induced membrane protrusions, including macropinocytic ruffling and systemic blebbing, consistent with the formation macropinosomes at the plasma membrane. Thus, it is

likely that motor neurons internalise extracellular aggregates directly *via* dynamic membrane rearrangements that eventually form large endocytic macropinosomes.

Activated RAC1 has previously been identified as an important and central player in triggering membrane ruffles and blebbing (Mercer and Helenius, 2009) associated with virus entry into cells, and has been found to do so by activating downstream effectors of actin polymerisation (Sanchez et al., 2012). While the precise role of PKC in virus entry is still unclear, its activation with PMA (as used in this current study and in Chapter 2) can induce ruffling and fluid uptake in the absence of ligands that bind the cell surface (Swanson, 1989). The activation of RAC1 by TDP-43, Htt_{ex1}46Q and α-synuclein aggregates and subsequent membrane ruffling was supported by results presented in the current study. Although SOD1-mediated activation of RAC1 in human iPSC derived motor neurons and primary neurons was not directly investigated in the current study, inhibition of RAC1 supressed the uptake of SOD1 aggregates into these cells, thus suggesting a role for RAC1 activation in aggregate entry. Of note, the study in chapter 1 confirmed that activation of RAC1 is upstream of membrane ruffling, thus consistent with triggering the increased perturbation in the plasma membrane of human iPSC derived motor neurons and primary neurons upon incubation with SOD1 aggregates.

Macropinocytosis is a form of fluid phase endocytosis, characterised by internalisation of extracellular fluids and solutes at whatever concentrations they are found in the extracellular medium, rather than concentrating ligands at the cell surface (Swanson and Watts, 1995). The data presented here shows that the activation of macropinocytosis mediated by SOD1 aggregates in human iPSC derived motor neurons and primary neurons, and TDP-43, Htt_{ex1}46Q and α-syn in NSC-34 cells induced fluid uptake (dextran-Alexa 647 to quantify fluid-phase endocytosis), coinciding with the formation of membrane ruffling. Similarly, previous work has demonstrated that incubation with tau fibrils increased dextran uptake,

consistent with activation of macropinocytosis (Holmes et al., 2013). The model proteins α-lactalbumin RCM and amorphous proteins were also able to induce membrane perturbations that facilitate their cellular uptake in a similar manner to that of SOD1, suggesting that a broad range of aggregated proteins, both amorphous and amyloid-like, are able to induce membrane perturbations that facilitate their cellular uptake.

In addition to TDP-43, Htt_{ex1}46Q and α-synuclein aggregate, various viruses, such as the vaccinia virus, adenovirus 3, herpes simplex virus 1 and HIV, utilize macropinocytosis to gain entry to cells. This phenomenon is likely to be due to the fact that macropinosomes are not restricted in size, enabling even large virions to be internalised, and that many cell types, not just professional phagocytes (such as macrophages), have the ability to activate the macropinocytosis pathways (Swanson and Watts, 1995). Indeed, macropinocytosis can be activated in neurons by interactions with large viral particles (Kalia et al., 2013). Of note, amyloid fibrils including those associated with Alzheimer's disease (Aβ1-40) and Parkinson's disease (α-synuclein) and can enhance human immunodeficiency virus type 1 infection (Munch et al., 2007; Wojtowicz et al., 2002). Thus, it is interesting to speculate that this behaviour could be due to the potent ability of such aggregates to stimulate macropinocytosis and facilitate increased viral uptake. Recently, accumulating evidence suggests that the transcellular propagation of a wide range of disease-associated proteins, including SOD1, TDP-43, huntingtin with poly-Q repeats, α-synuclein, Aβ, tau mediate the progression of disease in a prion-like manner (reviewed in Ayers et al., 2016). Likewise, cellular uptake of the pathological prion protein has been reported to occur *via* by stimulated lipid-raft mediated macropinocytosis (Wadia et al., 2008)

In conclusion, this study represents the first report of SOD1 mediated activation of macropinocytosis in human neurons, consistent with the notion that protein aggregates could be an active part of ALS disease progression, possibly through secondary nucleation (Buell et

al., 2014), or another prion-like aggregate propagation process. In addition, the current study highlights the ability of neurons to undergo stimulated macropinocytosis. Furthermore, the current study suggests that aggregate induction of macropinocytosis may be a more generic principle and not restricted to one type of aggregate (Holmes et al., 2013). While further investigations are required to determine the exact mechanisms of TDP-43, huntingtin and α-synuclein uptake *in vivo*, additional mechanisms may also operate to facilitate their entry. Overall, the data is consistent with protein aggregates exploiting macropinocytosis as a novel route for entry into cells. It may therefore prove important to elucidate intracellular pathways that result in macropinosome formation and closure to generate effective therapeutic targets for halting the propagation of aggregation in these disorders.

Chapter 6

CONCLUSIONS AND SIGNIFICANCE

6.1 Overview

Amyotrophic lateral sclerosis (ALS) is a devastating neuromuscular degenerative disease that currently has no effective treatments or therapeutics. ALS is characterised by a focal onset of motor neuron loss, followed by contiguous outward spreading of pathology throughout the nervous system, resulting in paralysis and death within a few years after diagnosis. The aetiology of ALS is poorly defined and the complexity of the pathogenic mechanisms responsible for disease initiation and progression are not completely understood. However, multiple factors and cellular pathways including; protein aggregation and seeding of endogenous native proteins, aberrant secretion and the subsequent internalisation of aggregated proteins by neighbouring cells are implicated in disease pathogenesis. Both copper-zinc superoxide dismutase 1 (SOD1) and the 43-kDa trans-activating response region DNA-binding protein (TDP-43) have been implicated in these disease mechanisms, with recent evidence demonstrating a role for macropinocytosis in ALS disease progression. Thus, this thesis aimed to examine the prion-like activity of SOD1 and TDP-43, and determine the role of macropinocytosis in the propagation of ALS pathology, in cell lines and human neurons. From this, potential therapeutic targets may be identified and strategies developed.

6.2 Conclusions and Significance

The work presented in this thesis suggests that aggregates of SOD1 can stimulate macropinocytosis and result in the subsequent prion-like propagation of misfolding, both findings that may help explain patterns of ALS disease progression. Misfolded SOD1 is capable of transferring between neuronal cells, through release from cells *via* active and passive mechanisms and uptake *via* macropinocytosis–like pathways. In Chapter 2, the uptake of SOD1 aggregates by the murine motor-neuron like cell line (NSC-34) was confirmed. Furthermore, Chapter 2 demonstrated that inhibiting key regulators of

macropinocytosis in NSC-34 motor neurons, using pharmacological inhibitors significantly reduced the uptake of SOD1 aggregates into NSC-34 cells. This is consistent with previous evidence in the same and similar cell lines (N2a neuroblastoma cells) using misfolded SOD1. In these previous studies, similar pharmacological inhibitors of macropinocytosis resulted in a significant reduction in SOD1 internalisation (Grad et al., 2014; Münch et al., 2011; Sundaramoorthy et al., 2013) and subsequent induction of endoplasmic reticulum (ER) stress in neuronal cells (Sundaramoorthy et al., 2013). Although ER stress was not directly investigated in the current study, expression of misfolded WT and mutant SOD1 have been observed to induce ER stress, and when prolonged can promote and pro-apoptotic pathways in motor neurons reminiscent of ALS pathology (Nishitoh et al., 2008; Sundaramoorthy et al., 2013).

Furthermore, although these studies suggest a role for stimulated macropinocytosis in SOD1 uptake, the exact mechanisms that underlie internalisation *via* macropinocytosis are unknown. It is therefore possible that misfolded SOD1 may trigger macropinocytosis through a direct interaction with receptors on the cell surface. Therefore, further analysis into the specific pathways leading up to the activation of macropinocytosis will assist in identifying how SOD1 utilises macropinocytosis for entry into cells. Incubation of NSC-34 cells with SOD1 aggregates induced the activation of the signalling molecule RAC1 which in turn resulted in the induction of membrane perturbations in the form of ruffles and blebs in the plasma membrane and subsequent fluid-phase uptake into NSC-34 cells was also observed. Given that there is no evidence of activated macropinocytosis in the absence of aggregates, it is therefore reasonable to conclude that aggregated SOD1 triggered these signaling pathways to activate a macropinocytosis-like pathway. The above represents new evidence for the SOD1 aggregate mediated activation of macropinocytosis in ALS, however viruses have been

shown in prior studies to activate these same macropinocytosis-like pathways to facilitate cellular infection (Sanchez et al., 2012).

The murine motor neuron cell line NSC-34 is a hybrid cell line originally developed by fusing mouse derived neuron-enriched primary embryonic spinal cord cells and N18TG2 neuroblastoma cells (Cashman et al., 1992). Although the NSC-34 cell model may provide information that may not be completely applicable to human ALS disease, it is likely that misfolded toxic SOD1 proteins may also activate macropinocytosis in a similar manner *in vivo* to facilitate their entry into motor neurons. For decades, transgenic rodent models of ALS have been widely available for use and have provided important information on a range of areas including pathogenesis and disease progression in ALS disease. However, given that there are differences between humans and rodents, particularly genetically engineered rodents which develop ALS-like disease phenotypes, other physiologically relevant models should be used to strengthen the validity of the data obtained. The development of reprogramming biology and humanised models of ALS have been established in recent years to allow for complementary, and arguably more relevant, models. The generation of patient specific induced pluripotent stem cells (iPSCs) derived from reprogrammed somatic cells from a range familial and sporadic ALS patients now represent an effective model disease model of ALS (Hedges et al., 2016; Lee and Huang, 2015). A range of disease-relevant cell types including neurons and motor neurons can be differentiated from human induced pluripotent stem cells and used to study pathogenic mechanisms and elucidate specific drug targets.

Humanised models of ALS including iPSC derived motor neurons and human primary neurons were therefore used to investigate the role of SOD1 in triggering macropinocytosis (Chapter 5). In Chapter 5, internalisation of exogenously added WT and mutant SOD1 aggregates were also shown to be reduced in the presence of pharmacological inhibitors that interfere with regulators of the macropinocytosis pathway and signaling molecules. In

addition, SOD1 aggregates induced membrane ruffling and blebbing in the plasma membrane and subsequent fluid uptake into human neurons coinciding with the activation of macropinocytosis. Although the activation of the signalling molecule RAC1 was not investigated, inhibition of RAC1 reduced the uptake of SOD1 aggregates consistent with a role for RAC1 activation in this process. Although these human models provide relevant insight into the mechanisms of exogenous SOD1 aggregate uptake, future studies could focus on investigating the role of macropinocytosis in SOD1 internalisation in animal models, including zebra fish which provide many advantages such as they are transparent and therefore can visualise fluorescence in real time and are easy to handle and house.

Given the consistent structure and large size of most protein aggregates, it is likely that similar mechanisms are used by neurons to engulf such large aggregates. Intuitively, the large size of the protein aggregates argues against neuronal entry by most forms of endocytosis given their size limitations. Therefore, the process of macropinocytosis could potentially explain the uptake of such large structures. Thus, it reasonable to speculate that a wide range of proteins associated with other common neurodegenerative diseases including TDP-43, α-synuclein and fibrillar polyQ aggregates (e.g. Huntingtin protein) in ALS, Parkinson's and Huntington's disease respectively, may also trigger the activation of macropinocytosis in neuronal cells. In Chapter 5, exogenously applied TDP-43, α-synuclein and Huntingtin (Htt-46Q) protein aggregates were shown to be internalised by murine NSC-34 motor neurons *via* activated macropinocytosis, as similarly observed for SOD1 aggregates. This is consistent with previous reports that implicate fluid-phase endocytosis in the cellular uptake of α-synuclein and Tau (Alzheimer's Disease) aggregates (Holmes et al., 2013; Lee et al., 2008).

The panel of pharmacological inhibitors of macropinocytosis used in this study was sufficient for confirming the involvement of macropinocytosis, specifically the use of amiloride (EIPA) which is reported to specifically (in the context of other endocytosis pathways) inhibit

macropinocytosis (West et al., 1989) (Chapter 2 and Chapter 5). Given the effectiveness of EIPA, it may be worth investigating the effects of this drug in ALS mice or other animal models. However, it may also be worth utilising other available inhibitors specific to macropinocytosis or possibly developing new drugs for future experiments, to identify select processes that may be directly involved in the uptake of aggregates into neuronal cells among proteinopathies. However, macropinocytosis is important in a range of physiological processes, including its contribution to antigen presentation by the immune system (Kerr and Teasdale, 2009). Therefore a side effect of inhibiting macropinocytosis could be compromised immune function.

In addition, given that this study presents for the first time, evidence for the activation of macropinocytosis mediated by aggregates of SOD1, TDP-43, α-synuclein and Huntingtin proteins, it will be interesting to determine whether these proteins interact with a specific receptor upon cell contact and whether this receptor is the same among proteinopathies. Although there is no evidence in the context of protein aggregate activated macropinocytosis, previous work would suggest that receptor tyrosine kinases are involved in activation of macropinocytosis (Kerr and Teasdale, 2009). Activation of receptor tyrosine kinases causes an increase in actin polymerisation at the cell surface, resulting in an elevation in actin-mediated ruffling and therefore an increase in macropinosome formation, which is the mechanism distinguishing it from other endocytic pathways (Kerr and Teasdale, 2009). This cell surface receptor triggering activation of macropinocytosis may therefore represent a therapeutic target. Recent work suggests heparan sulfate proteoglycans are involved in the entry of tau aggregates, but how this relates to activation of macropinocytosis and to entry of other neurodegenerative disease associated aggregates is unclear (Holmes et al., 2013). In addition to this, inhibition of RAC1 activity inhibits ruffle formation irrespective of receptor tyrosine kinase signaling (Lanzetti et al., 2004). These are two examples of pathways that

could potentially be exploited to slow or stop the progression of toxic protein aggregates that enter cells *via* macropinocytosis. Furthermore, since macropinocytosis is incompletely understood, it is possible that different types of macropinocytosis pathways may exist, and therefore it will be interesting to investigate whether these proteins use the same or different pathways and how they induce relevant responses in varying neuronal cells.

The ability of the SOD1 aggregates to escape membrane bound compartments and enter into the cytosol is consistent with prion-like activity. By entering through macropinosomes, SOD1 aggregates can escape delivery into the endosomal compartments potentially due to the 'leaky' nature of macropinosomes, which is attributed to their lack of physical structure (Conner and Schmid, 2003). Although the precise mechanism by which these SOD1 aggregates escape macropinosomes and the relationship between escape and induced pathology is currently unknown. Given this, it may be worth investigating how SOD1 aggregates gain access to the cytosol and whether these aggregates interact with endogenous proteins using real-time imaging techniques including Fluorescence Resonance Energy Transfer (FRET) Microscopy which can be used to investigate molecular interactions between SOD1 aggregates and endogenous proteins in real-time.

The release of SOD1 into conditioned media was observed from cultured NSC-34 cells transiently expressing SOD1 proteins, coinciding with cell death (Chapter 3). However, how the protein aggregates relate to toxicity is currently unknown and it will therefore be interesting to determine whether misfolded and aggregated SOD1 proteins can directly induce cell death or whether other factors are operating simultaneously. These factors include deficient protein quality control, aberrant RNA metabolism, oxidative stress, endoplasmic reticulum stress, glutamate excitotoxicity, mitochondrial dysfunction, fragmentation of the Golgi apparatus, axonal transport defects and neuroinflammation. Furthermore, it is unknown whether the secreted SOD1 proteins were mediated by cell death or by active secretion

mechanisms. It is possible that both active and passive mechanisms of SOD1 secretion may have occurred, *via* cell death and exosomes respectively, as previously reported (Grad et al., 2014). Incubation of naïve neuronal cells with these conditioned media containing extracellular WT and mutant SOD1 was shown to be internalised by murine NSC-34 motor neurons. Toxicity and apoptotic cell death have been similarly observed in NSC-34 cells, which have taken up extracellular misfolded and aggregated WT and mutant SOD1 protein (Sundaramoorthy et al., 2013).

The prion-like propagation of a range protein aggregates mentioned above associated with neurodegenerative diseases is a hypothesis gaining much attention. Prior studies suggests that injection of brain/spinal cord extracts from symptomatic transgenic mice expressing human SOD1, Tau, or α-synuclein can seed pathology in the sites of injection and spread to other regions of the nervous system (Ayers et al., 2014; Clavaguera et al., 2009; Mougenot et al., 2012). Moreover, cell culture experiments also show that insoluble material from brain tissue can seed aggregation of neuropathological TDP-43, whose cytoplasmic accumulation is associated with ALS (Furukawa et al., 2011). However, only until very recently has ALS been implicated in the prion-like paradigm.

Cell-to-cell transfer of SOD1 aggregates between murine NSC-34 cells was observed here *in vivo* (Chapter 3). In addition, the ability of WT and mutant SOD1 as well as TDP-43 to induce the misfolding of native soluble proteins was quantified using a novel technique for measuring inclusions; flow cytometric characterisation of inclusions and trafficking (FloIT) (Chapter 3 and 4). Specifically, FloIT can be used to rapidly quantify cytosolic protein inclusions, including small inclusions and can be used to investigate the co-aggregation of different proteins into inclusions. Our data therefore, demonstrates the seeding of aggregation in a prion-like manner. Consistent with this, recent work provides striking evidence that this may indeed drive disease progression as focal injection of spinal cord homogenates from

symptomatic G93A SOD1 triggers progressive motor neuron disease in mice expressing G85R SOD1-YFP below the threshold for disease (Ayers et al., 2014). Furthermore, fibrils of TDP-43 can induce templated aggregation of TDP-43 in cells expressing WT TDP-43 or TDP-43 lacking nuclear localization signal (Shimonaka et al., 2016).

In vivo, aggregates of SOD1 were shown to induce TDP-43 mislocalisation NSC-34 cells and rapid fragmentation consistent with TDP-43 pathology observed in sporadic disease. Although the exact mechanism for this observation was not determined, it is likely that the proteotoxic stress induced by aggregate uptake was sufficient to trigger the mislocalisation of TDP-43. To the best of our knowledge, SOD1 induced TDP-43 pathology has not yet been reported in humans, and the mislocalisation of TDP-43 in SOD1 mouse models is contradictory (Shan et al., 2009; Turner et al., 2008) and therefore future investigations into the mechanisms and role of SOD1 aggregates in the formation of pathological TDP-43 are therefore warranted. This, however, provides a potential mechanistic link between sporadic and familial ALS cases. Interestingly, TDP-43 aggregates are present in other neurodegenerative diseases such as Huntington's and Alzheimer's disease and may reflect the proteotoxic stress in these diseases.

The use of WT and mutant forms of SOD1 as well as other pathological proteins including TDP-43 has been largely informative in the current study, given that these two proteins have been largely implicated in ALS. However, the use of one mutant form of the SOD1 protein ($SOD1^{G93A}$) and TDP-43 ($TDP\text{-}43^{G127X}$) may present a limitation of the study. Although the G93A mutation is one of the more common and well characterised mutations used widely as a model for familial ALS, future work should focus on a wider range of SOD1 mutations and possibly more mutations in TDP-43 protein.

6.3 Final remarks

Overall, this thesis demonstrated that misfolded SOD1 and other protein aggregates associated with other common neurodegenerative disease including TDP-43, α-synuclein and Huntingtin aggregates are capable of entering into NSC-34 motor neurons and that macropinocytosis plays a role in allowing the passage of protein aggregates into naïve cells. The SOD1-mediated activation of macropinocytosis on these cells induced actin dependant ruffling and blebbing in the plasma membrane triggered active RAC1 which lead to the internalisation of the aggregates. Once internalised into macropinosomes, the aggregates were capable of escaping into the cytosol, where the seeding of aggregation occurred, as detected using FloIT. Furthermore, the release of SOD1 aggregates from neuronal cells *via* passive and/or active mechanisms including cell death or potentially exosomes were observed and this may represent an early event in ALS disease. These extracellular (released) aggregates were able to internalise into other neighbouring motor neurons that may be more susceptible to cell damage and/or death, propagating cellular stress and aggregation from cell to cell, seeding aggregation consistent with previous evidence (Figure 6.1) (Grad et al., 2014; Münch et al., 2011; Sundaramoorthy et al., 2013).

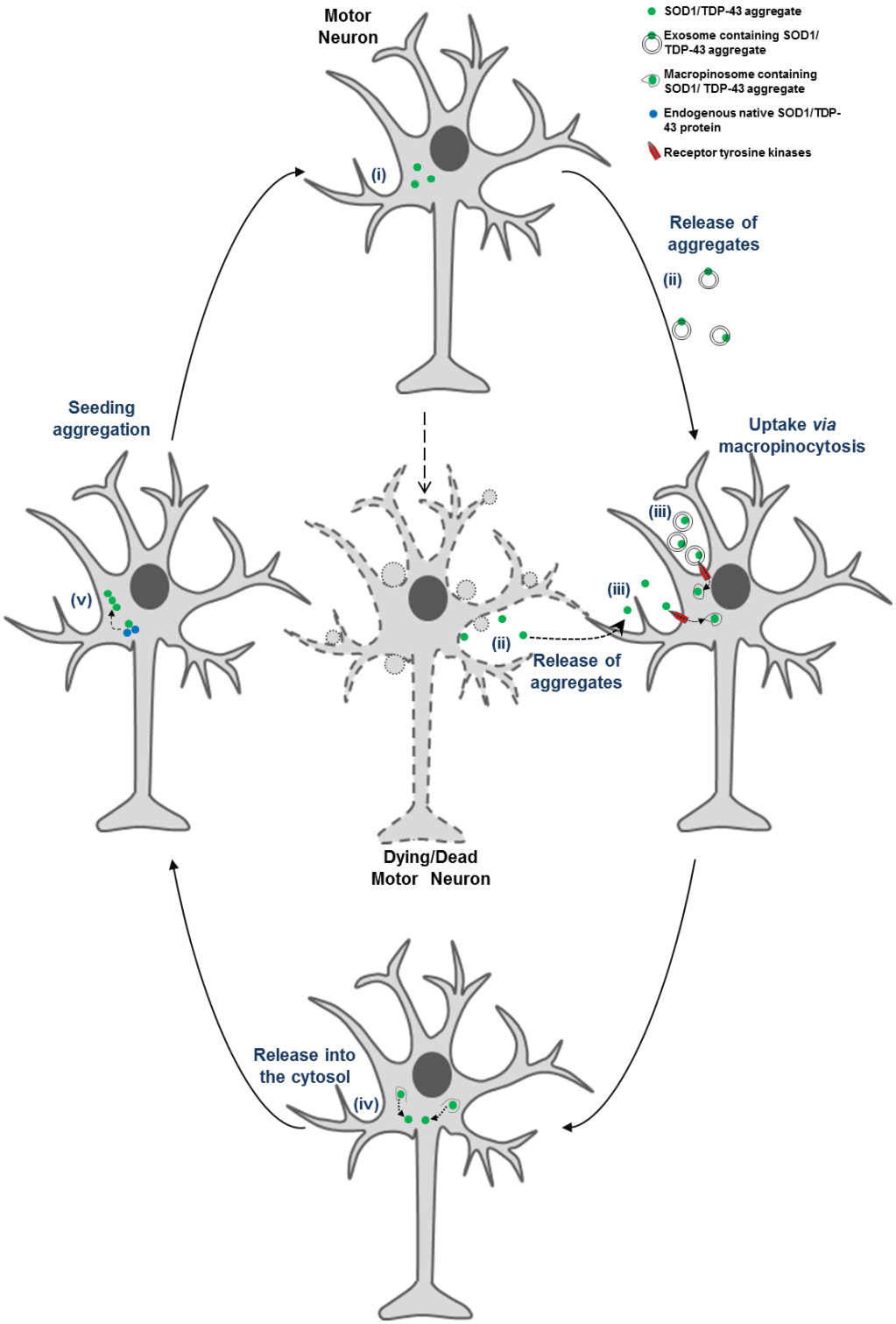

Figure 6.1 Summary of important findings in this study and how they may explain the role of macropinocytosis and SOD1 and TDP-43 protein aggregates in the pathogenic disease cycle of amyotrophic lateral sclerosis. (i) In ALS, SOD1 or TDP-43 may form spontaneous aggregates under non-physiological conditions or contain newly formed aggregates from seeded aggregation reaction in motor neurons. (ii) These aggregates can be released from motor neurons either *via* cell death (passive) or *via* exosomes (active) mechanisms. (iii) Once released into the extracellular environment, these can internalise into neuronal cells *via* the activation of macropinocytosis, and enter through newly formed macropinosomes, a process exploited by viruses. (iv) These aggregates may then escape these membrane bound vesicles and enter into the cytosol (v) to potentially seed the aggregation of endogenous soluble proteins.

Understanding neuron specific macropinocytosis mechanisms will be vital in identifying a target to slow disease progression. In particular, the intracellular pathways that result in activation of macropinocytosis, the formation and closure of macropinosomes, and importantly potential disintegration of macropinosomes must be examined. Lastly, while the ability of cellular uptake of misfolded SOD1 to induce TDP-43 pathology may be due to cellular stress rather than a specific result of SOD1 misfolding, this notion further supports the complex nature of ALS disease. However further study is required to decipher the mechanisms involved in these interactions, and potentially identify other proteins or processes that may be involved.

Given the prion-like properties of SOD1 and TDP-43 aggregates, an attractive therapeutic target would be to block the cell-to-cell propagation. One way of doing this is to target the aggregate entry mechanism. In an analogous situation, mechanisms underpinning Ebola virus entry *via* macropinocytosis are being scrutinized, with promising compounds targeting endocytosis and escape of viral particles from endosomes proving successful in mice (Sakurai et al., 2015). Macropinocytosis may be a viable target given that other cell types such as microglia that clear protein aggregates appear to be *via* different pathways (Roberts et al., 2013). It may be possible then to redirect aggregates from entering neurons by supressing macropinocytosis in pathological conditions while maintaining receptor mediated phagocytic pathways utilized by microglia to engulf extracellular protein aggregates.

Overall, the work presented in this thesis presents data that is consistent with the notion that protein aggregates could be an active part of ALS disease progression, possibly through secondary nucleation (Buell et al., 2014), or another prion-like aggregate propagation process. It presents novel data that now implicates the activation of macropinocytosis, a process used by viruses during infection. Therefore, a better understanding of the

pathological mechanisms involved and identifying targets may lead to halting the passage of the toxic aggregates in a strategy analogous to drugs blocking viral entry.

REFERENCES

Abdolvahabi A, Shi Y, Chuprin A, Rasouli S and Shaw BF (2016) Stochastic Formation of Fibrillar and Amorphous Superoxide Dismutase Oligomers Linked to Amyotrophic Lateral Sclerosis. *ACS chemical neuroscience*.

Aggarwal A and Nicholson G (2002) Detection of preclinical motor neurone loss in SOD1 mutation carriers using motor unit number estimation. *Journal of neurology, neurosurgery, and psychiatry* **73**:199-201.

Aguzzi A and Calella AM (2009) Prions: protein aggregation and infectious diseases. *Annual Review of Physiology* **89**:1105-1152.

Al-Chalabi A, Andersen PM, Chioza B, Shaw C, Sham PC, Robberecht W, Matthijs G, Camu W, Marklund SL, Forsgren L, Rouleau G, Laing NG, Hurse PV, Siddique T, Leigh PN and Powell JF (1998) Recessive amyotrophic lateral sclerosis families with the D90A SOD1 mutation share a common founder: evidence for a linked protective factor. *Hum Mol Genet* **7**:2045-2050.

Al-Chalabi A, Jones A, Troakes C, King A, Al-Sarraj S and van den Berg LH (2012) The genetics and neuropathology of amyotrophic lateral sclerosis. *Acta Neuropathol* **124**:339-352.

Alonso AC, Grundke-Iqbal I and Iqbal K (1996) Alzheimer's disease hyperphosphorylated tau sequesters normal tau into tangles of filaments and disassembles microtubules. *Nat Med* **2**:783-787.

Andersen PM and Al-Chalabi A (2011) Clinical genetics of amyotrophic lateral sclerosis: what do we really know? *Nat Rev Neurol* **7**:603-615.

Andersen PM, Nilsson P, Ala-Hurula V, Keranen ML, Tarvainen I, Haltia T, Nilsson L, Binzer M, Forsgren L and Marklund SL (1995) Amyotrophic lateral sclerosis associated with homozygosity for an Asp90Ala mutation in CuZn-superoxide dismutase. *Nat Genet* **10**:61-66.

Anderson RG (1998) The caveolae membrane system. *Annu Rev Biochem* **67**:199-225.

Arai T, Hasegawa M and Akiyama H (2006) TDP-43 is a component of ubiquitin-positive tau-negative inclusions in frontotemporal lobar degeneration and amyotrophic lateral sclerosis. *Biochemical and Biophysical Research Communications* **351**:602–611.

Arai T, Hasegawa M, Nonoka T, Kametani F, Yamashita M, Hosokawa M, Niizato K, Tsuchiya K, Kobayashi Z, Ikeda K, Yoshida M, Onaya M, Fujishiro H and Akiyama H (2010) Phosphorylated and cleaved TDP-43 in ALS, FTLD and other neurodegenerative disorders and in cellular models of TDP-43 proteinopathy. *Neuropathology* **30**:170-181.

Arber S, Han B, Mendelsohn M, Smith M, Jessell TM and Sockanathan S (1999) Requirement for the homeobox gene Hb9 in the consolidation of motor neuron identity. *Neuron* **23**:659-674.

Arosio P, Vendruscolo M, Dobson CM and Knowles TP (2014) Chemical kinetics for drug discovery to combat protein aggregation diseases. *Trends Pharmacol Sci* **35**:127-135.

Artalejo CR, Elhamdani A and Palfrey HC (2002) Sustained stimulation shifts the mechanism of endocytosis from dynamin-1-dependent rapid endocytosis to clathrin- and dynamin-2-mediated slow endocytosis in chromaffin cells. *Proc Natl Acad Sci U S A* **99**:6358-6363.

Atkin JD, Farg MA, Soo KY, Walker AK, Halloran M, Turner BJ, Nagley P and Horne MK (2014) Mutant SOD1 inhibits ER-Golgi transport in amyotrophic lateral sclerosis. *J Neurochem* **129**:190-204.

Atkin JD, Farg MA, Turner BJ, Tomas D, Lysaght JA, Nunan J, Rembach A, Nagley P, Beart PM, Cheema SS and Horne MK (2006) Induction of the unfolded protein response in familial amyotrophic lateral sclerosis and association of protein-disulfide isomerase with superoxide dismutase 1. *Journal of Biological Chemistry* **281**:30152-30165.

Atkin JD, Farg MA, Walker AK, McLean C, Tomas D and Horne MK (2008) Endoplasmic reticulum stress and induction of the unfolded protein response in human sporadic amyotrophic lateral sclerosis. *Neurobiol Dis* **30**:400-407.

Audet JN, Gowing G and Julien JP (2010) Wild-type human SOD1 overexpression does not accelerate motor neuron disease in mice expressing murine Sod1 G86R. *Neurobiol Dis* **40**:245-250.

Ayala YM, Zago P, D'Ambrogio A, Xu YF, Petrucelli L, Buratti E and Baralle FE (2008) Structural determinants of the cellular localization and shuttling of TDP-43. *Journal of cell science* **121**:3778-3785.

Ayers JI, Fromholt S, Koch M, DeBosier A, McMahon B, Xu G and Borchelt DR (2014) Experimental transmissibility of mutant SOD1 motor neuron disease. *Acta neuropathologica*.

Ayers JI, Fromholt SE, O'Neal VM, Diamond JH and Borchelt DR (2016) Prion-like propagation of mutant SOD1 misfolding and motor neuron disease spread along neuroanatomical pathways. *Acta Neuropathol* **131**:103-114.

Baker HF, Ridley RM, Duchen LW, Crow TJ and Bruton CJ (1993) Evidence for the experimental transmission of cerebral beta-amyloidosis to primates. *Int J Exp Pathol* **74**:441-454.

Baker HF, Ridley RM, Duchen LW, Crow TJ and Bruton CJ (1994) Induction of beta (A4)-amyloid in primates by injection of Alzheimer's disease brain homogenate. Comparison with transmission of spongiform encephalopathy. *Molecular neurobiology* **8**:25-39.

Banci L, Bertini I, Boca M, Calderone V, Cantini F, Girotto S and Vieru M (2009) Structural and dynamic aspects related to oligomerization of apo SOD1 and its mutants. *Proc Natl Acad Sci U S A* **106**:6980-6985.

Bar-Sagi D, McCormick F, Milley RJ and Feramisco JR (1987) Inhibition of cell surface ruffling and fluid-phase pinocytosis by microinjection of anti-ras antibodies into living cells. *Journal of cellular physiology Supplement* **Suppl 5**:69-73.

Basso M, Pozzi S, Tortarolo M, Fiordaliso F, Bisighini C, Pasetto L, Spaltro G, Lidonnici D, Gensano F, Battaglia E, Bendotti C and Bonetto V (2013) Mutant copper-zinc superoxide dismutase (SOD1) induces protein secretion pathway alterations and exosome release in astrocytes: implications for disease spreading and motor neuron pathology in amyotrophic lateral sclerosis. *J Biol Chem* **288**:15699-15711.

Beckman JS and Koppenol WH (1996) Nitric oxide, superoxide, and peroxynitrite: the good, the bad, and ugly. *The American journal of physiology* **271**:C1424-1437.

Belzil VV, Valdmanis PN, Dion PA, Daoud H, Kabashi E, Noreau A, Gauthier J, Hince P, Desjarlais A and Bouchard JP (2009) Mutations in FUS Cause FALS and SALS in French and French Canadian Populations. *Neurology* **73**:1176-1179.

Bendotti C, Marino M, Cheroni C, Fontana E, Crippa V, Poletti A and De Biasi S (2012) Dysfunction of constitutive and inducible ubiquitin-proteasome system in amyotrophic lateral sclerosis: implication for protein aggregation and immune response. *Prog Neurobiol* **97**:101-126.

Bick RJ, Poindexter BJ, Kott MM, Liang YA, Dinh K, Kaur B, Bick DL, Doursout MF and Schiess MC (2008) Cytokines disrupt intracellular patterns of Parkinson's disease-associated proteins alpha-synuclein, tau and ubiquitin in cultured glial cells. *Brain Res* **1217**:203-212.

Bilican B, Livesey MR, Haghi G, Qiu J, Burr K, Siller R, Hardingham GE, Wyllie DJ and Chandran S (2014) Physiological normoxia and absence of EGF is required for the long-term propagation of anterior neural precursors from human pluripotent cells. *PloS one* **9**:e85932.

Blokhuis AM, Groen EJ, Koppers M, van den Berg LH and Pasterkamp RJ (2013) Protein aggregation in amyotrophic lateral sclerosis. *Acta Neuropathol* **125**:777-794.

Boillée S, Velde CV and Cleveland DW (2006) ALS: A disease of motor neurons review and their nonneuronal neighbors. *Neuron* **52**:39-59.

Bolognesi B, Kumita JR, Barros TP, Esbjorner EK, Luheshi LM, Crowther DC, Wilson MR, Dobson CM, Favrin G and Yerbury JJ (2010) ANS binding reveals common features of cytotoxic amyloid species. *ACS Chem Biol* **5**:735-740.

Bosco DA, Morfini G, Karabacak M, Song Y, Gros-Louis F, Pasinelli P, Goolsby H, Fontaine BA, Lemay N, McKenna-Yasek D, Frosch MP, Agar JN, Julien J-P, Brady ST and Brown RH (2010) Wild-type and Mutant SOD1 Share an Aberrant Conformation and a Common Pathogenic Pathway in ALS. *Nature Neuroscience* **13**:1396-1403.

Braak H, Alafuzoff I, Arzberger T, Kretzschmar H and Del Tredici K (2006) Staging of Alzheimer disease-associated neurofibrillary pathology using paraffin sections and immunocytochemistry. *Acta neuropathologica* **112**:389-404.

Braak H, Brettschneider J, Ludolph AC, Lee VM, Trojanowski JQ and Del Tredici K (2013) Amyotrophic lateral sclerosis--a model of corticofugal axonal spread. *Nat Rev Neurol* **9**:708-714.

Braak H, Del Tredici K, Rub U, de Vos RA, Jansen Steur EN and Braak E (2003) Staging of brain pathology related to sporadic Parkinson's disease. *Neurobiol Aging* **24**:197-211.

Brettschneider J, Del Tredici K, Irwin DJ, Grossman M, Robinson JL, Toledo JB, Fang L, Van Deerlin VM, Ludolph AC, Lee VM, Braak H and Trojanowski JQ (2014) Sequential distribution of pTDP-43 pathology in behavioral variant frontotemporal dementia (bvFTD). *Acta Neuropathol*.

Brettschneider J, Del Tredici K, Lee VM and Trojanowski JQ (2015) Spreading of pathology in neurodegenerative diseases: a focus on human studies. *Nature reviews Neuroscience* **16**:109-120.

Brettschneider J, Del Tredici K, Toledo JB, Robinson JL, Irwin DJ, Grossman M, Suh E, Van Deerlin VM, Wood EM, Baek Y, Kwong L, Lee EB, Elman L, McCluskey L, Fang L, Feldengut S, Ludolph AC, Lee VM, Braak H and Trojanowski JQ (2013) Stages of pTDP-43 pathology in amyotrophic lateral sclerosis. *Ann Neurol* **74**:20-38.

Brettschneider J, Van Deerlin VM, Robinson JL, Kwong L, Lee EB, Ali YO, Safren N, Monteiro MJ, Toledo JB, Elman L, McCluskey L, Irwin DJ, Grossman M, Molina-Porcel L, Lee VM and Trojanowski JQ (2012) Pattern of ubiquilin pathology in ALS and FTLD indicates presence of C9ORF72 hexanucleotide expansion. *Acta Neuropathol* **123**:825-839.

Brodsky FM, Chen CY, Knuehl C, Towler MC and Wakeham DE (2001) Biological basket weaving: formation and function of clathrin-coated vesicles. *Annual review of cell and developmental biology* **17**:517-568.

Brotherton TE, Li Y and Glass JD (2013) Cellular toxicity of mutant SOD1 protein is linked to an easily soluble, non-aggregated form *in vivo*. *Neurobiol Dis* **49**:49-56.

Bruijn L, M.Miller T and W.Cleveland D (2004) Unraveling the mechanisms involved in motor neuron degeneration in ALS. *Annual Review of Neuroscience* **27**:723-749.

Bruijn LI, Becher MW, Lee MK, Anderson KL, Jenkins NA, Copeland NG, Sisodia SS, Rothstein JD, Borchelt DR, Price DL and Cleveland DW (1997) ALS-linked SOD1 mutant G85R mediates damage to astrocytes and promotes rapidly progressive disease with SOD1-containing inclusions. *Neuron* **18**:327-338.

Bruijn LI, Houseweart MK, Kato S, Anderson KL, Anderson SD, Ohama E, Reaume AG, Scott RW and Cleveland DW (1998) Aggregation and motor neuron toxicity of an

ALS-linked SOD1 mutant independent from wild-type SOD1. *Journal of Cell Science* **281**:1851-1854.

Brundin P, LY J, Holton J, Lindvall O and Revesz T (2008) Research in motion: the enigma of Parkinson's disease pathology spread. *Nature Reviews Neuroscience* **9**:741-745.

Brundin P, Melki R and Kopito R (2010) Prion-like transmission of protein aggregates in neurodegenerative diseases. *Nature Reviews* **11**:301-307.

Budini M, Romano V, Quadri Z, Buratti E and Baralle FE (2015) TDP-43 loss of cellular function through aggregation requires additional structural determinants beyond its C-terminal Q/N prion-like domain. *Hum Mol Genet* **24**:9-20.

Buell AK, Galvagnion C, Gaspar R, Sparr E, Vendruscolo M, Knowles TP, Linse S and Dobson CM (2014) Solution conditions determine the relative importance of nucleation and growth processes in alpha-synuclein aggregation. *Proc Natl Acad Sci U S A* **111**:7671-7676.

Buratti E and Baralle FE (2001) Characterization and functional implications of the RNA binding properties of Nuclear factor TDP-43, a novel splicing regulator of CFTR exon 9. *Journal of Biological Chemistry* **276**:36337-36343.

Buratti E and Baralle FE (2008) Multiple roles of TDP-43 in gene expression, splicing regulation, and human disease. *Frontiers in Bioscience* **13**:867-878.

Buratti E, Dörk T, Zuccato E, Pagani F, Romano M and Baralle FE (2001) Nuclear factor TDP-43 and SR proteins promote *in vitro* and *in vivo* CFTR exon 9 skipping. *EMBO Journal* **20**:1774-1784.

Burgold S, Filser S, Dorostkar MM, Schmidt B and Herms J (2014) *In vivo* imaging reveals sigmoidal growth kinetic of beta-amyloid plaques. *Acta Neuropathol Commun* **2**:30.

Bystrom R, Andersen PM, Grobner G and Oliveberg M (2010) SOD1 mutations targeting surface hydrogen bonds promote amyotrophic lateral sclerosis without reducing apo-state stability. *J Biol Chem* **285**:19544-19552.

Caetano-Pinto P, Janssen MJ, Gijzen L, Verscheijden L, Wilmer MJ and Masereeuw R (2016) Fluorescence-Based Transport Assays Revisited in a Human Renal Proximal Tubule Cell Line. *Molecular pharmaceutics* **13**:933-944.

Cairns NJ, Neumann M, Bigio EH, Holm IE, Troost D, Hatanpaa KJ, Foong C, White CL, 3rd, Schneider JA, Kretzschmar HA, Carter D, Taylor-Reinwald L, Paulsmeyer K, Strider J, Gitcho M, Goate AM, Morris JC, Mishra M, Kwong LK, Stieber A, Xu Y, Forman MS, Trojanowski JQ, Lee VM and Mackenzie IR (2007) TDP-43 in familial and sporadic frontotemporal lobar degeneration with ubiquitin inclusions. *Am J Pathol* **171**:227-240.

Cashman NR, Durham HD, Blusztajn JK, Oda K, Tabira T, Shaw IT, Dahrouge S and Antel JP (1992) Neuroblastoma x spinal cord (NSC) hybrid cell lines resemble developing motor neurons. *Dev Dynam* **194**:209-221.

Cattaneo E, Zuccato C and Tartari M (2005) Normal huntingtin function: an alternative approach to Huntington's disease. *Nature reviews Neuroscience* **6**:919-930.

Cereda C, Leoni E, Milani P, Pansarasa O, Mazzini G, Guareschi S, Alvisi E, Ghiroldi A, Diamanti L, Bernuzzi S, Ceroni M and Cova E (2013) Altered intracellular localization of SOD1 in leukocytes from patients with sporadic amyotrophic lateral sclerosis. *PLoS One* **8**:e75916.

Chang HY, Hou SC, Way TD, Wong CH and Wang IF (2013) Heat-shock protein dysregulation is associated with functional and pathological TDP-43 aggregation. *Nature communications* **4**:2757.

Chen S, Sayana P, Zhang X and Le W (2013) Genetics of amyotrophic lateral sclerosis: an update. *Molecular neurodegeneration* **8**:28.

Chia R, Tattum H, Jones S, Collinge J, Fisher E and Jackson GS (2010) Superoxide Dismutase 1 and tgSOD1G93A mouse spinal cord seed fibrils, suggesting a propagative cell death mechanism in amyotrophic lateral sclerosis. *Public Library of Science* **5**:e10627.

Chio A, Benzi G, Dossena M, Mutani R and Mora G (2005) Severely increased risk of amyotrophic lateral sclerosis among Italian professional football players. *Brain* **128**:472-476.

Chiti F and Dobson CM (2006) Protein misfolding, functional amyloid, and human disease. *Annu Rev Biochem* **75**:333-366.

Cimini V, Ruggiero G, Buonomo T, Seru R, Sciori S, Zanzi C, Santangelo F and Mondola P (2002) CuZn-superoxide dismutase in human thymus: immunocytochemical localisation and secretion in thymus-derived epithelial and fibroblast cell lines. *Histochemistry and Cell Biology* **118**:163-169.

Clavaguera F, Bolmont T, Crowther RA, Abramowski D, Frank S, Probst A, Fraser G, Stalder AK, Beibel M, Staufenbiel M, Jucker M, Goedert M and Tolnay M (2009) Transmission and spreading of tauopathy in transgenic mouse brain. *Nat Cell Biol* **11**:909-913.

Cleveland DW and Rothstein JD (2001) From Charcot to Lou Gehrig: Deciphering selective motor neuron death in ALS. *Nature Reviews* **2**:806-819.

Cohen SI, Linse S, Luheshi LM, Hellstrand E, White DA, Rajah L, Otzen DE, Vendruscolo M, Dobson CM and Knowles TP (2013) Proliferation of amyloid-beta42 aggregates occurs through a secondary nucleation mechanism. *Proc Natl Acad Sci U S A* **110**:9758-9763.

Colombrita C, Zennaro E, Fallini C, Weber M, Sommacal A, Buratti E, Silani V and Ratti A (2009) TDP-43 is recruited to stress granules in conditions of oxidative insult. *J Neurochem* **111**:1051-1061.

Conner SD and Schmid SL (2003) Regulated portals of entry into the cell. *Nature* **422**:37-44.

Correia AS, Patel P, Dutta K and Julien JP (2015) Inflammation Induces TDP-43 Mislocalization and Aggregation. *PLoS One* **10**:e0140248.

Dal Canto MC and Gurney ME (1997) A low expressor line of transgenic mice carrying a mutant human Cu,Zn superoxide dismutase (SOD1) gene develops pathological changes that most closely resemble those in human amyotrophic lateral sclerosis. *Acta Neuropathol* **93**:537-550.

Damiano S, Petrozziello T, Ucci V, Amente S, Santillo M and Mondola P (2013) Cu-Zn superoxide dismutase activates muscarinic acetylcholine M1 receptor pathway in neuroblastoma cells. *Mol Cell Neurosci* **52**:31-37.

Daoud H, Valdmanis PN, Kabashi E, Dion P, Dupre N, Camu W, Meininger V and Rouleau GA (2009) Contribution of TARDBP Mutations to Sporadic Amyotrophic Lateral Sclerosis. *Journal of Medical Genetics* **46**:112-114.

Dauer W and Przedborski S (2003) Parkinson's disease: mechanisms and models. *Neuron* **39**:889-909.

Davidson Y, Kelley T, Mackenzie IR, Pickering-Brown S, Du Plessis D, Neary D, Snowden JS and Mann DM (2007) Ubiquitinated pathological lesions in frontotemporal lobar degeneration contain the TAR DNA-binding protein, TDP-43. *Acta Neuropathol* **113**:521-533.

Davies SW, Turmaine M, Cozens BA, DiFiglia M, Sharp AH, Ross CA, Scherzinger E, Wanker EE, Mangiarini L and Bates GP (1997) Formation of neuronal intranuclear inclusions underlies the neurological dysfunction in mice transgenic for the HD mutation. *Cell* **90**:537-548.

Deng HX, Hentati A, Tainer JA, Iqbal Z, Cayabyab A, Hung WY, Getzoff ED, Hu P, Herzfeldt B, Roos RP and et al. (1993) Amyotrophic lateral sclerosis and structural defects in Cu,Zn superoxide dismutase. *Science* **261**:1047-1051.

Deng HX, Shi Y, Furukawa Y, Zhai H, Fu R, Liu E, Gorrie GH, Khan MS, Hung WY, Bigio EH, Lukas T, Dal Canto MC, O'Halloran TV and Siddique T (2006) Conversion to the amyotrophic lateral sclerosis phenotype is associated with intermolecular linked insoluble aggregates of SOD1 in mitochondria. *Proc Natl Acad Sci U S A* **103**:7142-7147.

Desplats P, Lee HJ, Bae EJ, Patrick C, Rockenstein E, Crews L, Spencer B, Masliah E and Lee SJ (2009) Inclusion formation and neuronal cell death through neuron-to-neuron transmission of alpha-synuclein. *Proc Natl Acad Sci U S A* **106**:13010-13015.

Dharmawardhane S, Schurmann A, Sells MA, Chernoff J, Schmid SL and Bokoch GM (2000) Regulation of macropinocytosis by p21-activated kinase-1. *Mol Biol Cell* **11**:3341-3352.

Diener TO, McKinley MP and Prusiner SB (1982) Viroids and prions. *Proc Natl Acad Sci U S A* **79**:5220-5224.

Dobson CM (2003) Protein folding and misfolding. *Nature* **426**:884-890.

Duyao M, Ambrose C, Myers R, Novelletto A, Persichetti F, Frontali M, Folstein S, Ross C, Franz M, Abbott M and et al. (1993) Trinucleotide repeat length instability and age of onset in Huntington's disease. *Nat Genet* **4**:387-392.

Eisbach SE and Outeiro TF (2013) Alpha-synuclein and intracellular trafficking: impact on the spreading of Parkinson's disease pathology. *J Mol Med (Berl)* **91**:693-703.

Eisele YS, Bolmont T, Heikenwalder M, Langer F, Jacobson LH, Yan ZX, Roth K, Aguzzi A, Staufenbiel M, Walker LC and Jucker M (2009) Induction of cerebral beta-amyloidosis: intracerebral versus systemic Abeta inoculation. *Proc Natl Acad Sci U S A* **106**:12926-12931.

Eisele YS, Obermuller U, Heilbronner G, Baumann F, Kaeser SA, Wolburg H, Walker LC, Staufenbiel M, Heikenwalder M and Jucker M (2010) Peripherally applied Abeta-containing inoculates induce cerebral beta-amyloidosis. *Science* **330**:980-982.

Elden AC, Kim HJ, Hart MP, Chen-Plotkin AS, Johnson BS, Fang X, Armakola M, Geser F, Greene R, Lu MM, Padmanabhan A, Clay-Falcone D, McCluskey L, Elman L, Juhr D, Gruber PJ, Rub U, Auburger G, Trojanowski JQ, Lee VM, Van Deerlin VM, Bonini NM and Gitler AD (2010) Ataxin-2 intermediate-length polyglutamine expansions are associated with increased risk for ALS. *Nature* **466**:1069-1075.

Elia AE, Lalli S, Monsurro MR, Sagnelli A, Taiello AC, Reggiori B, La Bella V, Tedeschi G and Albanese A (2016) Tauroursodeoxycholic acid in the treatment of patients with amyotrophic lateral sclerosis. *European journal of neurology* **23**:45-52.

Farrawell NE, Lambert-Smith IA, Warraich ST, Blair IP, Saunders DN, Hatters DM and Yerbury JJ (2015) Distinct partitioning of ALS associated TDP-43, FUS and SOD1 mutants into cellular inclusions. *Scientific reports* **5**:13416.

Feiler MS, Strobel B, Freischmidt A, Helferich AM, Kappel J, Brewer BM, Li D, Thal DR, Walther P, Ludolph AC, Danzer KM and Weishaupt JH (2015) TDP-43 is intercellularly transmitted across axon terminals. *The Journal of cell biology* **211**:897-911.

Fevrier B, Vilette D, Archer F, Loew D, Faigle W, Vidal M, Laude H and Raposo G (2004) Cells release prions in association with exosomes. *Proceedings Of The National Academy Of Sciences Of The United States Of America* **101**:9683–9688.

Forman MS, Trojanowski JQ and Lee VM (2004) Neurodegenerative Diseases: A Decade of Discoveries Paves the Way for Therapeutic Breakthroughs. *Nature Medicine* **10**:1055-1063.

Forsberg K, Jonsson PA, Andersen PM, Bergemalm D, Graffmo KS, Hultdin M, Jacobsson J, Rosquist R, Marklund SL and Brannstrom T (2010) Novel antibodies reveal inclusions containing non-native SOD1 in sporadic ALS patients. *PLoS One* **5**:e11552.

Freeman D, Cedillos R, Choyke S, Lukic Z, McGuire K, Marvin S, Burrage AM, Sudholt S, Rana A, O'Connor C, Wiethoff CM and Campbell EM (2013) Alpha-synuclein induces lysosomal rupture and cathepsin dependent reactive oxygen species following endocytosis. *PLoS One* **8**:e62143.

Frost B, Jacks RL and Diamond MI (2009) Propagation of Tau misfolding from the outside to the inside of a cell. *Journal of Biological Chemistry* **284**:12845–12852.

Fukada K, Nagano S, Satoh M, Tohyama C, Nakanishi T, Shimizu A, Yanagihara T and Sakoda S (2001) Stabilization of mutant Cu/Zn superoxide dismutase (SOD1) protein by coexpressed wild SOD1 protein accelerates the disease progression in familial amyotrophic lateral sclerosis mice. *The European journal of neuroscience* **14**:2032-2036.

Furukawa Y, Kaneko K, Watanabe S, Yamanaka K and Nukina N (2011) A seeding reaction recapitulates intracellular formation of Sarkosyl-insoluble transactivation response element (TAR) DNA-binding protein-43 inclusions. *J Biol Chem* **286**:18664-18672.

Furukawa Y, Kaneko K, Watanabe S, Yamanaka K and Nukina N (2013) Intracellular seeded aggregation of mutant Cu,Zn-superoxide dismutase associated with amyotrophic lateral sclerosis. *FEBS Lett* **587**:2500-2505.

Furukawa Y, Kaneko K, Yamanaka K, O'Halloran T and Nukina N (2008) Complete loss of post-translational modifications triggers fibrillar aggregation of SOD1 in the familial form of amyotrophic lateral sclerosis. *Journal of Biological Chemistry* **283**:24167–24176.

Furukawa Y and O'Halloran TV (2005) Amyotrophic lateral sclerosis mutations have the greatest destabilizing effect on the Apo- and reduced form of SOD1, leading to unfolding and oxidative aggregation. *Journal of Biological Chemistry* **280**:17266-17274.

Geevasinga N, Menon P, Ng K, Van Den Bos M, Byth K, Kiernan MC and Vucic S (2016) Riluzole exerts transient modulating effects on cortical and axonal hyperexcitability in ALS. *Amyotrophic lateral sclerosis & frontotemporal degeneration*:1-9.

Giordana MT, Piccinini M, Grifoni S, Marco GD, Vercellino M, Magistrello M, Pellerino A, Buccinnà B, Lupino E and Rinaudo MT (2010) TDP-43 redistribution is an early event in sporadic amyotrophic lateral sclerosis *Brain Pathology* **20**:351-360.

Gitcho MA, Baloh RH, Chakraverty S, Mayo K, Norton JB, Levitch D, Hatanpaa KJ, White CL, Bigio EH, Caselli R, Baker M, Al-Lozi MT, Morris JC, Pestronk A, Rademakers R, Goate AM and Cairns NJ (2008) TDP-43 A315T Mutation in Familial Motor Neuron Disease. *Annals of Neurology* **63**:535-538.

Goedert M, Klug A and Crowther RA (2006) Tau protein, the paired helical filament and Alzheimer's disease. *Journal of Alzheimer's disease : JAD* **9**:195-207.

Goetz CG (2000) Amyotrophic lateral sclerosis: early contributions of Jean-Martin Charcot. *Muscle & nerve* **23**:336-343.

Gomes C, Keller S, Altevogt P and Costa J (2007) Evidence for secretion of Cu,Zn superoxide dismutase *via* exosomes from a cell model of amyotrophic lateral sclerosis. *Neuroscience Letters* **428**:43-46.

Grad LI, Fernando SM and Cashman NR (2015) From molecule to molecule and cell to cell: prion-like mechanisms in amyotrophic lateral sclerosis. *Neurobiol Dis* **77**:257-265.

Grad LI, Guest WC, Yanai A, Pokrishevsky E, O'Neill MA, Gibbs E, Semenchenko V, Yousefi M, Wishart DS, Plotkin SS and Cashman NR (2011) Intermolecular

transmission of superoxide dismutase 1 misfolding in living cells. *Proc Natl Acad Sci U S A* **108**:16398-16403.

Grad LI, Yerbury JJ, Turner BJ, Guest WC, Pokrishevsky E, O'Neill MA, Yanai A, Silverman JM, Zeineddine R, Corcoran L, Kumita JR, Luheshi LM, Yousefi M, Coleman BM, Hill AF, Plotkin SS, Mackenzie IR and Cashman NR (2014) Intercellular propagated misfolding of wild-type Cu/Zn superoxide dismutase occurs *via* exosome-dependent and -independent mechanisms. *Proc Natl Acad Sci U S A*.

Gregory JM, Barros TP, Meehan S, Dobson CM and Luheshi LM (2012) The aggregation and neurotoxicity of TDP-43 and its ALS-associated 25 kDa fragment are differentially affected by molecular chaperones in Drosophila. *PLoS One* **7**:e31899.

Guillemin GJ, Smythe G, Takikawa O and Brew BJ (2005) Expression of indoleamine 2,3-dioxygenase and production of quinolinic acid by human microglia, astrocytes, and neurons. *Glia* **49**:15-23.

Guo W, Chen Y, Zhou X, Kar A, Ray P, Chen X, Rao EJ, Yang M, Ye H, Zhu L, Liu J, Xu M, Yang Y, Wang C, Zhang D, Bigio EH, Mesulam M, Shen Y, Xu Q, Fushimi K and Wu JY (2011) An ALS-associated mutation affecting TDP-43 enhances protein aggregation, fibril formation and neurotoxicity *Nature Structural and Molecular Biology* **18**:822-831.

Gurney ME, Pu H, Chiu AY, Canto MCD, Polchow CY, Alexander DD, Caliendo J, Hentati A, Kwon YW, Deng HX, Chen W, Zhai P, Sufit RL and Siddique T (1994) Motor Neuron Degeneration in Mice That Express a Human Cu/Zn Superoxide Dismutase Mutation. *Science* **264**:1772-1775.

Gustafsson G, Eriksson F, Moller C, da Fonseca TL, Outeiro TF, Lannfelt L, Bergstrom J and Ingelsson M (2016) Cellular Uptake of alpha-Synuclein Oligomer-Selective Antibodies is Enhanced by the Extracellular Presence of alpha-Synuclein and Mediated *via* Fcgamma Receptors. *Cellular and molecular neurobiology*.

Haidet-Phillips AM, Hester ME, Miranda CJ, Meyer K, Braun L, Frakes A, Song S, Likhite S, Murtha MJ, Foust KD, Rao M, Eagle A, Kammesheidt A, Christensen A, Mendell JR, Burghes AHM, Kaspar BK, 1The Research Institute at Nationwide Children's Hospital C, OH and 2Integrated Biomedical Science Graduate Program CoM, The Ohio State (2011) Astrocytes from familial and sporadic ALS patients are toxic to motor neurons. *Nature Biotechnology* **29**:824-828.

Haley RW (2003) Excess incidence of ALS in young Gulf War veterans. *Neurology* **61**:750-756.

Halle A, Hornung V, Petzold GC, Stewart CR, Monks BG, Reinheckel T, Fitzgerald KA, Latz E, Moore KJ and Golenbock DT (2008) The NALP3 inflammasome is involved in the innate immune response to amyloid-beta. *Nature immunology* **9**:857-865.

Hansen C, Angot E, Bergstrom AL, Steiner JA, Pieri L, Paul G, Outeiro TF, Melki R, Kallunki P, Fog K, Li JY and Brundin P (2011) alpha-Synuclein propagates from mouse brain to grafted dopaminergic neurons and seeds aggregation in cultured human cells. *J Clin Invest* **121**:715-725.

Harikrishnareddy D, Misra S, Upadhyay S, Modi M and Medhi B (2015) Roots to start research in amyotrophic lateral sclerosis: molecular pathways and novel therapeutics for future. *Reviews in the neurosciences* **26**:161-181.

Harraz MM, Marden JJ, Zhou W, Zhang Y, Williams A, Sharov VS, Nelson K, Luo M, Paulson H, Schoneich C and Engelhardt JF (2008) SOD1 mutations disrupt redox-sensitive Rac regulation of NADPH oxidase in a familial ALS model. *The Journal of clinical investigation* **118**:659-670.

Hasegawa M, Arai T, Nonaka T, Kametani F, Yoshida M, Hashizume Y, Beach TG, Buratti E, Baralle F, Morita M, Nakano I, Oda T, Tsuchiya K and Akiyama H (2008)

Phosphorylated TDP-43 in frontotemporal lobar degeneration and amyotrophic lateral sclerosis. *Annals of Neurology* **64**:60-70.

Haverkamp LJ, Appel V and Appel SH (1995) Natural history of amyotrophic lateral sclerosis in a database population. Validation of a scoring system and a model for survival prediction. *Brain* **118 (Pt 3)**:707-719.

Hedges EC, Mehler VJ and Nishimura AL (2016) The Use of Stem Cells to Model Amyotrophic Lateral Sclerosis and Frontotemporal Dementia: From Basic Research to Regenerative Medicine. *Stem cells international* **2016**:9279516.

Heiman-Patterson TD, Sher RB, Blankenhorn EA, Alexander G, Deitch JS, Kunst CB, Maragakis N and Cox G (2011) Effect of genetic background on phenotype variability in transgenic mouse models of amyotrophic lateral sclerosis: a window of opportunity in the search for genetic modifiers. *Amyotrophic lateral sclerosis : official publication of the World Federation of Neurology Research Group on Motor Neuron Diseases* **12**:79-86.

Herman AM, Khandelwal PJ, Stanczyk BB, Rebeck GW and Moussa CE (2011) beta-amyloid triggers ALS-associated TDP-43 pathology in AD models. *Brain Res* **1386**:191-199.

Herrera F, Tenreiro S, Miller-Fleming L and Outeiro TF (2011) Visualization of cell-to-cell transmission of mutant huntingtin oligomers. *PLoS currents* **3**:RRN1210.

Hewlett LJ, Prescott AR and Watts C (1994) The coated pit and macropinocytic pathways serve distinct endosome populations. *The Journal of cell biology* **124**:689-703.

Hollidge BS, Nedelsky NB, Salzano MV, Fraser JW, Gonzalez-Scarano F and Soldan SS (2012) Orthobunyavirus entry into neurons and other mammalian cells occurs *via* clathrin-mediated endocytosis and requires trafficking into early endosomes. *Journal of virology* **86**:7988-8001.

Holmes BB, DeVos SL, Kfoury N, Li M, Jacks R, Yanamandra K, Ouidja MO, Brodsky FM, Marasa J, Bagchi DP, Kotzbauer PT, Miller TM, Papy-Garcia D and Diamond MI (2013) Heparan sulfate proteoglycans mediate internalization and propagation of specific proteopathic seeds. *Proc Natl Acad Sci U S A* **110**:E3138-3147.

Hortschansky P, Schroeckh V, Christopeit T, Zandomeneghi G and Fandrich M (2005) The aggregation kinetics of Alzheimer's beta-amyloid peptide is controlled by stochastic nucleation. *Protein Sci* **14**:1753-1759.

Horwich AL and Weissman JS (1997) Deadly conformations--protein misfolding in prion disease. *Cell* **89**:499-510.

Huang CY, Lu TY, Bair CH, Chang YS, Jwo JK and Chang W (2008) A novel cellular protein, VPEF, facilitates vaccinia virus penetration into HeLa cells through fluid phase endocytosis. *Journal of virology* **82**:7988-7999.

Huttner WB, Gerdes HH and Rosa P (1991) The granin (chromogranin/secretogranin) family. *Trends in Biochemical Sciences* **16**:27-30.

Iba M, Guo JL, McBride JD, Zhang B, Trojanowski JQ and Lee VM (2013) Synthetic tau fibrils mediate transmission of neurofibrillary tangles in a transgenic mouse model of Alzheimer's-like tauopathy. *The Journal of neuroscience : the official journal of the Society for Neuroscience* **33**:1024-1037.

Ibrahim T and McLaurin J (2016) alpha-Synuclein aggregation, seeding and inhibition by scyllo-inositol. *Biochem Biophys Res Commun* **469**:529-534.

Ilieva EV, Ayala V, Jove M, Dalfo E, Cacabelos D, Povedano M, Bellmunt MJ, Ferrer I, Pamplona R and Portero-Otin M (2007) Oxidative and endoplasmic reticulum stress interplay in sporadic amyotrophic lateral sclerosis. *Brain* **130**:3111-3123.

Ivanov AI (2008) Pharmacological inhibition of endocytic pathways: is it specific enough to be useful? *Methods in molecular biology* **440**:15-33.

Ivanova MI, Sievers SA, Guenther EL, Johnson LM, Winkler DD, Galaleldeen A, Sawaya MR, Hart PJ and Eisenberg DS (2014) Aggregation-triggering segments of SOD1 fibril formation support a common pathway for familial and sporadic ALS. *Proc Natl Acad Sci U S A* **111**:197-201.

Jaarsma D, Haasdijk ED, Grashorn JA, Hawkins R, van Duijn W, Verspaget HW, London J and Holstege JC (2000) Human Cu/Zn superoxide dismutase (SOD1) overexpression in mice causes mitochondrial vacuolization, axonal degeneration, and premature motoneuron death and accelerates motoneuron disease in mice expressing a familial amyotrophic lateral sclerosis mutant SOD1. *Neurobiol Dis* **7**:623-643.

Jacobsson J, Jonsson PA, Andersen PM, Forsgren L and Marklund SL (2001) Superoxide dismutase in CSF from amyotrophic lateral sclerosis patients with and without CuZn-superoxide dismutase mutations. *Brain* **124**:1461-1466.

Jarrett JT, Berger EP and Lansbury PT, Jr. (1993) The carboxy terminus of the beta amyloid protein is critical for the seeding of amyloid formation: implications for the pathogenesis of Alzheimer's disease. *Biochemistry* **32**:4693-4697.

Jarrett JT and Lansbury PT, Jr. (1993) Seeding "one-dimensional crystallization" of amyloid: a pathogenic mechanism in Alzheimer's disease and scrapie? *Cell* **73**:1055-1058.

Jaunmuktane Z, Mead S, Ellis M, Wadsworth JD, Nicoll AJ, Kenny J, Launchbury F, Linehan J, Richard-Loendt A, Walker AS, Rudge P, Collinge J and Brandner S (2015) Evidence for human transmission of amyloid-beta pathology and cerebral amyloid angiopathy. *Nature* **525**:247-250.

Johnson BS, McCaffery JM, Lindquist S and Gitler AD (2008) A yeast TDP-43 proteinopathy model: Exploring the molecular determinants of TDR-43 aggregation and cellular toxicity. *P Natl Acad Sci USA* **105**:6439-6444.

Johnson BS, Snead D, Lee JJ, McCaffery JM, Shorter J and Gitler AD (2009) TDP-43 is intrinsically aggregation-prone, and amyotrophic lateral sclerosis-linked mutations accelerate aggregation and increase toxicity. *J Biol Chem* **284**:20329-20339.

Jucker M and Walker LC (2013) Self-propagation of pathogenic protein aggregates in neurodegenerative diseases. *Nature* **501**:45-51.

Juenemann K, Wiemhoefer A and Reits EA (2015) Detection of ubiquitinated huntingtin species in intracellular aggregates. *Frontiers in molecular neuroscience* **8**:1.

Jurney WM, Gallo G, Letourneau PC and McLoon SC (2002) RAC1-mediated endocytosis during ephrin-A2- and semaphorin 3A-induced growth cone collapse. *J Neurosci* **22**:6019-6028.

Kabashi E, Valdmanis PN, Dion P and Rouleau GA (2007) Oxidized/misfolded superoxide dismutase-1: the cause of all amyotrophic lateral sclerosis? *Ann Neurol* **62**:553-559.

Kabashi E, Valdmanis PN, Dion P, Spiegelman D, McConkey BJ, Velde CV, Bouchard JP, Lacomblez L, Pochigaeva K, Salachas F, Pradat PF, Camu W, Meininger V, Dupre N and Rouleau GA (2008) TARDBP Mutations in Individuals with Sporadic and Familial Amyotrophic Lateral Sclerosis. *Nature Genetics* **40**:572-574.

Kabayama H, Takeuchi M, Taniguchi M, Tokushige N, Kozaki S, Mizutani A, Nakamura T and Mikoshiba K (2011) Syntaxin 1B suppresses macropinocytosis and semaphorin 3A-induced growth cone collapse. *J Neurosci* **31**:7357-7364.

Kalia M, Khasa R, Sharma M, Nain M and Vrati S (2013) Japanese encephalitis virus infects neuronal cells through a clathrin-independent endocytic mechanism. *J Virol* **87**:148-162.

Kane MD, Lipinski WJ, Callahan MJ, Bian F, Durham RA, Schwarz RD, Roher AE and Walker LC (2000) Evidence for seeding of beta -amyloid by intracerebral infusion of Alzheimer brain extracts in beta -amyloid precursor protein-transgenic mice. *The*

Journal of neuroscience : the official journal of the Society for Neuroscience **20**:3606-3611.

Karch CM, Prudencio M, Winkler DD, Hart PJ and Borchelt DR (2009) Role of mutant SOD1 disulfide oxidation and aggregation in the pathogenesis of familial ALS. *Proc Natl Acad Sci U S A* **106**:7774-7779.

Kato S (1999) Recent advances in research on neuropathological aspects of familial amyotrophic lateral sclerosis with superoxide dismutase 1 gene mutations: Neuronal Lewy body-like hyaline inclusions and astrocytic hyaline inclusions. *Histology and Histopathology* **14**:973-989.

Kaur SJ, McKeown SR and Rashid S (2016) Mutant SOD1 mediated pathogenesis of Amyotrophic Lateral Sclerosis. *Gene* **577**:109-118.

Kaus A and Sareen D (2015) ALS Patient Stem Cells for Unveiling Disease Signatures of Motoneuron Susceptibility: Perspectives on the Deadly Mitochondria, ER Stress and Calcium Triad. *Frontiers in cellular neuroscience* **9**:448.

Kayed R, Head E, Thompson JL, McIntire TM, Milton SC, Cotman CW and Glabe CG (2003) Common structure of soluble amyloid oligomers implies common mechanism of pathogenesis. *Science* **300**:486-489.

Kenna KP, van Doormaal PT, Dekker AM, Ticozzi N, Kenna BJ, Diekstra FP, van Rheenen W, van Eijk KR, Jones AR, Keagle P, Shatunov A, Sproviero W, Smith BN, van Es MA, Topp SD, Kenna A, Miller JW, Fallini C, Tiloca C, McLaughlin RL, Vance C, Troakes C, Colombrita C, Mora G, Calvo A, Verde F, Al-Sarraj S, King A, Calini D, de Belleroche J, Baas F, van der Kooi AJ, de Visser M, Ten Asbroek AL, Sapp PC, McKenna-Yasek D, Polak M, Asress S, Munoz-Blanco JL, Strom TM, Meitinger T, Morrison KE, Consortium S, Lauria G, Williams KL, Leigh PN, Nicholson GA, Blair IP, Leblond CS, Dion PA, Rouleau GA, Pall H, Shaw PJ, Turner MR, Talbot K, Taroni F, Boylan KB, Van Blitterswijk M, Rademakers R, Esteban-Perez J, Garcia-Redondo A, Van Damme P, Robberecht W, Chio A, Gellera C, Drepper C, Sendtner M, Ratti A, Glass JD, Mora JS, Basak NA, Hardiman O, Ludolph AC, Andersen PM, Weishaupt JH, Brown RH, Jr., Al-Chalabi A, Silani V, Shaw CE, van den Berg LH, Veldink JH and Landers JE (2016) NEK1 variants confer susceptibility to amyotrophic lateral sclerosis. *Nat Genet*.

Kerman A, Liu H-N, Croul S, Bilbao J, Rogaeva E, Zinman L, Robertson J and Chakrabartty A (2010) Amyotrophic lateral sclerosis is a non-amyloid disease in which extensive misfolding of SOD1 is unique to the familial form. *Acta Neuropathologica* **119**:335-344.

Kerr MC and Teasdale RD (2009) Defining macropinocytosis. *Traffic* **10**:364-371.

Kfoury N, Holmes BB, Jiang H, Holtzman DM and Diamond MI (2012) Trans-cellular propagation of Tau aggregation by fibrillar species. *J Biol Chem* **287**:19440-19451.

Kiernan MC, Vucic S, Cheah BC, Turner MR, Eisen A, Hardiman O, Burrell JR and Zoing MC (2011) Amyotrophic lateral sclerosis. *Lancet* **377**:942-955.

Kirkham M and Parton RG (2005) Clathrin-independent endocytosis: new insights into caveolae and non-caveolar lipid raft carriers. *Biochim Biophys Acta* **1745**:273-286.

Knowles TP, Vendruscolo M and Dobson CM (2014) The amyloid state and its association with protein misfolding diseases. *Nature reviews Molecular cell biology* **15**:384-396.

Knowles TP, Waudby CA, Devlin GL, Cohen SI, Aguzzi A, Vendruscolo M, Terentjev EM, Welland ME and Dobson CM (2009) An analytical solution to the kinetics of breakable filament assembly. *Science* **326**:1533-1537.

Knowles TP, White DA, Abate AR, Agresti JJ, Cohen SI, Sperling RA, De Genst EJ, Dobson CM and Weitz DA (2011) Observation of spatial propagation of amyloid assembly from single nuclei. *Proc Natl Acad Sci U S A* **108**:14746-14751.

Koivusalo M, Welch C, Hayashi H, Scott CC, Kim M, Alexander T, Touret N, Hahn KM and Grinstein S (2010) Amiloride inhibits macropinocytosis by lowering submembranous pH and preventing RAC1 and Cdc42 signaling. *The Journal of cell biology* **188**:547-563.

Kolpak AL, Jiang J, Guo D, Standley C, Bellve K, Fogarty K and Bao ZZ (2009) Negative guidance factor-induced macropinocytosis in the growth cone plays a critical role in repulsive axon turning. *The Journal of neuroscience : the official journal of the Society for Neuroscience* **29**:10488-10498.

Kulig M and Ecroyd H (2012) The small heat-shock protein alphaB-crystallin uses different mechanisms of chaperone action to prevent the amorphous versus fibrillar aggregation of alpha-lactalbumin. *The Biochemical journal* **448**:343-352.

Kumar S, Rezaei-Ghaleh N, Terwel D, Thal DR, Richard M, Hoch M, Mc Donald JM, Wullner U, Glebov K, Heneka MT, Walsh DM, Zweckstetter M and Walter J (2011) Extracellular phosphorylation of the amyloid beta-peptide promotes formation of toxic aggregates during the pathogenesis of Alzheimer's disease. *EMBO J* **30**:2255-2265.

Kwong LK, Uryu K, Trojanowski JQ and Lee VM (2008) TDP-43 proteinopathies: neurodegenerative protein misfolding diseases without amyloidosis. *Neurosignals* **16**:41-51.

Lagier-Tourenne C, Polymenidou M and Cleveland DW (2010) TDP-43 and FUS/TLS: emerging roles in RNA processing and neurodegeneration. *Human Molecular Genetics* **19**:R46-R64.

Lanzetti L, Palamidessi A, Areces L, Scita G and Di Fiore PP (2004) Rab5 is a signalling GTPase involved in actin remodelling by receptor tyrosine kinases. *Nature* **429**:309-314.

Lee DY, Jeon GS, Shim YM, Seong SY, Lee KW and Sung JJ (2015) Modulation of SOD1 Subcellular Localization by Transfection with Wild- or Mutant-type SOD1 in Primary Neuron and Astrocyte Cultures from ALS Mice. *Experimental neurobiology* **24**:226-234.

Lee EB, Lee VMY and Trojanowski JQ (2012) Gains or losses: Molecular mechanisms of TDP-43-mediated neurodegeneration *Nature Reviews Neuroscience* **13**:38-50.

Lee HJ, Suk JE, Bae EJ, Lee JH, Paik SR and Lee SJ (2008) Assembly-dependent endocytosis and clearance of extracellular alpha-synuclein. *The international journal of biochemistry & cell biology* **40**:1835-1849.

Lee HJ, Suk JE, Patrick C, Bae EJ, Cho JH, Rho S, Hwang D, Masliah E and Lee SJ (2010) Direct transfer of α-Synuclein from neuron to astroglia causes inflammatory responses in synucleinopathies. *Journal of Biological Chemistry* **285**:9262-9272.

Lee S and Huang EJ (2015) Modeling ALS and FTD with iPSC-derived neurons. *Brain Res*.

Leigh PN, Whitwell H, Garofalo O, Buller J, Swash M, Martin JE, Gallo JM, Weller RO and Anderton BH (1991) Ubiquitin-immunoreactive intraneuronal inclusions in amyotrophic lateral sclerosis. Morphology, distribution, and specificity *Brain* **114**:775-788.

Li HF and Wu ZY (2016) Genotype-phenotype correlations of amyotrophic lateral sclerosis. *Translational neurodegeneration* **5**:3.

Li JY, Englund E, Holton JL, Soulet D, Hagell P, Lees AJ, Lashley T, Quinn NP, Rehncrona S, Bjorklund A, Widner H, Revesz T, Lindvall O and Brundin P (2008) Lewy bodies in grafted neurons in subjects with Parkinson's disease suggest host-to-graft disease propagation. *Nat Med* **14**:501-503.

Li Q, Yokoshi M, Okada H and Kawahara Y (2015) The cleavage pattern of TDP-43 determines its rate of clearance and cytotoxicity. *Nature communications* **6**:6183.

Lindberg MJ, Tibell L and Oliveberg M (2002) Common denominator of Cu/Zn superoxide dismutase mutants associated with amyotrophic lateral sclerosis: Decreased stability of the apo state. *Proceedings Of The National Academy Of Sciences Of The United States Of America* **99**:16607-16612.

Liu-Yesucevitz L, Bilgutay A, Zhang YJ, Vanderweyde T, Citro A, Mehta T, Zaarur N, McKee A, Bowser R, Sherman M, Petrucelli L and Wolozin B (2010) Tar DNA binding protein-43 (TDP-43) associates with stress granules: analysis of cultured cells and pathological brain tissue. *PLoS One* **5**:e13250.

Logroscino G, Traynor BJ, Hardiman O, Chio A, Mitchell D, Swingler RJ, Millul A, Benn E, Beghi E and Eurals (2010) Incidence of amyotrophic lateral sclerosis in Europe. *Journal of neurology, neurosurgery, and psychiatry* **81**:385-390.

Lomen-Hoerth C, Anderson T and Miller B (2002) The overlap of amyotrophic lateral sclerosis and frontotemporal dementia. *Neurology* **59**:1077-1079.

Loov C, Scherzer CR, Hyman BT, Breakefield XO and Ingelsson M (2016) alpha-Synuclein in Extracellular Vesicles: Functional Implications and Diagnostic Opportunities. *Cellular and molecular neurobiology* **36**:437-448.

Lu H, Le WD, Xie YY and Wang XP (2016) Current Therapy of Drugs in Amyotrophic Lateral Sclerosis. *Current neuropharmacology* **14**:314-321.

Luk KC, Kehm V, Carroll J, Zhang B, O'Brien P, Trojanowski JQ and Lee VM (2012a) Pathological alpha-synuclein transmission initiates Parkinson-like neurodegeneration in nontransgenic mice. *Science* **338**:949-953.

Luk KC, Kehm VM, Zhang B, O'Brien P, Trojanowski JQ and Lee VM (2012b) Intracerebral inoculation of pathological alpha-synuclein initiates a rapidly progressive neurodegenerative alpha-synucleinopathy in mice. *The Journal of experimental medicine* **209**:975-986.

Mackenzie IR, Rademakers R and Neumann M (2010) TDP-43 and FUS in amyotrophic lateral sclerosis and frontotemporal dementia. *Lancet Neurology* **9**:995-1007.

Mackenzie IRA, Bigio EH, Ince PG, Geser F, Neumann M, Cairns NJ, Kwong LK, Forman MS, Ravits J, Stewart H, Eisen A, McClusky L, Kretzschmar HA, Monoranu CM, Highley JR, Kirby J, Siddique T, Shaw PJ, Lee VMY and Trojanowski JQ (2007) Pathological TDP-43 distinguishes sporadic amyotrophic lateral sclerosis from amyotrophic lateral sclerosis with SOD1 mutations *Annals of Neurology* **61**:427-434.

Maier O, Marvin SA, Wodrich H, Campbell EM and Wiethoff CM (2012) Spatiotemporal dynamics of adenovirus membrane rupture and endosomal escape. *Journal of virology* **86**:10821-10828.

Mancuso R, Olivan S, Rando A, Casas C, Osta R and Navarro X (2012) Sigma-1R agonist improves motor function and motoneuron survival in ALS mice. *Neurotherapeutics : the journal of the American Society for Experimental NeuroTherapeutics* **9**:814-826.

Marangi G and Traynor BJ (2015) Genetic causes of amyotrophic lateral sclerosis: new genetic analysis methodologies entailing new opportunities and challenges. *Brain Res* **1607**:75-93.

Marciniuk K, Taschuk R and Napper S (2013) Evidence for prion-like mechanisms in several neurodegenerative diseases: potential implications for immunotherapy. *Clinical & developmental immunology* **2013**:473706.

Marmor MD and Julius M (2001) Role for lipid rafts in regulating interleukin-2 receptor signaling. *Blood* **98**:1489-1497.

Matias-Guiu J, Galan L, Garcia-Ramos R and Barcia JA (2008) Superoxide dismutase: the cause of all amyotrophic lateral sclerosis? *Ann Neurol* **64**:356-357; author reply 358.

McAlary L, Aquilina JA and Yerbury JJ (2016) Susceptibility of Muatnt SOD1 to form a destabilized monomer predicts cellular aggregation and toxicity but not in vitro aggregation propensity. *Frontiers in neuroscience* **10**:499

McGuire KA, Barlan AU, Griffin TM and Wiethoff CM (2011) Adenovirus type 5 rupture of lysosomes leads to cathepsin B-dependent mitochondrial stress and production of reactive oxygen species. *Journal of virology* **85**:10806-10813.

Meier O, Boucke K, Hammer SV, Keller S, Stidwill RP, Hemmi S and Greber UF (2002) Adenovirus triggers macropinocytosis and endosomal leakage together with its clathrin-mediated uptake. *Journal Of Cell Biology* **158**:1119-1131.

Meier O and Greber UF (2003) Adenovirus endocytosis. *The journal of gene medicine* **5**:451-462.

Mercado PA, Ayala YM, Romano M, Buratti E and Baralle FE (2005) Depletion of TDP 43 overrides the need for exonic and intronic splicing enhancers in the human apoA-II gene. *Nucleic Acids Research* **33**:6000-6010.

Mercer J and Helenius A (2009) Virus entry by macropinocytosis. *Nat Cell Biol* **11**:510-520.

Mercer J and Helenius A (2012) Gulping rather than sipping: macropinocytosis as a way of virus entry. *Current opinion in microbiology* **15**:490-499.

Meyer-Luehmann M, Coomaraswamy J, Bolmont T, Kaeser S, Schaefer C, Kilger E, Neuenschwander A, Abramowski D, Frey P, Jaton AL, Vigouret JM, Paganetti P, Walsh DM, Mathews PM, Ghiso J, Staufenbiel M, Walker LC and Jucker M (2006) Exogenous Induction of Cerebral Beta-amyloidogenesis is Governed by Agent and Host. *Science* **22**:1781-1784.

Milanesi L, Sheynis T, Xue WF, Orlova EV, Hellewell AL, Jelinek R, Hewitt EW, Radford SE and Saibil HR (2012) Direct three-dimensional visualization of membrane disruption by amyloid fibrils. *Proc Natl Acad Sci U S A* **109**:20455-20460.

Mizusawa H (1993) Hyaline and Skein-like Inclusions in Amyotrophic Lateral Sclerosis. *Neuropathology* **13**:201-210.

Mohamed NV, Herrou T, Plouffe V, Piperno N and Leclerc N (2013) Spreading of tau pathology in Alzheimer's disease by cell-to-cell transmission. *The European journal of neuroscience* **37**:1939-1948.

Mondola P, Annella T, Santillo M and Santangelo F (1996) Evidence for secretion of cytosolic CuZn superoxide dismutase by hep G2 cells and human fibroblasts. *The International Journal of Biochemistry & Cell Biology* **28**:677-681.

Mondola P, Ruggiero G, Seru R, Damiano S, Grimaldi S, Garbi C, Monda M, Greco D and Santillo M (2003) The Cu,Zn superoxide dismutase in neuroblastoma SK-N-BE cells is exported by a microvesicles dependent pathway. *Molecular Brain Research* **110**:45-51.

Moon M, Hong HS, Nam DW, Baik SH, Song H, Kook SY, Kim YS, Lee J and Mook-Jung I (2012) Intracellular amyloid-beta accumulation in calcium-binding protein-deficient neurons leads to amyloid-beta plaque formation in animal model of Alzheimer's disease. *Journal of Alzheimer's disease : JAD* **29**:615-628.

Mougenot AL, Nicot S, Bencsik A, Morignat E, Verchere J, Lakhdar L, Legastelois S and Baron T (2012) Prion-like acceleration of a synucleinopathy in a transgenic mouse model. *Neurobiol Aging* **33**:2225-2228.

Mousavi A and Hotta Y (2005) Glycine-rich proteins: a class of novel proteins. *Applied biochemistry and biotechnology* **120**:169-174.

Muller FJ, Schuldt BM, Williams R, Mason D, Altun G, Papapetrou EP, Danner S, Goldmann JE, Herbst A, Schmidt NO, Aldenhoff JB, Laurent LC and Loring JF (2011) A bioinformatic assay for pluripotency in human cells. *Nature methods* **8**:315-317.

Munch C, O'Brien J and Bertolotti A (2011) Prion-like propagation of mutant superoxide dismutase-1 misfolding in neuronal cells. *Proc Natl Acad Sci U S A* **108**:3548-3553.

Munch J, Rucker E, Standker L, Adermann K, Goffinet C, Schindler M, Wildum S, Chinnadurai R, Rajan D, Specht A, Gimenez-Gallego G, Sanchez PC, Fowler DM, Koulov A, Kelly JW, Mothes W, Grivel JC, Margolis L, Keppler OT, Forssmann WG and Kirchhoff F (2007) Semen-derived amyloid fibrils drastically enhance HIV infection. *Cell* **131**:1059-1071.

Murayama S, Ookawa Y, Mori H, Nakano I, Ihara Y, Kuzuhara S and Tomonaga M (1989) Immunocytochemical and ultrastructural study of Lewy body-like hyaline inclusions in familial amyotrophic lateral sclerosis. *Acta Neuropathology* **78**:143–152.

Nagai M, Aoki M, Miyoshi I, Kato M, Pasinelli P, Kasai N, Brown RH, Jr. and Itoyama Y (2001) Rats expressing human cytosolic copper-zinc superoxide dismutase transgenes with amyotrophic lateral sclerosis: associated mutations develop motor neuron disease. *The Journal of neuroscience : the official journal of the Society for Neuroscience* **21**:9246-9254.

Nara A, Aki T, Funakoshi T, Unuma K and Uemura K (2012) Hyperstimulation of macropinocytosis leads to lysosomal dysfunction during exposure to methamphetamine in SH-SY5Y cells. *Brain Res* **1466**:1-14.

Nath S, Agholme L, Kurudenkandy FR, Granseth B, Marcusson J and Hallbeck M (2012) Spreading of neurodegenerative pathology *via* neuron-to-neuron transmission of beta-amyloid. *The Journal of neuroscience : the official journal of the Society for Neuroscience* **32**:8767-8777.

Neumann M, Kwong LK, Truax AC, Vanmassenhove B, Kretzschmar HA, Van Deerlin VM, Clark CM, Grossman M, Miller BL, Trojanowski JQ and Lee VM (2007) TDP-43-positive white matter pathology in frontotemporal lobar degeneration with ubiquitin-positive inclusions. *Journal of neuropathology and experimental neurology* **66**:177-183.

Neumann M, Sampathu DM, Kwong LK, Truax AC, Micsenyi MC, Chou TT, Bruce J, Schuck T, Grossman M, Clark CM, McCluskey LF, Miller BL, Masliah E, Mackenzie IR, Feldman H, Feiden W, Kretzschmar HA, Trojanowski JQ and Lee VMY (2006) Ubiquitinated TDP-43 in frontotemporal lobar degeneration and amyotrophic lateral sclerosis. *Journal of cell science* **314**:130-133.

Nishitoh H, Kadowaki H, Nagai A, Maruyama T, Yokota T, Fukutomi H, Noguchi T, Matsuzawa A, Takeda K and Ichijo H (2008) ALS-linked mutant SOD1 induces ER stress- and ASK1-dependent motor neuron death by targeting Derlin-1. *Genes & development* **22**:1451-1464.

Nixon RA, Cataldo AM and Mathews PM (2000) The endosomal-lysosomal system of neurons in Alzheimer's disease pathogenesis: a review. *Neurochemical research* **25**:1161-1172.

Nizard P, Tetley S, Le Drean Y, Watrin T, Le Goff P, Wilson MR and Michel D (2007) Stress-induced retrotranslocation of clusterin/ApoJ into the cytosol. *Traffic* **8**:554-565.

Nonaka T, Arai T, Buratti E, Baralle FE, Akiyama H and Hasegawa M (2009a) Phosphorylated and ubiquitinated TDP-43 pathological inclusions in ALS and FTLD-U are recapitulated in SH-SY5Y cells. *FEBS Lett* **583**:394-400.

Nonaka T, Kametani F, Arai T, Akiyama H and Hasegawa M (2009b) Truncation and pathogenic mutations facilitate the formation of intracellular aggregates of TDP-43. *Hum Mol Genet* **18**:3353-3364.

Nonaka T, Masuda-Suzukake M, Arai T, Hasegawa Y, Akatsu H, Obi T, Yoshida M, Murayama S, Mann DM, Akiyama H and Hasegawa M (2013) Prion-like properties of pathological TDP-43 aggregates from diseased brains. *Cell reports* **4**:124-134.

Okamoto K, Mizuno Y and Fujita Y (2008) Bunina bodies in amyotrophic lateral sclerosis. *Neuropathology* **28**:109-115.

Orsini M, Oliveira AB, Nascimento OJ, Reis CH, Leite MA, de Souza JA, Pupe C, de Souza OG, Bastos VH, de Freitas MR, Teixeira S, Bruno C, Davidovich E and Smidt B (2015) Amyotrophic Lateral Sclerosis: New Perpectives and Update. *Neurology international* **7**:5885.

Otomo A, Kunita R, Suzuki-Utsunomiya K, Mizumura H, Onoe K, Osuga H, Hadano S and Ikeda JE (2008) ALS2/alsin deficiency in neurons leads to mild defects in macropinocytosis and axonal growth. *Biochem Biophys Res Commun* **370**:87-92.

Ou SHI, Wu F, Harrich D, Garcia-Martinez LF and Gaynor RB (1995) Cloning and characterization of a novel cellular protein, TDP-43, that binds to human immunodeficiency virus type 1 TAR DNA sequence motifs. *Journal of Virology* **69**:3584-3596.

Pasinelli P and Brown RH (2006) Molecular biology of amyotrophic lateral sclerosis: insights from genetics. *Nature reviews Neuroscience* **7**:710-723.

Pearce MM, Spartz EJ, Hong W, Luo L and Kopito RR (2015) Prion-like transmission of neuronal huntingtin aggregates to phagocytic glia in the Drosophila brain. *Nature communications* **6**:6768.

Pedersen JS, Christensen G and Otzen DE (2004) Modulation of S6 fibrillation by unfolding rates and gatekeeper residues. *J Mol Biol* **341**:575-588.

Petrasch-Parwez E, Nguyen HP, Lobbecke-Schumacher M, Habbes HW, Wieczorek S, Riess O, Andres KH, Dermietzel R and Von Horsten S (2007) Cellular and subcellular localization of Huntingtin [corrected] aggregates in the brain of a rat transgenic for Huntington disease. *The Journal of comparative neurology* **501**:716-730.

Piao Y-S, Wakabayashi K, Kakita A, Yamada M, Hayashi S, Morita T, Ikuta F, Oyanagi K and Takahashi H (2003) Neuropathology with clinical correlations of sporadic amyotrophic lateral sclerosis: 102 Autopsy cases examined between 1962 and 2000. *Brain Pathology* **13**:10-22.

Pinotsi D, Michel CH, Buell AK, Laine RF, Mahou P, Dobson CM, Kaminski CF and Kaminski Schierle GS (2016) Nanoscopic insights into seeding mechanisms and toxicity of alpha-synuclein species in neurons. *Proc Natl Acad Sci U S A* **113**:3815-3819.

Pokrishevsky E, Grad LI, Yousefi M, Wang J, Mackenzie IR and Cashman NR (2012) Aberrant localization of FUS and TDP-43 is associated with misfolding of SOD1 in amyotrophic lateral sclerosis. *PLoS One* **7**:e35050.

Polling S, Mok YF, Ramdzan YM, Turner BJ, Yerbury JJ, Hill AF and Hatters DM (2014) Misfolded polyglutamine, polyalanine, and superoxide dismutase 1 aggregate *via* distinct pathways in the cell. *J Biol Chem* **289**:6669-6680.

Prudencio M, Durazo A, Whitelegge JP and Borchelt DR (2009a) Modulation of mutant superoxide dismutase 1 aggregation by co-expression of wild-type enzyme. *J Neurochem* **108**:1009-1018.

Prudencio M, Durazo A, Whitelegge JP and Borchelt DR (2010) An examination of wild-type SOD1 in modulating the toxicity and aggregation of ALS-associated mutant SOD1. *Hum Mol Genet* **19**:4774-4789.

Prudencio M, Hart J, Borchelt DR and Andersen PM (2009) Variation in aggregation propensities among ALS-associated variants of SOD1: Correlation to human disease. *Human Molecular Genetics* **18**:3217-3226.

Prusiner SB (1982) Novel proteinaceous infectious particles cause scrapie. *Science* **216**:136-144.

Prusiner SB (1984) Some speculations about prions, amyloid, and Alzheimer's disease. *N Engl J Med* **310**:661-663.

Prusiner SB (1998) Prions. *Proceedings Of The National Academy Of Sciences Of The United States Of America* **95**:13363-13383.

Radunovic A and Leigh PN (1996) Cu/Zn superoxide dismutase gene mutations in amyotrophic lateral sclerosis: Correlation between genotype and clinical features. *Journal of Neurological sciences* **61**:565-572.

Rakhit R, Crow J and Lepock J (2004) Monomeric Cu, Zn superoxide dismutase is a common misfolding intermediate in the oxidation models of sporadic and familial amyotrophic lateral sclerosis. *Journal of Biological Chemistry* **279**:15499–15504.

Rakhit R, Robertson J, Vande Velde C, Horne P, Ruth DM, Griffin J, Cleveland DW, Cashman NR and Chakrabartty A (2007) An immunological epitope selective for pathological monomer-misfolded SOD1 in ALS. *Nat Med* **13**:754-759.

Ramdzan YM, Nisbet RM, Miller J, Finkbeiner S, Hill AF and Hatters DM (2010) Conformation sensors that distinguish monomeric proteins from oligomers in live cells. *Chemistry & biology* **17**:371-379.

Ravits J (2014) Focality, stochasticity and neuroanatomic propagation in ALS pathogenesis. *Exp Neurol* **262 Pt B**:121-126.

Ravits J, Paul P and Jorg C (2007) Focality of upper and lower motor neuron degeneration at the clinical onset of ALS. *Neurology* **68**:1571–1575.

Ravits JM and La Spada AR (2009) ALS motor phenotype heterogeneity, focality, and spread: deconstructing motor neuron degeneration. *Neurology* **73**:805-811.

Ray K, Bobard A, Danckaert A, Paz-Haftel I, Clair C, Ehsani S, Tang C, Sansonetti P, Tran GV and Enninga J (2010) Tracking the dynamic interplay between bacterial and host factors during pathogen-induced vacuole rupture in real time. *Cellular microbiology* **12**:545-556.

Raymond GJ, Bossers A, Raymond LD, O'Rourke KI, McHolland LE, Bryant PK, 3rd, Miller MW, Williams ES, Smits M and Caughey B (2000) Evidence of a molecular barrier limiting susceptibility of humans, cattle and sheep to chronic wasting disease. *EMBO J* **19**:4425-4430.

Reaume AG, Elliott JL, Hoffman EK, Kowall NW, Ferrante RJ, Siwek DF, Wilcox HM, Flood DG, Beal MF, Brown RH, Jr., Scott RW and Snider WD (1996) Motor neurons in Cu/Zn superoxide dismutase-deficient mice develop normally but exhibit enhanced cell death after axonal injury. *Nat Genet* **13**:43-47.

Redler RL and Dokholyan NV (2012) The complex molecular biology of amyotrophic lateral sclerosis (ALS). *Progress in molecular biology and translational science* **107**:215-262.

Ren PH, Lauckner JE, Kachirskaia I, Heuser JE, Melki R and Kopito RR (2009) Cytoplasmic penetration and persistent infection of mammalian cells by polyglutamine aggregates. *Nat Cell Biol* **11**:219-225.

Ren WQ, Tian ZM, Yin F, Sun JZ and Zhang JN (2016) Extracellular alpha-synuclein--a possible initiator of inflammation in Parkinson's disease. *Die Pharmazie* **71**:51-55.

Renton AE, Chio A and Traynor BJ (2014) State of play in amyotrophic lateral sclerosis genetics. *Nature neuroscience* **17**:17-23.

Riancho J, Gonzalo I, Ruiz-Soto M and Berciano J (2016) Why do motor neurons degenerate? Actualization in the pathogenesis of amyotrophic lateral sclerosis. *Neurologia*.

Richter T, Floetenmeyer M, Ferguson C, Galea J, Goh J, Lindsay MR, Morgan GP, Marsh BJ and Parton RG (2008) High-resolution 3D quantitative analysis of caveolar ultrastructure and caveola-cytoskeleton interactions. *Traffic* **9**:893-909.

Ridley AJ, Paterson HF, Johnston CL, Diekmann D and Hall A (1992) The small GTP-binding protein rac regulates growth factor-induced membrane ruffling. *Cell* **70**:401-410.

Ripps M, Huntley G, Hof P, Morrison J and Gordon J (1995) Transgenic mice expressing an altered murine superoxide dismutase gene provide an animal model of amyotrophic lateral sclerosis *Proceedings Of The National Academy Of Sciences Of The United States Of America* **92**:689-693.

Roberts K, Zeineddine R, Corcoran L, Li W, Campbell IL and Yerbury JJ (2013) Extracellular aggregated Cu/Zn superoxide dismutase activates microglia to give a cytotoxic phenotype. *Glia* **61**:409-419.

Robertson J, Sanelli T, Xiao S, Yang W, Horne P, Hammond R, Pioro EP and Strong MJ (2007) Lack of TDP-43 abnormalities in mutant SOD1 transgenic mice shows disparity with ALS. *Neurosci Lett* **420**:128-132.

Rosen DR, Siddique T, Patterson D, Figlewicz DA, Sapp P, Hentati A, Donaldson D, Goto J, O'Regan JP, Deng HX, Rahmani Z, Krizus A, McKenna-Yasek D, Cayabyab A, Gaston SM, Berger R, Tanzi RE, Halperin JJ and Herzfeldt B (1993) Mutations in Cu/Zn superoxide dismutase gene are associated with familial amyotrophic lateral sclerosis. *Nature* **362**:59-62.

Ross CA and Poirier MA (2004) Protein aggregation and neurodegenerative disease. *Nature Medicine* **10**:10-17.

Rowland LP and Shneider NA (2001) Amyotrophic lateral sclerosis. *The New England Journal of Medicine* **344**:1688-1700.

Rutherford NJ, Zhang YJ, Baker M, Gass JM, Finch NA, Xu YF, Stewart H, Kelley BJ, Kuntz K, Crook RJ, Sreedharan J, Vance C, Sorenson E, Lippa C, Bigio EH, Geschwind DH, Knopman DS, Mitsumoto H, Petersen RC, Cashman NR, Hutton M, Shaw CE, Boylan KB, Boeve B, Graff-Radford NR, Wszolek ZK, Caselli RJ, Dickson DW, Mackenzie IR, Petrucelli L and Rademakers R (2008) Novel mutations in TARDBP (TDP-43) in patients with familial amyotrophic lateral sclerosis. *PLoS Genet* **4**:e1000193.

Sakurai Y, Kolokoltsov AA, Chen CC, Tidwell MW, Bauta WE, Klugbauer N, Grimm C, Wahl-Schott C, Biel M and Davey RA (2015) Ebola virus. Two-pore channels control Ebola virus host cell entry and are drug targets for disease treatment. *Science* **347**:995-998.

Saman S, Kim W, Raya M, Visnick Y, Miro S, Saman S, Jackson B, McKee AC, Alvarez VE, Lee NCY and Hall GF (2012) Exosome-associated tau is secreted in tauopathy models and is selectively phosphorylated in cerebrospinal fluid in early Alzheimer disease. *The Journal of Biological Chemistry* **287**:3842-3849.

Sanchez EG, Quintas A, Perez-Nunez D, Nogal M, Barroso S, Carrascosa AL and Revilla Y (2012) African swine fever virus uses macropinocytosis to enter host cells. *PLoS pathogens* **8**:e1002754.

Santillo M, Secondo A, Seru R, Damiano S, Garbi C, Taverna E, Rosa P, Giovedı S, Benfenati F and Mondola P (2007) Evidence of calcium- and SNARE-dependent release of CuZn superoxide dismutase from rat pituitary GH3 cells and synaptosomes in response to depolarization. *journal of Neurochemistry* **102**:679-685.

Saxena S, Cabuy E and Caroni P (2009) A role for motoneuron subtype-selective ER stress in disease manifestations of FALS mice. *Nat Neurosci* **12**:627-636.

Scarmeas N, Shih T, Stern Y, Ottman R and Rowland LP (2002) Premorbid weight, body mass, and varsity athletics in ALS. *Neurology* **59**:773-775.

Scherzinger E, Lurz R, Turmaine M, Mangiarini L, Hollenbach B, Hasenbank R, Bates GP, Davies SW, Lehrach H and Wanker EE (1997) Huntingtin-encoded polyglutamine

expansions form amyloid-like protein aggregates *in vitro* and *in vivo*. *Cell* **90**:549-558.

Schmid SL (1997) Clathrin-coated vesicle formation and protein sorting: an integrated process. *Annu Rev Biochem* **66**:511-548.

Schneider D, Greb C, Koch A, Straube T, Elli A, Delacour D and Jacob R (2010) Trafficking of galectin-3 through endosomal organelles of polarized and non-polarized cells. *European journal of cell biology* **89**:788-798.

Schonn I, Hennesen J and Dartsch DC (2010) Cellular responses to etoposide: cell death despite cell cycle arrest and repair of DNA damage. *Apoptosis : an international journal on programmed cell death* **15**:162-172.

Schwab C, Akiyama H, McGeer EG and McGeer PL (1998) Extracellular neurofibrillary tangles are immunopositive for the 40 carboxy-terminal sequence of beta-amyloid protein. *Journal of neuropathology and experimental neurology* **57**:1131-1137.

Scotter EL, Vance C, Nishimura AL, Lee YB, Chen HJ, Urwin H, Sardone V, Mitchell JC, Rogelj B, Rubinsztein DC and Shaw CE (2014) Differential roles of the ubiquitin proteasome system and autophagy in the clearance of soluble and aggregated TDP-43 species. *Journal of cell science* **127**:1263-1278.

Sekiguchi T, Kanouchi T, Shibuya K, Noto Y, Yagi Y, Inaba A, Abe K, Misawa S, Orimo S, Kobayashi T, Kamata T, Nakagawa M, Kuwabara S, Mizusawa H and Yokota T (2014) Spreading of amyotrophic lateral sclerosis lesions--multifocal hits and local propagation? *Journal of neurology, neurosurgery, and psychiatry* **85**:85-91.

Serio TR, Cashikar AG, Kowal AS, Sawicki GJ, Moslehi JJ, Serpell L, Arnsdorf MF and Lindquist SL (2000) Nucleated conformational conversion and the replication of conformational information by a prion determinant. *Science* **289**:1317-1321.

Shan X, Vocadlo D and Krieger C (2009) Mislocalization of TDP-43 in the G93A mutant SOD1 transgenic mouse model of ALS. *Neurosci Lett* **458**:70-74.

Shaw PJ (2002) Toxicity of CSF in motor neurone disease: a potential route to neuroprotection. *Brain* **125**:693-694.

Shibata N, Hirano A, Kobayashi M, Sasaki S, Kato T, Matsumoto S, Shiozawa Z, Komori T, Ikemoto A, Umahara T and et al. (1994) Cu/Zn superoxide dismutase-like immunoreactivity in Lewy body-like inclusions of sporadic amyotrophic lateral sclerosis. *Neurosci Lett* **179**:149-152.

Shimonaka S, Nonaka T, Suzuki G, Hisanaga S and Hasegawa M (2016) Templated Aggregation of TAR DNA-binding Protein of 43 kDa (TDP-43) by Seeding with TDP-43 Peptide Fibrils. *J Biol Chem* **291**:8896-8907.

Silverman JM, Fernando SM, Grad LI, Hill AF, Turner BJ, Yerbury JJ and Cashman NR (2016) Disease Mechanisms in ALS: Misfolded SOD1 Transferred Through Exosome-Dependent and Exosome-Independent Pathways. *Cellular and molecular neurobiology*.

Soo KY, Farg M and Atkin JD (2011) Molecular motor proteins and amyotrophic lateral sclerosis. *International journal of molecular sciences* **12**:9057-9082.

Sreedharan J, Blair LP, Tripathi VB, Hu X, Vance C, Rogelj B, Ackerley S, Durnall JC, Williams KL, Buratti E, Baralle F, Belleroche Jd, Mitchell D, Leigh N, Chalabi AA, Miller CC, Nicholson G and Shaw CE (2008) TDP-43 mutations in familial and sporadic amyotrophic lateral sclerosis. *Journal of Cell Science* **319**:1668-1672.

Stancu IC, Vasconcelos B, Ris L, Wang P, Villers A, Peeraer E, Buist A, Terwel D, Baatsen P, Oyelami T, Pierrot N, Casteels C, Bormans G, Kienlen-Campard P, Octave JN, Moechars D and Dewachter I (2015) Templated misfolding of Tau by prion-like seeding along neuronal connections impairs neuronal network function and associated behavioral outcomes in Tau transgenic mice. *Acta Neuropathol* **129**:875-894.

Stefani M and Dobson CM (2003) Protein aggregation and aggregate toxicity: new insights into protein folding, misfolding diseases and biological evolution. *J Mol Med (Berl)* **81**:678-699.

Steiner JA, Angot E and Brundin P (2011) A deadly spread: cellular mechanisms of alpha-synuclein transfer. *Cell Death Differ* **18**:1425-1433.

Stieber A, Gonatas JO and Gonatas NK (2000) Aggregation of ubiquitin and a mutant ALS-linked SOD1 protein correlate with disease progression and fragmentation of the Golgi apparatus *Journal of the Neurological Sciences* **173**:53-62.

Stohr J, Watts JC, Mensinger ZL, Oehler A, Grillo SK, DeArmond SJ, Prusiner SB and Giles K (2012) Purified and synthetic Alzheimer's amyloid beta (Abeta) prions. *Proc Natl Acad Sci U S A* **109**:11025-11030.

Strong M and Rosenfeld J (2003) Amyotrophic lateral sclerosis: a review of current concepts. *Amyotrophic lateral sclerosis and other motor neuron disorders : official publication of the World Federation of Neurology, Research Group on Motor Neuron Diseases* **4**:136-143.

Sun P, Yamamoto H, Suetsugu S, Miki H, Takenawa T and Endo T (2003) Small GTPase Rah/Rab34 is associated with membrane ruffles and macropinosomes and promotes macropinosome formation. *J Biol Chem* **278**:4063-4071.

Sundaramoorthy V, Walker AK, Yerbury J, Soo K, Farg MA, Hoang V, Zeineddine R, Spencer D and Atkin JD (2013) Extracellular wildtype and mutant SOD1 induces ER-Golgi pathology characteristic of amyotrophic lateral sclerosis in neuronal cells. *Cellular and Molecular Life Sciences* **70**:4181-4195.

Sung JY, Kim J, Paiki SR, Park JH, Ahn YS and Chung KC (2001) Induction of neuronal cell death by Rab5A-dependent endocytosis of alpha-synuclein. *The Journal of Biological Chemistry* **276**:27441-27448.

Suzuki H, Lee K and Matsuoka M (2011) TDP-43-induced death is associated with altered regulation of BIM and Bcl-xL and attenuated by caspase-mediated TDP-43 cleavage. *J Biol Chem* **286**:13171-13183.

Swanson JA (1989) Phorbol esters stimulate macropinocytosis and solute flow through macrophages. *Journal of cell science* **94 (Pt 1)**:135-142.

Swanson JA (2008) Shaping cups into phagosomes and macropinosomes. *Nature reviews Molecular cell biology* **9**:639-649.

Swanson JA and Watts C (1995) Macropinocytosis. *Trends in cell biology* **5**:424-428.

Talekar A, Pessi A and Porotto M (2011) Infection of primary neurons mediated by nipah virus envelope proteins: role of host target cells in antiviral action. *Journal of virology* **85**:8422-8426.

Tandan R and Bradley WG (1985) Amyotrophic lateral sclerosis: Part 1. Clinical features, pathology, and ethical issues in management. *Ann Neurol* **18**:271-280.

Tasaki M, Ueda M, Ochiai S, Tanabe Y, Murata S, Misumi Y, Su Y, Sun X, Shinriki S, Jono H, Shono M, Obayashi K and Ando Y (2010) Transmission of circulating cell-free AA amyloid oligomers in exosomes vectors *via* a prion-like mechanism. *Biochem Biophys Res Commun* **400**:559-562.

Tjernberg LO, Callaway DJ, Tjernberg A, Hahne S, Lilliehook C, Terenius L, Thyberg J and Nordstedt C (1999) A molecular model of Alzheimer amyloid beta-peptide fibril formation. *J Biol Chem* **274**:12619-12625.

Tom VJ, Steinmetz MP, Miller JH, Doller CM and Silver J (2004) Studies on the development and behavior of the dystrophic growth cone, the hallmark of regeneration failure, in an *in vivo* model of the glial scar and after spinal cord injury. *J Neurosci* **24**:6531-6539.

Tortelli R, Conforti FL, Cortese R, D'Errico E, Distaso E, Mazzei R, Ungaro C, Magariello A, Gambardella A, Logroscino G and Simone IL (2013) Amyotrophic lateral sclerosis: a new missense mutation in the SOD1 gene. *Neurobiol Aging* **34**:1709 e1703-1705.

Traub LM (2009) Clathrin couture: fashioning distinctive membrane coats at the cell surface. *PLoS Biol* **7**:e1000192.

Trevino RS, Lauckner JE, Sourigues Y, Pearce MM, Bousset L, Melki R and Kopito RR (2012) Fibrillar structure and charge determine the interaction of polyglutamine protein aggregates with the cell surface. *Journal of Biological Chemistry* **287**:29722-29728.

Trump BF, Berezesky IK, Chang SH and Phelps PC (1997) The pathways of cell death: oncosis, apoptosis, and necrosis. *Toxicologic pathology* **25**:82-88.

Turner B and Talbot K (2008) Transgenics, toxicity and therapeutics in rodent models of mutant SOD1-mediated familial ALS. *Progress in Neurobiology* **85**:94-134.

Turner BJ, Atkin JD, Farg MA, Zang DW, Rembach A, Lopes EC, Patch JD, Hill AF and Cheema SS (2005) Impaired extracellular secretion of mutant superoxide dismutase 1 associates with neurotoxicity in familial amyotrophic lateral sclerosis. *The Journal of Neuroscience* **25**:108-117.

Turner BJ, Baumer D, Parkinson NJ, Scaber J, Ansorge O and Talbot K (2008) TDP-43 expression in mouse models of amyotrophic lateral sclerosis and spinal muscular atrophy. *BMC Neurosci* **9**:104.

Turner BJ, Lopes EC and Cheema SS (2003) Neuromuscular accumulation of mutant superoxide dismutase 1 aggregates in a transgenic mouse model of familial amyotrophic lateral sclerosis. *Neurosci Lett* **350**:132-136.

Urushitani M, Ezzi SA, Matsuo A, Tooyama I and Julien JP (2008) The endoplasmic reticulum-Golgi pathway is a target for translocation and aggregation of mutant superoxide dismutase linked to ALS. *FASEB journal : official publication of the Federation of American Societies for Experimental Biology* **22**:2476-2487.

Urushitani M, Sik A, Sakurai T, Nukina N, Takahashi R and Julien J (2006) Chromogranin-mediated secretion of mutant superoxide dismutase proteins linked to amyotrophic lateral sclerosis. *Nature Neuroscience* **9**:108-118.

Uversky VN (2007) Neuropathology, biochemistry, and biophysics of alpha-synuclein aggregation. *J Neurochem* **103**:17-37.

Valentine JS and Hart PJ (2003) Misfolded CuZnSOD and amyotrophic lateral sclerosis. *Proceedings Of The National Academy Of Sciences Of The United States Of America* **100**:3617-3622.

Van Deerlin VM, Leverenz JB, Bekris LM, Bird TD, Yuan W, Elman LB, Clay D, Wood EM, Chen-Plotkin AS, Martinez-Lage M, Steinbart E, McCluskey L, Grossman M, Neumann M, Wu IL, Yang WS, Kalb R, Galasko DR, Montine TJ, Trojanowski JQ, Lee VM, Schellenberg GD and Yu CE (2008) TARDBP mutations in amyotrophic lateral sclerosis with TDP-43 neuropathology: a genetic and histopathological analysis. *The Lancet Neurology* **7**:409-416.

van der Kant R and Goldstein LS (2015) Cellular functions of the amyloid precursor protein from development to dementia. *Developmental cell* **32**:502-515.

van Eersel J, Ke YD, Gladbach A, Bi M, Gotz J, Kril JJ and Ittner LM (2011) Cytoplasmic accumulation and aggregation of TDP-43 upon proteasome inhibition in cultured neurons. *PLoS One* **6**:e22850.

Vasconcelos B, Stancu IC, Buist A, Bird M, Wang P, Vanoosthuyse A, Van Kolen K, Verheyen A, Kienlen-Campard P, Octave JN, Baatsen P, Moechars D and Dewachter I (2016) Heterotypic seeding of Tau fibrillization by pre-aggregated Abeta provides

potent seeds for prion-like seeding and propagation of Tau-pathology *in vivo*. *Acta Neuropathol* **131**:549-569.

Veldink JH, Kalmijn S, Groeneveld GJ, Titulaer MJ, Wokke JH and van den Berg LH (2005) Physical activity and the association with sporadic ALS. *Neurology* **64**:241-245.

Volpicelli-Daley LA, Luk KC, Patel TP, Tanik SA, Riddle DM, Stieber A, Meaney DF, Trojanowski JQ and Lee VM (2011) Exogenous alpha-synuclein fibrils induce Lewy body pathology leading to synaptic dysfunction and neuron death. *Neuron* **72**:57-71.

Wadia JS, Schaller M, Williamson RA and Dowdy SF (2008) Pathologic prion protein infects cells by lipid-raft dependent macropinocytosis. *PLoS One* **3**:e3314.

Walker AK and Atkin JD (2011) Stress signaling from the endoplasmic reticulum: A central player in the pathogenesis of amyotrophic lateral sclerosis. *IUBMB life* **63**:754-763.

Walker AK, Soo KY, Sundaramoorthy V, Parakh S, Ma Y, Farg MA, Wallace RH, Crouch PJ, Turner BJ, Horne MK and Atkin JD (2013) ALS-associated TDP-43 induces endoplasmic reticulum stress, which drives cytoplasmic TDP-43 accumulation and stress granule formation. *PLoS One* **8**:e81170.

Wang J, Xu G and Borchelt DR (2002) High Molecular Weight Complexes of Mutant Superoxide Dismutase 1: Age-Dependent and Tissue-Specific Accumulation. *Neurobiology of Disease* **9**:139-148.

Wang L, Deng HX, Grisotti G, Zhai H, Siddique T and Roos RP (2009) Wild-type SOD1 overexpression accelerates disease onset of a G85R SOD1 mouse. *Hum Mol Genet* **18**:1642-1651.

Wang Q, Johnson JL, Agar NY and Agar JN (2008) Protein aggregation and protein instability govern familial amyotrophic lateral sclerosis patient survival. *PLoS biology* **6**:e170.

Watanabe M, Dykes-Hoberg M, Culotta VC, Price DL, Wong PC and Rothstein JD (2001) Histological evidence of protein aggregation in mutant SOD1 transgenic mice and in amyotrophic lateral sclerosis neural tissues. *Neurobiol Dis* **8**:933-941.

Watts C and Marsh M (1992) Endocytosis: what goes in and how? *Journal of cell science* **103 (Pt 1)**:1-8.

Webster CP, Smith EF, Bauer CS, Moller A, Hautbergue GM, Ferraiuolo L, Myszczynska MA, Higginbottom A, Walsh MJ, Whitworth AJ, Kaspar BK, Meyer K, Shaw PJ, Grierson AJ and De Vos KJ (2016) The C9orf72 protein interacts with Rab1a and the ULK1 complex to regulate initiation of autophagy. *EMBO J*.

Weisberg SJ, Lyakhovetsky R, Werdiger AC, Gitler AD, Soen Y and Kaganovich D (2012) Compartmentalization of superoxide dismutase 1 (SOD1G93A) aggregates determines their toxicity. *Proc Natl Acad Sci U S A* **109**:15811-15816.

West MA, Bretscher MS and Watts C (1989) Distinct endocytotic pathways in epidermal growth factor-stimulated human carcinoma A431 cells. *The Journal of cell biology* **109**:2731-2739.

Williams KL, Topp S, Yang S, Smith B, Fifita JA, Warraich ST, Zhang KY, Farrawell N, Vance C, Hu X, Chesi A, Leblond CS, Lee A, Rayner SL, Sundaramoorthy V, Dobson-Stone C, Molloy MP, van Blitterswijk M, Dickson DW, Petersen RC, Graff-Radford NR, Boeve BF, Murray ME, Pottier C, Don E, Winnick C, McCann EP, Hogan A, Daoud H, Levert A, Dion PA, Mitsui J, Ishiura H, Takahashi Y, Goto J, Kost J, Gellera C, Gkazi AS, Miller J, Stockton J, Brooks WS, Boundy K, Polak M, Munoz-Blanco JL, Esteban-Perez J, Rabano A, Hardiman O, Morrison KE, Ticozzi N, Silani V, de Belleroche J, Glass JD, Kwok JB, Guillemin GJ, Chung RS, Tsuji S, Brown RH, Jr., Garcia-Redondo A, Rademakers R, Landers JE, Gitler AD, Rouleau GA, Cole NJ, Yerbury JJ, Atkin JD, Shaw CE, Nicholson GA and Blair IP (2016)

CCNF mutations in amyotrophic lateral sclerosis and frontotemporal dementia. *Nature communications* **7**:11253.

Wilson AC, Dugger BN, Dickson DW and Wang DS (2011) TDP-43 in aging and Alzheimer's disease - a review. *International journal of clinical and experimental pathology* **4**:147-155.

Wilson MR, Yerbury JJ and Poon S (2008) Potential roles of abundant extracellular chaperones in the control of amyloid formation and toxicity. *Mol Biosyst* **4**:42-52.

Winer L, Srinivasan D, Chun S, Lacomis D, Jaffa M, Fagan A, Holtzman DM, Wancewicz E, Bennett CF, Bowser R, Cudkowicz M and Miller TM (2013) SOD1 in cerebral spinal fluid as a pharmacodynamic marker for antisense oligonucleotide therapy. *JAMA neurology* **70**:201-207.

Wojtowicz WM, Farzan M, Joyal JL, Carter K, Babcock GJ, Israel DI, Sodroski J and Mirzabekov T (2002) Stimulation of enveloped virus infection by beta-amyloid fibrils. *J Biol Chem* **277**:35019-35024.

Wu JW, Herman M, Liu L, Simoes S, Acker CM, Figueroa H, Steinberg JI, Margittai M, Kayed R, Zurzolo C, Di Paolo G and Duff KE (2013a) Small misfolded Tau species are internalized *via* bulk endocytosis and anterogradely and retrogradely transported in neurons. *J Biol Chem* **288**:1856-1870.

Wu JW, Herman M, Liu L, Simoes S, Acker CM, Figueroa H, Steinberg JI, Margittai M, Kayed R, Zurzolo C, Paolo GD and Duff KE (2013b) Small misfolded Tau species are internalized *via* bulk endocytosis and anterogradely and retrogradely transported in neurons. *The Journal of Biological Chemistry* **288**:1856-1870.

Yamaguchi H, Nakazato Y, Kawarabayashi T, Ishiguro K, Ihara Y, Morimatsu M and Hirai S (1991) Extracellular neurofibrillary tangles associated with degenerating neurites and neuropil threads in Alzheimer-type dementia. *Acta Neuropathol* **81**:603-609.

Yamamoto K, Seki T, Yamamoto H, Adachi N, Tanaka S, Hide I, Saito N and Sakai N (2014) Deregulation of the actin cytoskeleton and macropinocytosis in response to phorbol ester by the mutant protein kinase C gamma that causes spinocerebellar ataxia type 14. *Front Physiol* **5**:126.

Yamasaki T, Suzuki A, Shimizu T, Watarai M, Hasebe R and Horiuchi M (2012) Characterization of intracellular localization of PrP(Sc) in prion-infected cells using a mAb that recognizes the region consisting of aa 119-127 of mouse PrP. *The Journal of general virology* **93**:668-680.

Yang C, Tan W, Whittle C, Qiu L, Cao L, Akbarian S and Xu Z (2010) The C-Terminal TDP-43 fragments have a high aggregation propensity and harm neurons by a dominant-negative mechanism. *PLoS ONE* **5**:e15878.

Yang W, Dunlap JR, Andrews RB and Wetzel R (2002) Aggregated polyglutamine peptides delivered to nuclei are toxic to mammalian cells. *Human Molecular Genetics* **11**:2905-2917.

Yerbury JJ, Gower D, Vanags L, Roberts K, Lee JA and Ecroyd H (2013) The small heat shock proteins alphaB-crystallin and Hsp27 suppress SOD1 aggregation *in vivo*. *Cell stress & chaperones* **18**:251-257.

Yerbury JJ, Ooi L, Dillin A, Saunders DN, Hatters DM, Beart PM, Cashman NR, Wilson MR and Ecroyd H (2016) Walking the tightrope: Proteostasis and neurodegenerative disease. *J Neurochem*.

Yim MB, Kang JH, Yim HS, Kwak HS, Chock PB and Stadtman ER (1996) A gain-of-function of an amyotrophic lateral sclerosis-associated Cu,Zn- superoxide dismutase mutant: An enhancement of free radical formation due to a decrease in K(m) for hydrogen peroxide. *Proceedings Of The National Academy Of Sciences Of The United States Of America* **93**:5709-5714.

Yokoseki A, Shiga A, Tan C-F, Tagawa A, Kaneko H, Koyama A, Eguchi H, Ikeuchi T, Okamoto K, Nishizawa M, Takahashi H and Onodera O (2008) TDP-43 Mutation in Familial Amyotrophic Lateral Sclerosis. *Annals of Neurology* **63**:538-542.

Zeineddine R, Pundavela JF, Corcoran L, Stewart EM, Do-Ha D, Bax M, Guillemin G, Vine KL, Hatters DM, Ecroyd H, Dobson CM, Turner BJ, Ooi L, Wilson MR, Cashman NR and Yerbury JJ (2015) SOD1 protein aggregates stimulate macropinocytosis in neurons to facilitate their propagation. *Molecular neurodegeneration* **10**:57.

Zeineddine R and Yerbury JJ (2015) The role of macropinocytosis in the propagation of protein aggregation associated with neurodegenerative diseases. *Frontiers in physiology* **6**:277.

Zetterstrom P, Andersen PM, Brannstrom T and Marklund SL (2011) Misfolded superoxide dismutase-1 in CSF from amyotrophic lateral sclerosis patients. *J Neurochem* **117**:91-99.

Zetterstrom P, Stewart HG, Bergemalm D, Jonsson PA, Graffmo KS, Andersen PM, Brannstrom T, Oliveberg M and Marklund SL (2007) Soluble misfolded subfractions of mutant superoxide dismutase-1s are enriched in spinal cords throughout life in murine ALS models. *Proc Natl Acad Sci U S A* **104**:14157-14162.

Zhang T, Baldie G, Periz G and Wang J (2014) RNA-processing protein TDP-43 regulates FOXO-dependent protein quality control in stress response. *PLoS Genet* **10**:e1004693.

Zhang YJ, Xu YF, Cook C, Gendron TF, Roettges P, Link CD, Lin WL, Tong J, Castanedes-Casey M, Ash P, Gass J, Rangachari V, Buratti E, Baralle F, Golde TE, Dickson DW and Petrucelli L (2009) Aberrant cleavage of TDP-43 enhances aggregation and cellular toxicity. *Proc Natl Acad Sci U S A* **106**:7607-7612.